RCA Review

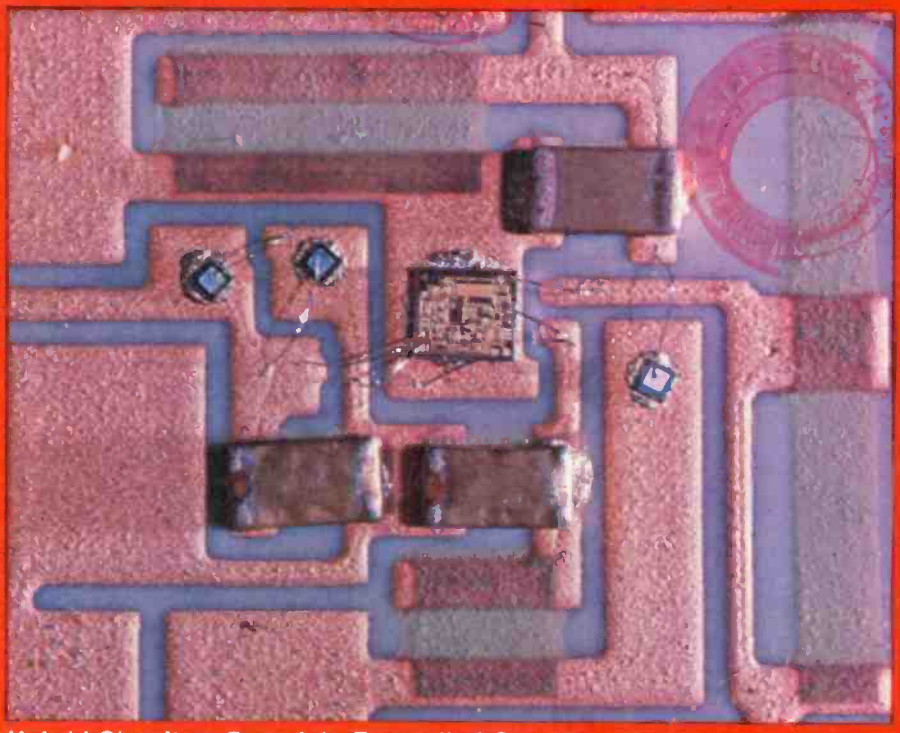

Hybrid Circuit on Porcelain-Enamelled-Steel Board

June 1981 Volume 42 No. 2

RCARCI 42(2) 131–330 (1981)

RCA Review, published quarterly in March, June, September and December by RCA Research and Engineering, RCA Corporation, Princeton, New Jersey 08540. Entered as second class matter July 3, 1950 under the Act of March 3, 1879. Second-class postage paid at Princeton, New Jersey, and at additional mailing offices. Effective January 1, 1978, subscription rates as follows: United States and Canada: one year $8.00, two years $14.00, three years $18.00; in other countries, one year $8.60, two years $15.20, three years $19.80. Single copies (except for special issues) up to five years old $3.00.

RCA Review

RCA Review (ISSN 0033-6831) is a technical journal published quarterly by RCA Research and Engineering in cooperation with the subsidiaries and divisions of RCA.

Contents

June 1981 Volume 42 Number 2 ISSN 0033-6831

Introduction to Special Issue on Porcelain-Enamelled-Steel Boards for Electronic Applications

Lubomyr S. Onyshkevych,

RCA Laboratories, Princeton, NJ 08540

Enamelling is a very ancient art. Originally, enamelled gold and other metals were used almost exclusively to embellish jewelry, weapons, and art objects. In more recent times enamelling has been utilized for such mundane purposes as passivating or otherwise protecting from the ambient environment metal surfaces of everyday objects such as pots and pans, kitchen utensils, washtubs, and bathroom fixtures. Enamelled steel has proved to be inexpensive, yet durable, rugged, reliable, and safe.

These properties are also desirable for electronic applications. This fact was recognized in the 1960's when the first attempts to fabricate electronic-grade enamelled-steel substrates were made jointly by GE and Ferro Companies. Those attempts were only partially successful, but interest in the idea has persisted.[1–15] The main attraction of the technology is the ability to use these substrates in two different ways, as a replacement for a printed circuit board or as a substrate for thick films (or a combination of the two).

Because of their obvious advantages, many different companies and researchers have toyed with enamelled boards during the last dozen years. The technology was not, however, widely accepted in the industry because the available porcelain-enamel materials had serious deficiencies for electronic use.

At RCA Laboratories, we started in 1976 to investigate various metal-core substrates including porcelain-coated-steel substrates (PCSS), for possible use in television sets and other products. Very soon it was realized that the concept of PCSS's offers some basic performance

advantages and is potentially extremely cost-effective. However, the materials and processes available at the time were not capable of meeting RCA product requirements. The idea thus either had to be abandoned or the technology had to be extended and developed, including some technical breakthroughs.

The latter course was followed. A research team was assembled, consisting mainly of the authors of the papers in the present issue of *RCA Review*. A number of technical breakthroughs resulted from this effort, mainly in the areas of novel porcelain and thick-film materials. During the period 1978–1980, the team developed a complete, self-consistent porcelain-enamel technology[16–19] that is vastly superior to anything previously available.

In 1980 a decision was made at RCA to license this technology to outside companies in order to disseminate the use of this promising new approach as widely as possible within the industry. In this introduction, I will first briefly describe the concept of the porcelain coated steel board and the reasons for choosing it, then the shortcomings of commercially available materials, and last the RCA-developed system that overcomes these shortcomings. The ten papers in this issue of RCA Review describe in some detail the various aspects of the system.

1. Advantages of Porcelain-Coated-Steel Boards

Fig. 1 illustrates schematically the basic structure of the porcelain-

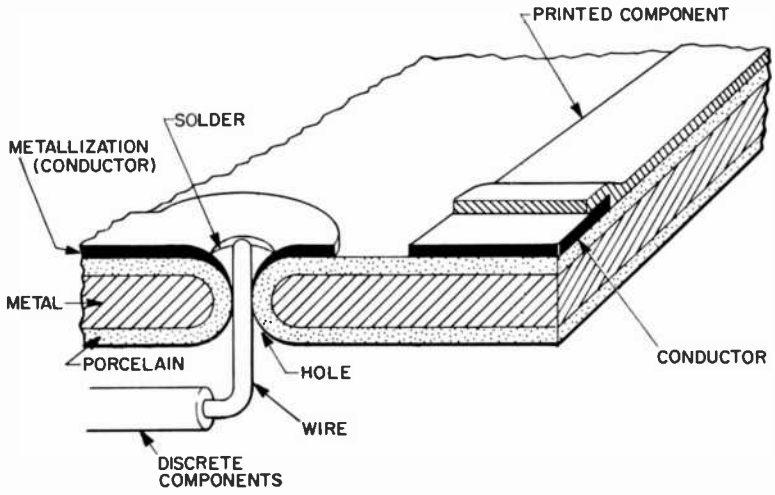

Fig. 1—Schematic representation of porcelain-coated-steel board.

coated-steel board. One starts with a metal core, which usually is a sheet of enamelling-grade (low-carbon) steel. This metal is pre-punched, at which time all of the necessary holes and other apertures are formed. Any sharp edges and burrs on the holes, which are to be electrically insulated, have to be rounded off at this time to prevent the possibility of electrical shorts. The surface of the metal is then cleaned and prepared for enamelling. Last, porcelain powder is applied to the surface, usually using electrophoretic deposition techniques, and fired on. If done correctly, the process produces an impervious, tough, electrically insulating porcelain coating that adheres tightly to the steel core. The board is then ready for circuit assembly.

Electrical circuits can be formed by screening-on and firing thick films, by inserting leaded discrete components and soldering them in place, by placing leadless-chip components and bonding them to the circuit, or by some combination of the above.

As was mentioned earlier, the porcelain-coated steel boards can be used either as regular printed circuit boards or as substrates for thick films. Thick films or hybrids have been used for decades in military, space, and medical applications. They are known for their high reliability, long life, and small size (micro-miniaturization). They are not widely used, however, in consumer applications, because of their relatively high cost when used on traditional ceramic substrates.

The enamelled board offers a very inexpensive substrate for thick- and thin-film components. Moreover, it is a substrate that is not limited in size to a few square inches, as are the alumina-ceramic substrates traditionally used for hybrid circuits. Therefore, the high-reliability thick-film technology, limited up till now to military and other expensive applications, becomes available to consumer-type, mass-market designers.

Cost-effectiveness is thus one of the chief attractions of the new technology. Per square-inch, the PCSS is comparable in cost to the epoxy-glass-laminate PC board, but the inherently small size of printed resistors leads to a substantial decrease in the board size. Compared to the alumina-ceramic substrate, the PCSS can, of course, be orders of magnitude less expensive. The cost-effectiveness are even further enhanced if base-metal ink systems (Cu conductors) can be used, rather than the traditional noble-metals (Au, Ag-Pd, Pt) used in the hybrid industry. Less expensive conductors and resistor inks are possible with the RCA developed porcelains, as will be discussed later.

Resistors typically account for 60% to 80% of electronic components in an electronic circuit. Thus, the use of printed resistors very substantially reduces the component count, as well as the number of solder joints and holes, with corresponding improvements in reliability. Other com-

ponents can also be printed: crossovers, some capacitors, by-passes, microwave components, strip-lines, even inductors and fuses. The metal-core board is fairly rigid and mechanically strong. Thus various frames, brackets, and other hardware can usually be eliminated when switching over to PCSS structures, with further substantial cost-reductions. The board is also a fairly good heat sink, allowing direct placement of power devices onto the board and eliminating costly heat-sink structures.

The metal core is electrically conductive; usually it is electrically grounded in a circuit. The presence of the ground plane can be a nuisance, because the parasitic capacitance has to be taken into account by the designer. It can also be an advantage, however, because it provides shielding, reduces crosstalk, and protects the IC's from static and other overloads. The ground-plane can be also used in microwave and other high-frequency applications. Lines-above-ground structures can be directly formed; the metal in such applications should be copper, or a copper-laminate, to reduce electric losses.

The porcelain structure is inherently durable, tough, resistant to chemicals, solvents, corrosive atmospheres, shock, vibration, extreme temperatures and other environments where no other technology would survive without special precautions. Automotive applications are especially attractive.

The weight of the metal board is higher than that of a standard PC board, but with the decrease in the board area and the elimination of resistors, heat-sinks, hardware, and other devices, the resultant system weight usually is decreased when a given system is converted from the traditional PC board to PCSS technology.

Reliability, as stated previously, can be expected to improve substantially. Safety is also improved, because the porcelain coated steel board is inherently nonflammable. It also provides the mechanical designer with a very flexible technology. The "board" need not be flat, but can be cylindrical or box-like in shape. The metal can simultaneously serve many purposes: beside holding the electrical circuit, it can serve as a mechanical structural member, a heat-dissipation structure, and even as the outer enclosure of the device. The enamel can be multi-colored and very ornamental.

Table 1 compares some widely-used electrical packaging technologies with the PCSS technology. The enamelled boards, by the way, are quite compatible with the leadless-chip devices. A very attractive combination might be enamelled boards, with printed resistors and conductors, multilayer dielectrics, chip capacitors, and IC's on leadless chip-carriers.

Table 1—Comparison of Various Technologies

	Discrete Leaded Components	Leadless/Chip Components on Phenolic Boards	Conventional Hybrids on Ceramic Substrates	Thick Films on Porcelain Substrates	Printed Epoxy Resistors on Phenolic Boards
Production costs	Medium	At present, higher than leaded	Very high	Low	Comparable to discrete resistors
Manufacturing steps	Manual or automatic insertion (discrete)	Automatic placing and adhesion with epoxy (discrete)	Silk-screening (batch)	Silk-screening (batch)	Silk-screening (limited to low-power resistors) (batch)
Reliability	Good	Good	Very high	Very high	Low
Stability	Good	Good	Very good	Very good	Poor (unless special precautions are taken)
Flammability and safety	Some problems	Some problems	Non-flammable	Non-flammable	Some problems
Board sizes available	Full chassis or larger	Full chassis or larger	Limited to ~4″ × 4″	Full chassis or larger	Full chassis or larger
Capital investment required	Low to medium	High	High	High	Medium

2. Limitations of Commercially Available Materials

With all the advantages listed above, why has the PCSS technology had only limited application? The answer lies with the rather severe materials limitations of the available porcelains. The main shortcomings of these materials are:

(1) *The presence of sodium and/or potassium.* These elements are usually added in quantities of up to 10% to match the expansion coefficient of the enamel to that of steel. As mobile ions, however, these elements lead to eventual crazing of enamel (under voltage/temperature cycling), decrease the bulk resistivity of the porcelain at elevated temperatures, and can contaminate semiconductors and resistors.

(2) *"Brown plague".* This is a phenomenon, possibly connected with the presence of Na and K, where thick-film conductors on an enamel surface turn brown and become unsolderable if in contact with or close to the steel substrate.

(3) *Presence of voids, bubbles and other imperfections.* The most difficult to control are hydrogen bubbles caused by outgassing of the steel during the porcelain cool-down period, i.e., while the porcelain is viscous. The voids lead to electrical breakdowns and to low yields and limit the usefulness of the enamel to <1000 V.

(4) *The rather low refire capability of the conventional porcelains—600° to 650°C.* Porcelains capable of higher refire temperatures are difficult to achieve, because the *initial firing temperature* is limited to 900° or 1000°C by the steel core. Most thick films available on the market require much higher refire temperatures: 850°–1000°C. Specifically, there exist today no Cu-compatible resistors for the lower temperatures. Thus one is forced into a noble-metal system and most of the cost-advantages are lost.

(5) *Energy and environmental constraints.* Typical "wet" metal preparation methods have problems with sludge-disposal, while the typical aqueous electrophoresis is energy inefficient.

(6) *Flatness problems* with the conventional enamelled boards, particularly a meniscus around a hole, makes screen-printing and lazer-trimming difficult.

(7) *Poor hole coverage.*

(8) *Expense in tooling.* This is particularly true for the required punching and coining dies. For a typical PC board with hundreds of holes, the dies are so expensive that they can be made cost-effective only for runs of ~300,000, or more.

3. RCA Developed System

Realizing the above difficulties, the RCA Laboratories decided to develop new materials that would be free of such limitations. From the very beginning of the program, it was decided that:

(1) An entirely new approach was necessary, not just an improvement in existing technology.
(2) A *total system* had to be developed. Beside the enamel and its deposition techniques, it was also necessary to develop a complete, compatible family of thick-film inks, various processing steps, interconnect devices, design rules, etc.

The objectives of the program that have been achieved are listed in Table 2. The key breakthrough was an entirely novel porcelain material[20-21] that is fired at ~850°C, at which temperature it devitrifies, forming a tough glass-ceramic enamel, which can then withstand multiple refirings at 900°–1000°C. Because of the way the enamel is formed, the incidence of voids is decreased by orders of magnitude. Sodium and potassium have been entirely eliminated and so, therefore, has the "brown plague." Thickness can be controlled and meniscus has been eliminated.

This new porcelain is described in the article "High-Temperature Porcelain-Enamel PC Boards," by K. Hang and J. Andrus; the properties of the porcelain are described in the articles, "Electrical Properties of RCA Porcelain-Enamelled PC Boards" by B. J. Thaler, et al, and "Mechanical Properties of RCA Porcelain-Enamelled PC Boards," by J. H. McCusker et al.

Table 2—Materials and Technology Developed for New Porcelain-Enamelled-Steel Boards

1. Novel and superior type of porcelain composition.
2. New completely automatic method of electrophoretic porcelain deposition (process understanding and process controls evolved).
3. Automatic method of firing porcelain.
4. An environmentally compatible metal-preparation technology developed for good porcelain–metal adhesion.
5. Method of rounding (coining) holes improved.
6. Method of coining holes for small lots developed and an inexpensive programmable machine designed.
7. Compatible thick-film base-metal ink system developed:
   —inexpensive copper conductors
   —compatible base-metal resistors
   —compatible cross-over dielectrics
8. Methods of making multilayer devices on porcelain invented.
9. Method of fabricating inductors on porcelain boards invented.
10. Various hardware designed (pins, connectors, and wire-wraps; chassis structures; methods of mounting parts).
11. Technology for fabricating various electronic circuits and devices up to ~50 MHz.
12. Methods of wire-bonding, laser trimming, and wave- and reflow-soldering adapted to these materials.

The metal preparation steps were also improved; an alternate "dry" method was proposed to eliminate environmental problems. An entirely automated deposition method was developed. The method is non-aqueous, low-energy consuming, yet safe. It is expected that very good thickness and property control will be possible in production. The firing step was also optimized, to minimize the incidence of voids [see "Electrophoretic Deposition of Coatings from Isopropenol/Glass Slurries," by A. Sussman and T. Ward]. The coining process was improved,[22] resulting in coining tools that are tolerant to wear and thickness variations. A single-hole piercing/coining machine was developed to allow economic production of short runs (<100,000 units) and prototyping. The manufacturing processes used in porcelain board fabrication are described in "Manufacturing steps in Production of Porcelain-Enamel PC Boards," by L. S. Onyshkevych et al.

A base-metal thick-film ink system was developed[23–25] that consists of Cu conductors and compatible, novel resistors, as well as a multilayer crossover dielectric and overglare. The inks, fired at 900°C in nitrogen, form a self-consistent ink system for our enamel. A series of noble-metal inks (Au, Ag, Pt, etc. conductors with Ru-based resistors) was also adapted to the substrate. [See the articles "Optimization of RCA Porcelain Composition for Compatibility with Thick Films," and "Characterization of RCA Thick-Film Compositions on RCA Porcelain Coated Steel Substrates," by A. N. Prabhu, et al.]

Various processing steps were adapted to our substrate, including wave-soldering, laser-trimming, wire-bonding, automatic insertion, and others. [See the article "Fabrication of Large Area Thick-Film Hybrid Circuits Using RCA Porcelain Coated Steel Substrates," by A. Prabhu, et al.] Connectors, potentiometers, switches, inductors and other structures were invented. Calculations, using computer modeling and finite element analysis, were performed on thermal flow within the boards and on stress distributions in them [see "Finite-Element Analysis of Stresses and Thermal Flow in Porcelain-Enamel PC Boards," by J. McCusker].

Finally, using the new technology, a number of actual working circuits were designed, constructed and successfully tested in real applications, ranging from TV sets to control circuits (see Figs. 2–5). The experience gained in this work allowed us to establish the feasibility of the concept and to develop practical design rules for the electrical and mechanical engineers. [See "The Design of Electronic Circuits on Porcelain-Enamelled PC Boards and Hybrids," by D. P. Dorsey, et al]. The circuits built and tested on enamelled-steel boards ranged from dc to 50 Mhz and included high-voltage and high-power devices. Manufacturability and cost studies were also performed.

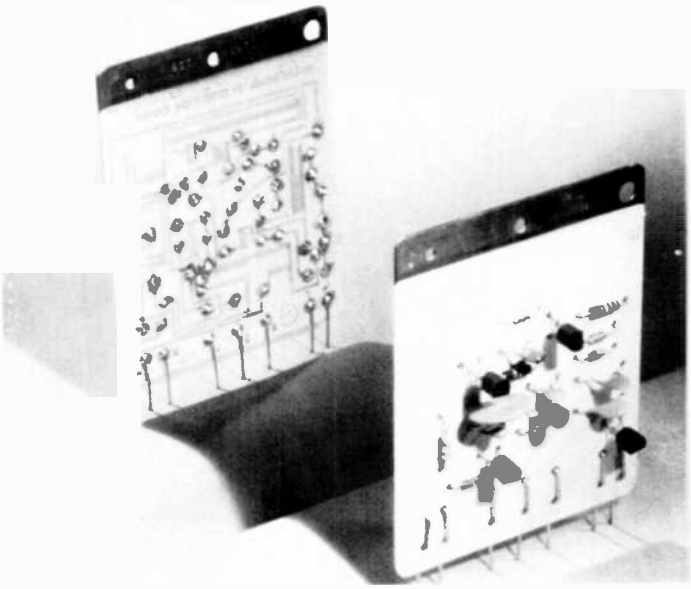

Fig. 2—Television circuit on enamelled-steel board.

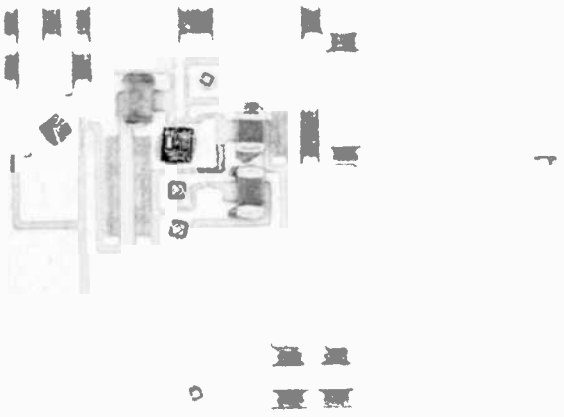

Fig. 3—Hybrid circuit on enamelled-steel board.

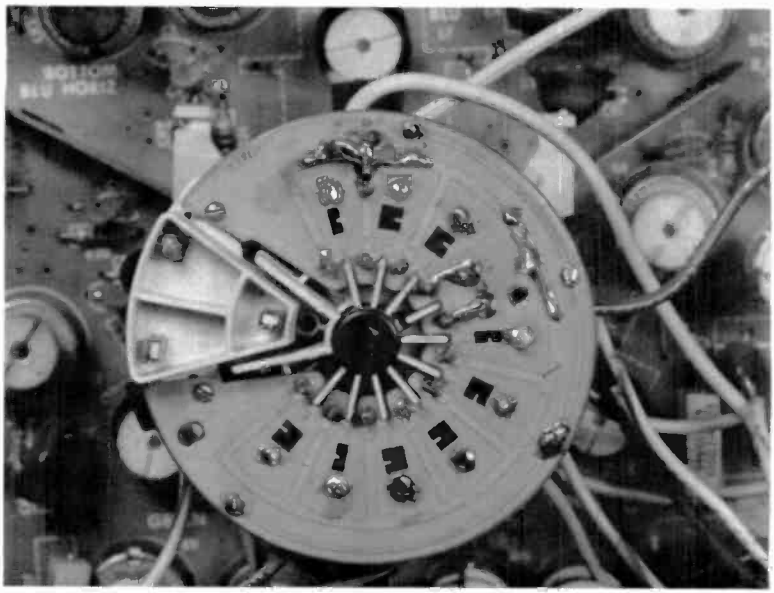

Fig. 4—TV kinescope-socket board using porcelain-coated steel.

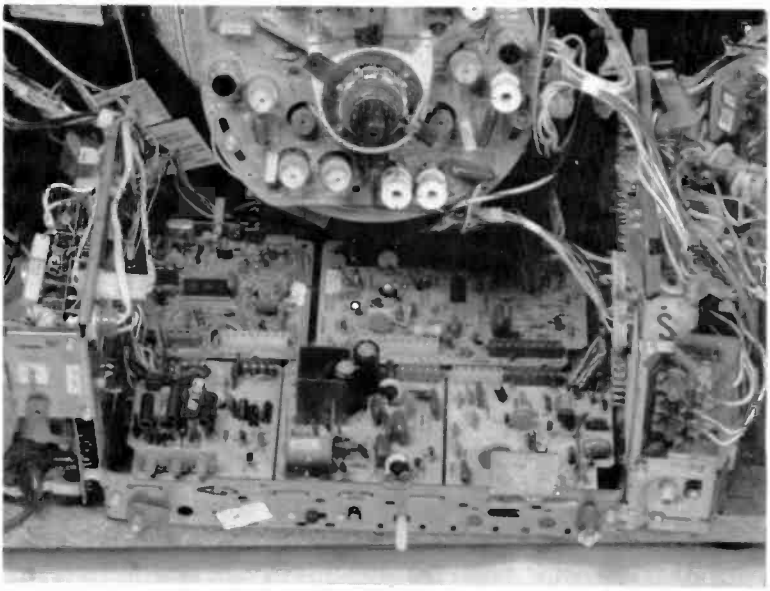

Fig. 5—Circuits in a TV set, with many of the modules built on porcelain-coated-steel boards.

4. Conclusions

A complete, self-consistent system has been developed by considering all aspects of the new technology and finding workable answers for all the problems studied. Specifically, all of the limitations of the previously available porcelain technology have been successfully overcome.

The work done in this system up till now (Summer 1981) has been done in the laboratory and was of a research type. No production pilot lines were set up to establish yields, true cost-effectiveness, and reliability in the field for the proposed technology. The technology is presently being transferred to licensees, who, hopefully, will put it into production to fully establish the feasibility of this promising new development.

Presently, porcelain-coated-steel boards are used only in a few applications in consumer electronics: flash-bars for cameras (where they provide a very cheap throw-away item), telephones[15] (touch-tone dials, where they eliminate the need for a backing-plate), and music synthesizers. We predict that the availability of the newly developed materials and techniques described in this issue of RCA Review will allow the use of the technology in the following areas:

- Consumer products such as games, toys, appliance controllers, TV and other entertainment products, regulators, etc. There the PCS boards will be used mostly as replacements for PC boards with hybrid performance advantages and cost-effectiveness.
- Automotive electronics, where the main advantages will be ruggedness and ability to withstand hostile environment.
- Computers, especially mini- and micro-systems, where a multilayer, possibly strip-line structure, will be employed to interconnect IC packages.
- Military and Space electronics, where traditional high reliability can be achieved at a lower cost. The ability to withstand hostile environments should be also very attractive.
- Solar panels, where they will provide reliability, ruggedness, and low cost.

Acknowledgments

The program described in this article was performed in the Electronic Packaging Research Group, TV Systems Laboratory (D.D. Holmes, Director) at the David Sarnoff Research Center, in Princeton, New Jersey. All of the authors of the PCSS-related articles in this issue of the RCA Review contributed to this effort, as did many others, among them K. Bube, W. Anderson, G. Whittley, B. Greenstein, G. Lord, and numerous others.

References:

[1] D. Hilson and G. Johnson, "New Materials for Low Cost Thick Film Circuits," *Sol. St. Tech.*, p. 49, Oct. 1977.

[2] W. Hatfield and D. Wicher, "A Microelectronic Packaging Technology for Consumer Product Applications," *Proc. 1978 ECC*, p. 271.

[3] D. Wicher and W. Hatfield, "Porcelain Steel Technology: A Bonafide Alternative," *Proc. 1978 Int. Microel. Symposium*, p. 176.

[4] T. Allington and R. Coté, "Characterization of Thick Film Compositions on Porcelainised Steel Substrates," *Proc. 1978 Int. Microel. Symposium*, p. 188.

[5] M. Spector, "A New Metal Core Hybrid Substrate," *Proc. 1978 Int. Microel. Symposium*, p. 193.

[6] W. Hatfield and D. Wicher, "Metal Board Technologies-Substrates for Alumina or PCB's," *Circuits Manufacturing*, p. 7, July 1978.

[7] R. Schabacker, "Porcelain Enamelled Steel as a Substrate for Circuit Boards," *Proc. Nepcon West*, 1978.

[8] M. Spector, "New Metal Core Boards in High Density Applications," *Proc. IPC*, 1978.

[9] S. Stein, C. Huang, and A. Gelb, "Thick Film Materials on Porcelain Enamelled Steel Substrates," *Proc. 1979 ECC*, p. 121.

[10] A. Schwarzmann, "Performance of the Porcelain-Metal Substrate at Microwaves," *Proc. 1979 ECC*, p. 132.

[11] M. Spector, "Characteristics of Porcelain Coated Steel Substrates," *Proc. 1979 ECC*, p. 141.

[12] M. Spector, "Porcelain Coated Steel Substrates for High Density Component Inter-connection," *Insulation/Circuits*, p. 15, Jan. 1979.

[13] S. Stein, C. Huang, and A. Gelb, "Comparison of Enamelled Steel Substrate Properties for Thick Film Use," *Europ. Hybrid Microelectr. Conf.*, 1979.

[14] R. Perks, "Porcelain on Steel Applications in the Telecommunications Industry," *IPC-TP-326*, April 1980.

[15] P. Dudley and G. Lenaerts, "Evolution of a Circuit Design on Porcelainized Steel," ECC 1981.

[16] L. Onyshkevych, "Porcelain-Enamelled Steel Substrates for Electronic Applications," *Appliance*, p. 46, Apr. 1981.

[17] L. Onyshkevych, "Porcelain-Enamelled Steel Substrates for Electronic Applications," *Proc. of 1980 PEI Forum.*

[18] L. Onyshkevych, "Overcoming Problems with Porcelainized Steel Substrates," submitted to *Insulation/Circuits*, 1981.

[19] L. Onyshkevych, "Electronic Applications of Porcelain-Metal Boards," submitted to *Ceramic Industry*, 1981.

[20] K. Hang, "High Temperature Porcelain Coated Steel Substrates for Electronic Applications," presented at the 1981 Annual Meeting of the Am. Ceramic Soc.

[21] K. Hang and W. Anderson, "Partially Devitrified Porcelain Composition and Articles Prepared with Same," U.S. Patent #4,256,796.

[22] G. Whittley, "Method fo Forming Aperture with Rounded Edges in Sheet Metal," U.S. Patent #4,248,075.

[23] A Prabhu, K. Hang, E. Conlon, and T. Hitch, "Properties of Base Metal Thick Film Materials on High Temperature Procelain Coated Steel Substrates," *Proc. of 1981 ECC*, p. 36.

[24] A. Prabhu, K. Hang, and E. Conlon, "Interaction between Base Metal Thick Film Inks and High Temperature Porcelain Coated Steel Substrates," Submitted to the 1981 ISHM Symposium.

[25] A. Prabhu, K. Hang, E. Conlon, "Characterization of Precious Metal and Base Metal Thick Films on High Temperature Porcelain Coated Steel Substrates," submitted to the 1981 Meeting of the Electronics Division of the Am. Cer. Soc.

Manufacturing Steps in the Production of Porcelain-Enamel PC Boards

L. S. Onyshkevych, W. H. Tsien, T. T. Hitch and P. R. Smith

RCA Laboratories, Princeton, NJ 08540

Abstract—The various manufacturing steps used in production of the RCA developed porcelain-enamelled PC Boards are described, including the necessary equipment, automation possibilities, material requirements, labor content, and anticipated problem areas. The technology is new, but most of the processing steps and equipment are fairly standard. Particular emphasis is placed on the hole-preparation step, which is of critical importance.

Introduction

This paper describes the manufacturing steps to be used in production of the RCA porcelain-enamel PC boards.[1] The proposed technology is new but much thought was given during its development to potential manufacturing problems. The operations involved in the manufacture of porcelain-enamelled boards (PEB's) with printed thick-film components can be divided into three basic groups:

(1) making the porcelainized-steel substrates;
(2) printing thick-film components on the substrate;
(3) assembling discrete components onto the board.

Only the first group of operations contains novel processes that had to be developed in the laboratory. The second group comprises standard techniques used in hybrid microelectronics, and the last group consists of standard PC board assembly steps.

In this paper, we describe each step in more or less detail, depending

upon its novelty. Where appropriate, we also describe alternative techniques. For each step, we describe the task to be accomplished, equipment required (including costs and facilities), automation possibilities and labor content, and special problem areas. We also briefly discuss materials specifications and quality control requirements and give suggestions for testing operations. Many of the manufacturing steps described in this paper are treated more fully in the other papers in this issue of *RCA Review*.

Overview

Fig. 1 shows an idealized flow-chart for fabrication of an electronic instrument based on a porcelain-board chassis. It is assumed that the instrument contains both printed thick-films and leaded discrete components that require insulated holes. The flow chart might look somewhat different if leadless chip components were placed on the board and connected using reflow soldering and wire-bonding. Both these possibilities are treated in this paper.

The assembly line can be made more or less automated, depending upon the particular application, but, in general, the technology lends itself to almost total automation. For small production runs, a semi-manual, labor-intensive production line is also possible.

The research program resulted, in addition to new materials (e.g.,

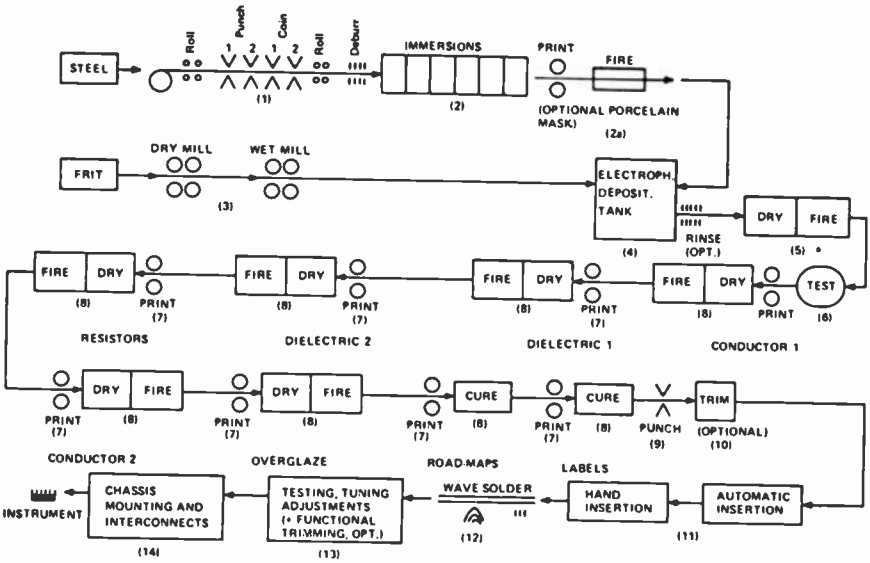

Fig. 1—Flow chart of porcelain-enamelled board manufacture.

porcelain-frit, and compatible inks), in some novel manufacturing processes. We also adapted standard processes (e.g., wire-bonding, laser-trimming, wave-soldering) to the porcelain substrate technology. Indeed, some work was performed on practically every step shown in Fig. 1. What follows is a step-by-step description of the various processes and our contributions to each manufacturing step.

Core Metal and Metal Handling

Enamelling-grade ultra-low-carbon ($\leq 0.01\%$) steel (e.g., Inland Steel INamel, Armco Steel Univit, or U.S. Steel Vitrenamel Type I) is usually the core metal for the PEB's. This material is fairly standard and inexpensive and is used widely in the appliance industry. Low-carbon steel is used for the commercially available enamels to minimize the carbon reaction, which forms carbon dioxide bubbles and results in "boiling" and "reboiling" bubbles in porcelain. The RCA porcelain is much less prone to "boiling"[2] and thus it is not absolutely necessary to limit the choice of metal to the ultra low-carbon steels. Other high-temperature and mechanically stronger steels are probably usable with these porcelains for many applications. Other possible core metals include copper, copper-clad steel, and copper-clad Invar. Such metals have some significant advantages over steel, e.g., better electrical and thermal conductivity, but the porcelains developed so far at the RCA Laboratories will not work well with copper without significant modifications.

The enamelling can work with steel of almost any shape and size. Typically, flat sheet steel in sizes from #20 (nominal thickness 0.036 inch) to #24 (nominal thickness 0.024 inch) is used. Since the steel usually comes in rolls of 2 to 10 tons each, the first step in the production flow is to unroll and flatten the sheet-metal. Next, panels, which may contain one board or a multiplicity of boards, are stamped out of the sheet metal. It is cost effective to work with panels that are as large as can be handled by the furnaces, screen-printers, etc. Typically, for large through-put production lines, the panels could be 2×3 feet or even larger.

If multiple-board panels are used, the individual boards should be separated from each other at this time by punching narrow slots around each board, leaving just narrow bridges to hold the board to the panel.[3] Typically, the slots are $\frac{1}{8}$ inch wide and the bridges are $\frac{1}{4}$ inch wide. The bridges will be cut through later to separate the boards from the panel.

It is important to provide for tabs and holes to facilitate parts handling during processing steps, particularly, during porcelainization. Typically an unporcelainized strip located along the top edge of the panel contains

holding and registration holes. In general, if any holes in the board are to be used for registration (e.g. during screen-printing), they should also be left bare of porcelain. Next, the holes that are to be electrically insulated are punched and rounded—usually by coining methods, as described in the next section. A de-burring operation can be used, in addition to coining, to round off edges of slots. Use of a second flattening step (rollers) may be desirable after punching.

It is possible to fabricate enamelled boards in other than flat configurations. Cylindrical geometries, boxes, and other shapes might be used for special applications. In this case, metal-forming steps would be necessary at this point in the production line.

All the equipment needed for the above operations (with the possible exception of coining) is fairly standard. The cost of the presses is relatively high and, if they are purchased new, may constitute from $\frac{1}{4}$ to $\frac{1}{2}$ the total cost of the equipment needed to set up the production line. The labor requirements for these operations depends upon the degree of automation used. The equipment will require a fair amount of floor space and power. Quality control on the incoming metal is advisable.

Punching and Coining

The holes and other apertures in the enamelled board that are to be electrically insulated have to be punched, deburred, and their edges must be radiused. In prototype samples, holes can be drilled and countersunk or filed by hand, but this method is obviously too slow, poorly reproducible, and expensive for mass production. Punching and coining is the preferred method for manufacturing.

Coining is done by specially designed forming dies; it must be done from *both* sides of the board simultaneously. The profile of the die is very important to accommodate variations in metal thickness and tool wear. RCA has developed a coining-die profile to achieve optimum results.[4] Fig. 2 shows a typical cross-section of the edge of a hole before and after coining.

In low-voltage applications, it may be sufficient to round off the hole edges by 50–75%. This is enough to reduce any nonuniformity in porcelain thickness, as well as to reduce stress concentrations in the porcelain at the hole.

For large-lot production ($\geq$250,000 boards), it is most economical to use the RCA-developed multiple coining die sets with an automatic punch press. Hundreds of holes may be coined in a single stroke (for >200 small holes, a two-stroke punching and a two-stroke coining operation is recommended).

The multihole progressive coining dies are relatively very expensive,

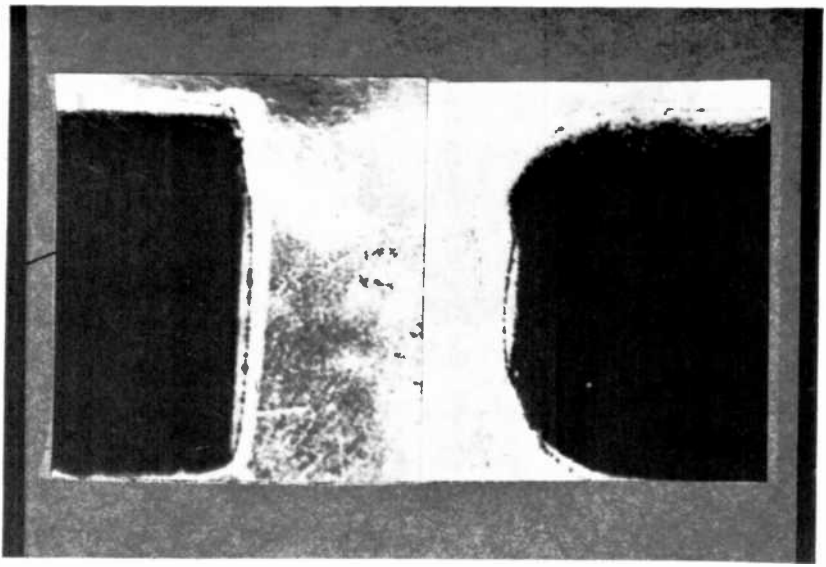

Fig. 2—Cross section of an edge of a hole: left shows hole as punched and right shows hole after coining.

and the precision required is on the order of 0.0005 inch. Therefore this method is not economical for small production quantities (100 to 250,000 boards).

For small runs, an automatic one-hole-at-a-time punch/coin machine might be the most economic tool. We have designed such an automatic, template-controlled, pneumatically activated device. It can be easily programmed by insertion of pins in templates to punch and then to coin the holes one at a time. The machine has multiple heads to permit more than one size or shape of holes to be done at any one run. The coining die is registered to within 0.0005 inch of the punch-die. The operation is fairly fast. Production quantities of up to 100,000 boards per year are possible with one such machine; the machine is relatively inexpensive, so parallel operation with multiple machines of this type would be cost-effective.

Other possible approaches to the small production quantity include:

(1) *Commercial numerically-controlled or template-controlled punch presses.* Most punch presses available presently can register only to a precision of ~0.005 inch which is not sufficient. However, some such machines can be modified to provide better precision.
(2) *Jet-etching.* Special apparatus for jet-etching exists and may be considered, provided the hole density is not too high and disposal of chemicals is not a problem.

(3) *Abrasive Brushing Machines.* These are very fast and inexpensive for removing burrs but are not able to radius the hole-edges sufficiently. They may be included in the production line to deburr straight edges.
(4) *Spindle Abrasive Finish System.* In this system, the work pieces are mounted on the end of a rotating spindle and lowered into an abrasive slurry inside a rotating tube. The combination of motions removes sharp edges very efficiently. The equipment is simple and relatively inexpensive, but the method works well only with small boards and slight coining. It is relatively labor-intensive.

In summary, then, we recommend hand coining or countersinking for prototypes (up to ~100 units), a single-hole-at-a-time automatic punch/coin machine for small production runs (100 to 250,000 units), and multiple-hole single or progressive die-sets for large runs (≥250,000 units).

Metal Surface Preparation

To assure porcelain-to-metal adhesion, the surface of the steel must be properly prepared. This preparation consists of removing any dirt, especially oil and grease, from the surface, roughening the surface to enable a mechanical bond, and treating the surface chemically to improve the chemical bond.

De-greasing has to be done by washing in water and detergents. The use of Petroleum-Free Lubricants during machining operations is very desirable to minimize the effort required in getting rid of the oils.

The surface preparation of cleaned metal to ensure good adhesion can be accomplished either by the "wet" method, used traditionally by the enamelling industry, or by a new "dry" method. The wet method consists of a series of immersion steps, which usually include a pickling operation and Ni-plating. This method works satisfactorily with RCA porcelains and produces PEB's with excellent porcelain adhesion. The method, however, has some environmental problems, mainly with sludge disposal. Therefore, a dry method is proposed that consists mainly of oxidation/reduction steps. This method also can produce excellent adhesion.

The equipment required for wet treatment consists mainly of a series of tanks, with some heaters and materials-handling equipment. The chemicals used are relatively inexpensive, as is the equipment. The processes are messy, however, and require ventilation, water, and sludge disposal. The dry method requires furnaces for the oxidation-reduction steps, more energy, and forming gas, or cracked ammonia, etc. (for reduction). The equipment and facilities are more expensive than those for the wet method, but government regulations may make the dry method more attractive. Both methods can be completely automated.

Enamel Masking

The metal surface can be coated with materials that will prevent porcelain particles from adhering to the surface during the enamelling (electrophoresis). It may be desirable to do this in selected areas on the board to allow for electrical connections to ground or to leave bare metal for subsequent weld attachment or machining (bending at seams, separation of boards from panel at bridges, cutting off of tabs, sheet-metal screws, etc.).

Masking can be done simply by taping or by screening on a special material. This material repels particles during electrophoresis and is then burned off during porcelain firing. The bare metal surface will be oxidized during the firing step. This oxide can be subsequently removed by a reducing-atmosphere firing step (which could be combined with one of the ink firings). Alternately, the masking compound can be formulated to leave a protective residue on the metal surface.

Frit and Slurry Preparation

The glass frit used in making the RCA porcelain[2,5] is produced by melting the raw materials in platinum crucibles, either continuously or in batches. The basic ingredients are fairly ordinary and inexpensive compounds; very high purities are not required. After melting, the glass is quenched on steel rollers. Quenching in water is to be avoided.

The frit can be stored in sacks or drums and transported. Before use, the frit is ball-milled, first dry and then in the non-aqueous fluid that will later be used in the electrophoretic deposition tank.

Quality control of both the incoming raw materials and of the frit is very important. This is a highly engineered glass and care must be taken in its preparation. The milling must also be controlled, since the particle-size distribution is important.

The equipment required includes platinum crucibles, quenching equipment, and ball-mills—all fairly standard equipment. Platinum crucibles are relatively expensive, but a continuous melter can produce large quantities of glass with a relatively small investment in platinum. The equipment requires relatively small floor space, but does require considerable power. It can be highly automated. The crucial parts of this operation are the quality control facilities.

Enamelling

The milled glass powder can be deposited onto the prepared metal surface in a number of different ways: wet spraying, dry electrostatic spraying, fluidized bed deposition, doctor-blading, and other methods.

Electrophoretic deposition[6,7] was found to be best. It is relatively easy to set up and to control thoroughly, it can cover insulated holes and other hard-to-reach places, it results in no material loss (as in spraying), and it can be completely automated.

Aqueous suspension electrophoresis is normally used for porcelain PC boards. Water, however, is not the optimum fluid for this purpose, because it results in large power losses and can produce voids in the porcelain. We therefore developed a nonaqueous technology that uses an organic fluid with a low volatility. The system reduces significantly the energy consumption, as well as the void count in the porcelain. The system is also safe (non-explosive and non-toxic). Loss of fluid through evaporation is minimal.

We have developed an automated electrophoretic deposition system, consisting of a deposition tank with a circulating slurry and control electronics. The thickness of the porcelain deposit can be controlled automatically. Various parameters are monitored during deposition; the readings are digitized and fed into a controlling minicomputer that can correct for small deviations or stop and sound an alarm if the process deviates from acceptable limits. Thus, deposition can be made almost completely automatic.

The cost of the equipment and processing is relatively very low, including energy consumption. The fluid can be reused again and again; evaporation is very low.

For very large throughput, an alternative deposition tank has been suggested: a long trough, with metal boards traveling along it while submerged in the slurry that is pumped in a flow pattern designed to assure uniform deposition.

Porcelain Drying and Firing

After electrophoretic deposition, the coated panel is dried and fired in air at 850–900°C,[6,7] The drying and firing furnaces can be combined into one. It is preferable to fire enamelled boards suspended vertically in a kiln-furnace rather than use of a belt furnace, because the enamel on the panel is at first fragile and then molten on both sides. Using fixtures to stand off the boards horizontally is not advisable, because at the firing temperature the metal might sag.

The firing profile has to be controlled, as discussed elsewhere in this issue.[6,7] The firing requires load/unload operations, which can be automated. The furnace required is standard and its cost medium. To conserve energy, the furnace should be well insulated. Power, cooling water, and modest ventilation are needed, as is a fair amount of floor space.

Testing of Porcelain

After firing it is advisable to test the porcelain insulation for defects, which can cause electrical shorts in operation. This will probably be necessary only during pilot production. It is our feeling that the void count in RCA porcelain will be found to be so low in actual production, that 100% testing for shorts will not be necessary.

There are many ways to perform this test. If porcelain is not masked off any portions of the board, the simplest test is an immersion in a conductive fluid. Otherwise, test with a sponge wetted in conductive fluid, tests with plasma, with fluorescent paints, and other methods have been successfully used in our porcelain development.

The cost of equipment, floorspace, and facilities for this operation will be relatively low, but the step may be relatively labor-intensive. Some automation is possible.

Thick-Film Ink Screening and Firing

The thick films (conductors, resistors, dielectrics) are usually screened onto the substrate, then dried and fired in belt-furnaces. All of these operations are standard, as are the screen-printers, belt-furnaces, and materials-handlers, which are routinely used in the hybrids industry. What is novel is the size of the boards. Whereas typical ceramic substrates are in the 1 to 20 square inch range, porcelain panels can be in the 1 to 10 square foot range. Equipment for such large-area panels is not readily available as yet, though there are no basic reasons why it could not be built. At the present time one can easily purchase 18 inch-belt furnaces and 3 × 3 foot screen-printers.

The tolerances obtainable in screen-printing depend upon the quality of equipment and the size of the board and can range from 0.002 to 0.025 inch. Printing of metallized holes (with conductor on the walls of the hole, or the so-called plated-through hole) can be done readily with vacuum suction of ink during the screening. Screen-printers are relatively inexpensive, do not require much floor-space or facilities, and can be automated.

Firng of noble-metal inks is done in air, but most base-metal inks have to be fired under a protective atmosphere.[8] Typical oxygen content in a modern nitrogen furnace is ~10 ppm, which is more than adequate for our inks. The belt-furnaces are relatively expensive and require energy, floor-space, and cooling water. Again, energy savings will result from furnace insulation.

The screening and firing of conductors, resistors and dielectrics can be all done on a single set of equipment in series—for small throughputs.

Alternately, for larger production runs, each thick-film layer can have a printer and furnace devoted to it. Various schemes for materials handling are possible. Fig. 3 illustrates one possible approach, where standardized print–dry–fire units are used. The panels are loaded in magazines, and the magazines are automatically loaded/unloaded at each unit. This approach can eliminate almost all of the labor from this part of production cycle.

Quality control of incoming thick-film inks is essential, but utilizes standard techniques. The fabrication of our base-metal inks is also standard. No exotic or ultrahigh-purity ingredients are used.

Overglazing and Overcoating

After the last ink is fired, the thick-film board should usually be protected, especially if base metals are used. Either the RCA-developed overglaze, or an organic overcoat can be used. The overglaze is printed and fired like other inks, but at a much lower temperature (500°C) to avoid disturbing the resistor values. Organic overcoats are usually also screen-printed and then either temperature or UV cured. Other organic thick films that might be used include solder-masks, roadmaps, circuit markings, etc. Most standard inks used for these purposes are compatible with our porcelain.

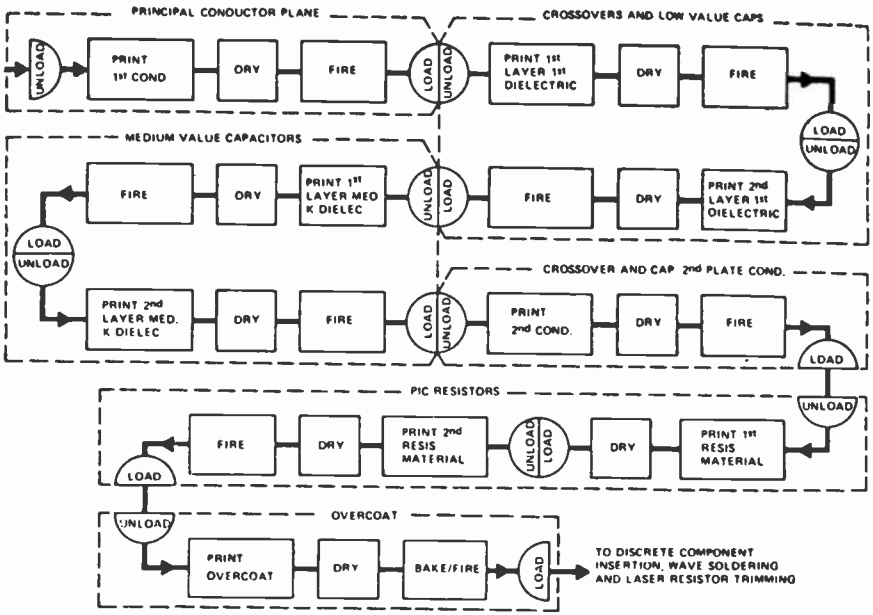

Fig. 3—Possible arrangement for automation of thick-film printing and firing steps.

Equipment used for these inks includes screen-printers and curing ovens or UV lights for curing. All of this equipment is standard and rather inexpensive. The steps can again be automated.

Resistor Trimming

Trimming of resistors can be performed either after firing, to bring them to value (trimming to within $\pm\frac{1}{2}\%$ is quite feasible), or after complete assembly (so-called functional trimming), to make the circuit perform. Both are possible with circuits on our porcelain boards. Trimming can be done either by abrasion (sand-blasting) or by laser; again, both types of trimming have been successfully adapted to the enamelled boards.[9]

Abrasive trimming requires rather simple and inexpensive equipment and can be either manual or semiautomatic. It is ideally suited to small production runs or prototyping. Laser-trimming is much more sophisticated, requires relatively very expensive equipment, but can be totally automated and is best used for large production runs. Laser trimmers are very fast.

Many laser trimmers are at present limited in the board-size available to beam deflection to $\sim 4 \times 4$ inches. Other trimmers employ a mechanically movable $X-Y$ table. Large-area trimmers are being developed and will probably become available when there is a need for them. However, the large-area laser-trimmer will probably be the single most expensive item on the porcelain-enamelled board production line.

The trimmer does not require large floor area, or special facilities. The abrasive trimmer, however, should be placed in a separate enclosure, otherwise, the sand can cause problems with other equipment.

Assembly of Discrete Components

Discrete components come in many sizes and shapes, leaded and unleaded, radial, linear, chip-form, etc. They comprise capacitors, coils, transformers, electrolytics, IC's, transistors, diodes, and many other devices. In addition, pins and various other connectors have to be assembled onto the board. Some of these devices had to be especially developed for the enamelled boards—pins, end-connectors, and stakes, as well as half-printed half-discrete potentiometers, switches, and inductors.

The discrete components can be assembled either manually or automatically. Most of the usual assembly machines can be used with the PEB's: automatic inserters of leaded components, chip-placement machines, and pin-inserters. Only machines that physically break the board,

such as the pin-staking machine, can not be used with PEB's; that is why special pins had to be developed. A whole family of assembly machines will probably be developed specially for the PEB's to make their asembly easier.

Because of the great variety of discrete components and assembly machines, not much more can be said here about this aspect of PEB manufacturing. The exact processing steps and equipment selected will depend upon the application, throughput, and degree of automation desired.

One type of discrete component should be mentioned—the unpackaged silicon chip (IC, transistor, diode). Such chips can be mounted directly onto the porcelain using conductive epoxy, solder, or eutectic bonding (on gold conductor).[9] The expansion coefficients of steel and silicon are not matched, however, and chips larger than $\sim 1/4 \times 1/4$ inch should be mounted with care.

Wire Bonding

IC chips and other semiconductor components are usually electrically connected to the circuit by ultrasonically or thermocompressively attached wires. We have found it readily possible to use ultrasonic bonding of aluminum wire with Cu conductors.[10] Thermocompression bonding of gold wire can be used with many of the precious-metal conductors. Equipment used for these operations is conventional.

Soldering

Most of the discrete components will be electrically connected to the board metallization by some soldering process—simple hand soldering, wave or dip-soldering, or a solder reflow technique. All of these are usable with PEB's. In particular, wave soldering was studied by us and found to be compatible with the metal-core board.[9] Conventional soldering equipment can be used.

Board Separation and Final Forming Operations

It is advantageous to work with unseparated panels during most of the fabrication steps. At some point in the assembly, however, the boards must be separated out of the multiple-board panels and excess selvage, tabs, and other waste cut off. This will probably have to be done before the resistor trimming operation because of the current limitations on maximum-size trimming field of the laser trimmers. Whether discrete component assembly, soldering, and wire-bonding take place before or

after separation will depend upon the particular application. The separation can be done in a conventional press, as in the original punching operation, with similar tooling costs and labor content.

It is also possible to form the PEB at this point into non-planar shapes if appropriate unporcelainized seams have been provided.

Final Assembly

The final mechanical and electrical assembly of the PEB into an instrument, as well as alignment, testing, etc., are conventional in nature. The exact process steps and equipment requirements depend upon the application.

Materials Handling

As stated previously, manual, semiautomatic, and fully automatic materials handling systems are possible, the exact type of system depending upon the application, size, and shape of the panel, throughput, and other factors. The following generalized observations can be made:

(1) The steel in the PEB's is magnetic, thus the board can be picked up and carried by electromagnets. In particular, in screen-printing and laser-trimming, where flatness is imperative, the board can be held down and even *flattened* during the operation by magnetic chucks.
(2) The PEB's are fairly rugged and do not have to be handled particularly gently. Even when dropped on the floor they usually sustain no damage. Selvage around a panel (to be separated and discarded later) will further protect the boards.
(3) Magazines that stack boards with space between them will be very convenient for automatic machinery, especially during the hybrid-circuit processing. Carousels of these magazines can improve the automation.
(4) Unprocelainized carrying tabs or selvage must be provided, with unporcelainized location holes for printing, laser trimming, etc.

Conclusions

As can be seen from the discussion in this paper, the exact form of the PEB manufacturing assembly line will depend upon the particular circumstances. Nevertheless, our work has investigated most of the assembly steps to adapt them to the peculiarities of this technology. Enough information has been gathered about these operations to allow the design of pilot lines. This information, only outlined in this paper, is being made available to licensees.

Acknowledgments

The authors wish to acknowledge the contributions of all the members of the Porcelain Board Project, which formed the basis upon which the information contained in this artible is built. In particular, we wish to acknowledge K. Hang, A. Prabhu, J. McCusker, B. Thaler, D. Dorsey, E. Conlon, A. Miller, S. Boardman, T. Ward, R. Filson, and A. Kusenko. Others who contributed include G. Whitley, R. Demers, and L. Potter. The work was performed mainly in the TV System Research Laboratory, D. D. Holmes, Director.

References:

[1] L. S. Onyshkevych, "Porcelain-Enamelled Steel Substrates for Electronic Applications," *Appliance*, Apr. 1981, p. 46.

[2] R. W. Hang, "High Temperature Porcelain Coated Steel Substrates for Electronic Applications," paper presented at the 1981 Annual Meeting of the American Ceramic Society.

[3] J. R. Harford, "Modular Printed Circuit Board," US Patent #4,216,523.

[4] G. J. Whitley, "Method of Forming Aperture With Rounded Edges in Sheet Material," US Patent #4,248,075.

[5] K. W. Hang and W. M. Anderson, "Partially Devitrified Porcelain Composition and Articles Prepared With Same," US Patent #4,256,796.

[6] A. Sussman and T. Ward, "Electrophoretic Deposition of Coatings from Isopropanol/Glass Slurries," *RCA Review*, **42**, p. 000, June 1981 (this issue).

[7] K. W. Hang and J. Andrus, "High-Temperature Porcelain-Enamel Substrates—Compositions and Interface Studies," *RCA Review*, **42**, p. 159, June 1981 (this issue).

[8] A. N. Prabhu, K. W. Hang, E. J. Conlon, T. T. Hitch, and A. Kusenko, "Characterization of Thick Film Compositions on RCA Porcelain-Coated Steel Substrates," *RCA Review*, **42**, p. 239, June 1981 (this issue).

[9] A. N. Prabhu, E. J. Conlon, A. Z. Miller, J. H. McCusker, and T. T. Hitch, "Fabrication of Large-Area Thick-Film Hybrid Circuits on RCA Porcelain-Coated Steel Substrates," *RCA Review*, **42**, p. 259, June 1981 (this issue).

High-Temperature Porcelain-Coated-Steel Electronic Substrates—Composition and Properties

K. W. Hang, J. Andrus, and W. M. Anderson

RCA Laboratories, Princeton, NJ 08540

Abstract—An alkali-free devitrifiable glass coating on steel suitable for use as a hybrid thick-film substrate or printed circuit board is described. The coating, applied by electrophoresis, is fused at 800–900°C until the coating crystallizes to a high volume fraction of crystal phase in a glass matrix. The resulting "ceramic on steel" coating has reheat capability of in excess of 900°C without change in the ceramic layer. Physical, thermal, and electrical properties of the board are reported. The RCA porcelain is a high quality substrate for thick- and thin-film circuits.

1. Introduction

Porcelain coated steel has attracted attention since the 1960's as a substrate material for electronic applications because of its ruggedness, ease of manufacture in special shapes, and low cost compared to ceramic substrates. So far the porcelain-board technology has not been broadly accepted in the electronic industry due to material limitations in the available porcelain materials. These materials have relatively low dielectric breakdown strengths and low refire temperatures (650°C). The thick-film materials available for use on commercial porcelain boards are, therefore, limited to less demanding electronic applications.

This paper discusses the composition and properties of a new porcelain material developed at RCA Laboratories. The porcelain is an alkali-free glass that is applied as a powder to the surface of a prepared low-carbon-steel substrate by electrophoresis then fused at 800–900°C. During the fusion of the glass, a high volume fraction of crystal phase is formed

in the glass layer. This composite glass and crystal dielectric layer is perhaps better described as a ceramic-dielectric-on-steel board. The RCA porcelain board has a smooth dielectric surface (4–15 micro-inch), >4000 volt breakdown strength, is refirable at high temperature (900°C) with structural stability for thick-film applications, and is stable in environmental exposures. The board is mechanically strong and has excellent bond strength between the porcelain and low-carbon-steel core. It can be manufactured economically in large, small, or irregular shapes with or without porcelain coated holes through the board. The RCA board makes possible the application of high reliability thick- and thin-film electronic circuits to a strong relatively inexpensive substrate. The board is also compatible with traditional printed-circuit components.

For porcelain steel technology to achieve wide application to high volume electronics, however, mutual compatibility between porcelain, conductor, resistor, and dielectric interfaces must also be achieved. The development of a high-refire-temperature porcelain is only the first step in the process. The chemical inertness of the porcelain surface is of primary importance, because the potential for compatible thick-film inks is otherwise severely limited. Thick-film materials that are compatible with the new porcelain were developed at RCA Laboratories under a concurrent program and are described in other papers in this issue of *RCA Review*.[10-12]

2. Material and Fabrication Processes

2.1 Metal Preparation

Inland steel and Armco steel in low-carbon (<0.01% C) grades (0.030–0.035 inch thick) have been used primarily in this study. The metal as received requires a surface cleaning and preparation to assure good bond adhesion between the porcelain and steel. Considerable literature exists on the glass-metal interface.[2-9] Metal preparation is conventionally done by wet chemical processing of the metal parts through several stages. The important generic steps are the cleaning of grease, oil, and soap films from the metal surface, an expansion of the metal surface area, usually done by grain boundary etching, and the deposition of an adherence-promoting metal such as nickel or cobalt on the surface of etched steel. The amount of metal deposited is normally in the range of 0.7–1.2 grams/square foot. The surface reaction kinetics between the liquid glass and steel during the thermal fusion (850°C), dictate the amount of nickel required for optimum adhesion.

Nickel is usually deposited by exchange plating in hot (70°C) $NiSO_4$

solutions filtered to remove Fe precipitates. Nickel may also be applied by electroplating (Watt's bath using low deposition currents to prevent nonuniform deposition around holes of edges). The layer of nickel deposited is not a complete film, it tends to deposit on the peaks of the etched metal surface. The nickel in this incomplete film serves two primary purposes. First, it stimulates a high temperature glass–metal galvanic corrosion reaction that promotes the solution of the substrate metal oxides into the glass. Upon reaching a solution saturation condition at the glass–metal interface, a chemical-mechanical bond is established between metal and glass. The amount of nickel controls the extent of these solution reactions and allows optimum adhesion to be developed between the porcelain and steel. This adhesion can be made to remain stable after repeated (>10) reheats to 900°C. The amount of nickel used may be varied over somewhat broad limits as long as the nickel layer remains incomplete. The higher the nickel deposit within an acceptable range, the more stable the structure is to repeated reheat.

Second, the nickel also alloys with the iron and increases the capacity of the metal to hold H_2 in the metal structure[4–6] and is responsible for reducing H_2 bubbles which can form near the glass metal interface.

2.2 Glass Preparation

The glass is prepared from oxide raw materials. Selected compositions are presented in Table 1. The principal contituents of the glass are MgO, BaO, B_2O_3, SiO_2. The raw materials were selected from commercial sources (Fisher Scientific and Alpha Ventron) to be low in alkali and transition metal contaminants (<100 ppm alkali and <100 ppm transition metals). These materials were weighed and mixed prior to melting at 1500°C for 30 min. The glass is then quenched between counter-rotating stainless steel rollers at 12 feet/min. surface speed, with a roller gap of 10 mils. The glass frit flake is then milled to a 3–7 micron mean

Table 1—Sample Compositions

	Composition in Weight (%)					
I.D. #	MgO	BaO	B_2O_3	SiO_2	P_2O_5	ZrO_2
#22	27.82	37.16	20.45	14.56	**	**
#36	27.96	37.34	16.95	17.73	**	**
#37	26.99	36.05	19.83	14.13	**	3.00
#38	26.99	36.05	19.83	14.13	**	3.00
#43	27.55	36.78	16.70	17.47	1.5	**
#72	40.91	18.78	25.58	14.72	**	**
#72 mod.	40.30	18.50	25.20	14.50	**	1.50
#72 mod.	40.30	18.50	25.20	14.50	1.50	**
#75	40.98	18.82	24.41	15.80	**	**
#77	41.05	18.85	23.22	16.88	**	**

size in two stages. The first step is a dry milling for 2 hours to a coarse powder. The glass is then milled in 2-propanol for 8–20 hours to produce a particle size distribution as shown in Fig. 11. The resultant liquid slurry (2-propanol and glass powder) is used as the stock solution for electrophoretic deposition of the glass powder on the substrate steel.

2.3 Glass Deposition

The glass particles possess a strong, positive, surface charge after milling which is believed to be due to surface dissociation reactions between the glass surface and the small amounts of water present in the milling liquid. The deposition slurry is formed by adding amounts of glass stock solution to 2-propanol to form a slurry with 1–2 volume percent glass solids. The glass is deposited cathodically between anode plates separated by 2–5 cm. A voltage of 300 volts applied for 3–4 minutes applies a coating of glass particles 15–20 mils thick. The slurry resistivity is normally measured in the range 6–18 megohm-cm using a Balsbaugh 900-18M meter. The deposition current is normally 40 mA/square foot or less. The dense powder compact on the substrate is dried at 120°C for 10 minutes, then fired at 800–900°C soon after deposition. A fired coating 7–8 mils thick has been used as a standard thickness for electronic substrate applications.

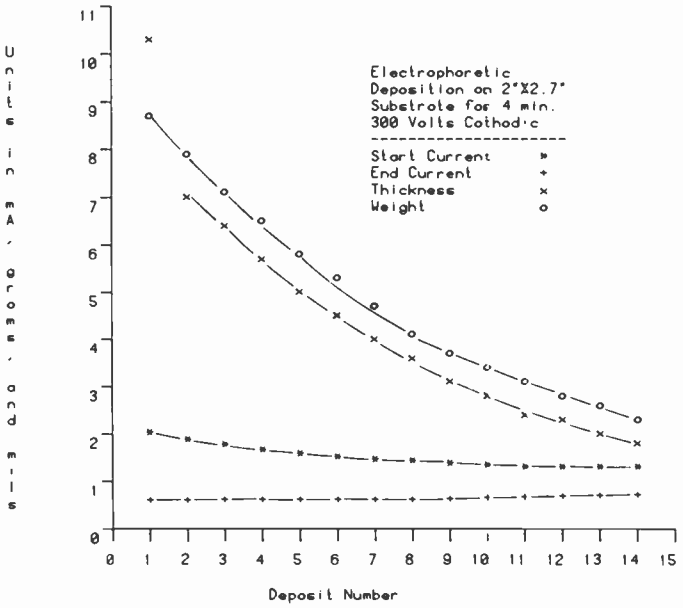

Fig. 1—Electrophoretic deposition of glass data plot.

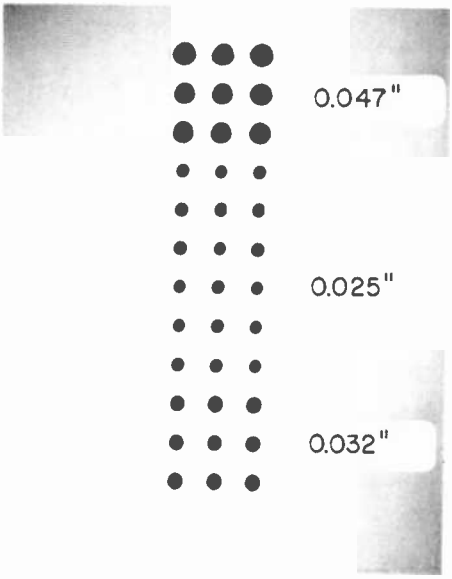

Fig. 2—Example of porcelain-coated holes in steel board.

A series of samples was deposited at a constant voltage of 300 volts dc for 4 minutes on steel substrates (2.75 × 2 inches). The data from this series is shown in Fig. 1. The deposit weight, fired thickness, starting current, and ending current are plotted as a function of the deposit number. No glass replenishment was made during the tests. Close correlation of deposit weight and fired thickness is apparent from the data.

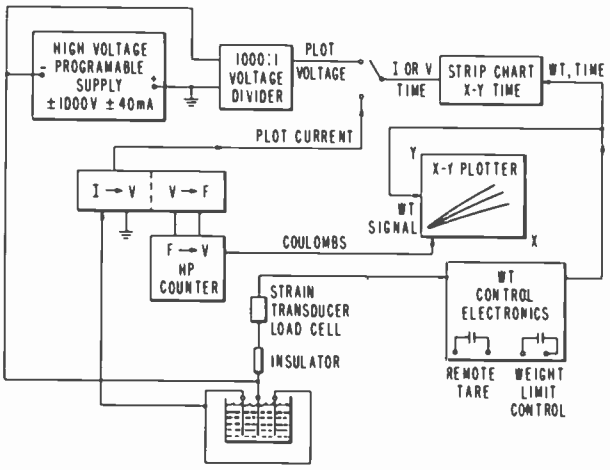

Fig. 3—Electrophoretic deposition monitoring system.

The deposition was continued until essentially no glass particles were remaining, indicating that nearly all particles are transportable in the electric field.

Holes punched and deburred prior to coating with glass have been successfully coated with porcelain down to approximately 30 mil holes in the metal board. Fig. 2 shows an array of holes coated with porcelain with openings as small as 25 mils after firing.

The deposition conditions are monitored by control electronics designed at RCA to provide information on the process of deposition. A diagram of the deposition system is shown in Fig. 3. A weight transducer is used to monitor the weight gain during deposition. A coulomb counting circuit is used to monitor the electrical energy consumed in deposition. After each deposit, the glass slurry is replenished. Deposition parameters such as grams/coulomb, weight versus time, and current and voltage versus time may be plotted.

2.4 Glass Firing

The deposited dry-powder compacts on the steel surface are fused by heating at 600–1000°C/minute to 800–900°C. Since the crystallization kinetics control the flow period of the glass during fusion, firing time is not critical. Usually, firing times of 3 to 10 minutes are used. The samples are cooled rapidly (quenched in air).

3. Studies of Glass Fusion

The glass system from which the present porcelain compositions are derived is the MgO-BaO-B_2O_3-SiO_2 system. Glasses from this system exhibit large regions of immiscibility.[1] The glass is quenched from high

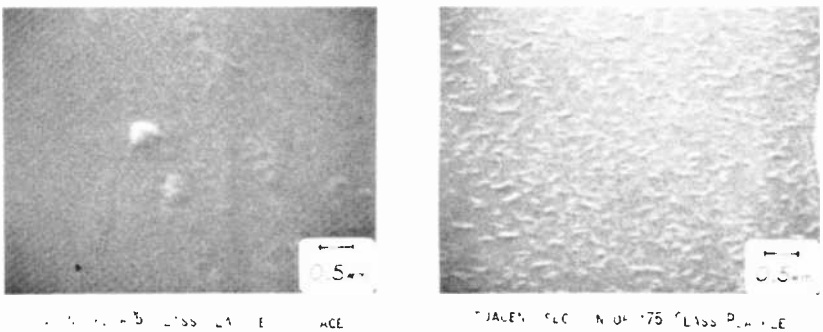

Fig. 4—Example of liquid–liquid phase separation: (left) as-quenched glass platelet and (right) glass platelet heat treated 700°C for 1 hour

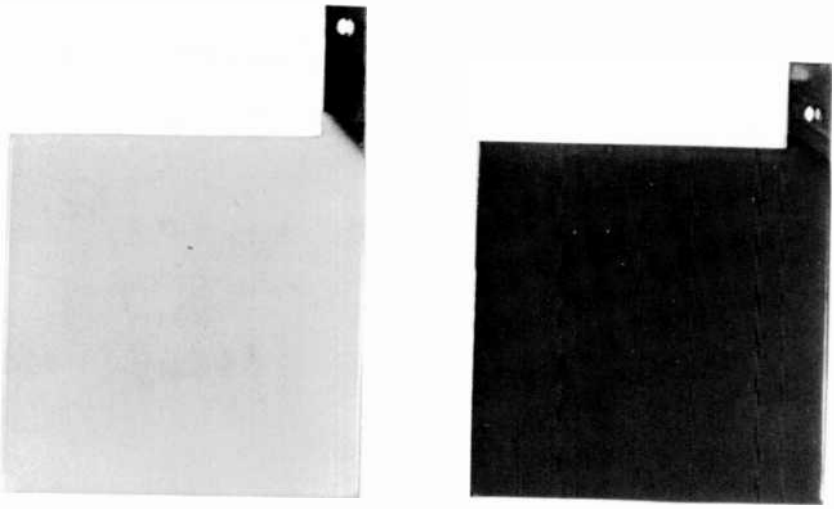

Fig. 5—Fusion of porcelain sample, initial (dark colored) and final (light colored) stages.

temperatures (>1400°C). When the glass in the form of compacted fine powder is fused on the surface of low carbon steel at 830°C, the glass flows, levels, and crystallizes to a high volume fraction of crystal in a remnant glass matrix. Liquid–liquid phase separation in the glass precedes the crystallization. Fig. 4 shows a scanning electron micrograph of a quenched glass platelet and an adjacent section heat treated at 700°C for 1 hour. The heat-treated sample has a surface roughened by the liquid–liquid separation. When a porcelain substrate sample is fused, two distinct visual stages are observed. The first is the thermal fusion of the glass particles to a clear, transparent, "vitreous" coating on steel. This stage is observed by quenching the fusion after about 10 seconds. If the sample is fused for 30–60 seconds and then cooled, the sample becomes opaque, slightly off-white, and crystallized. The fired surface upon cooling will show a slight "sheen" due to the matrix glass. Fig. 5 shows the appearance of samples in these two stages of fusion.

The viscosity of the glass is very low during the early stages of fusion; however its viscosity climbs with time determined by the kinetics of the crystallization process. This low-viscosity fusion period gives rise to many benefits not usually possible with conventional enamel interfaces. The first is the low incidence of interfacial bubbles at the metal surface. This appears to be due to the short vitreous period and the H_2 adsorption capability of Ni which is applied to the Fe interface to promote adhesion. Secondly, the interface becomes stabilized more quickly than conven-

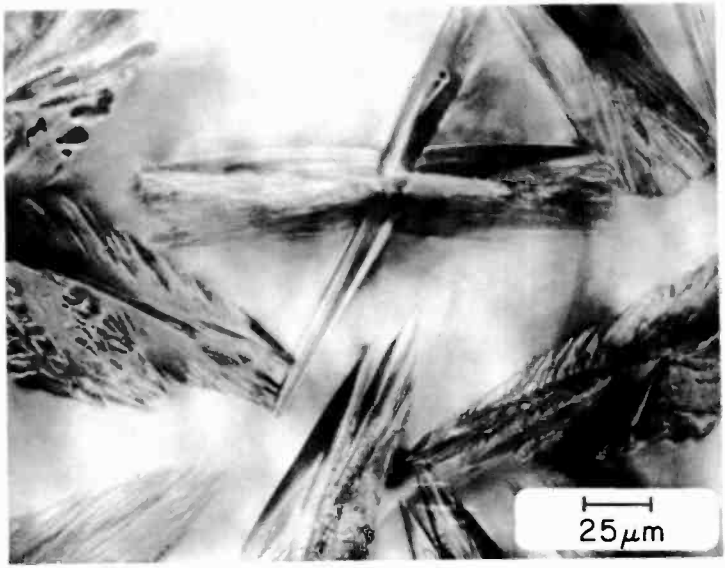

Fig. 6—Crystal growth from the melt—initial stage.

tional enamel systems due to the mechanical rigidity obtained with the growth of crystals. The solution reactions that occur near the metal-glass interface slow and effectively halt as the liquid phase is consumed by crystallization. Hence, the adhesion reactions become more dependent

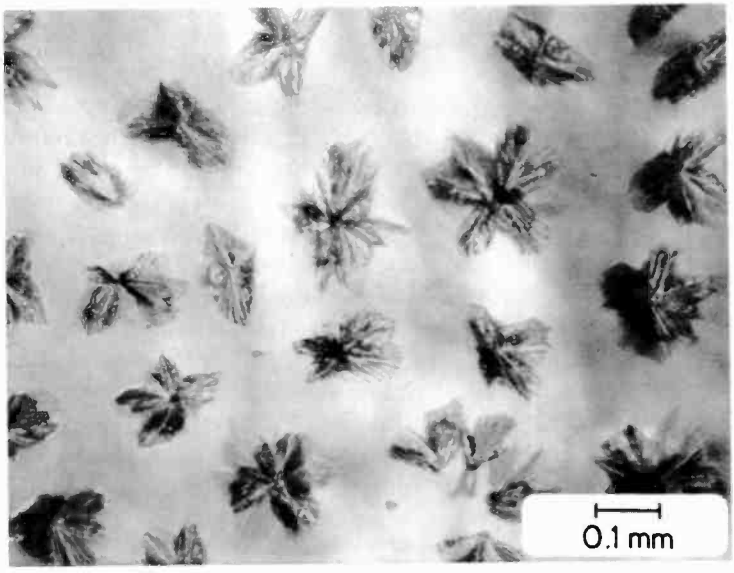

Fig. 7—Crystal growth from the melt—progression stage.

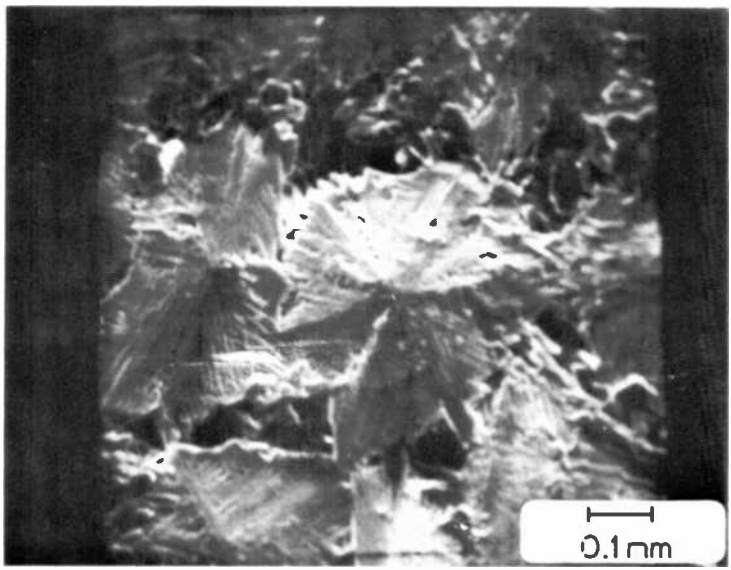

Fig. 8—Crystal growth from the melt—final stage.

upon the crystallization kinetics and temperature and less on the firing time. The ceramic–steel laminate structure has a significantly reduced tendency to warp upon cooling due to the mechanical stiffness of the ceramic layer. The surface smoothness is in the range 4–15 micro-inches as fired. This smoothness is a significant benefit to thick-film print quality.

In an effort to characterize the morphology of crystals produced during the fusion of the glass, samples of virgin glass surface were made by fusion in a platinum foil container at 1400°C. The samples were quenched then heat treated at temperatures between 720–830°C for a few seconds and quenched again. Fig. 6 shows an SEM of small growing nuclei in a predominately "vitreous" melt. Fig. 7 reveals the development of a fan like cluster growth. The growth is shown to be intersected with adjacent crystals in Fig. 8.

X-ray powder diffraction studies of crystallized glass have shown that $BaO\text{-}2MgO\text{-}2SiO_2$ and $2MgO\text{-}B_2O_3$ are among the crystal phases present.

4. Microstructural and Thermal Analysis Studies

The ultimate suitability of the glass-crystal composite layer for substrate applications depends on the control that can be exerted on the course of crystallization and the composition of the vitreous remnant glass. Fig.

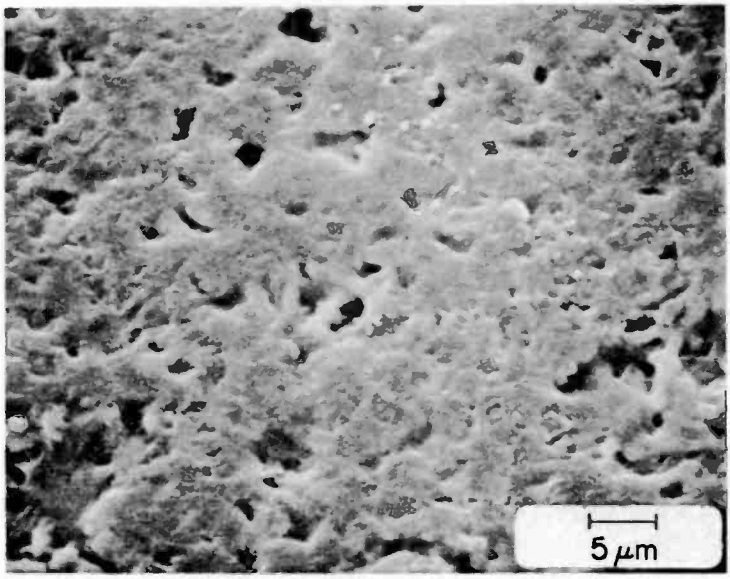

Fig. 9—Scanning electron micrographs of #75 porcelain surface (starting powder 6.4 μm mean diameter).

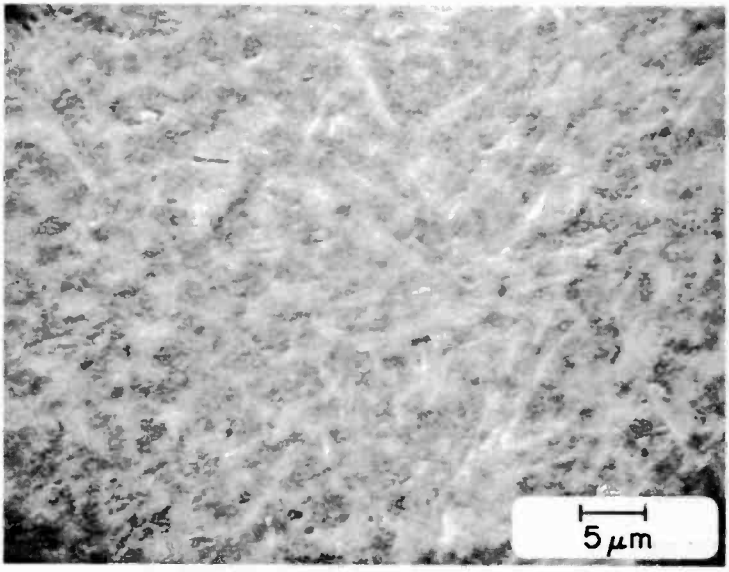

Fig. 10—Scanning electron micrograph of #75 porcelain surface (starting powder 3.7 μm mean diameter).

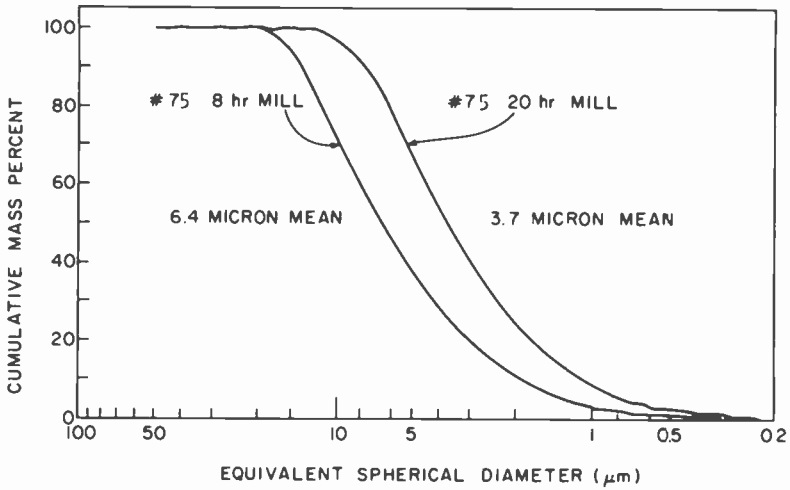

Fig. 11—Particle size distribution of #75 glass.

9 shows the porcelain surface for composition #75. The grain size of the microstructure is dependent upon the starting particle size of the glass. This sample had a 6.4 micron mean diameter. As the mean particle diameter is reduced, the grain size is reduced. A sample of #75 porcelain with 3.7 micron mean particle size is shown in Fig. 10 for comparison. The surface is more defect-free with the smaller mean size. The particle size distributions were measured by X-ray sedimentation using a Micromeritics Sedigraph. Fig. 11 presents data on the particle distributions

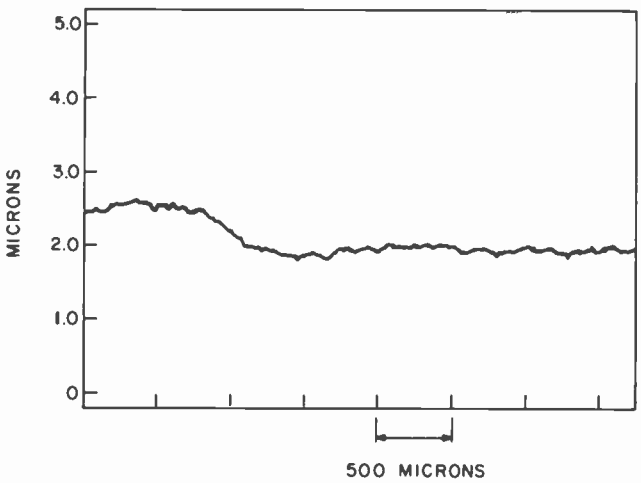

Fig. 12—Surface smoothness of #75 porcelain (Tallysurf).

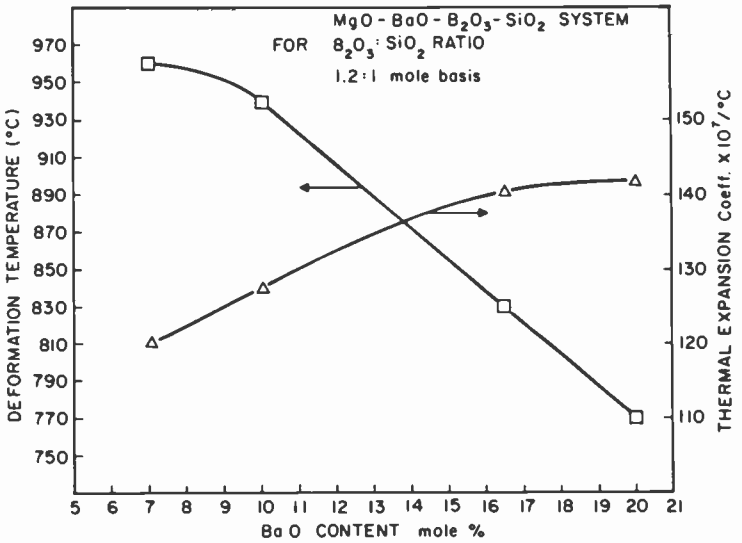

Fig. 13—Thermal expansion and deformation temperature versus glass composition.

for #75 after 8 and after 20 hours of milling. Surface smoothness measurements are presented in Fig. 12 for the finer particle #75 (Tally-surf).

Selected compositions are shown in Table 1 in wt.% oxide. This table

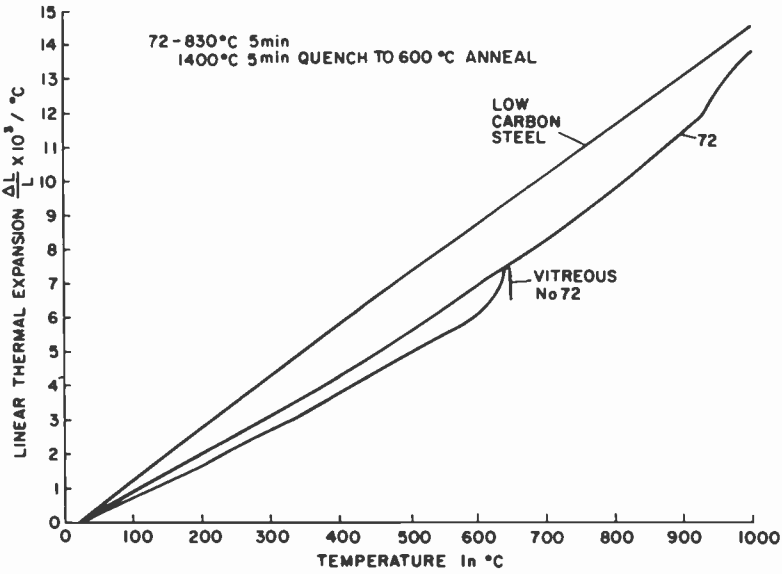

Fig. 14—Thermal expansion of "vitreous" and crystalline #72 versus steel.

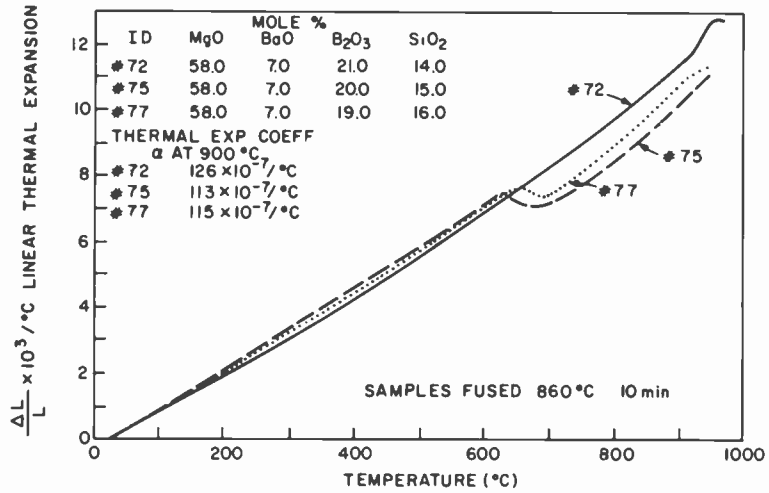

Fig. 15—Thermal expansion of #72, #75, and #77 versus temperature.

reveals some modifications in composition that have been made to study the influence of an additive on crystallization and the vitreous remanent glass. In order to measure the effects of composition on the reheat temperature, thermal expansion behavior, and crystallization kinetics, measurements by fused silica dilatometer and differential thermal analysis (DTA) were used. Fig. 13 presents a graph of thermal expansion coefficient and the deformation temperature as a function of composition. The B_2O_3:SiO_2 mole ratio was fixed (1.2:1). It can be observed that high BaO contents favor higher expansion and lower deformation temperature. Fig. 14 presents the thermal expansion behavior of composition #72 in the "vitreous" state and crystallized form plotted with the expansion of low-carbon steel. The vitreous sample was prepared by quenching from 1400°C, and annealing at 600°C, and then measured. The crystallized sample is fired from glass powder at 830°C for 5 minutes then cooled. In Fig. 15, three thermal expansion curves are shown for compositions #72, #75, and #77. These compositions have the same MgO and BaO contents in mole percent. The amounts of B_2O_3 and SiO_2 are varied in mole percent increments. As can be seen from the curves for #75 and #77, a peaked inflection in the expansion curve is observed at 625°C. This corresponds to the deformation peak in "vitreous #72" shown in Fig. 14 and indicates that the addition of SiO_2 at the expense of B_2O_3 reduces the crystal content of the fused samples. The composite structure yields, while heating, until crystalline particles support the deforming composite and begin to expand dominated by the crystal expansion. Examination of these compositions fired on steel shows in-

creasingly glossy surfaces with increasing SiO_2 content. In Fig. 16, the expansion behavior of composition #72, modified with the addition of 1.5 wt.% P_2O_5 to the melted composition, shows the same inflection and behavior as produced by changing the SiO_2 to B_2O_3 ratio as shown in Fig. 15. The addition of 1.5 wt.% ZrO_2 to the melted composition of #72 produced an increase in the expansion, without inflections, which reheats to a temperature in excess of 1000°C before deformation. The use of P_2O_5 as an additive to the four component base composition (#72) reduces the ultimate crystal content of the fired composite and also slows the crystallization kinetics (determined by DTA studies). The addition of ZrO_2 improves the thermal reheat stability of the fired composite structure with slight slowing of the kinetics of crystallization.

A DTA (differential thermal analyzer) was used to study the crystallization kinetics. The DTA was modified for rapid conversion without thermal upset to isothermal mode plotting. In Fig. 17, the DTA curve on heating at 30°C/minute is shown for compositions #72, #75, and #77. In #72, the crystallization is rapid, reaching its peak exotherm at 775°C. In #75, the crystallization exotherm is raised to 814°C. The kinetics are further slowed in #77 and a second crystal phase is indicated. The first peak at 825°C and the second at 875°C indicate that the course of crystallization has been altered.

Samples of #75 porcelain (6.5 micron mean size) heated at 9.8°C/minute to an isothermal soak temperature and then monitored with time are shown in Fig. 18. The plot shows the thermal dependence of the crystallization kinetics. A sample of #75 fired at 830°C completes its crystallization in less than a minute. The metal surface preparation must be optimized for the crystallization kinetics to achieve a high level of bond adhesion. Therefore, compositions with somewhat slower kinetics place less constraints on metal preparaton, heating rate, and fusion temperature to control the adhesion at a reliable level. Measurements of bond adhesion are normally done indirectly due to difficulties in pull testing glass–metal interfaces. Fig. 19 shows a sample of porcelain-steel twisted in torsion to 50 degrees on a 2 × 2 inch section and then released. The sample illustrates the high level adhesion between the ceramic layer and steel. A cross-section of porcelain-steel polished with a 16.5 degree angle-lapped interface is shown in Fig. 20. The metal has been etched with 5% nitric acid in 2-propanol to reveal its grain structure. The interlocking ceramic-metal interface indicates the conditions existing for high bond strength.

The ceramic-steel substrate has been used to develop compatible base-metal thick-film conductor, resistor, and dielectric inks[10,11] for routine firing at 900°C. The surface smoothness of the porcelain (4 micro-inches) is quite adequate for the use of metallo-organic films for

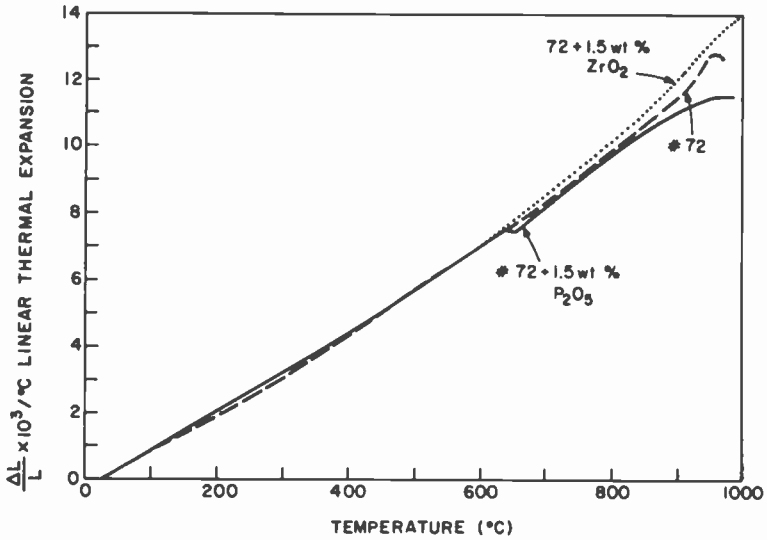

Fig. 16—Thermal expansion of #72 with additives of P_2O_5 and ZrO_2 in glass versus temperature.

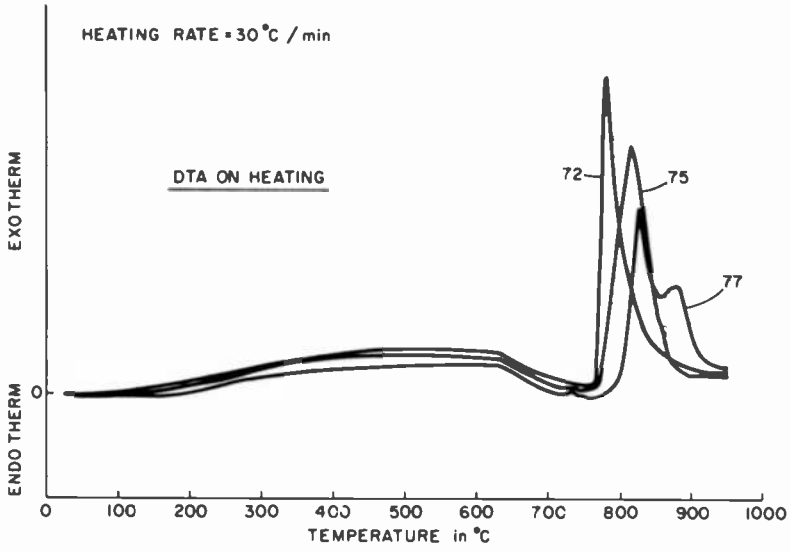

Fig. 17—Differential thermal analysis of #72, #75, and #77 upon heating.

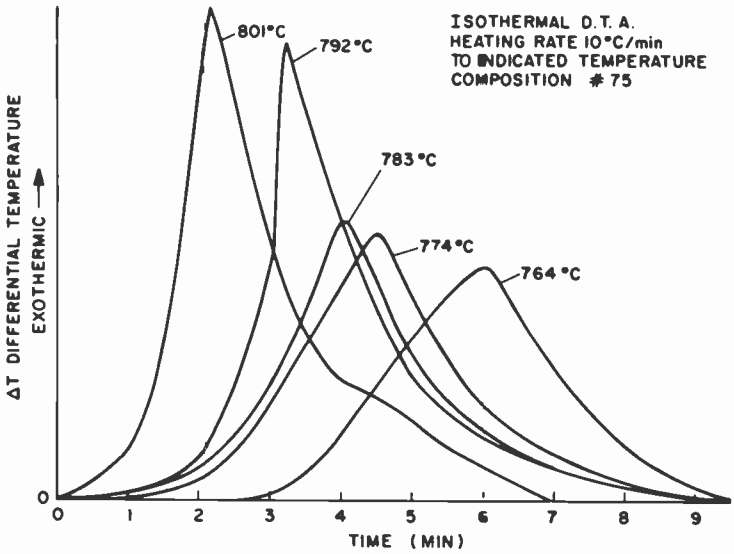

Fig. 18—Isothermal D.T.A. measurements on composition #75.

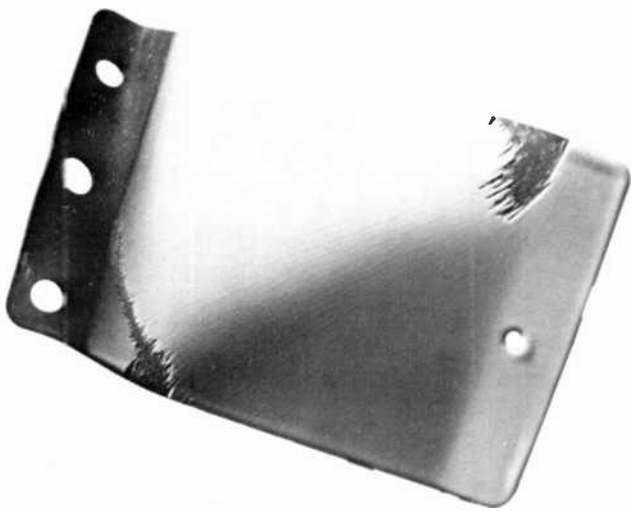

Fig. 19—Torsion tested sample of RCA porcelain.

Table 2—Properties of RCA Ceramic-Steel Board

Thermal Properties
(1) High refire temperature in excess of 900°C without degrading after 10 refirings
(2) Thermal emissivity: 0.9–0.95
(3) Thermal conductivity: 0.014 Watts/(cm × °C) steel 0.7 Watts/(cm × °C)
(4) Thermal expansion coefficient: 100–140 × 10^{-6}/°C

Electrical Properties
(1) Dielectric breakdown strength at 25°C, 7.5 mils thick: 4000 V dc
(2) Dielectric constant (100 Hz–10 MHz, 25°C): 7.5–8.5
(3) Dissipation factor (100 Hz–10 MHz, 25°C): 0.005–0.01
(4) Bulk resistivity (25°C, dry): 10^{17} ohm-cm
(5) Surface resistivity (25°C, dry): 10^{15} ohm/sq
(6) ASTM-495 Arc Tracking test passed at 12.5 Kv applied
(7) Capacitance thermal coefficient: 200–300 ppm/°C
(8) Dielectric *Q* at 30 MHz versus time at 50°C, 85% R.H. is stable for >1000 hr. at 158

Mechanical Properties
(1) Adhesion of ceramic layer to steel: excellent
(2) Surface Microhardness Vickers 50 g. load 700 Kg/mm^2
(3) Density of glass enamel: 3.1–3.6 g/cc
(4) Young's Modulus at 25°C: 18 × 10^6 psi
(5) Flexure of ceramic-steel board without fracture: 18 inch radius
(6) Surface smoothness 4–15 micro-inch as fired

conductor and resistor circuits. Noble-metal inks presently available may also be used successfully on the ceramic–steel board fired as high as 900°C.

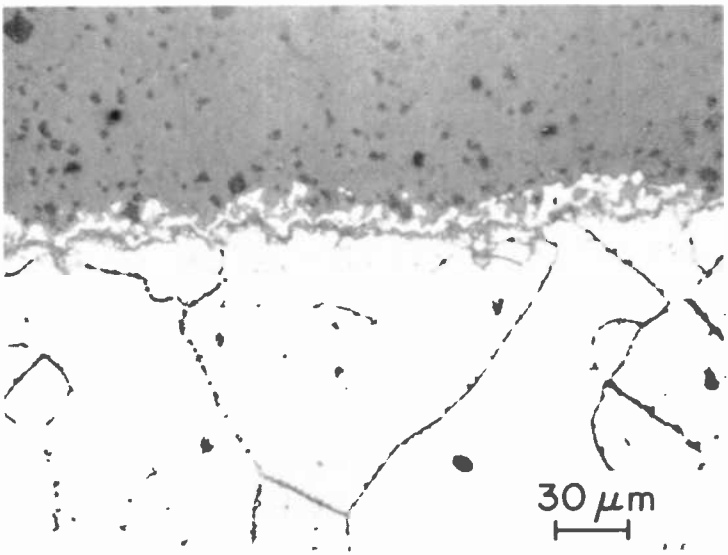

Fig. 20—Cross-sectional optical micrograph of RCA porcelain angle lapped at 16.5 degrees.

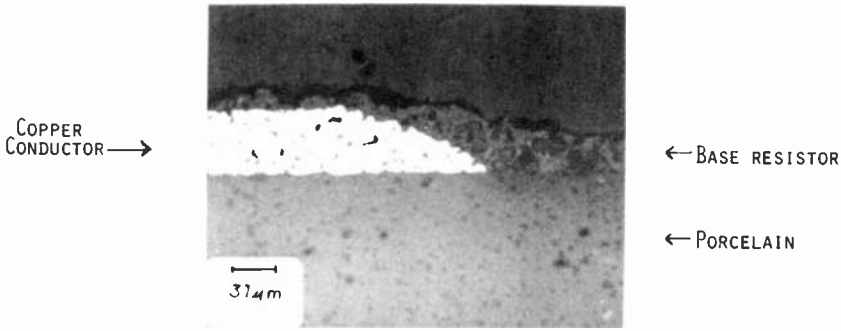

Fig. 21—Cross-sectional optical micrograph of RCA porcelain with thick-film copper and base-metal resistor layers angle lapped at 16.5 degrees.

In Table 2, a summary of mechanical, electrical, and thermal properties is presented for RCA ceramic-steel board. The superior electrical properties and high thermal reheat make the RCA porcelain board a highly versatile electronic substrate. The smooth as-fired surface is shown in Fig. 21 as a low angle cross-section of a copper conductor and base metal resistor printed on the porcelain surface. Little reaction between the substrate and the thick film layers is apparent. The porcelain remains unfluxed by the bonding materials in the thick-film inks. The RCA porcelain board has been used in a printed-circuit-board application to fabricate (on an experimental basis) complete TV sets (except for the tuner) with excellent performance results. Other control circuits using hybrid thick-film technology have been made using copper conductor, base-metal resistors, dielectric, and silicon chips wire bonded to copper with excellent results. Many applications of the porcelain board technology are forseen in the future.

Conclusions

The compositions, deposition, and glass–metal sealing technology developed in this study, were accomplished in conjunction with the simultaneous development of thick-film base-metal conductor, resistor, and dielectric inks formulated to be mutually compatible with each other at contact interfaces and with the porcelain board. The high refire temperature, excellent electrical properties of the porcelain and stability of the porcelain surface to applied thick-film layers are critical to the success of the porcelain. The development of a high temperature porcelain circuit substrate, described here, is the foundation for a complete circuit-substrate system. It should make possible the application of high-reliability thick- and thin-film circuits to high volume electronics at low cost.

Acknowledgments

This work was performed with the support of the Electronic Packaging Research Group (L. Onyshkevych, Group Head) in the Consumer Electronics Research Laboratories (D. Holmes, Director). We wish to thank A. Prabhu, B. Thaler, D. Dorsey, and A. Sussman for their helpful discussions during the course of this work; A. Kusenko for metal preparation; and T. Ward for glass depositions. Many other people, too numerous to mention contributed to the success of this study.

References:

[1] Ernest M. Levin, "Liquid Immissibility in Oxide Systems," in *Phase Diagrams Material Science and Technology, Vol. III, The Use Of Phase Diagrams in Electronic Materials and Glass Technology*, Ed. by Allen M. Alper, p. 143–233, Academic Press, NY and London, (1970).

[2] B. W. King, H. P. Tripp, and W. H. Duckworth, "Nature of Adherence of Porcelain Enamels to Metals," *J. Amer. Ceramic Soc.*, **42** (11), p. 504 (1959).

[3] M. P. Borom and J. A. Pask, "Role of 'Adherence Oxides' in the Development of Chemical Bonding at Glass-Metal Interfaces," *J. Amer. Ceramic Soc.*, **49** (1), p. 1 (1966).

[4] C. E. Sims, "Behavior of Gases in Solid Iron and Steel," *Gases in Metals*, **152**, Amer. Soc. for Metals (1953).

[5] D. P. Smith, *Hydrogen in Metals*, p. 61, Univ. of Chicago Press (1948).

[6] T. D. Sullivan, D. H. Nelson, and F. W. Nelson, "Effect of Moisture in Furnace Atmosphere on Hydrogen Defects in Glass Coated Steel," *J. Amer. Ceramic Soc.*, **45** (11), p. 509 (1962).

[7] Kubaschewski and Hopkins, *Oxidation of Metals and Alloys*, 2nd ed., p. 230–288, Academic Press (1962).

[8] K. Kauffe, *Oxidation of Metals*, p. 272–314, Plenum Press, New York (1965).

[9] C. E. Hoge, *The Effect of Atmosphere on Interfacial Reactions and Wetting Behavior in Glass-Metal Systems*, (MS Thesis) Lawrence Radiation Laboratory, Univ. of Calif., Berkley (UCRL-20334).

[10] A. N. Prabhu, K. W. Hang, E. J. Conlon, T. T. Hitch, and A. Kusenko, "Characterization of Thick-Film Compositions on RCA Porcelain Coated Steel Substrates," *RCA Rev.*, **42**, p. 239, June 1981 (this issue).

[11] A. N. Prabhu, K. W. Hang, E. J. Conlon, and S. M. Boardman, "Optimization of RCA Porcelain Composition for Compatibility with Thick Films," *RCA Rev.*, **42**, p. 221, June 1981 (this issue).

[12] A. N. Prabhu, E. J. Conlon, S. Z. Miller, J. H. McCusker, and T. T. Hitch, "Fabrication of Large-Area Thick-Film Hybrid Circuits Using RCA Porcelain-Coated-Steel Substrates," *RCA Rev.*, **42**, p. 259, June 1981 (this issue).

Electrophoretic Deposition of Coatings from Glass-Isopropanol Slurries

Alan Sussman and Thomas J. Ward

RCA Laboratories, Princeton, NJ 08540

Abstract—Physico-chemical properties of glass–isopropanol slurries were determined to evaluate production of uniform coatings by electrophoretic deposition. Positive charging of the glass is believed to occur by a reaction with water. Kinetics of deposition were investigated for constant voltage and constant current modes. The deposit forms without obvious electrode reaction. Stability of the initial coating, initial and overall deposition rates, and deposit wet resistance depend on the slurry conductance. That conductance is influenced by many electrolytes and additives, particularly water. Carbon dioxide affects the deposit packing and resistance in an abnormal fashion. An experimental deposition system is described. Firing of the deposit results in a physical structure that depends both on the particle size and composition of the original glass deposit. Time and temperature of firing affect the kinetics of melting and subsequent recrystallization.

Introduction

Electrophoretic deposition of coatings is an old art[1] that has recently become a method suitable for large-scale industrial production. One of the more appealing features of the technique is the uniformity of the deposit, without the waste encountered in dipping or spraying operations typical of the enamelling industry. It was for these reasons that electrophoresis was developed for the deposition onto metal of special glasses that could then be converted by heat treatment to crystalline substrates suitable for hybrid thick-film use.[2] Such coatings applied simultaneously to both sides of the metal are conformal, providing uniform coverage of all edges. Another advantage is that electrophoresis is adaptable to

continuous, rather than batch, processing. This paper briefly covers the chemical and physical properties of the glass that make it suitable for electrophoretic deposition, the deposition system and kinetics of the deposition process, and the conversion of the glass deposit to a ceramic bonded to the substrate. This substrate is a literal foundation for the building of hybrid circuits; the development of a typical system is described elsewhere.[3]

Electrophoresis

The interface between two materials in contact usually becomes charged, the sign and magnitude of the charge being controlled by the properties of the two substances. If a particle is in suspension, and the dimensions over which the charge compensating the surface charge relaxes to the neutrality of the continuous phase are large compared to the particle radius, the particle, when placed in an electric field, will move with respect to the continuous phase. This phenomenon, electrophoresis, is generally observed in colloidal materials when particles are smaller than 1 μm. Such particles remain in suspension for long periods of time because of Browniun motion. Large particles (up to 50 μm), which are the subject of this study, require constant hydrodynamic agitation to keep them distributed as a slurry. With such large particles, the dimensions of the compensating charge region, the double layer, must increase to maintain electrophoresis. This requires low ionic concentration in the continuous phase, which can be accomplished by using liquids of low dielectric constant. Such solvents reduce the solubility of inorganic materials and are themselves less conducting. Higher alcohols such as propanol, butanol, and pentanol are found to be suitable. We have chosen isopropanol because of its availability, reasonable cost, low toxicity, and environmental compatibility.

The glasses used for the study are barium magnesium boro silicates.[4] The surface of the particles in this glass system becomes positively charged in isopropanol. (The mechanism for charging will be discussed later.) Therefore the particles move toward a negatively charged electrode. By having the slurry conductance very low, any simultaneous electrochemical reactions at the metal surface that could interfere with the deposition are eliminated. The charge present on the surface of the particles contributes to the formation of a stable wet deposit by a mechanism that is only partially understood. After a layer is deposited and dried, the material may be resuspended and deposited without loss of efficiency; it is not known whether the material has lost its charge by electron transfer, and then become recharged, or does not lose its charge at all. Since the deposit is porous, the electrode is always accessible to

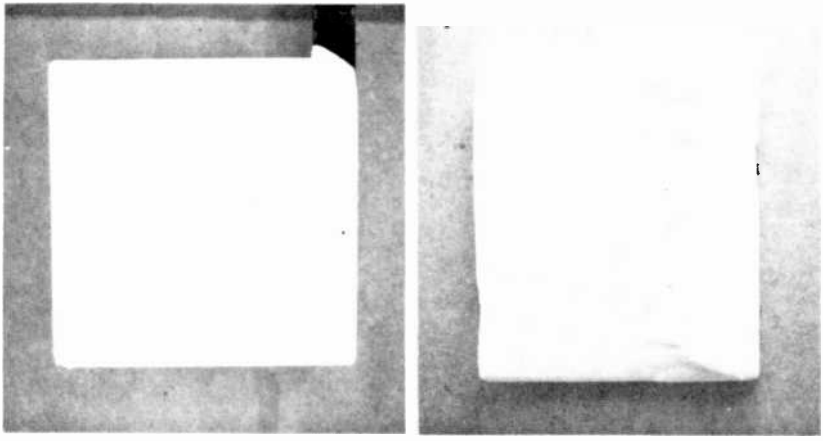

Fig. 1—Electrophoretically deposited glass layer (left) after removal from slurry. Photo on the right shows a similar piece replaced in slurry, without field. Note that deposition has continued by impingement. The resulting deposit distribution depends on the stirring pattern.

free ions in the alcohol; the measured current represents the sum of ion and particle charge transport. The kinetics of deposition have been developed assuming all particles that reach the surface are deposited. In that sense, except for the particle size distribution of the deposit, the process is similar to settling.

In settling, the largest particles settle first, resulting in a deposit whose particle size decreases from bottom to top. In electrophoresis, all the particles generally have the same velocity[5] and, therefore, the particle size distribution is the same at all levels of the deposit. In the stirred bath, the deposition continues by impingement after the voltage is turned off. Fig. 1 (left), illustrates a deposit removed from the bath after deposition. If the deposit is allowed to remain, it builds up as the stirring deposits more material.

Kinetics of Deposition

Assume that the rate of deposition, dn/dt (where n is the number of particles per unit area of the deposit), is proportional to the slurry particle density N and the velocity component of the slurry particles normal to the surface, v. Then $dn/dt = Nv$. The velocity has two parts, the electrophoretic contribution $v_e = ZV/d$ and the hydrodynamic (stirred) velocity v_h. The electrophoretic velocity depends on the field, V/d and the electrophoretic mobility Z, which depends in turn on the dielectric

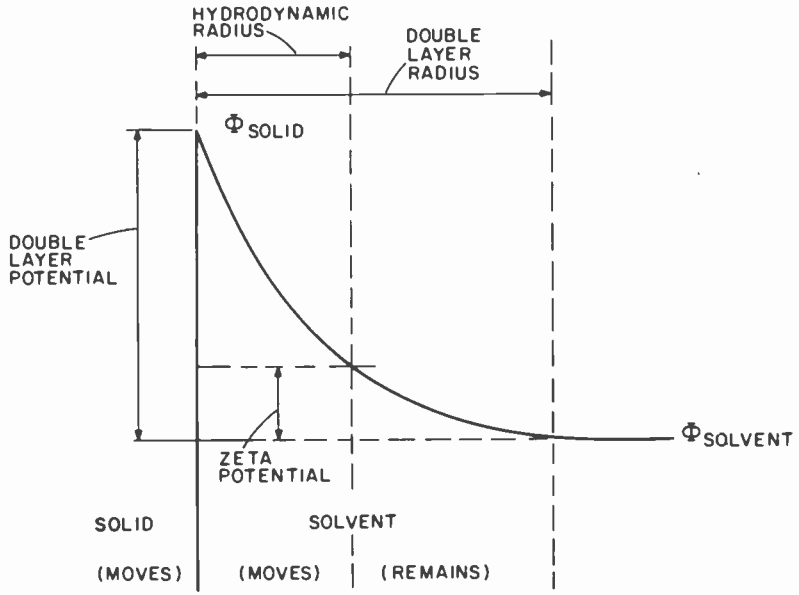

Fig. 2—The electrostatic potential at the surface of an insulating particle—the double layer. The hydrodynamic radius defines the zeta potential.

constant ϵ and viscosity η of the solvent, a geometric shape factor, and the zeta potential $\zeta = \epsilon/4\pi\eta$. The zeta potential may be defined as the value of the double-layer potential at a particular distance from the surface of the particle. That distance, the hydrodynamic radius, separates the fluid that travels with the particle from that which remains behind. It is clear from Fig. 2 that ζ is always less than the total double-layer potential. The kinetics of the deposition will be derived for the reasonable conditions that the hydrodynamic (stirring) contribution to the deposition may be neglected and that the slurry particle concentration does not change during the deposition. There are two regimes to consider: deposition at constant voltage and deposition at constant current.

In the constant-voltage mode, a voltage drop appears across the deposit as its thickness increases. Therefore, the decreasing voltage across the slurry results in particles being deposited at ever decreasing velocities. As this occurs, a point may be reached when the rate of deposition will be matched by the rate of wash-off. Normally, this does not take place in the range of deposit variables of interest. Fig. 3, shows the rates of deposition for several different constant voltages. The rates have been normalized for comparison. Only in the case of deposition at 50 volts is

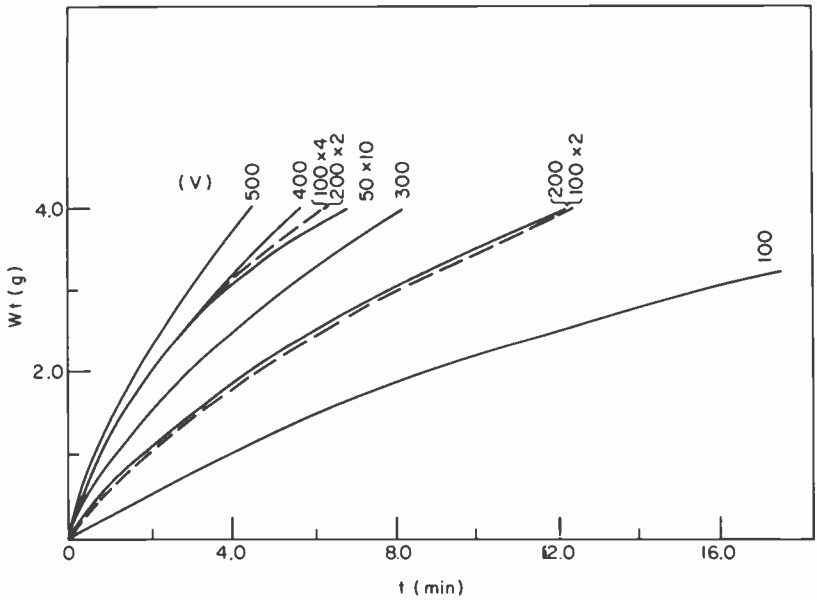

Fig. 3—Deposition at constant voltages, demonstrating the range of voltages over which proportionality is maintained. The rates also have been normalized to some of the voltages to facilitate comparison.

the difference between the 50 V rate × 10 and the 500 V rate appreciable.

The constant-current mode supplies a constant voltage drop across the slurry, so all particles arrive with the same velocity over the deposition time, and the deposition rate is uniform. This is a consequence of the independence of the particle velocity on particle size. Although constant voltage is easier to achieve, the analysis of the data is much more complicated, as will be shown by examining the solutions of the kinetic equations.

The initial conditions are

$$\frac{dn}{dt} = NZ\frac{V}{d} \qquad [1]$$

$$= NZ\,(V_{app} - V_f) \qquad [2]$$

where V_{app} is the applied voltage and V_f is the voltage drop across the film. Now

$$I(t) = \frac{V_{app}}{R_s + R_f}, \qquad [3]$$

where R_s is the slurry resistance and the film resistance is

$$R_f = \frac{N\nu}{\sigma A}. \quad [4]$$

Here ν is the particle volume, σ the film conductance, and A the film area.

For constant current,

$$I = I_0 = \frac{V_s}{R_s} \quad [5]$$

where V_s is the voltage drop across the slurry. From Eq. [1],

$$\frac{dn}{dt} = \frac{nZ}{d} Vs = \frac{nZ}{d} I_0 R_s. \quad [6]$$

After integration, the deposit variation $n(t)$ is obtained,

$$n(t) = NZ\, I_0\, R_s t, \quad [7]$$

which is linear with time. The voltage required to maintain this constant current is

$$V(t) = I_0\,(R_s + R_f) = I_0 \left(R_s + \frac{N\nu}{\sigma A}\right) \quad [8]$$

$$= I_0 \left(R_s + \frac{\nu NZ}{\sigma A d} I_0 R_s t\right). \quad [9]$$

Since $I_0 R_s = V_0$, the initial voltage is

$$V_t = V_0 \left(1 + \frac{\nu NZ}{\sigma A d} I_0 t\right), \quad [10]$$

which is also linear with time.

The expected behavior is shown in Fig. 4. Any departures from linearity of either the weight or voltage with time must be considered a problem (e.g., loss of the deposit, change in slurry concentration, etc).

For the constant voltage mode, we obtain from Eqs. [2] and [3] the relation

$$\frac{dn}{dt} = \frac{NZ}{d} V_0 \left(1 - \frac{n\nu/\sigma A}{R_s + n\nu/\sigma A}\right), \quad [11]$$

with a solution

$$n(t) = \left[\left(\frac{R_s \nu}{2A\sigma}\right)^2 + \frac{R_s \nu}{A\sigma} \frac{NZ}{d} V_0 t\right]^{1/2} - \frac{R_s \nu}{2A\sigma}. \quad [12]$$

This is an awkward expression, but for small values of t, the limiting

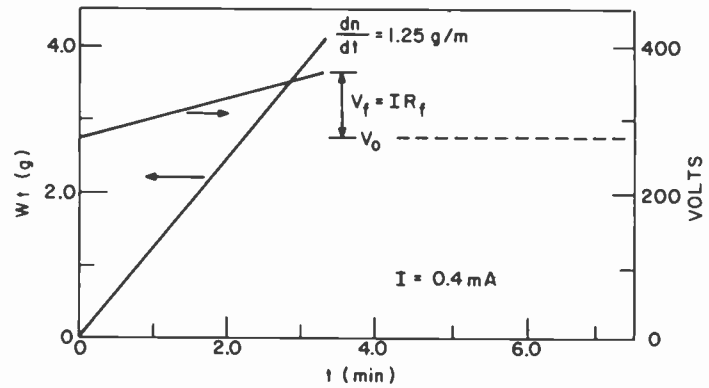

Fig. 4—Deposition at constant current. The increase in deposit weight with time is given by Eq. [8], while the voltage required to maintain the constant current is given by Eq. [11]. (Compare with Fig. 5.)

relation for the initial rate of deposition may be obtained:

$$\frac{dn(0)}{dt} = \frac{NZV_0}{d}. \qquad [13]$$

The weight increase is shown in Fig. 5, along with the value of $I(t)$. Because of the complexity of Eq. [12], the substitution into Eq. [3] to give the analytic value of the current $I(t)$ does not result in a very good process variable. Thus, by maintaining a constant slurry concentration and uniform stirring, deposits of constant thickness may be obtained either

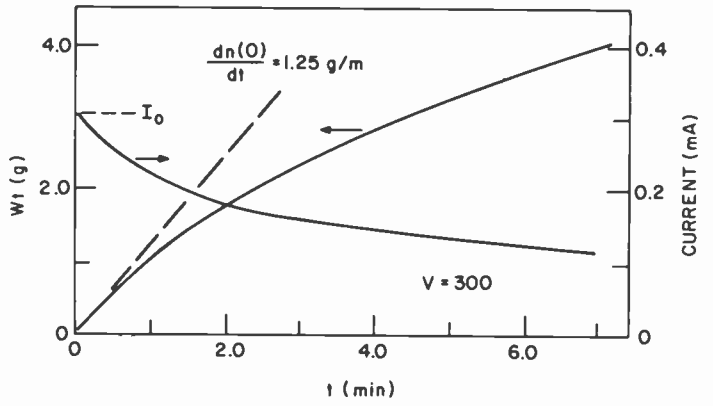

Fig. 5—Deposition at constant voltage. The increase in deposit weight with time is given by Eq. [13]. The functional dependence of the current is not usable as a process variable (see text).

at constant voltage or constant current by controlling the deposition time.

Film Resistance

In some electrophoretic depositions, e.g., that of paint, a film forms whose resistance is sufficient to give a self-limiting thickness.[6] The resistance of the glass layers is too low to use this technique, but it still would be desirable to use the film resistance to control the film thickness. The conductance of the film, σ, is given by $P_L\sigma_L + P_s\sigma_s$, where the subscripts L and s indicate liquid and solid and P their volume fractions and σ their conductances. If $\sigma_L \gg \sigma_S$, and since $P_L + P_s = 1$, the film conductance σ equals $\sigma_L\ (1 - P_s)$. Therefore, increased conductance of the fluid and reduced packing fraction of the solid both increase the conductance of the deposited film. Unfortunately, the conductance of the fluid and the packing portion of the deposit are not independent, since the conductance influences the packing by altering the zeta potential.[7] We may see these interrelated effects by observing some experimental results.

First we may recall, from Eq. [13], that the initial rate of deposition is directly proportional to the electrophoretic mobility Z. Fig. 6 shows the changes in conductance brought about by addition of water, which is a likely contaminant of isopropanol. Below a conductance of about 2

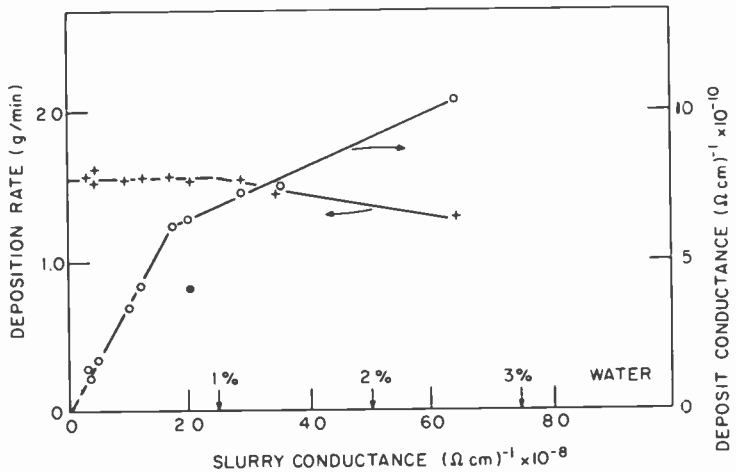

Fig. 6—The initial deposition rate and conductance of the completed film as influenced by the conductance of the slurry. Changes in the slurry conductance are made by adding water, a likely impurity of the isopropanol. (The isolated conductance point is produced by very agitated stirring.)

$\times 10^{-8}$ $(\Omega\ \text{cm})^{-1}$, the initial deposition rate is constant; above that conductance, corresponding to a 0.5 volume percent of water, the rate decreases. This suggests that there is a decrease in zeta potential of the glass surface. Also shown in Fig. 6 is the conductance of films of equal weight as influenced by the fluid conductance. These films show an increase of conductance proportional to the conductance of the slurry, as might be expected. At the same conductance at which the initial rate decreases (which is not influenced by the film), there is a corresponding decrease in the proportionality between the conductance of the film and the conductance of the slurry. Since the latter is dependent on the ionic conductance of the alcoholic solution, the only conclusion is that the packing of the particles must change. The reduced conductance suggests that the glass particles become more closely compacted above an 0.5% concentration of water.

The zeta potential also influences the adherence of the particles to the substrate.[8] No effort to quantify this complex phenomenon is made here, but it has been observed that at low slurry conductance, the particles do not form a stable compact layer, the deposit showing a tendency to slide off the substrate. At high conductance, the electrophoretic mobility falls because the dimensions of the double layer become reduced with respect to the hydrodynamic radius. The influence of particle

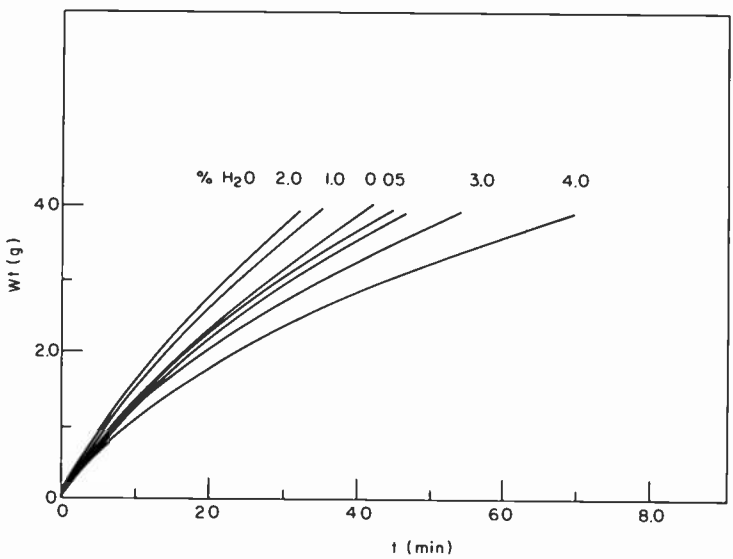

Fig. 7—Overall deposition rate as affected by water. Numbers indicate water concentration in percent. Note that the overall rate first increases, then decreases with increasing water content.

packing may also be seen in the isolated point of Fig. 6, where stirring was extremely vigorous and the deposit would, therefore, be expected to be less compact.

The influence of the film resistance on overall rate may be understood in a qualitative fashion if Eq. [11] is rewritten

$$\frac{dn}{dt} = \text{const}\left(1 - \frac{R_f}{R_f + R_s}\right); \qquad [14]$$

clearly, as the resistance of the film increases, the deposition rate decreases. Thus as packing changes, the rate at constant voltage will be changed, complicating an already awkward expression. Fig. 7 illustrates the changes in overall rate as influenced by water content. These are the same data from which the initial deposition rates and film resistances of Fig. 6 were obtained. Note that the overall rate first increases, then decreases as the conductance is increased by adding water.

Charging Mechanism

The influence of water on the conductance and also the charging of the particle surface may depend on the dissolution of barium oxide on the glass surface, $H_2O + BaO \rightarrow Ba^{++} + 2\,OH^-$, and a resorption of barium

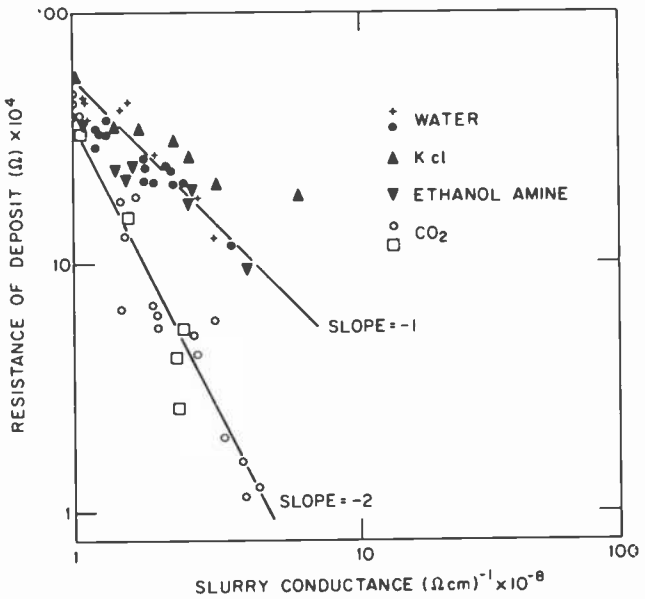

Fig. 8—Influence of ionic deposits in the slurry on the resistance of the deposited film. The behavior for carbon dioxide is seen to be "abnormal".

ions on the surface. This process leaves the surface positively charged, with the negative counter ions forming the rest of the double layer. Such mechanisms have been proposed for other systems.[9] Leaching of glass powder with wet isopropanol and of fired glass with water both result in a large dissolution of barium ions but not of magnesium ions, the other element likely to be affected. This is presumed to result because of the different chemical environments of the ions in the glass. The barium ion is large and crowded into the glass structure, while the magnesium ion is smaller and more easily accommodated.

The addition of barium oxide to slurries with poor deposition characteristics (low charge) improves the deposition rate, while magensium compounds are ineffective. [The use of standard charging agents, such as polyglycols, increases the conductance of the slurry too greatly to be useful.] The addition of other ionophores to slurries also increases the conductance and reduces the resistance of the deposited layer. Fig. 8 shows the result of the addition of typical compounds. The resistance of the film is inversely proportional to the conductance of the fluid. In the case of carbon dioxide, a seemingly abnormal affect is observed—the resistance of the film depends on the inverse square of the fluid conductance. If a small amount of CO_2 gas is introduced into a slurry before

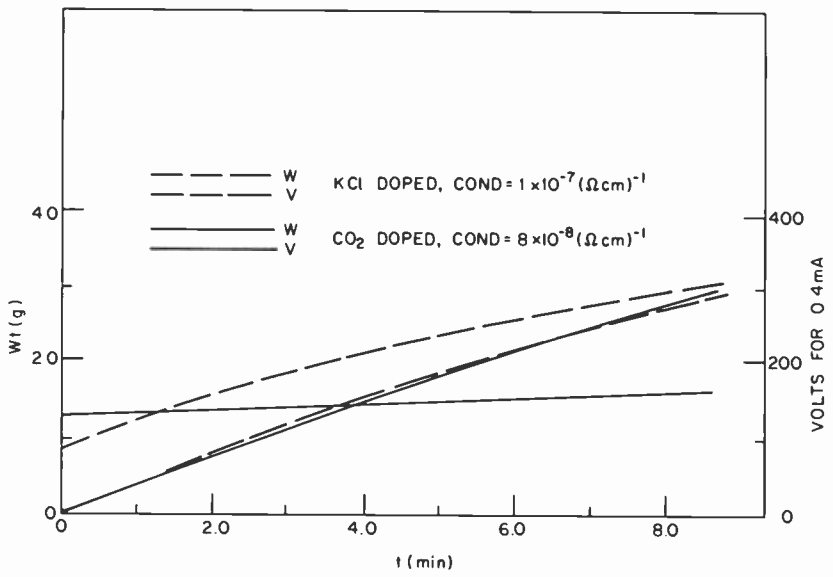

Fig. 9—Comparison between carbon dioxide and potassium chloride as dopants. Although the deposition rates are the same, the resistance of the deposit influenced by carbon dioxide is very small compared to the "normal" resistance.

deposition, the resistance of the deposit becomes very low, but otherwise the deposition rate is unchanged.

Fig. 9 shows a comparison between a slurry doped with KCl and one with CO_2, both with approximately the same conductance. The deposition rates are almost identical, but the voltage necessary to maintain that deposition rate for the KCl-doped slurry increases, while that for the CO_2-doped slurry remains substantially constant. For the latter slurry, therefore, the film resistance is insignificant, possibly because of very loose packing. Indeed, the CO_2-doped deposit is found to be "soupy" rather than stiff. A normal deposit is firm to the touch, similar to wet plaster. (However, both produce satisfactory deposits when fired.) This strong influence of carbon dioxide is one reason that deposit resistance is not a satisfactory control variable. The influence of the CO_2 is entirely reversible; by bubbling nitrogen gas through the slurry, both initial conductance and the deposition characteristics of the slurry are restored.

The role of doping on the mechanical stability of the deposits may be evaluated by observing the ability of settled slurries to resist upsetting. Fig. 10 shows the stability of a settled slurry as the concentration of water is increased. The specimen is prepared by allowing the slurry to settle in a small flat-bottomed vial, then turning the vial on its side. The instability is measured by the amount of the slurry that slides from the bottom. Note that the stability increases above a water concentration of about 1.5% by volume. This figure is in rough agreement with that for the volume percent of water that influences the packing of the electrodeposited layers (Fig. 6). The agreement should be considered only

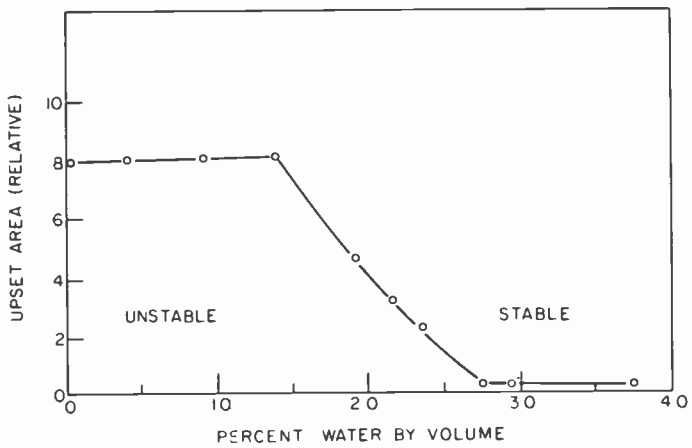

Fig. 10—Mechanical stability of settled deposits as influenced by water.

qualitative, because of the difference between the structure of the deposits made by electrophoresis and settling, as previously noted.

By studying the stability of slurries in this fashion, some general properties imparted by added dopants may be demonstrated (even though they interfere with the electrodeposition).

First, stability increases with addition of water alone. If water and/or an electrolyle is added, there is no other change in stability unless the electrolyle reacts chemically with the glass. Strong bases, such as hydroxide ion, first increase and then decrease the stability with increasing concentration. They also cause faster settling of the slurry (flocculation) and increase the volume of the settled deposit, both as a usual consequence of reduced zeta potential. This result is not paradoxical—the faster settling prevents the particles from compacting and, as a result, the deposit is less dense. The mechanism for controlling the stability of deposited charged particles is complex but depends to a large extent on the counter-ions remaining between the particles,[10] which imparts an electrostatic "stiffness" to the deposit. This stiffness vanishes when the dimensions of the double layer become small (high electrolyte concentration) or when the surface charge vanishes, such as at the iso-electric point.

Deposition

The experimental deposition system is shown in Fig. 11. The vessel is polymeric to prevent dissolution of ions from glass surfaces. The workpiece, which may be prepared to improve adhesion by passing it once

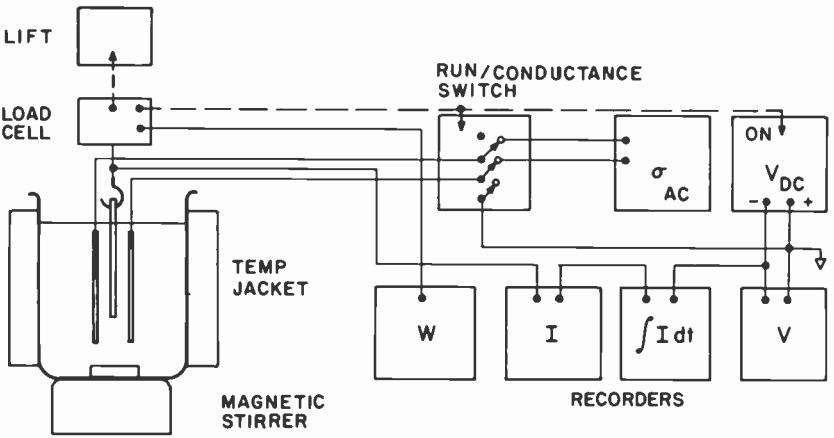

Fig. 11—Schematic of experimental electrodeposition apparatus.

through the firing oven, is placed parallel to and equidistant from two counter electrodes, which are about 2.5 cm apart; the counter electrodes are larger than the workpiece by at least one electrode spacing. Agitation to keep the slurry properly mixed is accomplished by means of a magnetic stirring bar. A suitable concentration of the slurry is approximately 3% by volume as determined by centrifugation. This concentration gives, at 300 V, a deposit equivalent to 0.025 cm fired thickness in about 3 minutes. The weight of the deposit is monitored by a load cell, and both current and voltage are recorded. Figs. 4 and 5 are records of typical depositions at constant current and voltage, respectively. The depositions begin without delay effects sometimes observed.[11] For the same initial rate, constant current deposition is faster.

Drying and Firing

When the deposition is completed, the workpiece is lifted rapidly from the bath. The excess slurry, which wets the surface, begins to drain and the isopropanol begins to evaporate. The small amount of slurry left at the edges results in a slight thickening of the coating at the board edges and around holes. The diameter of holes after firing compared to the (original) size of the hole in the metal can be determined empirically (see Fig. 12). Draining of excess slurry from part holders may lead to wash

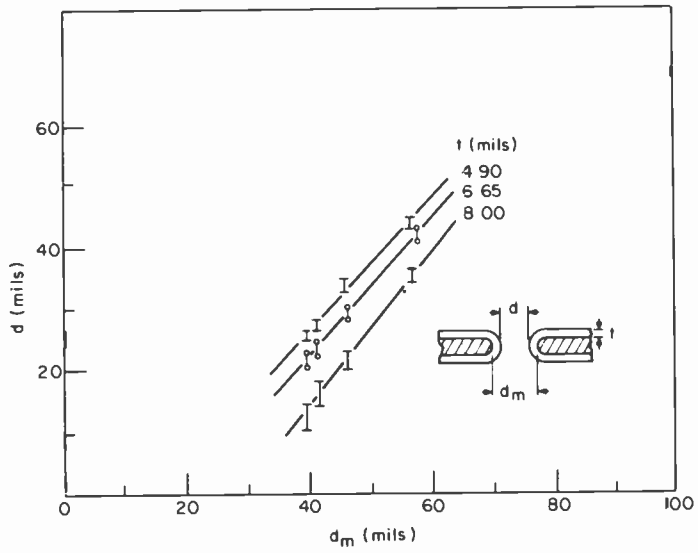

Fig. 12—Diameter of fired hole compared with original hole diameter for different deposit thicknesses.

lines; this may be prevented by using small-area fixturing or by not immersing the part completely.

The evaporation of solvent can present a problem if it brings the material to below the dew point, since the condensation of water could allow generation of steam when the part is fired. For this reason, after initial draining is completed, when the part is still damp with alcohol and still hydrophobic, it is placed for 2 minutes in a preheat section of the oven and preheated at about 60°–80° C. Once dried this way, the work may be kept indefinitely in a dry environment until it is fired.

The firing accomplishes two things: (1) it begins the formation of the ceramic by melting the glass, which then may crystallize spontaneously, and (2) it encourages the creation of the bond between the iron substrate and the ceramic. Both these processes are complex, and are treated in detail elsewhere.[12] If no metal preparation except pre-oxidation is employed, the adherence of the ceramic to the substrate is sufficient to permit evaluation of the electrical properties of the ceramic surface and of the conductor and resistor inks that are subsequently fired onto it.[3]

Firing

The scanning electron micrographs in Fig. 13 show the effect of time and temperature on the formation of a ceramic film. This substrate passed

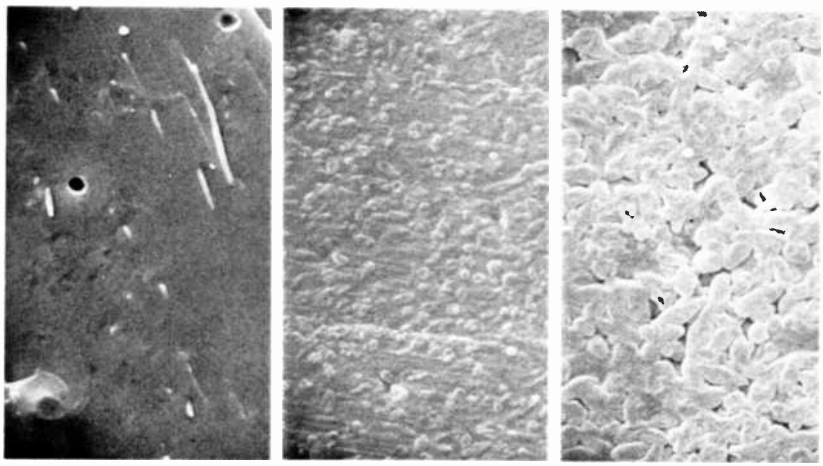

Fig. 13—Kinetics of ceramic formation from glass. The layer was passed through the furnace giving a thermal gradient: (left) the glass has melted but did not have enough time to crystallize (observe trapped bubbles); (center) crystallization has begun; (right) crystallization is complete. Magnification 2000X.

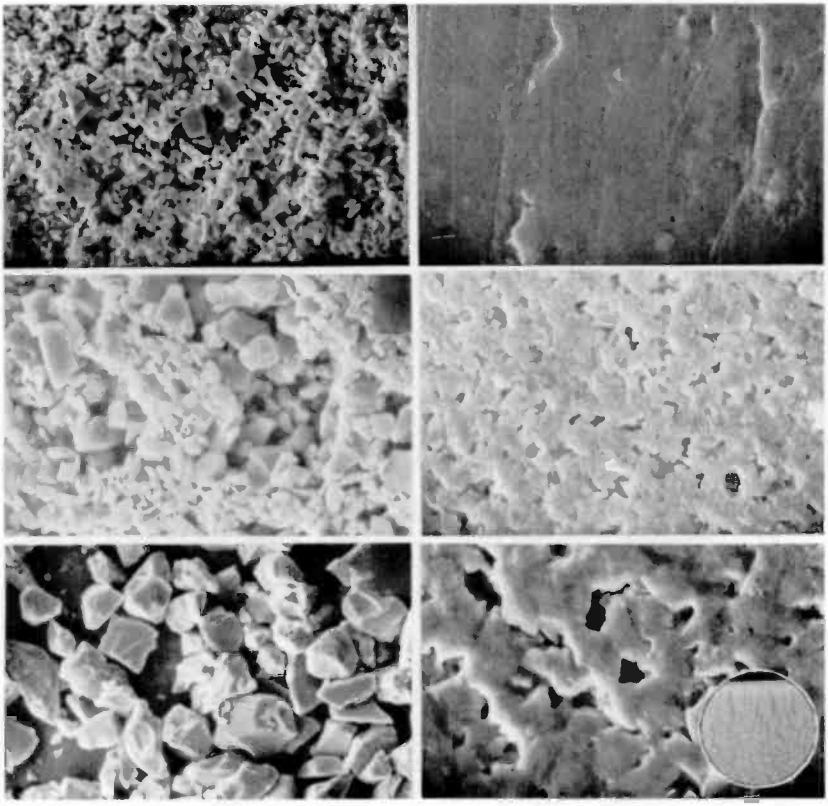

Fig. 14—Effect of glass particle size on crystallization. Left side is the deposited particles, right the fired ceramic. The top pair was made with fine particles (less than 10 μm) and gives a smooth ceramic layer; the middle with 1–50 μm particles; and the bottom with coarse particles. Note the vestiges of the original structure. The inset bottom right (actual size) shows the iron oxide veining that occurs with coarse particles. Magnification (except for inset) 1000X.

through the furnace at a rapid rate, but because of a thermal gradient the top and bottom differed in temperature by an estimated 30 K. The particulate deposit (similar to that shown in the left center photo in Fig. 14) melted to give a glass that, because of the rapid passage through the furnace, had insufficient time to crystallize (Fig. 13 left). The center SEM in Fig. 13 shows the beginning of crystallization, while the right shows an almost fully formed crystalline ceramic.

The effect of particle size of the slurry can be observed in Fig. 14. Here, the deposits are made from the same glass, with the different particle size distributions in the slurry obtained by fractional settling. The firing conditions are those that usually result in complete crystallization of the

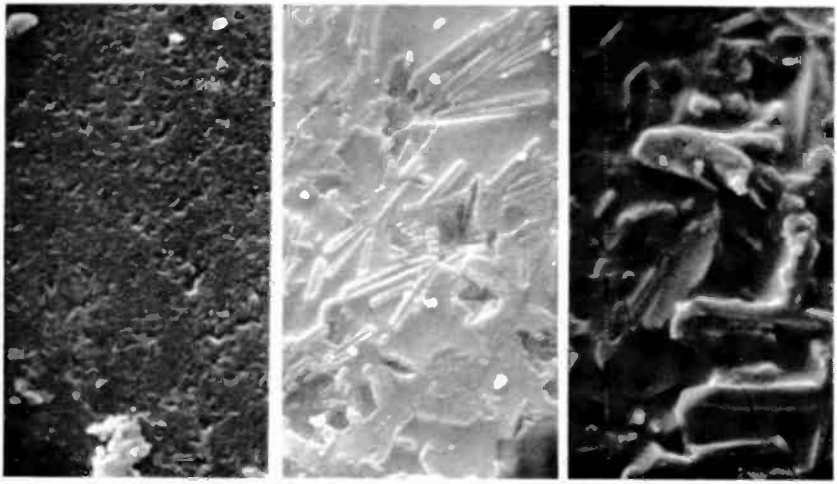

Fig. 15—Continued crystallization upon reheating (undesirable). Left photo shows the original; center, after 5 minutes refiring at 850°C; and right, after 3 hours at 850°C. (1000X)

ceramic. Note in Fig. 14 that the coarse particles (greater than 10 μm) fired to give a ceramic that has a structure containing vestiges of the original particles. This is believed to occur for two reasons: (1) the glass doesn't have time enough to melt and level before sintering and crystallization occurs and (2) the iron substrate oxidizes because of the

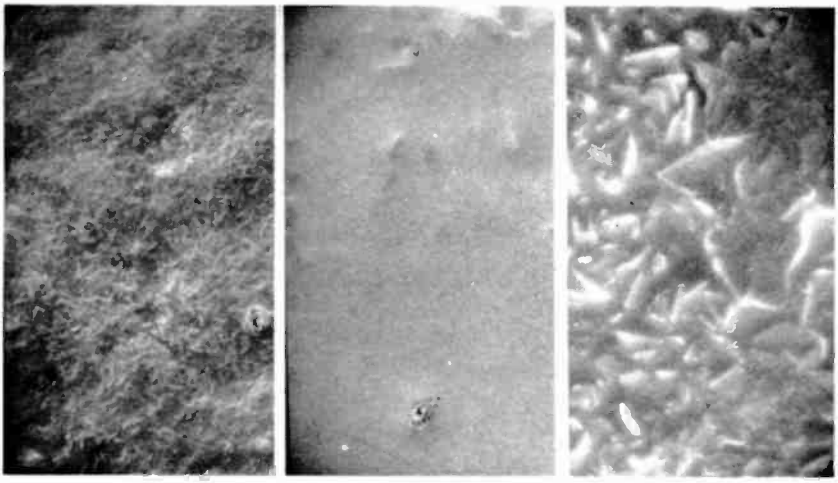

Fig. 16—Remelting after original crystallization, followed by a second crystallization (undesirable). Left photo shows the original; center, after 5 minutes refiring at 850°C; and right after 3 hours at 850°C. (1000X)

"open" character of the particles. This oxide surface apparently is not easily wet by the glass, thereby discouraging spreading of the liquid glass. Also veins of iron-rich glass are observed (inset). For glass of fine particle size (less than 10 μm), as shown in Fig. 14 (top) there is rapid melting/sintering of the surface. A continuous glass film forms and crystallizes, but because of the multiplicity of nucleation sites, a very fine-grained crystalline structure results.

Different glass compositions respond to reheating in ways that depend on the rate of crystallization and recrystallization. After the ceramic is formed, it may continue to crystallize upon reheating, resulting in a change in surface topography. Fig. 15 shows this in system 36 for various post-crystallization heating times at 875°C. These changes of structure are undesirable, because they may cause a loss of adhesion of other inks. Additionally, in this system, the diffusion of iron from the substrate in ferrous oxidation state continued with post firing. The ferrous iron, a reducing agent, reacted with many of the metal-oxide components of the resistor inks, which is of course undesirable. Fig. 16 shows another system in which post-heating resulted in complete melting of the original ceramic followed by another crystallization, which is also unsatisfactory. Fig. 17 shows System 72, which has desirable reheat characteristics; it

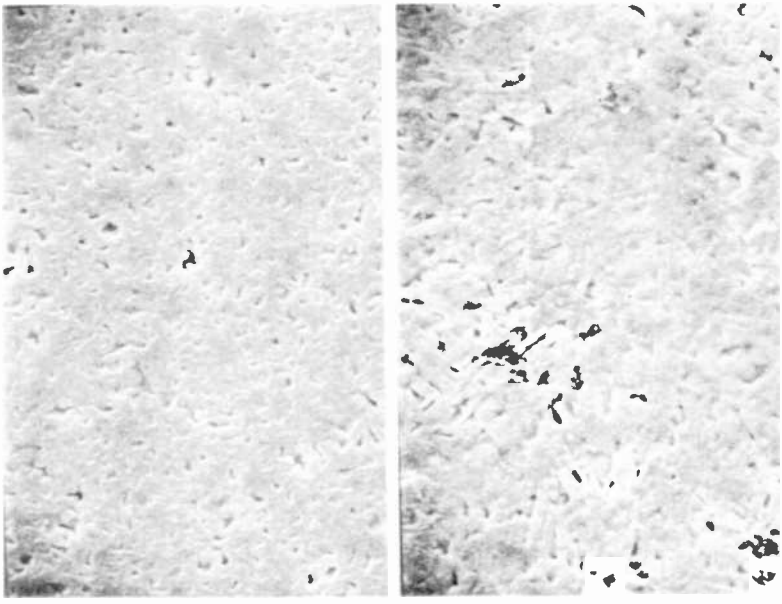

Fig. 17—Desirable reheat characteristics. The surface is structurally unchanged after 18 hours at 850°C (left is original). (1000X)

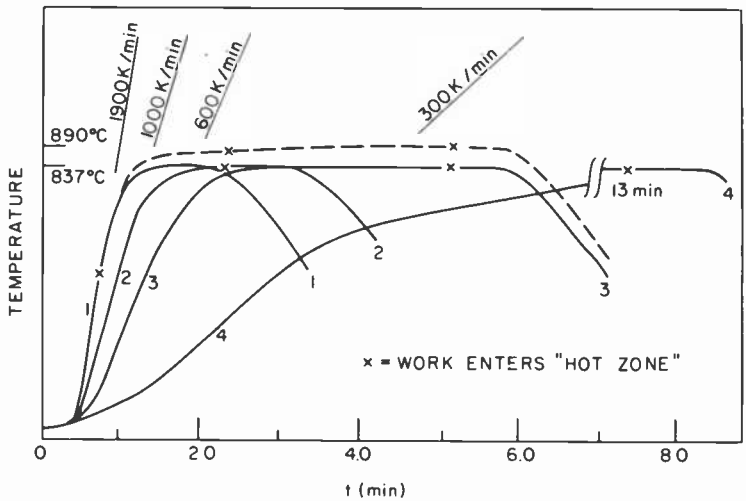

Fig. 18—Heating rates as determined for different furnace temperatures and belt speeds.

is topologially unchanged after 18 hours at 850°C. Such stability of structure is a necessary prerequesite for an enamel system but is not sufficient, since the substrate must also not interact adversely or in any uncontrolled fashion with any of the layers that are fired on subsequently. Several such post-firings are necessary to produce a circuit, and a satisfactory system is usually the result of many iterations of compositions and processing variables.[3]

An investigation of heating rates and temperature was made to find how much of a processing "window" is available with a desired substrate composition. For System 72, for example, satisfactory results (as determined by satisfactory performance of the overall system) were obtained for the range of temperatures and heating rates shown in Fig. 18. The temperatures are measured at the center of a (uncoated) plate of the same size as the work. Most of the heating is by radiation. There is a maximum heating rate for each temperature, but over the range studied, no differences could be resolved.

Acknowledgments

The authors would like to acknowledge the continuing technical interchanges with Ken Hang and Ashok Prabhu, and the superb scanning electron microscopy work of Ben Seabury. Much of the instrumentation was designed by the late Gerry Lozier.

References:

[1] C. P. Gutierrez, J. R. Mosley, and T. C. Wallace, "Electrophoretic Deposition: a Versatile Coating Method," *J. Electrochem. Soc.*, **109**, p. 923 (1962).

[2] L. S. Onyshkevych, "Porcelain-Enamelled Boards for Electronic Applications," *RCA Rev.*, **42**, p. 133 June 1981 (this issue).

[3] A. N. Prabhu, K. W. Hang, E. J. Conlon, and S. M. Boardman, "Optimization of RCA Porcelain Composition for Compatibility with Thick Films," *RCA Rev.*, **42**, p. 221, June 1981 (this issue).

[4] K. W. Hang and J. Andrus, "High-Temperature Porcelain-Enamel Substrates-Compositions and Interface Studies," *RCA Rev.*, **42**, p. 159, June 1981 (this issue).

[5] S. Stotz, "Field Dependence of the Electrophoretic Mobility of Particles Suspended in Low-Conductivity Liquids," *J. Colloid and Interface Sci.*, **65**, p. 118 (1978).

[6] F. Beck "Fundamental aspects of Electrodeposition of Paint," p. 1 in *Progress in Organic Coatings*, **4**, Elsevier, Lausanne (1976).

[7] H. Van Olphan, *Clay Colloid Chemistry* 2nd Ed. Wiley, New York (1977), Chap. 3, "The Theory of the Stability of Hydrophobic Sols."

[8] B. V. Deryagin, N. A. Krotova and V. P. Smilga, *Adhesion of Solids*, Chapter VIII, Consultants Bureau, New York (1978).

[9] A. Kitahara, "Zeta Potential in Non-aqueous Media and its Effect on Dispersion Stability," p. 81 in *Progress in Organic Coatings*, **2**, Elsevier, Lausanne (1973).

[10] H. van Olphen, *Clay Colloid Chemistry*, 2nd Ed., J. Wiley and Sons, New York (1977), Chap. 4, "Successes of the Theory of Stability—Further Theories and Refinements."

[11] H. Koelmans and J. Th. G. Overbeek, "Stability and Electrophoretic Deposition of Suspensions in Non-aqueous Media," *Disc. Faraday Soc.*, **18**, p. 53 (1954).

[12] W. B. Shook, "The Ceramic-Metal Interface," *Proc. Porcelain Enamel Inst.*, **41**, p. 105 (1979).

Electrical Properties of RCA Porcelain-Enamelled Steel PC Boards

B. J. Thaler, J. H. McCusker, and J. P. Honoré, III

RCA Laboratories, Princeton, NJ 08540

Abstract—The electronic properties of RCA porcelain-enamelled substrates are reviewed in this paper. The electrical resistivity, dielectric strength, capacitance, and dielectric loss were all studied. Additionally, the environmental stability of the dielectric loss and dielectric strength were investigated. Particular emphasis was placed on the properties that are significantly influenced by minor composition modifications. These results served as guidelines for development of porcelain formulations.

1. Introduction

To gain widespread acceptance within the consumer electronics field, a porcelainized steel substrate must be able to withstand repeated firings at 900 to 1000°C, and also be a high-voltage insulator. To attain the high-temperature refire stability, it was necessary to synthesize a partially devitrified glass instead of the usual amorphous porcelain used by commercial porcelainized steel substrate manufacturers. High-voltage insulating qualities were attained by only using alkali-free materials. These two properties have been incorporated in a family of porcelain compositions having electrical properties that are significantly different from those of commercial electronic porcelains. This paper examines these electrical properties and their material dependence. The details of the material preparation have been described elsewhere.[1,2]

2. DC Electrical Resistivity

When porcelainized steel substrates are used as printed circuit boards in consumer electronics applications, it is expected that the boards will have thick-film conductor (most likely a copper base) patterns, and the operating temperatures will be below 150°C. The following resistivity measurements were intended to observe the response of the RCA porcelain under such conditions.

Electrical conduction in ceramics is generally governed by ionic conduction. If the electrodes cannot replenish ions depleted by movement due to the applied electric field, an internal electric field is set up in opposition to the applied field and the electrical resistivity increases. It is expected that Cu or steel electrodes will cause such effects. Furthermore, since these porcelains are not single crystals, these materials will also exhibit a time dependent (decaying) absorption current,[3] suggesting the formation of one or more internal space charge regions.

All resistivities described in this paper were measured with 500 volts applied across the porcelain, and the specimens resided in a chamber having a positive, dry N_2 pressure (for all room-temperature measurements) to minimize humidity effects. The voltage was applied between a thick-film Cu cover electrode and the steel ground plane. Upon application of the voltage across the sample, a transient current that was several orders of magnitude larger than the "steady state" current necessitated allowing the samples to stabilize overnight before noting the "steady state" current of 0.1-1 pA. Fig. 1 shows the initial stages of this transient, which is indicative of the formation of space-charge regions in the porcelain.

The temperature dependence of the dc electrical resistivity may provide some clues to the conduction mechanisms. The electrical resistivity of a 5.7-mil-thick specimen of porcelain formulation #78 (refired 10 times at 900°C in an N_2 atmosphere) was measured between 25 and 150°C in a forced-air laboratory oven. Fig. 2 shows an Arrhenius plot of the resistivity of porcelain #78. It is quite clear from this plot that the activation energy is quite a bit less than 0.8 eV, the normal value for porcelainized steel substrates and some high-voltage porcelains.[4] This means that the electrical conduction mechanism is not limited by alkali ion diffusion. It appears that, once formed, the space-charge region at low temperatures ($T < 150$°C) is relatively stable with respect to temperature.

When porcelainized steel substrates are fabricated, the porcelain is deposited on the bare steel and then fired in air. Thus an iron oxide interface is formed that is highly conducting relative to the porcelain. The

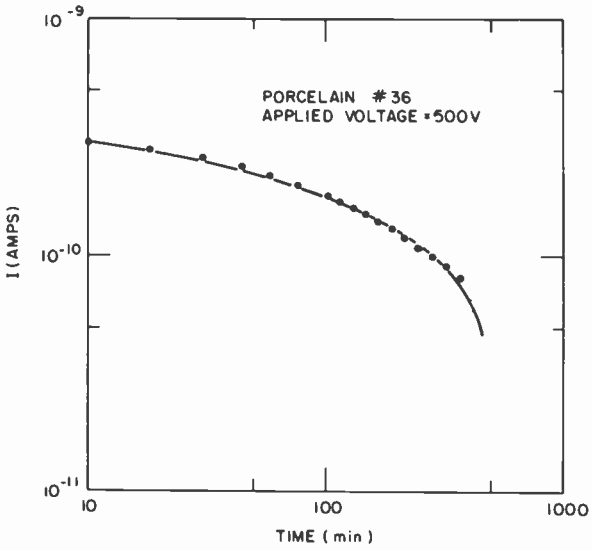

Fig. 1—Initial stages of the current transient upon voltage application to a porcelainized steel substrate.

porcelain, therefore, must be deposited to a thickness that will contain this iron oxide layer, but yet maintain the insulating qualities required for a printed circuit board.

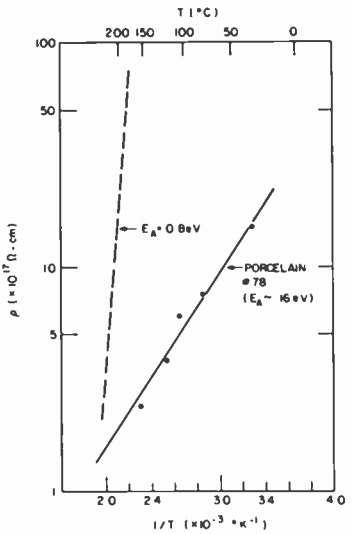

Fig. 2—Log of the resistivity as a function of the reciprocal of the absolute temperature.

Electrical resistivity measurements on substrates having different porcelain thicknesses provide a very effective tool for determining the thickness of the electrically active region. Measurements were performed on porcelain formulation #36, a porcelain that permitted the largest amount of iron diffusion of all the porcelains studied.[5] The cover electrodes were 1-inch square, thick-film copper conductors (DuPont #9923) fired at 850°C in an N_2 atmosphere. Fig. 3 shows the results of measurements made at room temperature. The resistivity is relatively independent of porcelain thickness for thicknesses greater than 4.5 mils; indicating that the highly conducting iron oxide and the Cu thick-film ink do not penetrate more than about 4.5 mils into the porcelain. One should also note that the resistivity of the thicker porcelain samples is approximately 10^{18} Ω-cm, which is comparable to or better than many high-voltage-grade porcelains.[4]

3. DC Dielectric Strength

A study was performed to determine the effect of porcelain thickness on the dielectric strength of porcelainized steel substrates prepared with well controlled deposition and metal preparation processes.[6] Porcelain

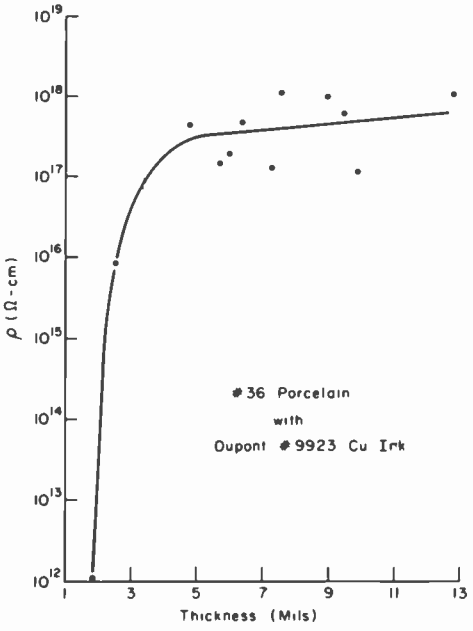

Fig. 3—Resistivity as a function of the porcelain thickness of a porcelainized steel substrate.

compositions included in this study were #36, #72, #75, #76, and #78.

The #36 porcelain specimens were prepared by screening a 1-inch square top electrode (DuPont #9923 thick-film Cu ink) onto the porcelain and firing at 850°C (in an N_2 atmosphere). Specimens of the other compositions were all fired first at 850°C and then at 950°C (both in an N_2 atmosphere) to complete the recrystallization process, and the specimens were not metallized. Instead, these specimens were placed in a holder that pressed 1.5-inch diameter copper electrodes against the porcelain. In all cases, the high voltage was applied to the Cu electrodes and the steel was grounded. Porcelain thickness was determined with an Elecometer Magnetic Thickness Gauge. The high voltage was raised in 500 volt steps, with the specimens remaining at a given step for 5 minutes, unless the specimen exhibited high-voltage breakdown. High-voltage breakdown is defined as visible arcing or detectable current spikes (~100 μA). The maximum voltage applied was 4 kV, and if a sample did not exhibit breakdown, this voltage was applied for at least half an hour.

Fig. 4 shows the breakdown voltage as a function of porcelain thickness. No obvious compositional dependence of the breakdown potential is apparent. The figure also shows that porcelain thicknesses greater than 6 mils should be able to support a 3 kV stress and seem to be capable of supporting more than 4 kV.

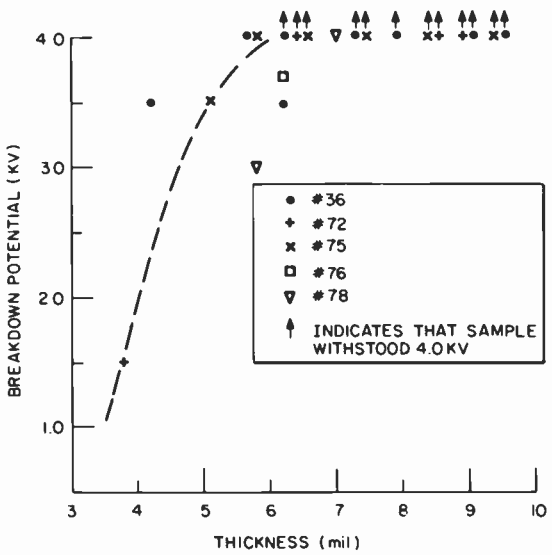

Fig. 4—Dielectric strength as a function of the porcelain thickness of a porcelainized steel substrate.

4. Dielectric Properties

When a circuit is designed for use on a porcelainized steel substrate, the engineer must take into account the capacitance of the substrate to ground as well as the dielectric loss* of the porcelain. The dielectric constants of all members of the RCA porcelain family are in the range of 7.5–8.5. Fig. 5 shows the effect of temperature on the dielectric constant of #78 porcelain; from this figure we calculate a thermal coefficient of capacitance of about 300 ppm/°C. By contrast, the dielectric loss is very sensitive to composition, as will be discussed later, because the RCA porcelains are all made of partially devitrified glasses and not amorphous glasses.

Except for porcelain #72 (with no additives) and the amorphous #75 specimen, all specimens employed in the studies described in this section were pieces of porcelain that had chipped off the steel substrates during the glass recrystallization firing step, leaving an iron oxide layer on the back of the porcelain. The #72 (with no additives) specimen was made from a much more finely divided glass powder and was fired on a Pt, not steel, substrate. The amorphous #75 specimen was a slab made by melting the glass at a temperature below its recrystallization temperature. This specimen was approximately 27 mils thick, while the devitrified glass ones were 6–10 mils thick. All the partially devitrified glass samples were subsequently fired (in an N_2 atmosphere) at 850°C and then at 950°C to "complete" the recrystallization process. Finally, 3000 Å thick Cu electrodes were evaporated onto the porcelain; the electrodes

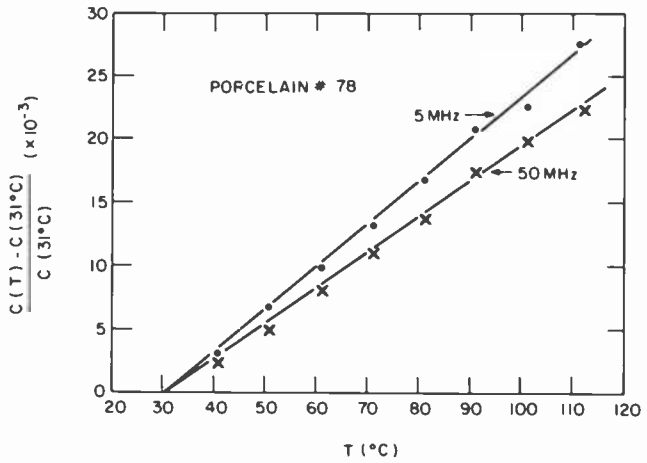

Fig. 5—Thermal variation of the capacitance of porcelain #78.

* For a general discussion of dielectric constant and dielectric loss see, e.g., Ref. [3], p. 686 ff.

were either 1/4, 3/8, or 1/2 inch diameter circles. Leads were then soldered to the electrodes. The dielectric properties of these porcelain chips are the same as those of porcelainized steel substrates having a thick-film Cu cover electrode. Capacitance and dielectric loss were measured between 10 kHz and 50 MHz using commercial LCR meters or admittance bridges.

Fig. 6 shows the effect on dielectric loss, for the same composition, of initially firing the porcelain above or below the glass recrystallization temperature. Q, the reciprocal of dielectric loss (tan δ), is plotted in this figure as a function of frequency for these two conditions. The amorphous material shows a significantly higher Q than the partially devitrified material for three reasons:

(1) The amorphous and crystallized regions of the partially devitrified porcelains are likely to have different chemical compositions than the totally amorphous porcelain.
(2) The dielectric properties of a material are determined by the local electric fields, which are in turn determined by the *local* atomic order; so crystalline materials can behave quite differently than their amorphous counterparts. Thus, devitrified glasses might be expected to have their own unique properties when compared to their amorphous counterparts.
(3) The residual material from nonstoichiometric mixtures, as well as any impurities, are likely to end up in high concentrations in the

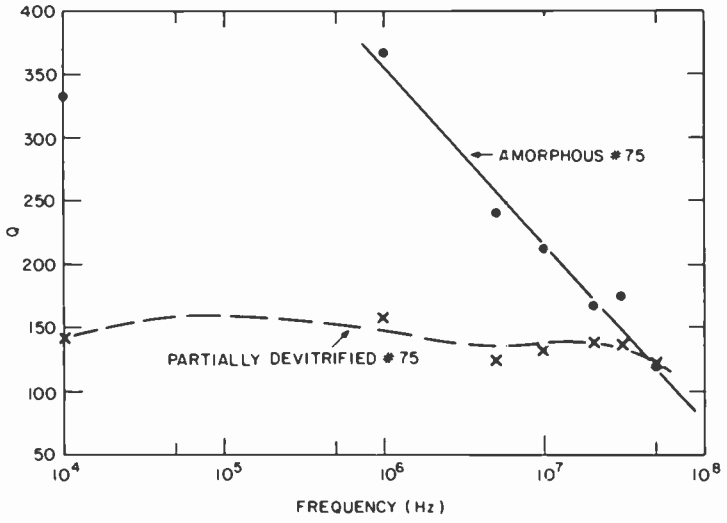

Fig. 6—Effect of crystallization of the Q versus frequency characteristics of porcelain #75.

grain boundaries of the devitrified porcelain. The grain boundaries can be quite conducting, causing a decrease in Q.

Also, the microstructure of the porcelain, which can significantly influence the dielectric loss of the material, is intimately connected with the crystallization kinetics of the glass mixture. Small composition changes and minor component additions (1–5%) can profoundly influence the crystallization kinetics and, therefore, ultimately affect the dielectric loss. In addition, minor material additions can act as fluxes, washing all residual components and impurities into the grain boundaries where they become highly concentrated. Sometimes these grain boundaries are quite conducting compared to major phases in the porcelain and degrade an otherwise electrically acceptable porcelain. It is clear, therefore, that the dielectric loss characteristics of a devitrified glass can be expected to be a rather sensitive material property.

Fig. 7 shows room temperature plots of Q versus frequency for several porcelains that differ only by minor component modifications. Although quantitatively different, all porcelains show qualitatively the same frequency characteristics, indicating that the frequency variation of the RCA family of porcelains is primarily determined by the major component phases. However, this figure also shows that small composition changes can change Q by a factor of 3; which can be the difference between a high-grade and a low-grade electrical substrate. The difference between porcelains #72 and #75 stems only from a change in reaction

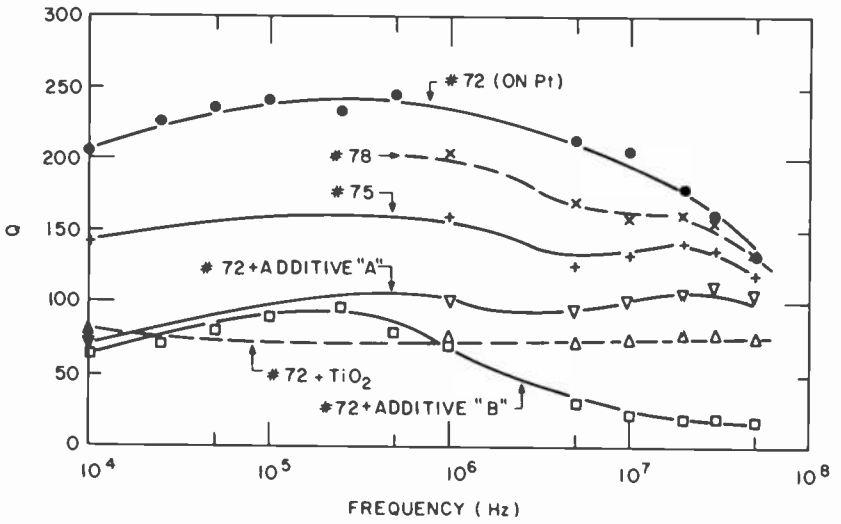

Fig. 7—Effect of composition on the Q versus frequency characteristics of some partially devitrified porcelains.

kinetics, since both of the materials contain only the 4 basic constituents of RCA porcelain and no minor additives. The effect of changing the reaction kinetics and incorporating a minor phase into the porcelain is illustrated in Fig. 7 by the #72 + an additive and the #78 specimens. The low Q values of the #72 + TiO_2 specimen in the figure results because TiO_2 is a strong flux for these types of glass systems, and thus all residual material is swept into the grain boundaries, degrading the Q of the porcelain.

5. Environmental Stability

The solubility of ceramics in water cover the range from quite soluble to almost insoluble. Since porcelain-enamelled steel printed-circuit boards must maintain their good insulating qualities for a period of many years, often in very humid environments, the porcelain must possess a resistance to water leaching. Since it only takes a very small number of conducting paths to completely degrade a good insulator, one must insure that all phases of the porcelain, both major and minor, are resistant to water absorption and leaching at all operational temperatures. To this end, a study was conducted to observe the influence of small porcelain composition changes on the degree of humidity degradation of dielectric loss and dielectric strength; also, several organic overcoats were tested to determine the amount of protection which they provide.

Unless noted, all samples were porcelain-enameled substrates[6] containing four thick-film Cu cover electrodes (1/4-, 3/8-, 1/2-, and 1-inch diameter circles); the substrates were fired at 850°C and 900°C (in an N_2 atmosphere) to fire the thick-film ink and also to "complete" the porcelain recrystallization; finally organic overcoats were applied to the 1/4- and 3/8-inch electrodes, with only a small area of Cu exposed for voltage application.

Specimens referred to as chips were prepared according to procedures outlined in Sec. 4 (Dielectric Properties). All specimens were aged in a temperature-humidity chamber that maintained an atmosphere of 51 ± 1°C with 84 ± 5% relative humidity. After removal from the chamber, the specimens were allowed to equilibrate at ambient atmosphere for one hour before any measurements commenced.

Fig. 8 shows the effect of humidity aging on Q for several members of the RCA porcelain family. Of the formulations shown in this figure, only formulation #75 is totally made up of the four major components; all of the other formulations contain minor additives (1–3%). Of the formulations shown in Fig. 8, only formulations #72 + Additive B and #75 exhibit catastrophic degradation. Furthermore, it should be noted that the application of an organic overcoat did *not* significantly retard the

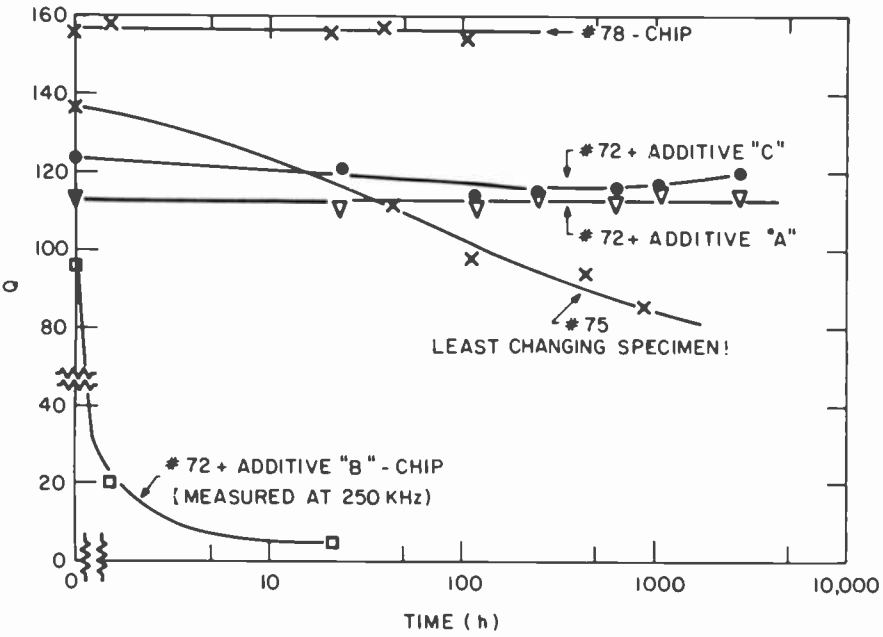

Fig. 8—Effect of composition on the environmental stability of *Q*. Unless noted, *Q* was measured at 30 MHz.

degradation of *Q* for #75 porcelain. The data shown in the figure reinforces the idea that *all* phases of an electronic grade porcelain must be resistant to water leaching. The fact that minor additives can be added to the porcelain mixture and produce superior humidity resistance suggests that either the additive forms a corrosion resistant coating over the entire substrate, or that a leachable minor phase of the four component mixture has been eliminated in favor of a new insoluble phase in the new mixture. Additional work is needed to uncover the mechanism responsible for the superior humidity resistance.

We also sought to observe the effect of humidity aging on the dielectric strength of the porcelain. The dielectric strength measurements were made by applying a dc voltage across the sample and monitoring the current flowing through the sample. Breakdown was defined as steady currents, or current spikes in excess of 1 μA. The voltage was applied for 5 minutes at each 500-volt increment, and if breakdown did not occur, the voltage was ramped to the next increment at a rate of 5 volts/sec, to a maximum of 4 kV, which was then applied for an additional 32 minutes. Aside from porcelain #75, only a small minority of the specimens showed any humidity degradation after 2000 hours of exposure to 50°C and 85% relative humidity, and none of the specimens in this group broke down at the organically overcoated electrode (the $\frac{1}{4}$-inch diameter cir-

cle). In contrast, of the six #75 porcelain electrodes, which initially withstood 4 kV, all but two electrodes (which happened to have organic overcoats) exhibited breakdown at greatly reduced voltages after 433 hours of exposure. It should also be noted that several of the #75 samples failed by exhibiting a steady leakage current that varied ohmically, in contrast to all other compositions which failed by exhibiting large current spikes above a threshold voltage. These failure modes are consistent with our hypothesis that #75 porcelain contains a minor phase that is leachable; properly chosen additives will eliminate this problem. Additionally, dielectric loss of this composition showed significant degradation after 50–100 hours (see Fig. 8), well in advance of high voltage breakdown (after 175–430 hours).

6. Conclusions

The electrical properties of the RCA family of high temperature porcelains have been studied. The data reported in this paper were obtained on small sample lot sizes. The test results show that the dc electrical resistivity is quite high and is not limited by alkali ion diffusion, as is the case with many electronic grade porcelains. Furthermore, the dielectric strength of these porcelains is quite good, probably because of the high resistivity of these material. The dielectric constants of the porcelain are in the range of 7.5–8.5, with a temperature coefficient of capacitance of about 300 ppm/°C. The dielectric loss of these devitrified glasses is a very sensitive material property, and small modifications can change this parameter by a factor of three. Minor composition modifications also have been shown to vastly improve the porcelain's resistance to environmental degradation. Therefore, the RCA porcelain family seems to meet the requirements of the consumer electronics industry, and shows the potential for being highly reliable substrates.

Acknowledgments

This work was performed within the Electronic Packaging Research Group (L. S. Onyshkevych, Group Head), in the Consumer Electronics Research Laboratories (D. D. Holmes, Director). We wish to thank K. W. Hang, A. N. Prabhu, and A. Sussman for many helpful discussions throughout this work, T. Ward for supplying the porcelain coated specimens, W. Anderson for preparing the glass compositions, and S. Boardman for printing and firing the thick film conductor patterns. The help of B. Halon and D. Hoffman in the evaporation of thin film electrodes is also acknowledged. M. Hamilton also made an important contribution to this research effort. Many other people, too numerous to mention individually, contributed to the success of this project.

References:

[1] K. W. Hang and J. Andrus, "High Temperature Porcelain-Enamel Substrates—Compositions and Interface Studies," *RCA Review*, **42**, p. 159, June 1981 (this issue).

[2] A. Sussman and T. Ward, "Electrophoretic Deposition Coatings from Isopropanol/Glass Slurries," *RCA Review*, **42**, p. 178, June 1981 (this issue).

[3] W. D. Kingery, *Introduction to Ceramics*, John Wiley and Sons, Inc., New York (1960), p. 659.

[4] H. Gibson and J. P. Ballard, "Some Effects of Long Term DC Stress on Porcelain Insulators Operated at High Temperature," *J. Mat. Sci.*, **7**, p. 303 (1972).

[5] A. N. Prabhu, K. W. Hang, E. J. Conlon, and S. M. Boardman, "Optimization of RCA Porcelain Composition for Compatibility With Thick Films," *RCA Review*, **42**, p. 221, June 1981 (this issue).

[6] The samples studied did not have optimal porcelain to steel adhesion, since the adhesion studies were performed concurrent with the high voltage studies. It is expected that good adhesion will improve the high voltage characteristics.

Mechanical Properties of RCA Porcelain-Enamelled Steel PC Boards

W. Tsien, J. McCusker and B. Thaler

RCA Laboratories, Princeton, NJ 08540

Abstract—Mechanical properties and interfacial adhesion of porcelain-enamelled-steel substrates were investigated. Four-point bend, three-point bend, torsion, and ball-and-ring tests were used to measure semiquantitatively the degree of adhesion. The four-point bending results were used to obtain a simple failure model. The thermal flow characteristics of the porcelainized-steel substrate were also investigated, both for resistor and transistor thermal heating.

1. Introduction

Porcelain enamels are strong in compression but weak in tension. Under moderate tensile stresses, they will fail with glass-like fractures. The sources for crack propagation under stresses include microcracks, surface imperfections, mechanical abrasion, and chemical etching of the surface. Once a crack has been initiated, a tensile stress can cause the crack to propagate.

In general, the fracture strength in ceramic materials is statistical in nature, depending on the probability that a flaw, capable of initiating fracture, is present under the applied stress. This is the common explanation of the great variance in the test results for the strength of ceramic materials. Also, since fracture strength is related to the volume of the material and the surface area under maximum stress, the observed results vary with the manner in which the test is conducted.

In this paper, we report on the mechanical testing of porcelains enamelled on carbon steel. These porcelain-enamelled-steel substrates were

developed at the RCA Laboratories for electronic applications. The substrates generally have a 0.030-inch low-carbon-steel core and a 0.0075-inch porcelain-enamel coating on both surfaces. The resultant substrate provides supports for electrical and mechanical components and surfaces suitable for thick- or thin-film technology. Testing methods to determine the degree of adhesion of porcelain and steel have been studied.

The last section of the paper reports on an investigation of the thermal characteristics of the substrates.

2. Thermal Stresses

To evaluate the results of adhesion tests for different porcelainized steel substrates, it is necessary to determine thermal stresses existing in the substrate. Since the thermal coefficient of expansion of the porcelain is normally chosen to be lower than that of the steel, the steel in the substrate is under thermal tension and the porcelain is under thermal compression after cooling from the firing temperature.

The thermal compressive stress in porcelain can be evaluated by the expression

$$S_p = \frac{(\alpha_s - \alpha_p)(T_F - T_R) E_p}{(1 - \mu)\left(1 + \frac{2t_p}{t_s}\frac{E_p}{E_s}\right)} \quad [1]$$

and the tensile stress in steel using the expression

$$S_s = Sp\,\frac{2t_p}{t_s}. \quad [2]$$

Here

α_s = thermal coefficient of expansion of steel = 14.4×10^{-6}/°C
α_p = thermal coefficient of expansion of porcelain = 13.0×10^{-6}/°C
T_F = firing temperature = 825°C
T_R = room temperature = 25°C
μ = Poisson's ratio = 0.25
t_p = thickness of porcelain = 0.0075 inch
t_s = thickness of steel = 0.030 inch
E_s = Young's Modulus of steel = 30×10^6 psi
E_p = Young's Modulus of porcelain = 18×10^6 psi

Young's modulus for porcelain, E_p, was determined by measuring the time of propagation of an acoustic wave through the porcelain length. PZT rods, which act as transducers, were used to generate and detect

Table 1— Velocity of Sound and Young's Modulus of Some Porcelain Compositions

Composition Number	Velocity cm/sec ($\times 10^5$)	*Ep* psi ($\times 10^6$)
26	5.74 ± .05	15.8 ± 0.3
36	5.43 ± .12	14.1 ± .6
67	5.79 ± .04	16.0 ± .2
69	5.95 ± .06	16.9 ± .3
69	6.16 ± .07	18.2 ± .4
70	5.61 ± .08	15.1 ± .4
70	5.84 ± .08	16.3 ± .4
72	6.10 ± .09	17.8 ± .5
73	6.02 ± .06	17.3 ± .3
74	6.2 ± .04	18.4 ± .2
75	6.08 ± .1	17.5 ± .6

mechanical waves. For steel, the velocity of sound was found to be 5.15×10^5 cm/sec, implying a Young's Modulus of 30×10^6 psi at room temperature.[1,2] No velocity change was observed at temperatures up to 100°C, either for steel or for porcelain samples. Table 1 shows the measured value of velocity and the calculated value of Young's Modulus for different porcelain compositions.[1]

Using the above constants in Eqs. [1] and [2], the thermal compression in porcelain is approximately 20,000 psi and the thermal tension in steel 10,000 psi. Different porcelain compositions have been made with a wide range of thermal expansion coefficients to control the thermal stresses.

3. Adhesion Testing

Adhesion of porcelain to the steel substrate can be a problem due to the intrinsic crystallization kinetics of the porcelain formulation. In processing of the usual amorphous porcelain, a strong interfacial layer can be formed by keeping the porcelain in the liquid phase for a sufficiently long time. Partially devitrified porcelain, however, recrystallizes rapidly at firing temperatures. To obtain good adhesion under this restriction, the steel must first be etched and then electroplated with nickel. The nickel plus the etching leads to good adhesion over a limited range of nickel thicknesses.[1]

Since poor adhesion means poor electrical and mechanical properties, failure under stresses, and separation of layers in refiring, it is desirable to at least semiquatitatively determine the degree of adhesion of the porcelain to the steel. Several different tests were used to evaluate the degree of adhesion, including impact testing, pull-push tests on cemented pieces, ball and ring testing, bend testing, and torsion testing.

3.1 Impact Testing

Impact testing was originally used to test adhesion. In the impact, or drop, tester (Gardner Laboratory), a known weight falls from various heights on a 5/8-inch-diameter vertical rod that, in turn, impacts the substrate being tested. In this case, the porcelain-steel-porcelain sandwich is mounted on a ring whose inner diameter is slightly larger than the diameter of the vertical rod.

One method of determining adhesion is to measure the threshold value in inch-pounds at which cracking or flaking occurred. The other method is to use an impact of known value and then assess the damage. The second approach is perhaps satisfactory when good adhesion has been obtained, but is not sensitive to small changes. Correlations were not made between the impact tester and other tests.

3.2 Pull-Push Test on Cemented Pieces

Attempts were made to measure the shear or tensile strength between porcelain and steel directly by cementing a metal piece to the porcelain surface and applying a pull or a push force to separate them. However, the cement used (epoxy or a low melting point glass) was not strong enough for the purpose. The failure point of the best cements was 3000 psi.

3.3 Ball-and-Ring Test

A simple ball-and-ring tester was made for use with the Instron Testing Machine, using a compression load cell. It consists of two parallel plates with a number of sets of holes in them. The test sample is inserted between the plates and a ball (running fit) is inserted into the top hole, directly above the "ring" hole in the lower plate. A compressive force is then applied to the ball, with the ring plate remaining stationary.

Fig. 1 shows the results of one set of tests applied to porcelain-steel boards with low or high adhesion. Other sets were tested with similar results. A 3/8-inch diameter ball was used because the sample pieces were small. To cause detectable cracking in a strongly adhesive porcelain requires twice the force needed for a weakly adhesive porcelain.

3.4 3-Point and 4-Point Bend Tests

The tensile strength of porcelain is usually measured by 3-point or 4-point bend tests. In a 3-point bend test, the maximum stress occurs along a line on the specimen surface opposite the middle support. Only a small

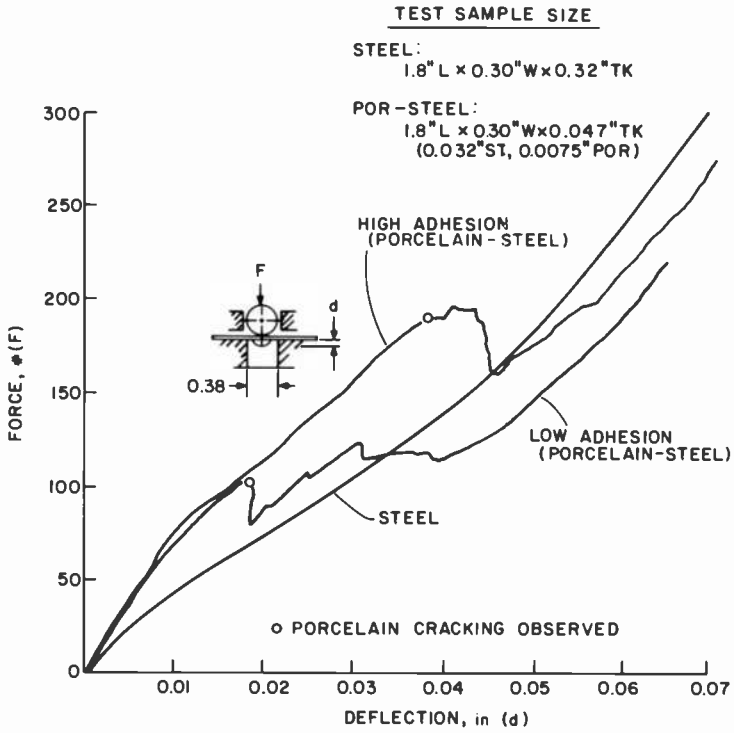

Fig. 1—Ball-and-ring test.

area under the load is subjected to maximum stress, and failures outside this limited area may not occur. In contrast, the 4-point bend test, which has a uniform bending moment between the two middle points, will reveal the substrate behavior over the whole area between the middle points.

The 3-point and 4-point bending test results are shown in Figs. 2 and 3, respectively. The 4-point bend test shows that twice as much force is required to cause detectable cracking for strongly adhesive porcelain as for weakly adhesive porcelain, whereas the 3-point bend test shows only 1-¼ times the force is required. However, the resultant stresses in porcelain at the cracking points are 20×10^3 psi tensile force for the 3-point bend test and about zero tensile force for the 4-point bend test.

3.5 Torsion Test

For this test, the porcelainized steel substrate was placed between a rotatable clamp and a fixed clamp (see Fig. 4). Since both the porcelain and steel were clamped, shearing stresses were set up in both porcelain

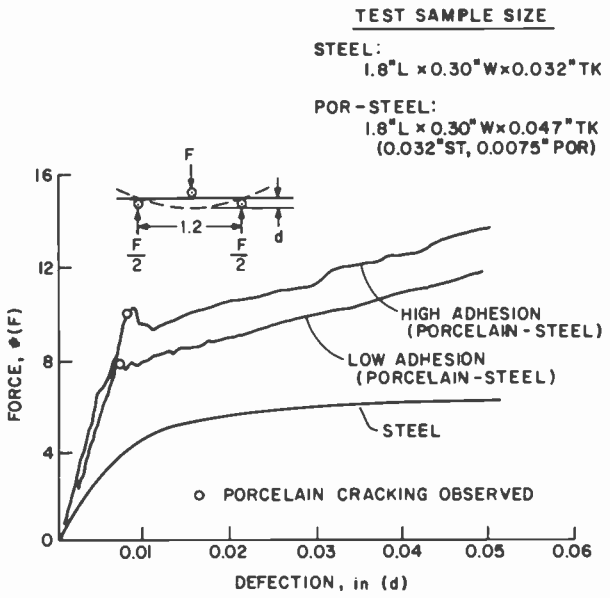

Fig. 2—Three-point bend test.

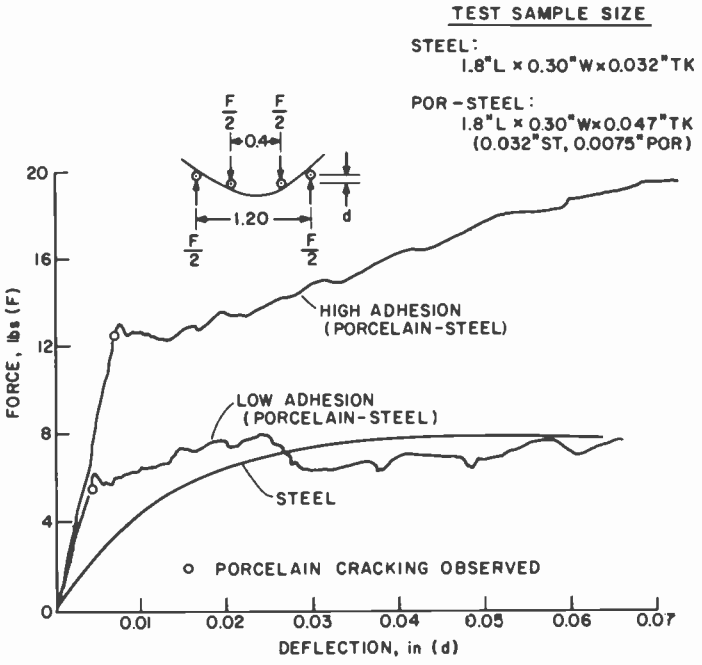

Fig. 3—Four-point bend test.

and steel as the sample was twisted. As can be seen in Fig. 5, about twice the force is required to cause detectable cracking for strongly adhesive porcelain as for weakly adhesive porcelain. It was also observed that substrates with low adhesion cracked into flakes along 45° lines, and that substrates with high adhesion cracked along very fine 45° lines with no visible flaking. The 45° lines indicate tension failure.

Table 2—Comparison of Adhesion Test Results for Two Different Porcelainized Steel Substrates

Type of Test	Force before Cracking Observed (lbs)		
	Specimen A	Specimen B	Ratio
3-point Bend Test	10.0	8.0	1.2
4-point Bend Test	12.2	6.0	2.0
Torsion Test	5.5	3.2	1.7
Ball-and-Ring Test	190	100	1.9

4. Conclusion On Adhesion Tests

Table 2 gives a comparison of results obtained from the various tests mentioned. With the exception of the 3-point bend test, all tests showed that about twice the force is required to cause detectable cracking for strongly adhesive (A) versus weakly adhesive (B) porcelainized steel substrates. All A or B specimens for different tests were made from a single piece of specimen type A or B.

Failure occurs in 4-point bending for porcelain when the tensile bending stresses are slightly larger than the thermal compressive stresses and for steel when the yield point is exceeded. The minimum bending radius is about 18 to 20 inches.

The degree of adhesion can be measured by 4-point bend tests, torsion tests, and the ball-and-ring tests. Poor adhesion reduced the failure limits by a factor of two in all tests except the 3-point bend test.

Samples with widely varying adhesion should be checked before and after refirings to determine loss of adhesion. The minimum final adhesion strengths should be such that the board should survive a drop test before and after assembly, packaging, shipping, and operation. In addition, shock tests at holes based on reasonable insertion procedures should be investigated.

5. Thermal Characteristics

The porcelainized steel substrate acts not only as a mechanical support for components but also as an isolated heat sink for thermal effects. The temperature of the substrate (exclusive of dimensional effects) is de-

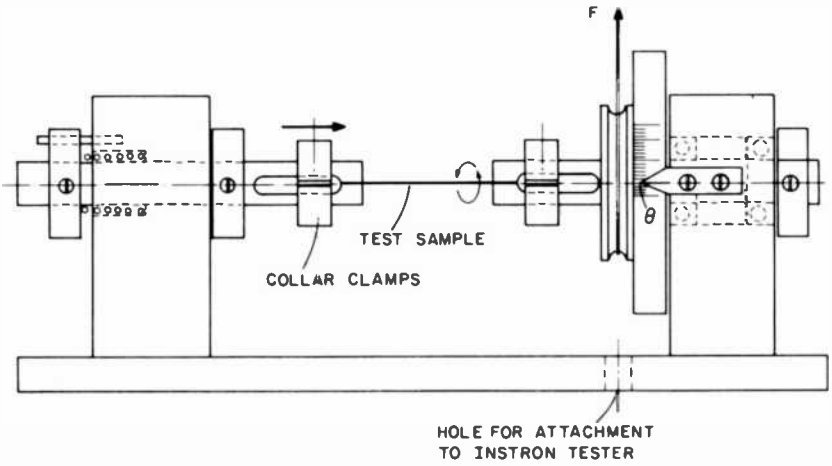

Fig. 4—Torsion tester.

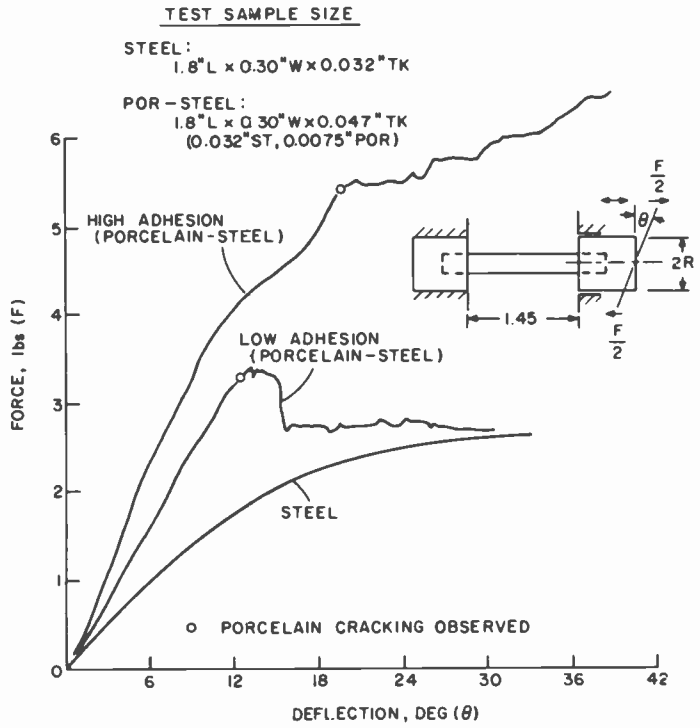

Fig. 5—Torsion test.

termined by the thermal conductivity of the board, its heat loss properties (convection and radiation), and by the thermal input.

The thermal conductivity of steel is about 0.7 W/cm/°C,[3] whereas that of porcelain is about 0.014 W/cm/°C.[4] As a basis of comparison, alumina is about 0.26 W/cm/°C.[5] The porcelain must therefore be thin (about 7 mils) to reduce the thermal drop. The steel must be thick (30 mils or more), both for better transverse thermal flow and for mechanical strength.

Radiation and convection are assumed to be the only heat loss mechanisms. The principal variable in the heat loss mechanisms is the emissivity, which is about 0.9 for porcelain.

The temperature rise on a 2 × 2 inch porcelainized steel substrate versus power input from a 1 × 1 inch thick-film resistor is shown in Fig. 6. The figure gives temperatures measured by 5-mil-diameter chromel-alumel thermocouples at the hot spot of the resistor, T_H, and at points ½-inch from the edges, as measured on the diagonal. These results are consistent with the thermal properties already stated for the porcelainized steel substrates as checked by finite element analysis.[6]

Measurements were also made of temperature versus power input for the same transistor (2N3055) mounted first on a porcelainized-steel and

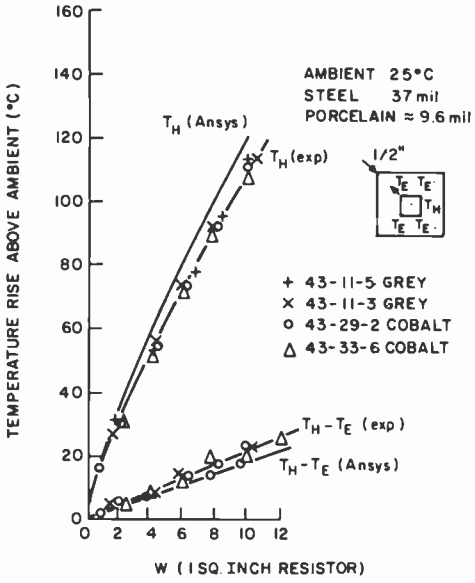

Fig. 6—Temperature rise versus power input (experimental and finite element analysis results).

then on an aluminum board. Temperature was measured using a thermocouple mounted on the outer wall of the transistor. Both substrates measured were 3 × 2½ inches, the aluminum being a section cut from a standard 1/16-inch aluminum chasis. The steel core is about half the thickness of the aluminum. As shown in Fig. 7, the wall temperature of the transistor was higher for the aluminum substrate than for the porcelainized steel substrate. This is because of the high emissivity of the porcelain. When the aluminum was painted, the wall temperature for the aluminum substrate was lower.

It was also desired to determine the temperature of a large porcelainized steel substrate with ¼ watt per square inch uniform heating to determine operating temperatures for moderate size boards and power. Since no large porcelainized steel substrates were available, a painted steel substrate (13-½ × 9 × 0.030 inches) was used. Fifteen 2-watt resistors were uniformly spread over the surface. As shown in Fig. 8, the average temperature for vertical mounting (short side vertical) was 50°C, 24°C above ambient temperature. For horizontal mounting, the average temperature was 7°C hotter.

The relatively good thermal response of the porcelainized steel substrates is primarily determined by the high emissivity of the porcelain and the moderately high thermal conductivity of the steel (about three times that of alumina) and by the thinness of the porcelain layer.

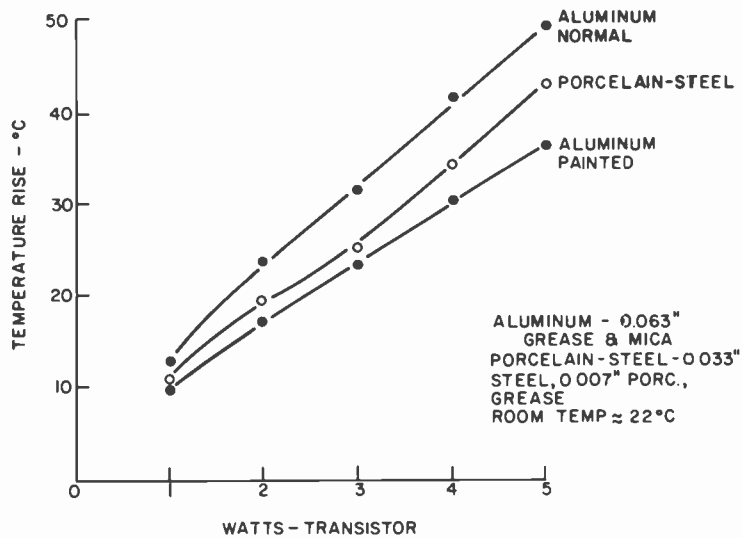

Fig. 7—Wall temperature of transistor mounted on aluminum and on porcelainized-steel substrates.

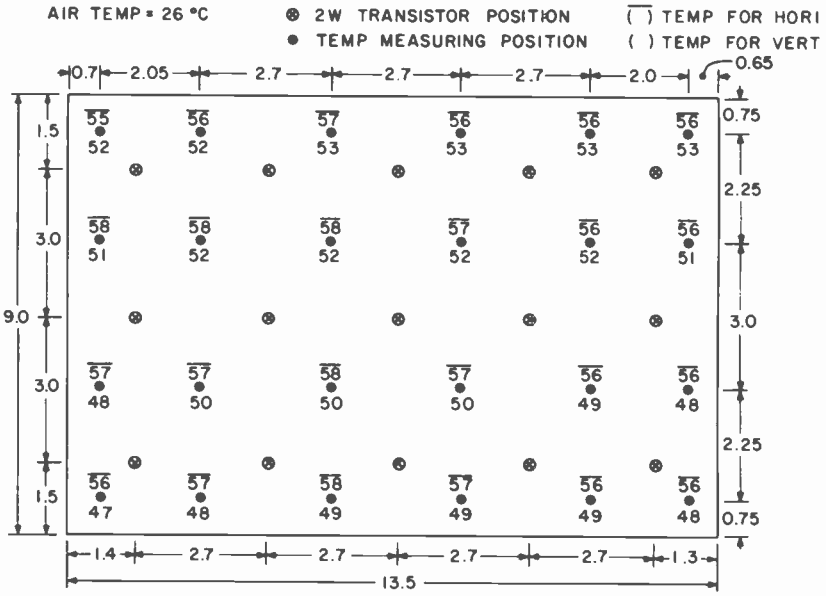

Fig. 8—Thermal distribution for 15 2-watt resistor heating. Top numbers (with bar over) are for horizontal and bottom figures are for vertical mounting.

Acknowledgments

This work was performed within the Electronic Packaging Research Group (L. Onyshkevych, Group Head) in the Consumer Electronics Research Laboratories (D. Holmes, Director). We wish to thank all members of this group for their cooperation, and in particular to thank T. Ward for supplying test specimens and K. Hang and J. Andrus for their helpful suggestions and demonstration of the adhesion tester of their own design.

References:

[1] K. W. Hang and J. Andrus, "High Temperature Porcelain-Enamel Substrate-Compositions and Interface Studies" *RCA Review*, **42**, p. 159, June 1981 (this issue).

[2] S. P. Timoshinko and J. N. Goodier, *Theory of Elasticity*, McGraw-Hill Book Co., New York, (1970).

[3] A. Goldsmith, T. Waterman, and H. Hirschhorn, *Handbook of Thermophysical Properties of Solid Materials*, Macmillan Co., New York (1961).

[4] E. Sichel, private communication.

[5] Coors Porcelain Co. Bulletin No. 955, 1976.

[6] J. McCusker, "Finite-Element Analysis of Stresses and Thermal Flow in Porcelain-Enamel PC Boards," *RCA Review*, **42**, p. 281, June 1981 (this issue).

Optimization of RCA Porcelain for Compatibility with Thick Films

A. N. Prabhu, K. W. Hang, E. J. Conlon, and S. M. Boardman

Abstract—Optimization of RCA porcelain coated steel substrates for compatibility with base-metal thick-film compositions is described in this paper. The interactions between thick films and several porcelain compositions were investigated by examining the microstructures of the fired films and the thick-film–porcelain interfaces and studying conductor film properties, such as conductivity, solderability, solder aged adhesion and wire-bondability, and sheet resistances of the base-metal resistor inks. Information obtained on each porcelain composition was utilized to tailor the composition of the next porcelain to obtain better compatibility with thick films. This process was continued until a porcelain-coated steel substrate that can be used for large-area thick-film hybrid circuits in consumer electronic applications was developed.

Introduction

The porcelain-coated steel substrate described in this issue of *RCA Review* can be used as a printed circuit board and/or a thick-film circuit substrate. If used in conjunction with non-noble metal thick films, it has the potential to make thick-film hybrid circuit technology cost effective in high volume electronic applications. The properties of the porcelain and the base metal thick film inks developed at RCA Laboratories for use on these substrates have been previously reported.[1–4] This paper deals primarily with the interactions between the thick films and several RCA porcelain compositions.

The copper conductor and SnO_2-containing resistor inks used for this study were formulated using glasses compatible with the porcelain. The base-metal resistor inks, described in the next paper in this issue of *RCA Review*,[4] are based upon certain other conductive ingredients and form a stable resistor system that is compatible over a wide sheet resistivity range with the copper conductor, cross-over dielectric, and overglaze compositions. SnO_2-containing resistor inks were formulated and used for this study because of their greater sensitivity to changes in the porcelain compositions.

During the initial stages of the development of the porcelain, com-

positional controls for reheat stability, electric properties and compatibility with the ink system were emphasized. The information obtained from the study of interactions between the porcelain and the thick film inks was used to optimize the porcelain composition to minimize these interactions. During the latter stages of the development of the porcelain, mutual compatibility between the porcelain, conductor, resistor and multi-layer dielectric interfaces was also achieved.

Process Conditions

The copper conductor and the SnO_2 containing resistor inks were formulated to be compatible with each other and with the porcelain. The inks were printed using 200 mesh and 0.0016-inch wire diameter stainless steel screens, dried in air at 125 ± 5°C for 5–15 minutes, and fired in nitrogen at a peak temperature of 900 ± 5°C. Firing was conducted in a 5 zone, Inconel muffle, BTU-Transheat belt furnace with a belt width of 6 inches. Total firing time was 30–35 minutes and the time at peak temperature was 4–6 minutes. The oxygen content of the nitrogen was determined using a Research Inc. Model 648A-5 oxygen monitor. The amount of oxygen in the nitrogen supply used for processing the inks was less than 10 ppm and the oxygen in the hot zone was typically 20–30 ppm as measured through the BTU installed sample port. The fired film thicknesses of the conductors and the resistors were 0.6–0.8 mil.

The microstructures of the fired films were examined using optical and scanning electron microscopy. The samples for the study of the interfaces between the conductor, resistor and the porcelain were prepared by cold mounting the substrate in an epoxy and metallographically sectioning the interface at a low angle so that an extended area could be examined. During the polishing, some grains of the porcelain were pulled from its surface. These areas, which appear as dark spots in the optical micrographs, do not indicate porosity.

The bulk resistivity of the copper film was calculated on conductor lines 2.5 inches long and 0.03 inch wide by measuring the sheet resistance using the four probe (Kelvin) technique and computing the cross-sectional areas of the Tallysurf plots using a Zeiss image analyzer. The solderability of the copper conductor was examined by measuring its contact angle with a 0.04-inch diameter 62Sn/36Pb/2Ag solder ball after it was melted on the film for 5 seconds at 215°C. The flux used was Kester 1544. The contact angle measurements were done on A-100, Rame-Hart contact angle goniometer system.

Adhesion of the copper film to the porcelain was measured on 0.1 × 0.1 inch copper pads using the soldered-wire peel adhesion test method. Annealed copper wires 0.032 inch in diameter were soldered to the copper

pads using Kester 1544 flux and 62Sn/36Pb/2Ag solder. Peel testing was performed on an Instron at 0.5 inch/minute crosshead speed. The wire-bondability of the copper film was studied using a Kulicke and Sofa ultrasonic wire bonder to bond 0.0015-inch diameter Al-1%Si wire to the copper films.

The compatibility of the base metal resistors with the porcelain and the copper conductor was investigated by examining their microstructure and by comparing the resistor values to those obtained on 96% alumina. The sheet resistance values were plotted as a function of the resistor aspect ratio. From the slope of the straight line obtained, the sheet resistivities were calculated for the resistor ink on various porcelain compositions. The properties of the thick films on various RCA porcelain compositions are described below.

Porcelain A

The properties of the base metal thick films on Porcelain A are described in Table 1. The conductivity of the copper film fired on this substrate is quite good. However, the other measured film properties are poor. The scanning electron micrographs of the porcelain shown in Fig. 1 indicate that the surface of the substrate is quite glassy from a liquid phase exuded from the surface and remains glassy after 2 firings at 900°C in nitrogen (Fig. 1B). This low viscosity of the glassy phase at the peak firing temperatures gives rise to blisters in the copper films, as shown in the opitcal micrographs of Fig. 2A. The optical micrograph of the cross-section of the conductor and porcelain (Fig. 2B) clearly shows bubbles under the copper film. These bubbles cause blisters in the copper films. The bubbles probably form due to the carbonaceous residue from the organic vehicle in the ink. The impressions left in the porcelain as a result of these bubbles are seen in Fig. 2C. In this SEMograph the copper pad has been separated from the porcelain. The reaction between the copper film and the porcelain gives rise to a thin layer of glass on the copper film. Because of this the solderability and the wire-bondability of the copper films are poor, as reported in Table 1.

The dependence of the base metal resistor values on aspect ratio is shown in Fig. 3. The sheet resistivity of this ink on porcelain A is com-

Table 1—Properties of Base-Metal Thick Films on Porcelain A

Conductivity: 50–60% of the bulk conductivity of copper.
Contact Angle between Solder and Copper Film: 140–150°, 5 seconds at 215°C, 62Sn/36Pb/2Ag solder.
Solder Peel Adhesion: 3.5 lbs, Copper pad size 0.1 × 0.1 inch.
Al Wire Bond Pull Strengths: 2–10 gms (Failures occur mostly due to bond lifts).
Sheet Resistivity of the Resistor Ink: 2946 kΩ/□.

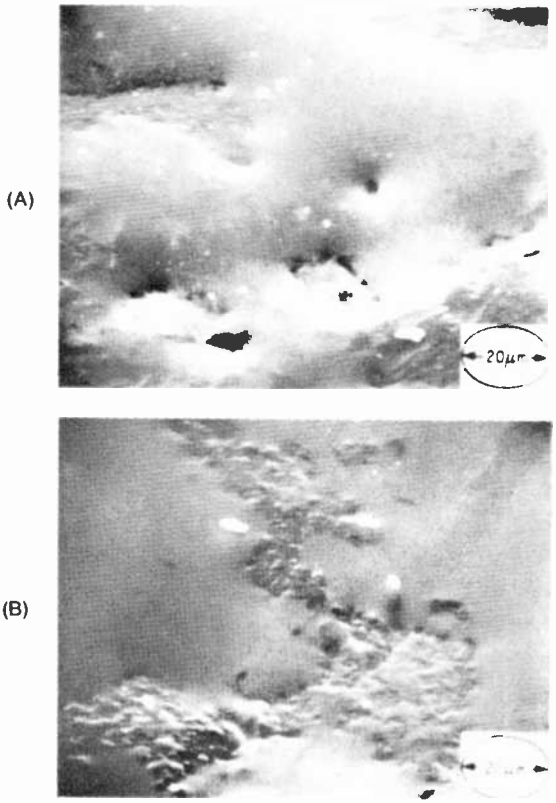

Fig. 1—Scanning electron micrographs of surface of porcelain A; bottom photo shows surface after two firings at 900°C.

puted to be 2946 kΩ/□ as compared to 24.6 kΩ/□ obtained on 96% alumina (Fig. 4). This high resistivity is due to considerable mixing between the low viscosity glassy phases and the resistor at the peak firing temperatures. It was clear from these observations that the crystal fraction of the porcelain had to be increased considerably and the remnant glass made more refractory in order to use it as a thick film substrate.

Porcelain B

The composition of porcelain B was formulated to provide a larger fraction of crystals during the initial firing of the deposited glass as compared to porcelain A. Scanning electron micrographs of the porcelain after one and after two firings are shown in Fig. 5. As can be seen in Fig. 5A, the porcelain surface is mostly crystalline. However, the reheat

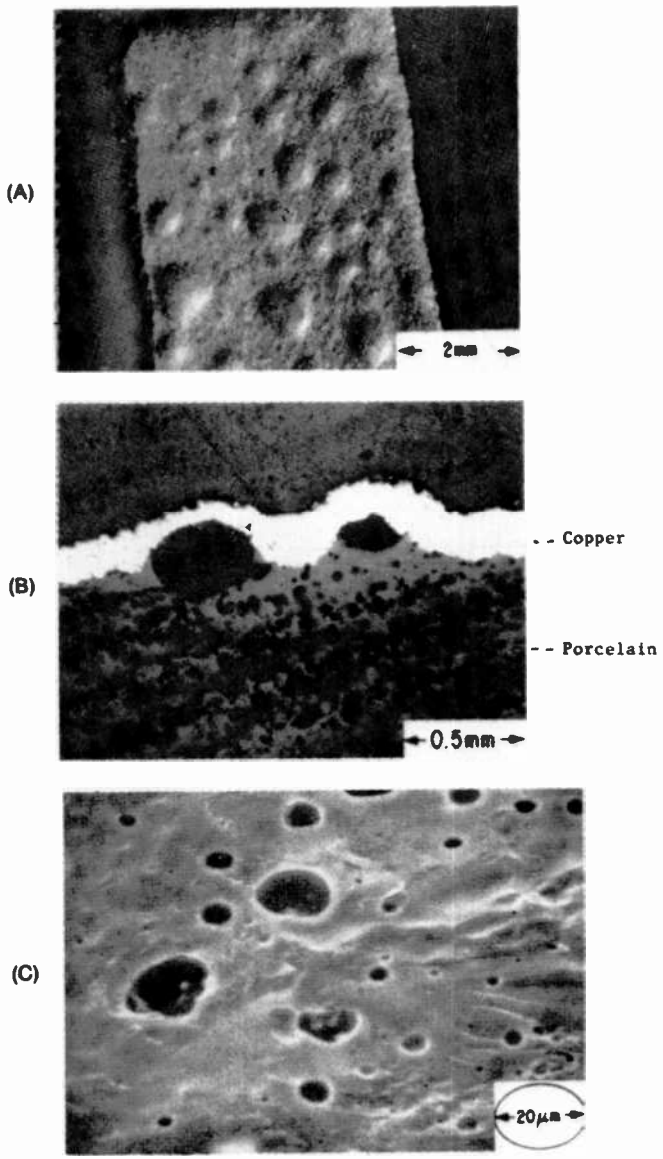

Fig. 2—(A) Optical micrograph of surface of copper film on porcelain A, (B) optical micrograph of cross section of copper–porcelain A interface, and (C) scanning electron micrograph of surface of porcelain A after separation of the copper pad.

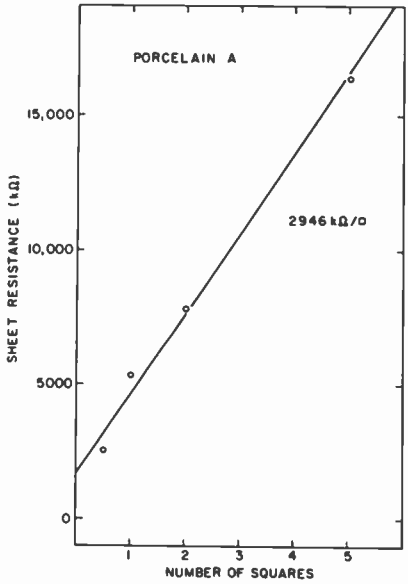

Fig. 3—Sheet resistance versus resistor aspect ratio (porcelain A).

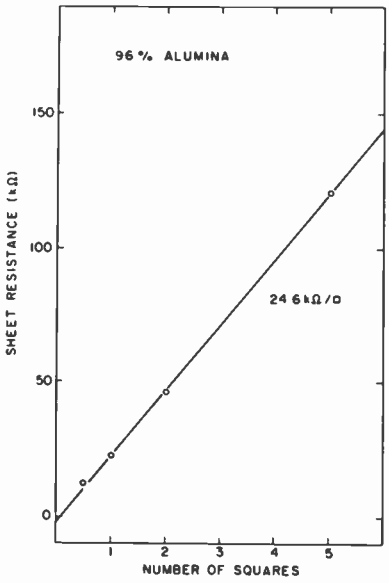

Fig. 4—Sheet resistance versus resistor aspect ratio (96% alumina).

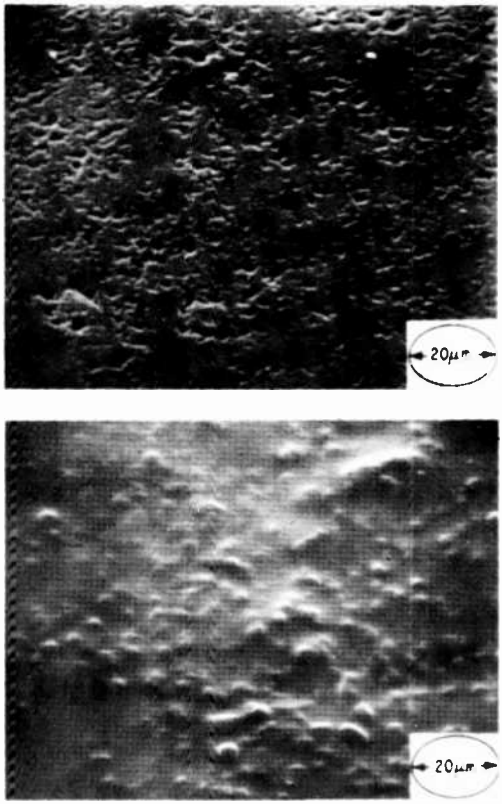

Fig. 5—Scanning electron micrographs of porcelain B; bottom photo shows surface after two firings at 900°C.

stability of the porcelain is not very good. Fig. 5B shows glassy phase formed after 2 firings at 900°C. The copper film fired on this porcelain does not contain any blisters, as shown in the optical micrograph of Fig. 6A. The optical micrograph of the cross-section of the resistor-copper-porcelain interface (Fig. 6B) shows better compatibility than for porcelain A. The contact angle of the solder to the copper film is 80–90°, which indicates poor solder wetting. This is because, during firing of the porcelain, the interaction between the copper film and the porcelain forms a thin layer of glass on the copper film, as shown in Fig. 6C. The poor reheat stability of this porcelain leads to poor solderability and wire-bondability and also resistor incompatibility. Better reheat stability was achieved by further increasing the crystal content of the porcelain.

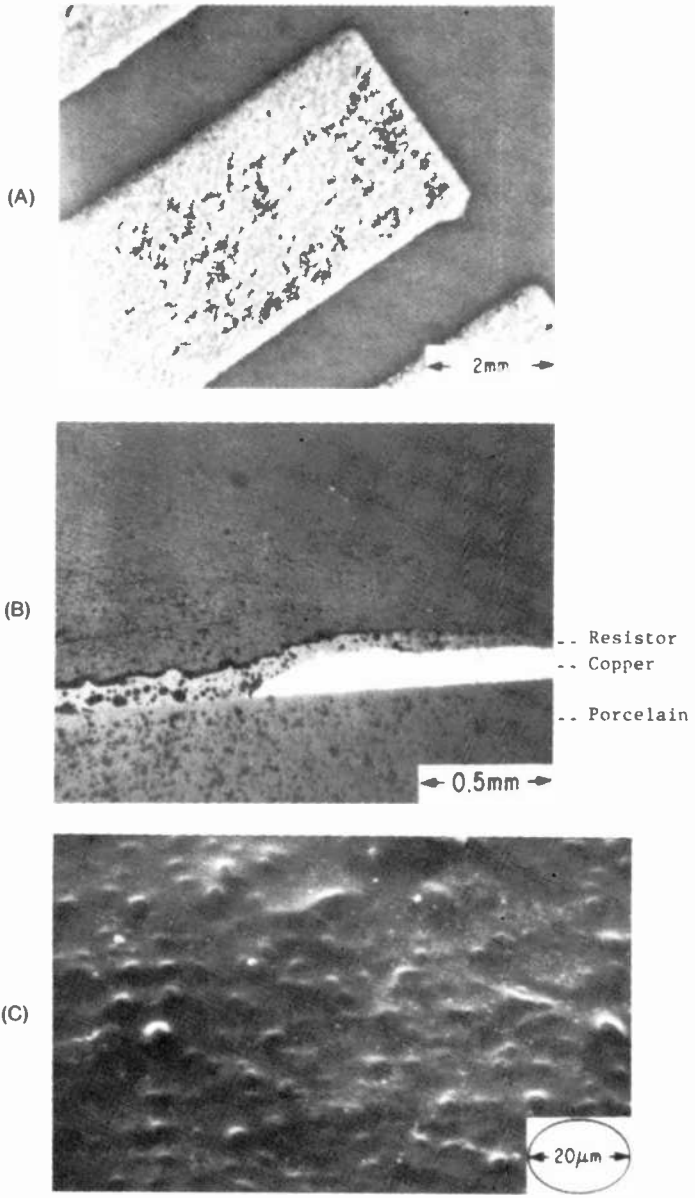

Fig. 6—(A) Optical micrograph of surface of copper film on porcelain B, (B) optical micrograph of cross section of resistor–copper–porcelain B, and (C) scanning electron micrograph of surface of copper film on porcelain B.

Table 2—Properties of Base-Metal Thick Films on Porcelain C

Conductivity: 50–60% of the bulk conductivity of copper.
Contact Angle between Solder and Copper Film: 30–40°, 5 seconds at 215°C, 62Sn/36Pb/2Ag solder.
Solder Peel Adbesion: 8 lbs, Copper pad size 0.1 × 0.1 inch
Al Wire Bond Pull Strengths: 7–16 gms (Failures occur due to wire breaks and bond lifts).
Sheet Resistivity of the Resistor Ink: 199.5 kΩ/□.

Porcelain C

The properties of the copper conductor and SnO_2-based resistor inks fired on porcelain C are described in Table 2. The properties of the copper films show a considerable improvement compared to porcelain A and porcelain B. Fig. 7 shows scanning electron micrographs of the

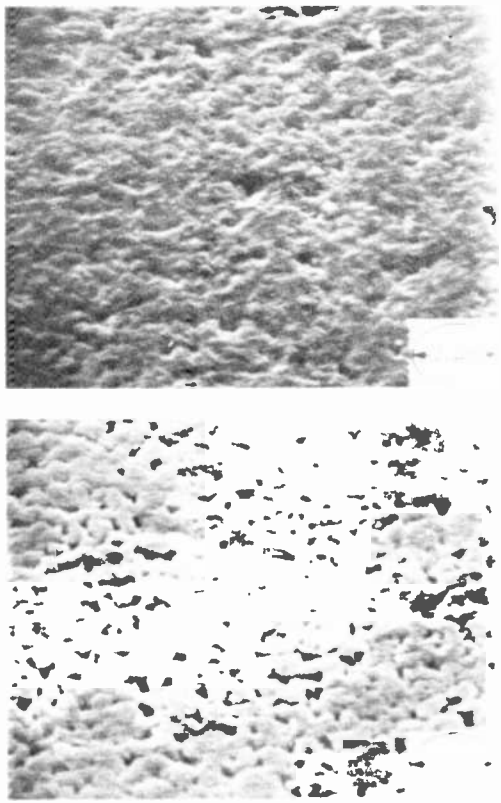

Fig. 7—Scanning electron micrographs of porcelain C; bottom photo shows surface after two firings at 900°C.

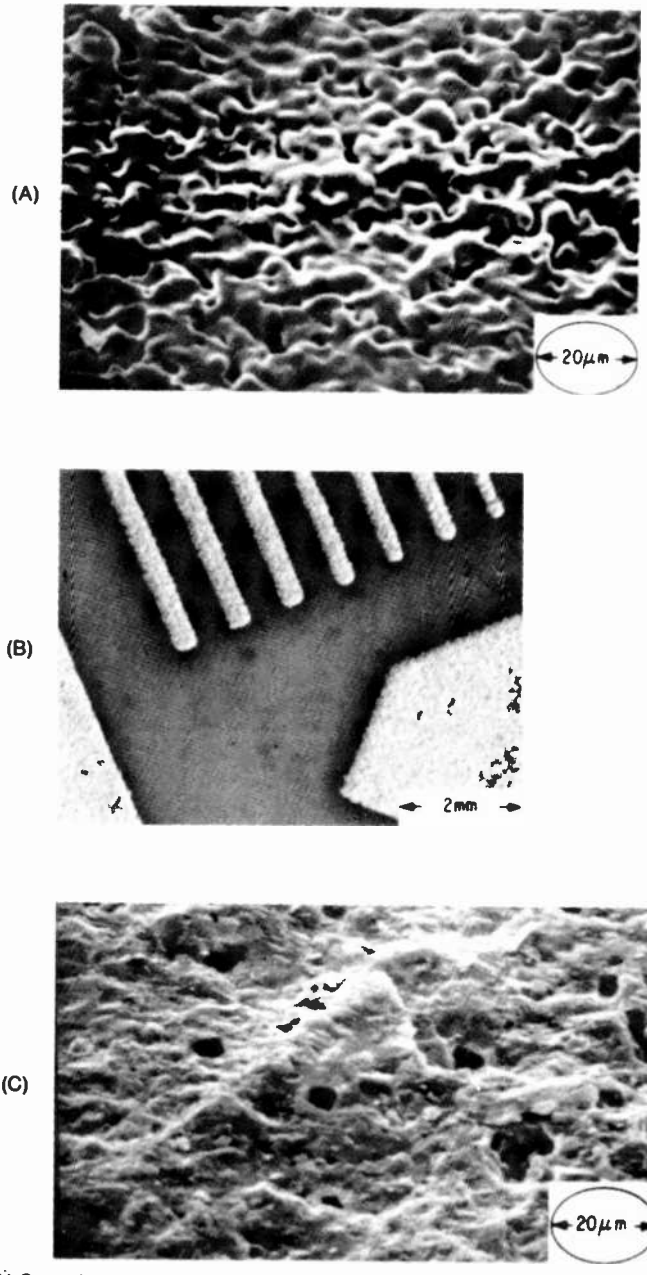

Fig. 8—(A) Scanning electron micrograph of surface of copper film fired on porcelain C, (B) optical micrograph of surface of copper film fired on porcelain C, and (C) scanning electron micrograph of surface of porcelain C after separation of the copper pad.

surface of porcelain C after one (top) and two (bottom) firings at 900°C; the porcelain is mostly crystalline and the microstructure does not change significantly even after 2 firings at 900°C. A scanning electron micrograph of the copper film fired on porcelain C is shown in Fig. 8A. The copper film has well sintered contacts with little glass on the surface. As a result the films have improved solder wetting and wire-bondability characteristics.

The optical micrograph of the copper film shown in Fig. 8B does not show any blisters. However, there is some staining of the porcelain in the areas adjacent to the conductor lines, probably due to reaction between the copper oxide and any liquid phase forming in the porcelain during processing the thick films. Fig. 8C shows a scanning electron micrograph of the porcelain surface after the separation of the copper pad. Some break within the porcelain can be noticed here. This might also be associated with the reaction between the liquid phase formed in the porcelain and the glass and the copper oxide from the conductor film.

The resistor values obtained on porcelain C are plotted in Fig. 9. The sheet resistivity is 199.5 kΩ/□. This is considerably higher than the value of 24.6 kΩ/□ obtained for this ink on 96% alumina. The optical micrograph of the cross-section of the resistor-conductor-porcelain interface

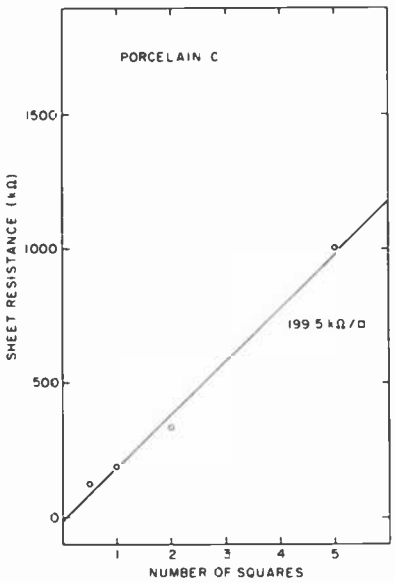

Fig. 9—Sheet resistance versus resistor aspect ratio (porcelain C).

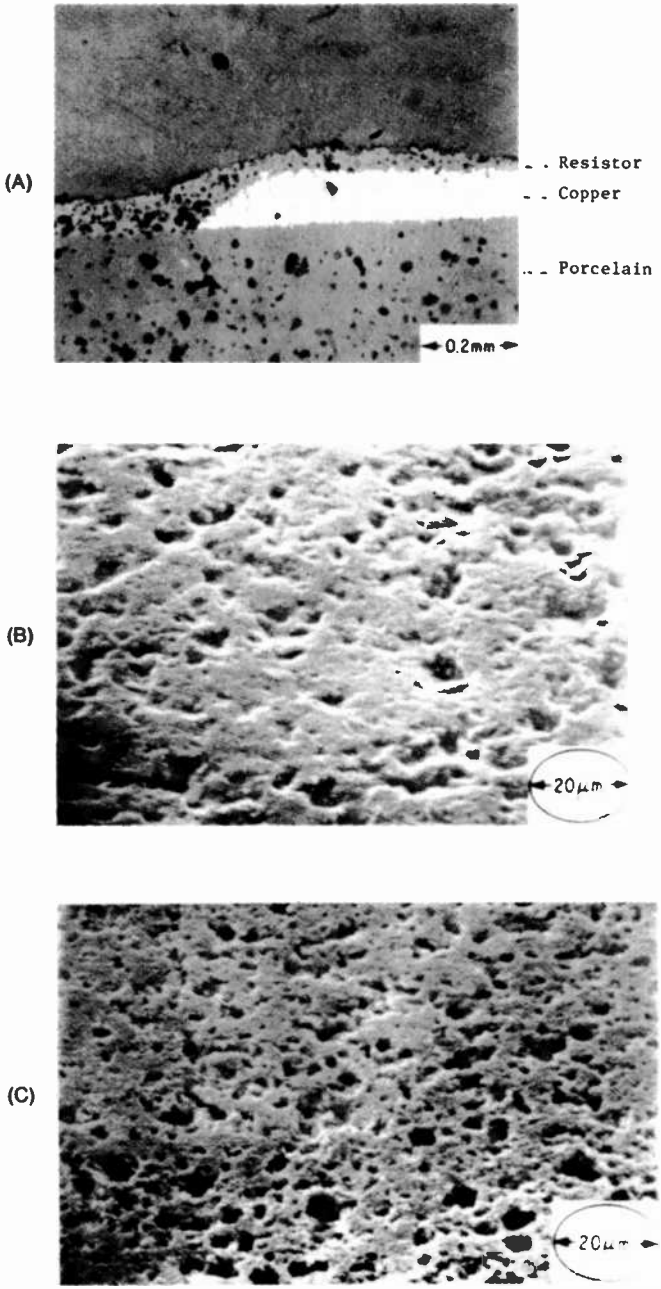

Fig. 10—(A) Optical micrograph of cross section of resistor–conductor–porcelain C and scanning electron micrographs (B) of surface of resistor fired on porcelain C and (C) of surface of resistor fired on 96% alumina.

is shown in Fig. 10A. The copper–porcelain, resistor–porcelain, and copper–resistor interfaces do not suggest any adverse reactions. The scanning electron micrographs of the resistor surfaces fired on the porcelain (Fig. 10B) and alumina (Fig. 10C) do not suggest any major differences. Careful investigation of this problem revealed that a small amount of iron had diffused from the core into the porcelain body. This iron reacted with the resistor causing some SnO_2 to reduce to tin, thus partially disrupting the conductive network. At the resistor–copper interface, tin formed from the reduction of SnO_2 reacted with copper, forming an alloy. This leads to poor contacts between the resistor and the conductor. Therefore, porcelain C could not be used to produce base-metal resistors. The diffusion of iron had to be decreased considerably to make it useful as a substrate for both the conductors and the resistors. This was achieved by further changes in the composition of the porcelain.

Porcelain D

The properties of the base-metal thick films obtained on porcelain D are reported in Table 3. The properties of the copper thick films are better than previously obtained and the resistor values are similar to those obtained on alumina, suggesting that the iron diffusion problem has been eliminated. Scanning electron micrographs of porcelain D are shown in Fig. 11. The porcelain is a crystallized material with fairly uniform grain size and does not undergo significant changes even after multiple firings at 900°C (Fig. 11B). The microstructure of the copper film shown in Fig. 12A indicates well sintered copper particles with very little glass on the surface. The films have good solderability and wire-bondability, as mentioned in Table 3. The optical micrograph of the copper thick film (Fig. 12B) does not indicate either the blisters observed in porcelain A or the staining in the porcelain adjacent to the copper lines observed in porcelain C. This suggests that porcelain D is quite inert even at the peak firing temperature. The scanning electron micrograph of the porcelain surface after the separation of the copper pad is shown in Fig. 12C. It does not indicate any break in the porcelain as was observed for

Table 3—Properties of Base-Metal Thick Film Inks on Porcelain D

Conductivity: 50–60% of the bulk conductivity of copper.
Contact Angle between Solder and Copper Film: <15°, 5 seconds at 215°C, 62Sn/36 Pb/2Ag solder.
Solder Peel Adhesion: 8 lbs, Copper pad size 0.1 × 0.1 inch
Al Wire Bone Pull Strengths: 11–16 gms (Failures occur mostly due to wire breaks).
Sheet Resistivity of the Resistor Ink: 21.7 kΩ/□.

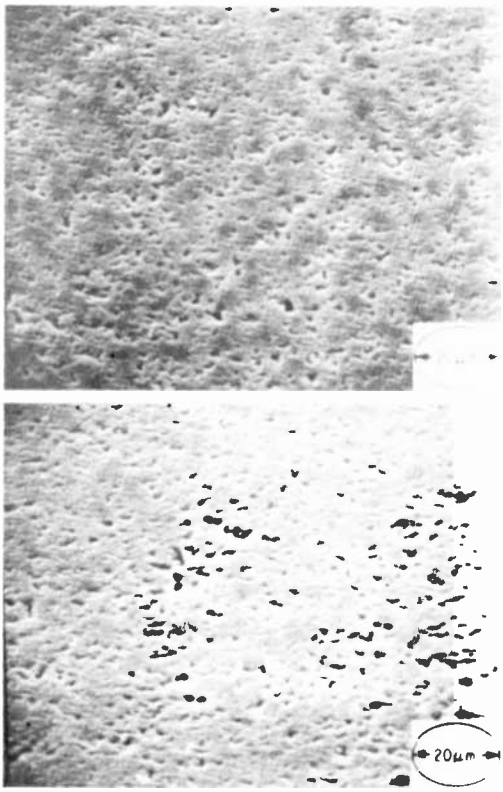

Fig. 11—Scanning electron micrographs of surface of porcelain D; bottom photo shows surface after two firings at 900°C.

porcelain C. The high adhesion between the copper film and the substrate is due to bonding between the conductor glass and the porcelain.

The resistor values obtained on the porcelain D are shown in Fig. 13. The sheet resistivity is calculated to be 21.7 kΩ/□, which is quite close to the 24.6 kΩ/□ value obtained on 96% alumina. This suggests that the presence of iron in the porcelain has been limited to the interface between steel and porcelain and is not present at the porcelain surface. There is no reduction of SnO_2 in the resistors fired on the procelain D and, hence, the alloy formation at the resistor–copper interface has been eliminated. Thus porcelain D can be used as a thick-film substrate for producing conductor as well as resistor films.

The surface of porcelain D is also considerably smoother than the previous porcelains, as illustrated in the Tallysurf plots of Fig. 14. Porcelain A is smooth but wavy, whereas porcelain C is fairly flat but has

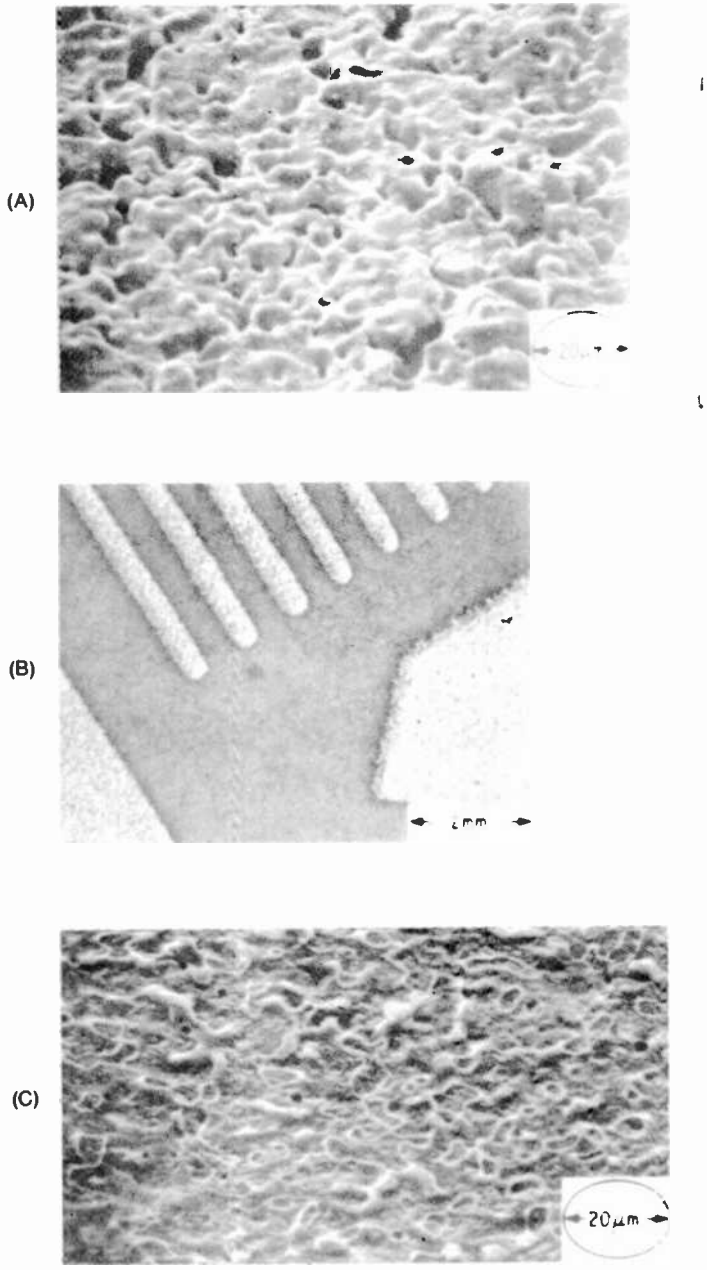

Fig. 12—(A) scanning electron micrograph of surface of copper film on porcelain D, (B) optical micrograph of surface of copper film on porcelain D, and (C) scanning electron micrograph of surface of porcelain after separation of the copper pad.

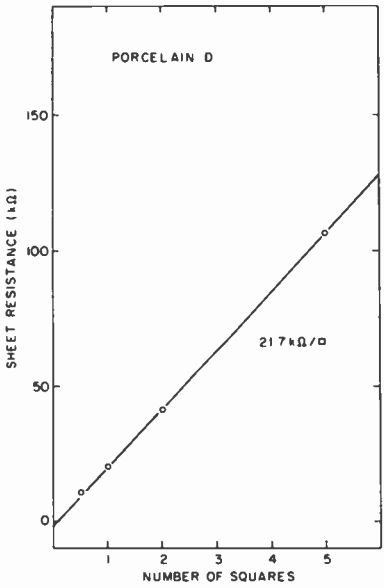

Fig. 13—Sheet resistance versus resistor aspect ratio (porcelain D).

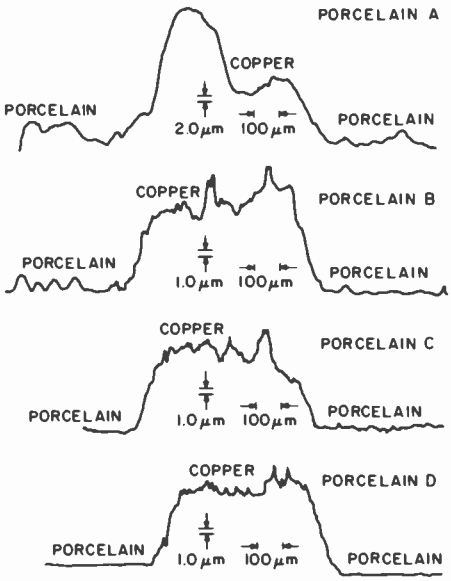

Fig. 14—Tallysurf plots of copper films on porcelains.

a rough surface. Porcelain D is both smooth and flat. The bump observed in the copper film profile of porcelain A indicates the blister in the copper films. Such bumps are absent in the copper films produced on other porcelain compositions. Further changes have been made in the composition of the porcelain and its fabrication procedure to obtain a porcelain-coated steel substrate that is smooth, flat and essentially pore free.

Porcelain E

The scanning electron micrographs of the porcelain E are shown in Figs. 15A and 15B. As can be seen, a very dense porcelain has been obtained from this composition. The microstructure of the porcelain remains essentially the same even after multiple firings at 900°C. This should

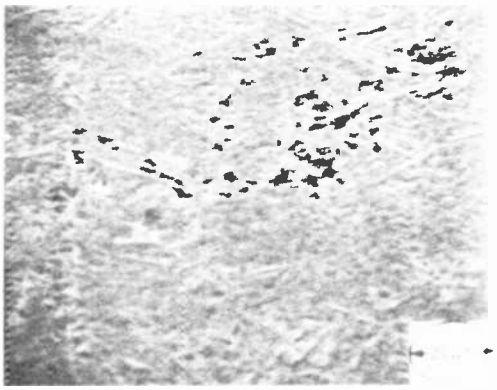

Fig. 15—Scanning electron micrographs of surface of porcelain E; bottom photo shows surface after two firings at 900°C.

make a very suitable composition for porcelain-coated steel substrates.

Conclusions

The sequential outline described in this paper has shown the development of a porcelain-coated steel substrate that is pore-free, smooth and stable after refiring; it is therefore suitable for producing large-area thick-film hybrid circuits. A complete base-metal thick-film system comprising copper conductor, base-metal resistor, cross-over dielectric, and overglaze ink has been formulated for use on these substrates. The glass compositions in the thick-film inks have been chosen for compatibility of the thick films with the porcelain and also to ensure mutual compatibility. The test results reported in this paper were obtained on the SnO_2-based resistor inks; the base-metal resistor system specifically developed for these substrates and as a part of the total ink system, however, is based upon certain other conductive ingredients. These resistor inks are less sensitive to the porcelain compositions than are the SnO_2 based inks. The properties of the base-metal thick films on the RCA porcelain-coated steel substrates show potential for the production of large area hybrid circuits on these substrates.

Acknowledgments

This work was performed within the Electronic Packaging Research Group (L. Onyshkevych, Group Head) in the Consumer Electronics Research Laboratories (D. Holmes, Director). We wish to thank D. Dorsey, T. Hitch, A. Sussman and B. Thaler for helpful discussions throughout the course of this work, T. Ward for supplying the porcelain coated steel samples, A. Kusenko for making the inks, W. Anderson for preparing the glass compositions, A. Miller for the wire bonding evaluations, and B. Seabury for scanning electron micrographs. Many other people, too numerous to mention, also contributed to the success of this undertaking.

References:

[1] L. S. Onyshkevych, "New Advances in Porcelainized Steel," ISHM Fall Seminar, Tri-State University, Indiana, Sept. 1980.

[2] K. W. Hang, "High Temperature Porcelain Coated Steel Substrates for Electronic Applications," presented at the 83rd Annual Meeting of the American Ceramic Society, Wash., D.C., May 1981.

[3] L. S. Onyshkevych, "Porcelain-Enamel Steel Substrates for Electronic Applications," PEI Technical Forum, University of Illinois, Oct. 1980.

[4] A. N. Prabhu et al., "Characterization of Thick Film Compositions on RCA Porcelain Coated Steel Substrates," *RCA Review*, **42**, p. 239, June 1981 (this issue).

Characterization of Thick-Film Compositions on RCA Porcelain-Coated Steel Substrates*

A. N. Prabhu, K. W. Hang, E. J. Conlon, T. T. Hitch, and A. Kusenko

RCA Laboratories, Princeton, NJ 07060

Abstract—A thick-film ink system comprising copper conductor, base metal resistor, low *K* dielectric, and overglaze compositions has been formulated for producing thick-film patterns and passive components on the RCA porcelain coated steel substrates. The properties of the copper film, such as conductivity, solderability, solder leach resistance, solder aged adhesion and wire bondability, are reported. Resistor properties such as TCR, noise, geometry dependence, and solder dip stability are described, as well as the resistance drifts of laser trimmed resistors after thermal storage, thermal shock, power loading, and exposure to humidity. The effects of overglazing on the resistor properties have been determined. Data are also presented on the properties of the cross-over dielectric films.

1. Introduction

The use of porcelain-coated steel boards as substrates with thick-film inks can make thick-film hybrid circuit technology cost effective in high-volume electronic applications. So far, however, this technology has not been widely accepted in the electronic industry because the commercially available porcelain materials contain mobile alkali elements, and thus their electrical breakdown strengths are low and their refire temperatures are limited to ~650°C. The properties of the thick films obtained from the available compositions (precious metal com-

* This paper was published under the title, "Properties of Base-Metal Thick-Film Materials on High-Temperature Porcelain Coated Steel Substrates," in the *Proc. 31st Electronic Components Conf.*, May 1981.

Fig. 1—Scanning electron micrograph of surface of RCA porcelain-coated steel substrate.

positions) deposited on these substrates are not satisfactory for many high-performance requirements, because the low processing temperatures are not sufficient to cause adequate sintering and alloying of the metal particles in the conductor films or the proper microstructural development in the resistor and dielectric films.

The new high-temperature porcelain coated steel substrates described in this issue of *RCA Review*, however, can be refired at temperatures as high as 950°C. Because of the higher refiring temperatures, it is possible to formulate will-sintered thick-film conductors (non-noble metal compositions) and resistor and dielectric films with stable microstructures.

This paper describes the properties of thick-film copper conductor, non-noble metal resistor, and low K dielectric compositions developed for use on the new RCA porcelain coated steel substrates. A scanning electron micrograph of the surface of the RCA porcelain-coated steel substrate is shown in Fig. 1 and the properties of the substrate are listed in Table 1. The formulation of the thick-film ink system was begun concurrently with the latter stages of development of the new porcelain

Table 1—Properties of RCA Porcelain Coated Steel Substrates

Steel Thickness: 20–40 mils
Porcelain Thickness: 5–10 mils
Reheat Stability: Able to withstand repeated firings at 900°C in nitrogen.
Dielectric Breakdown Strength (7.5 mils, 25°C): 3500 V
Dielectric Constant (10^2–10^7 Hz, 25°C): 7.5–8.5
Dissipation Factor (10^2–10^7 Hz, 25°C): 0.005–0.01
Bulk Resistivity (25°C): 10^{17} Ω-cm

material. Thus, the substrate and the ink system were tailored for compatibility with each other. In addition to the porcelain properties, conductor film adhesion, sintered density, and resistors and dielectric compatability with the other members of the system were emphasized. The copper conductor, non-noble metal resistor, and low K dielectric compositions were formulated for processing in nitrogen at temperatures as high as 950°C. The processing conditions and the properties of the thick films obtained are described below.

2. Process Conditions

Preparation and processing techniques for the base-metal thick-film inks were similar to those used for noble metal inks. The copper conductor, base-metal resistor, and low K dielectric compositions were formulated to have the same drying and firing conditions. Stainless steel screens with 200 mesh and 0.0016-inch wire diameter were used for the copper and the dielectric inks, whereas for the resistors 325 mesh and 0.0011-inch wire diameter stainless steel screens were used. The inks were screen printed, dried in air at 125 ± 5°C for 5–15 minutes, and fired in nitrogen at a peak temperature of 900 ± 5°C. Firing was conducted in a 5-zone BTU-Transheat belt furnace with a belt width of 6 inches. The furnace muffle was made of Inconel. Total firing time was 30–35 minutes, and the time at peak temperature was 4–6 minutes. The oxygen content of the nitrogen was determined using a Research Inc. Model 648A-5 oxygen monitor. The amount of oxygen in the nitrogen supply used for processing the inks was less than 10 ppm, and the oxygen in the hot zone was typically 20–30 ppm, as measured through the BTU-installed sampling port.

The fired film thicknesses of the copper conductors were 0.6–0.8 mil and the thicknesses of the resistors were 0.4–0.7 mil. All the resistors were tested with prefired copper terminations. The same copper ink was used to form the resistor terminations as well as the multilayer electrodes. Two layers of the low-K dielectric were used to prevent shorts between the top and the bottom copper electrodes. Each layer of conductor and of the dielectric was fired separately to ensure adequate removal of all carbon residue. The overglaze ink was formulated to be screen printed, dried in air at 125 ± 5°C for 5–15 minutes, and fired in nitrogen at a peak temperature of 500 ± 10°C with a time at peak temperature ranging from 4–6 minutes.

3. Properties of Copper Conductor Films

Microstructure

A scanning electron micrograph of the fired copper film surface is shown

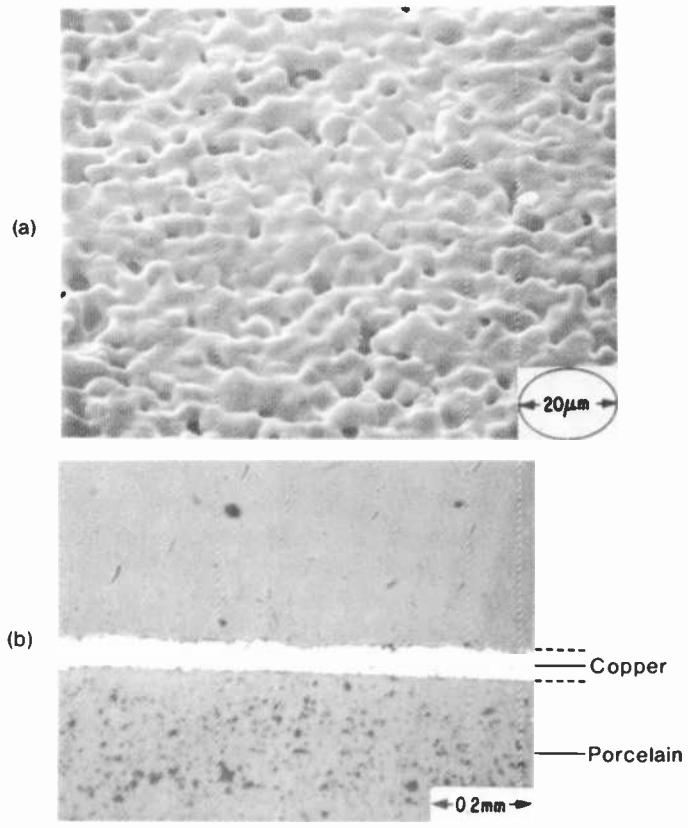

Fig. 2—(a) Scanning electron micrograph of surface of copper film and (b) optical micrograph of cross section of conductor-porcelain.

in Fig. 2a. Firing of the copper film at 900°C in nitrogen leads to well sintered contacts of the copper particles. Adequate sintering of the copper particles is necessary to obtain conductor films with good conductivity, solderability, and wire bondability. An optical micrograph of the cross-section of the conductor and porcelain is shown in Fig. 2b. The sample for this study was prepared by cold mounting the substrates in an epoxy and metallographically sectioning the interface at a 17° angle, so that an extended cross sectional area could be examined. During the polishing some grains were pulled from the surface of the porcelain. These areas appear as dark spots in Fig. 2b; they do not indicate porosity. Fig. 2b shows a sharp interface between the conductor and the porcelain, indicating that the porcelain is quite inert and that very little copper diffuses into it. This is desirable, as the diffusion of various thick film

materials into the porcelain could lead to degradation in its electrical properties.

Conductivity

The bulk resistivity of the copper film was measured on conductor lines 2.5 inches long and 0.03 inch wide. The sheet resistance was measured using the four-probe (Kelvin) technique. Three Tallysurf plots were taken on each line (at the center and near each end). The cross sectional areas were calculated with a Zeiss image analyser. The average of three areas was used to calculate the bulk resistivity of each sample. The conductivity of the copper thick film was calculated to be about 60% of the bulk conductivity of copper.

Solderability

The solderability of the copper conductor was compared with the solderability of OFHC copper foil by examining the spread of 0.04-inch diameter 62Sn/36Pb/2Ag solder balls after 5 seconds at 215°C. The flux used was Kester 1544. The solder spread on the copper films was greater than 75% of the spread on the copper foil.

Solder Leach Resistance

Solder leach resistance of the copper conductor was determined by observing the decrease in the size of the 0.1 × 0.1 inch copper pads after dipping them into solder. The parts were fluxed with Kester 1544 flux and dipped in 62Sn/36Pb/2Ag solder at 230°C. Each immersion lasted

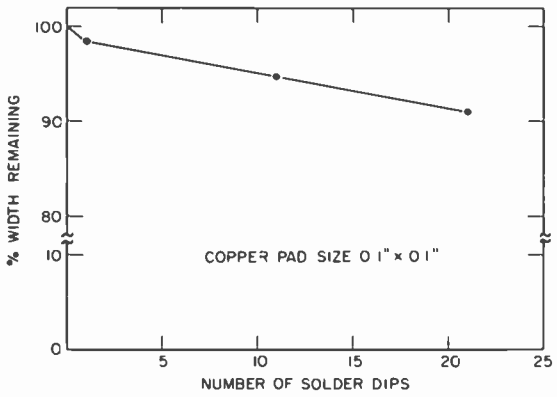

Fig. 3—Solder leach resistance of copper.

for 15 seconds. The conductor-pad width decrease after solder dipping is shown in Fig. 3. The decrease is about 5% after 11 dips and about 9% after 21 dips.

Adhesion

Adhesion of the copper films to the porcelain was measured on 0.1 × 0.1 inch copper pads using the soldered-wire peel adhesion test method.[5] Annealed copper wires, 0.032 inch in diameter, were soldered to the copper pads using Kester 1544 flux and 62Sn/36Pb/2Ag solder. Peel testing was performed on an Instron at 0.5-inch/minute crosshead speed. The initial adhesion values were 5–8 lbs. The failure mechanisms were separation at the copper–porcelain interface, a break within the porcelain, and, occasionally, a combination of the two. Fig. 4 is a scanning electron micrograph of a substrate after the copper pad was separated from the porcelain. Some fracture into the body of the porcelain coating can be seen in this scanning electron micrograph. The failure loads were essentially the same regardless of the failure mode.

The effect of thermal shock on the adhesion strength was determined by subjecting the soldered substrates to 5 cycles of temperature variation from +125°C to −80°C, holding for two minutes in each temperature bath, and allowing less than 10 seconds for transfer from the hot bath (Fluorinert FC-48) to the cold bath (dry ice and trichloroethylene mixture). The adhesion strengths of the copper pads subjected to thermal shock remained the same.

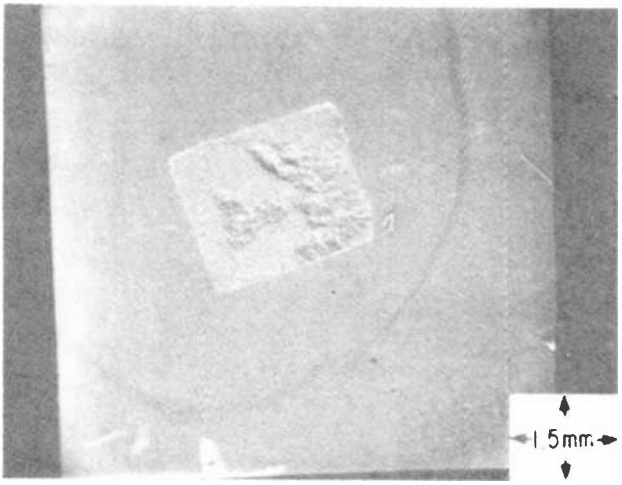

Fig. 4—Scanning electron micrograph of porcelain surface after separation of the copper pad.

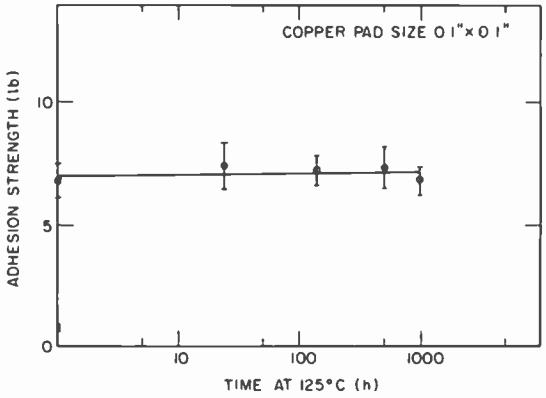

Fig. 5—Aged adhesion of copper (125°C).

Effects of heat and humidity on the adhesion of the copper films to the substrate are shown in Figs. 5 and 6. There is no decrease in the adhesion strength after aging for 1000 hours at 125°C. After storage at 50°C and 90% R.H. for 1000 hours, the copper-on-porcelain samples exhibited a decrease in adhesion strength of less than 20% of the initial value. In both the cases, all three failure modes were observed. The adhesion test results indicate that the adhesion of the copper film to the substrate is high and the effects of aging and humidity storage on adhesion are minimal.

Wire Bondability

A Kulicke and Sofa ultrasonic wire bonder was used to bond 0.0015-inch diameter Al-1%Si wire to the copper films. The wire bonds were pull

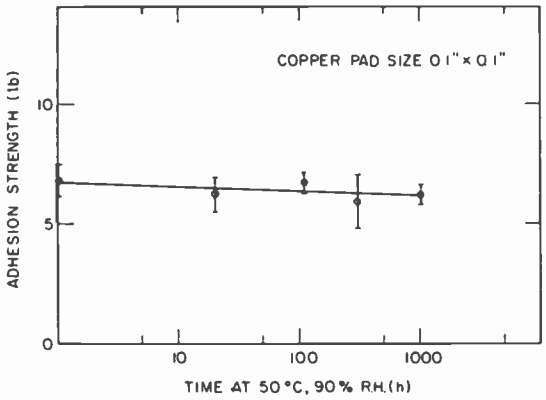

Fig. 6—Effect of humidity on adhesion of copper (50°C, 90% R.H.).

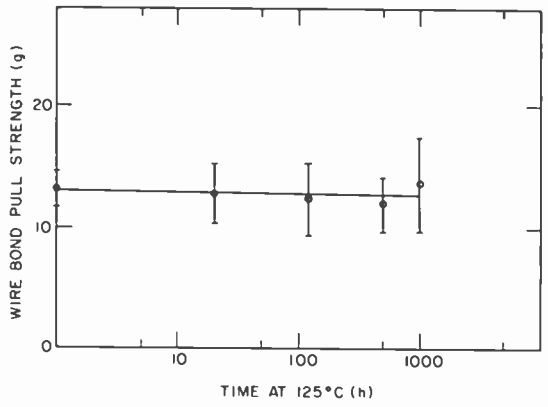

Fig. 7—Thermal aging of aluminum wire bonds on copper (125°C).

tested to destruction before and after aging at 125°C and storage at 50°C and 90% R.H. for times up to 1000 hours. The effects of heat and humidity on the wire bond strengths are shown in Figs. 7 and 8. Neither aging at 125°C nor exposure to 50°C and 90% R.H. had a significant effect on the wire-bond pull strengths. The pull strengths never fell below 7 gms. The failures after pull testing were mostly due to bond breaks. The pull strengths were generally higher when the failure mode was bond lifting. It appears from these test results that ultrasonic aluminum wire bonding can be used as a reliable interconnection method between IC's and the thick-film copper metallizations on these porcelain-coated steel substrates.

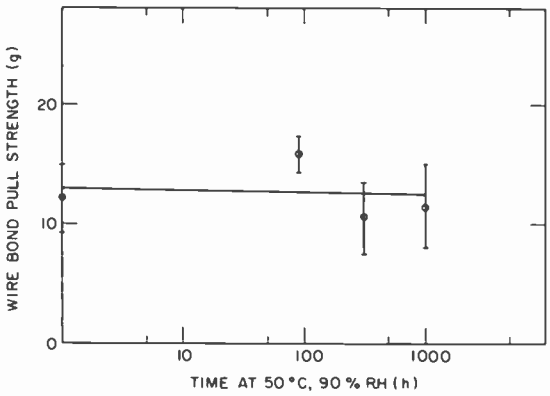

Fig. 8—Effect of humidity on Aluminum wire bonds (50°C, 90% R.H.).

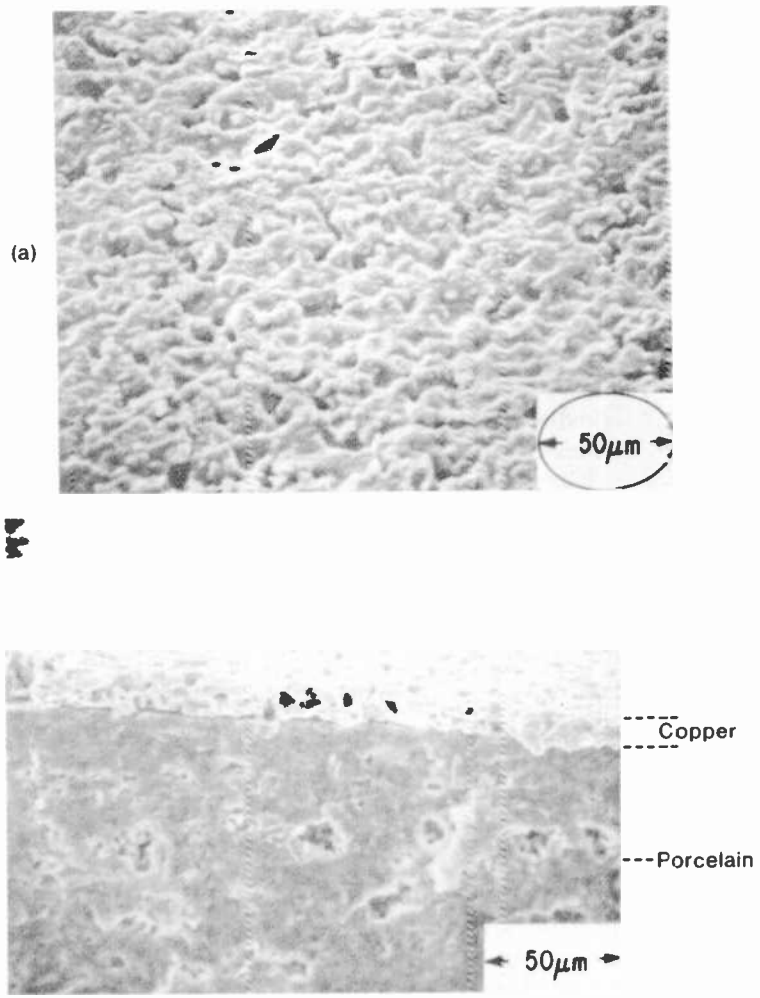

Fig. 9—Scanning electron micrographs (a) of surface of the dielectric film and (b) of cross section of conductor-dielectric.

4. Properties of the Low *K* Dielectric Films

A dielectric composition was formulated for use in producing multilayer structures on RCA porcelain-coated steel substrates. Fig. 9 shows scanning electron micrographs of the surface of the fired dielectric film and a fracture cross-section of the copper film fired over the dielectric. The dielectric film fires to a relatively dense structure with little porosity, in general, and with no open porosity, thus avoiding shorts between the

Table 2—Properties of the Multilayer Dielectric Films

Insulation Resistivity (25°C): $>10^{14}$ Ω cm
Dielectric Constant (10^3–10^4 Hz, 25°C): 9–10
Dissipation Factor (10^3–10^4 Hz, 25°C): ≤0.005
Dielectric Breakdown Strength (25°C): >500 volts

top and bottom electrodes. The composition of the dielectric film has been developed to minimize the blistering commonly observed in copper–dielectric multilayers. The copper film on the dielectric has a microstructure similar to that of well sintered copper particles on the porcelain. As a result they have similar properties. The pull strengths of the ultrasonic aluminum wire bonds formed on the top copper electrode are about 10–18 gms. The properties of the dielectric are shown in Table 2. The dielectric constant is 9–10 and the dissipation factor is quite low. The insulation resistivity and the breakdown voltage are adequate for multilayer applications.

5. Properties of the Base-Metal Resistors

Microstructure

Base-metal resistor compositions have been formulated to give sheet resistivities of 200Ω/□ to 1 MegΩ/□ when fired on the RCA porcelain coated steel substrates. Scanning electron micrographs of the resistor surfaces for different sheet resistivity compositions are shown in Fig. 10 and an optical micrograph of a cross section of the copper, resistor, and porcelain are shown in Fig. 11. The resistor microstructure does not show any segregation of the conducting particles and the glass. The optical micrograph of the cross section indicates good compatibility between the resistor and copper conductor and also between the resistor and the porcelain. Very little diffusion of copper into the resistor was noted even for high value resistors.

Effect of Resistor Geometry on Sheet Resistivity

The dependence of resistor values on aspect ratio is shown in Fig. 12 for five materials with different sheet resistivities. The resistor width for the resistors having aspect ratios of 0.5, 1, and 2 was 0.06 inch, and that of the resistors having an aspect ratio of 5 was 0.04 inch. The plots of sheet resistance versus number of squares are linear, indicating very little dependence of sheet resistivity on length. The slope of each straight line gives sheet resistivity in Ω/□ for that composition. The contact resistances are negative for all the sheet resistivities studied. The magnitude

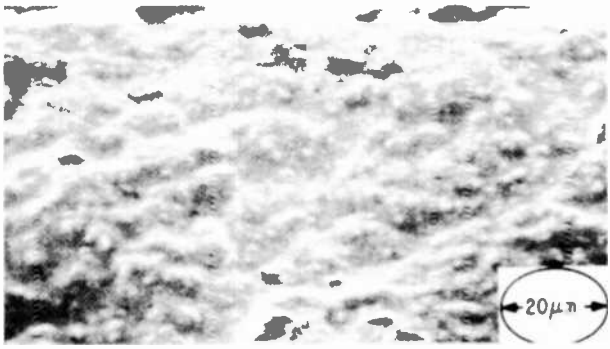

10 kΩ/□

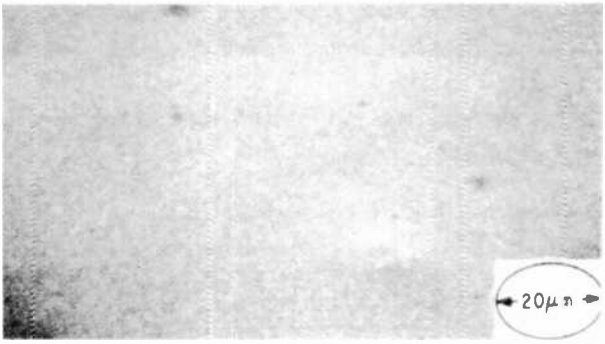

500 kΩ/□

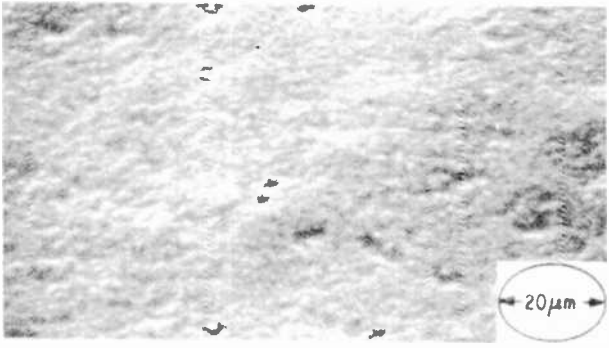

2 MegΩ/□

Fig. 10—Scanning electron micrographs of surface of three resistor films.

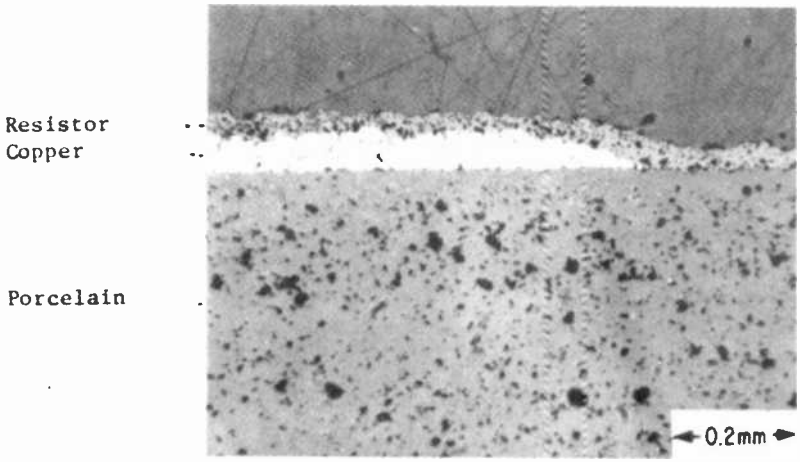

Fig. 11—Optical micrograph of cross section of resistor–conductor–porcelain.

of the contact resistance was minimized by careful selection of the composition of the glass.

Temperature Coefficient of Resistance (TCR)

The TCR's of the resistors were measured on 0.1 × 0.1 inch resistors for

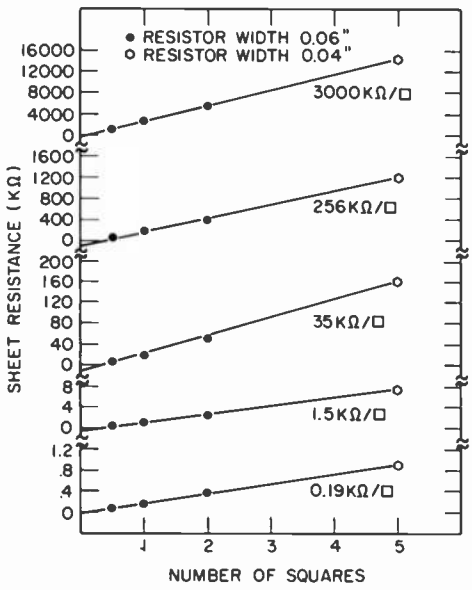

Fig. 12—Sheet resistance versus resistor aspect ratio.

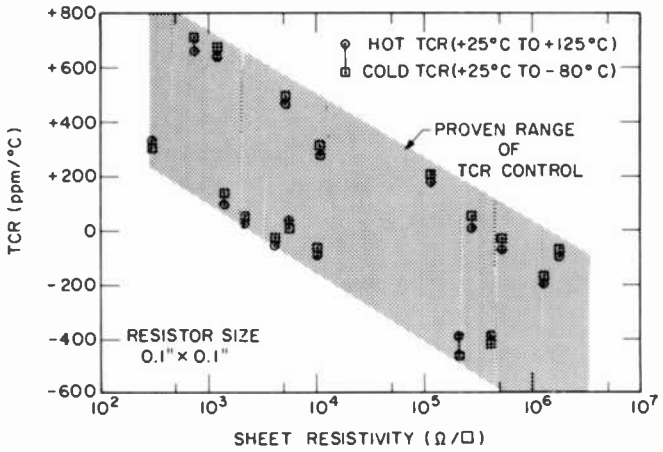

Fig. 13—TCR versus sheet resistivity.

temperatures varying from +125°C to −80°C. The hot and cold TCR data for various sheet resistivities are shown in Fig. 13. As can be seen, the TCR's for similar sheet resistivity can be varied considerably—as much as 500 ppm/°C in some cases—by the proper choice of TCR modifiers. For low-value resistors TCR modifiers are added to make the

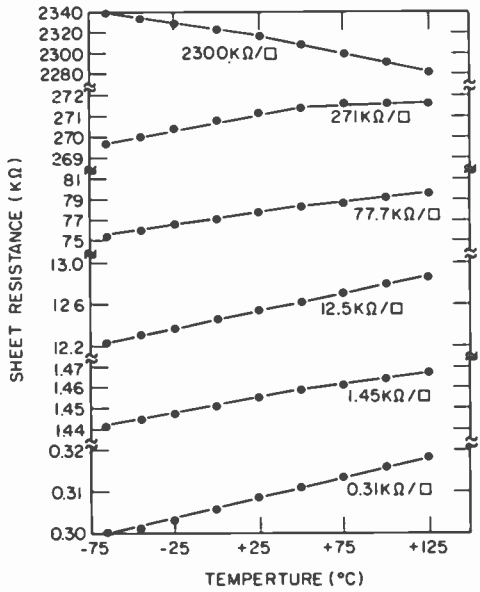

Fig. 14—Sheet resistance versus temperature.

TCR less positive, and for high-value resistors modifiers are added to make the TCR less negative. For the initial formulations it has been possible to control hot and cold TCR's to be within ±350 ppm/°C for the whole sheet resistivity range, and the midrange TCR's have been controlled to be within ±100 ppm/°C. The spread between the hot and cold TCR's is quite low for all sheet resistivities studied. As shown in Fig. 14, the sheet resistance variation of 0.1 × 0.1 inch resistors is linear with temperature from −65°C to +125°C. In general, the cold TCR's are slightly more positive than the hot TCR's.

Noise

The current noise of untrimmed 0.1 × 0.1 inch resistors was measured with a Quantech Model 315B noise meter. A plot of noise index versus sheet resistivity is shown in Fig. 15. As is typically observed with the thick-film resistor systems, the noise increases with sheet resistivity. Noise indexes are generally low for this resistor system, and for the high-value resistors they are comparable to those observed for air-fired ruthenium based resistors.

Laser Trimmability

The resistors were laser trimmed using a Quantronix Model 112-B YAG laser. The trimming parameters were, 3 mil/sec trim speed, 3 KHz pulse frequency, and 0.8-watt beam power. Resistors 0.1 × 0.1 inch, having sheet resistivities of 200 Ω/□ to 200 kΩ/□, were given a single plunge cut near the center of the resistor. The increases in the sheet resistances were 20–40%. The drift characteristics of the laser trimmed resistors were

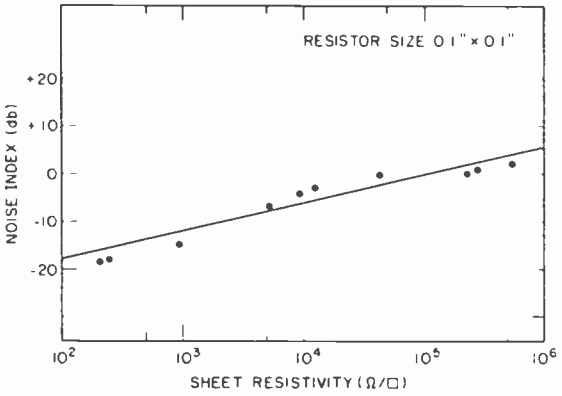

Fig. 15—Noise index versus sheet resistivity.

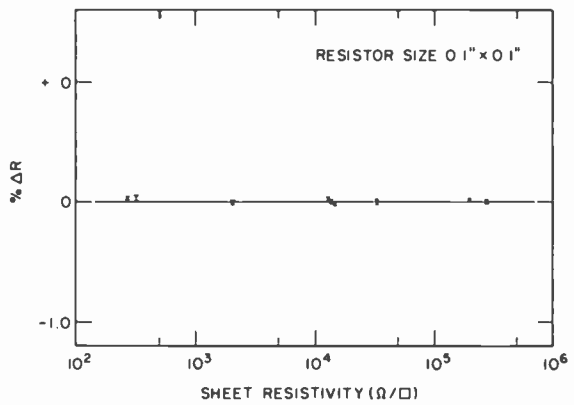

Fig. 16—Stability of laser-trimmed resistors (thermal shock).

studied. The results are plotted as minimum and maximum $\%\Delta R$ versus the sheet resistivity for various experimental conditions.

Resistance Changes Due to Thermal Shock

The laser-trimmed resistors were subjected to 5 cycles of temperature variation from +125°C to −80°C, holding for 2 minutes in each temperature bath, and allowing for less than 10 seconds to transfer from the hot bath to the cold bath. The sheet resistance changes of the resistors subjected to thermal shock are less than 0.1% throughout the sheet resistivity range studied, as shown in Fig. 16.

Solder Dip Stability

A solder-dip-stability study was conducted on the laser-trimmed resis-

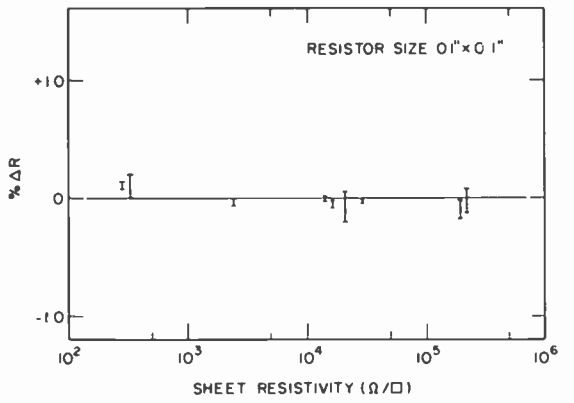

Fig. 17—Solder dip stability of laser-trimmed resistors.

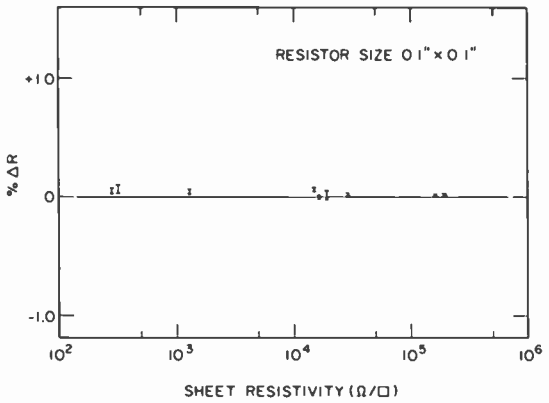

Fig. 18—1000-hour laser trim stability (125°C).

tors in 62Sn/36Pb/2Ag solder at 230°C with Kester 1544 flux. Immersion time was 10 seconds. As shown in Fig. 17, the changes are quite small, generally less than 0.1% and in all cases less than 0.2%. The composition of the glasses is not the same in all these resistor formulations. Some of the glass compositions provide better solder-dip stability to the resistors than others.

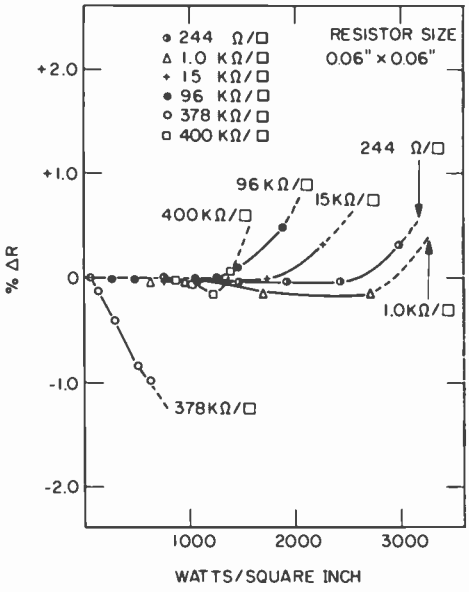

Fig. 19—STOL test data.

Thermal Stability

The sheet resistance changes of the laser-trimmed resistors upon aging at 125°C are shown in Fig. 18. The resistance changes after 1000 hours of aging are less than 0.1% throughout the sheet resistivity range studied.

STOL Data and Power Loading

Short time overload (STOL) test data are presented in Fig. 19 as the variation of $\%\Delta R$ with watts/inch^2 for 0.06 × 0.06 inch resistors having sheet resistivities of 0.244, 1, 15, 96, 378 and 400 kΩ/□. After application of more than 1000 watts/inch^2 overload, the resistor values changed by less than 0.1% for all the resistors except for the 378 kΩ/□ resistor, which changes about 1% after the application of the overload voltage of 625 watts/inch^2. The glass compositions in the formulations of 378 kΩ and 400 kΩ are different. The 400 kΩ/□ is an improved formulation giving resistors with better power handling characteristics. From these data the resistors can be rated at 100 watts/inch^2 since 625 watts/inch^2 overload caused drifts of 0.1% or less in all the resistors.

Load life tests were conducted on laser-trimmed resistors. The substrates were 1 × 1 inch and each substrate had three 0.1 × 0.1 inch resistors. Each resistor was powered at 1 watt (100 watts/inch^2) in an 80°C ambient environment chamber. Minimum and maximum resistance changes after 1000 hours are given in Fig. 20. The changes are less than 0.1% for some of the formulations. For other formulations the changes reached ~0.2% indicating the influence of the glass compositions on the resistor stability. By choosing appropriate glass compositions to formulate the resistors, it is possible to improve the stability of the resistors.

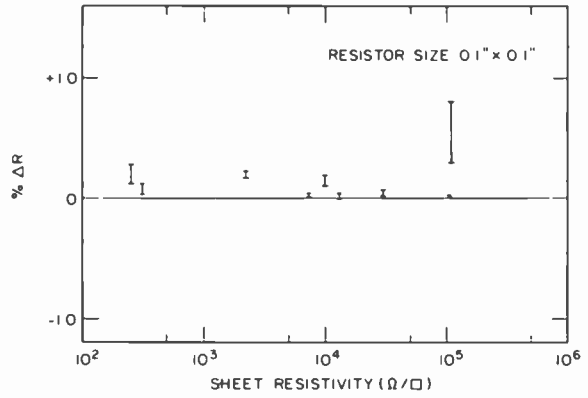

Fig. 20— 1000-hour laser trim stability (100 watts/inch^2).

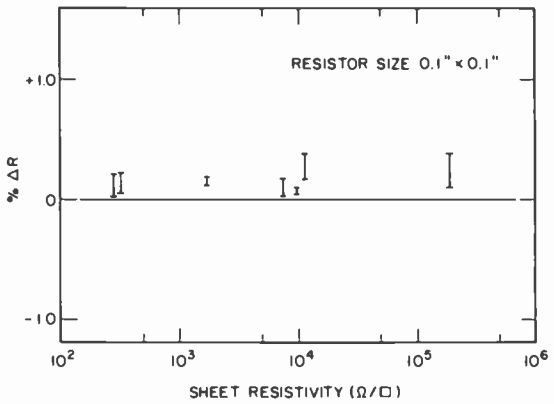

Fig. 21—1000-hour laser trim stability (50°C, 90% R.H.).

The resistor composition showing resistance drifts of 0.3–0.8%, also showed about 1%ΔR during STOL testing when overloaded at 625 watts/inch^2 for 5 seconds. The performance of the improved high-value resistor formulations is expected to be better.

Humidity Storage

The laser trimmed resistors were stored in a humidity chamber at 50°C and 90% R.H. for 1000 hours. Fig. 21 shows sheet resistance changes after 1000 hours. The drifts are generally less than 0.2% except for some formulations where the changes are about 0.4%. Again the results indicate that with proper choice of the glass compositions, the effect of humidity on the resistor drifts can be minimized.

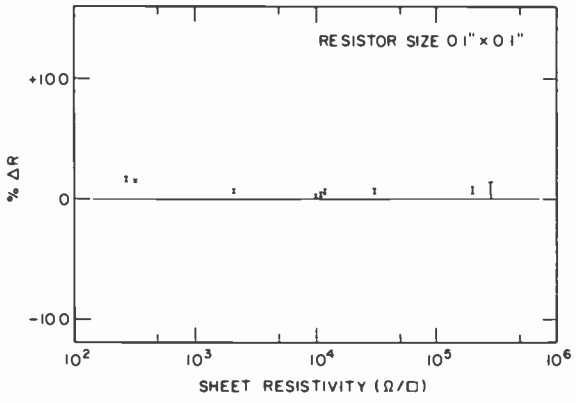

Fig. 22—Resistance changes after overglazing.

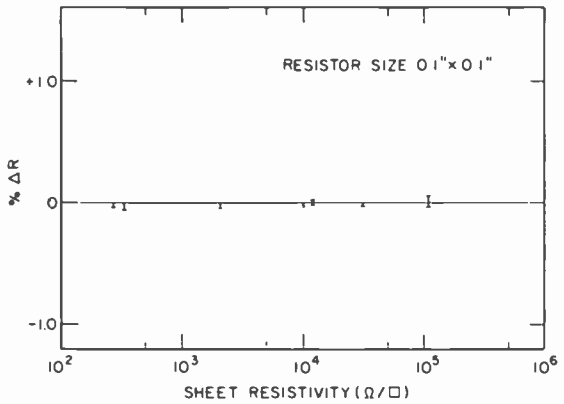

Fig. 23—Solder dip stability of the overglazed resistors.

6. Effect of Overglazing on Resistor Properties

The resistors were overglazed in nitrogen at the peak temperature of 500 ± 10°C. The sheet resistance increases that occurred during overglazing the resistors are typically 1–2%, with the amount of the increase dependent upon the resistor compositions, as shown in Fig. 22. Solder dip stability of the laser trimmed and overglazed resistors was determined by dipping for 10 seconds in 62Sn/36Pb/2Ag solder at 230°C. The results are shown in Fig. 23. The resistance changes are less than 0.1%. The overglazed resistors were stored for 1000 hours at 50°C and 90% R.H. The results are shown in Fig. 24. The resistance drifts are smaller than those observed for unglazed resistors. The changes are less than 0.1% for most of the overglazed resistors.

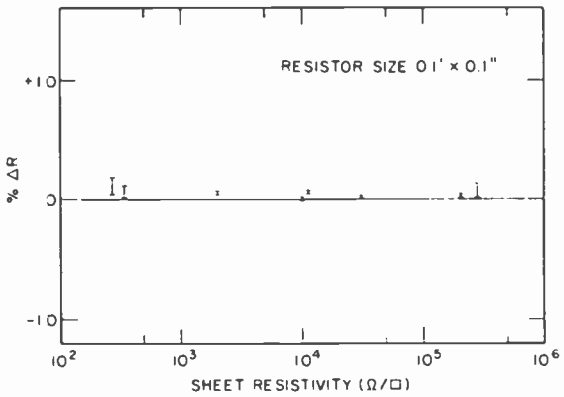

Fig. 24—1000-hour stability of the laser-trimmed and overglazed resistors (50°C, 90% R.H.).

7. Conclusions

The porcelain coated steel substrates described in this paper have the ability to withstand multiple firings at 900°C in nitrogen during thick film processing. Properties of the copper conductor, base metal resistor, and low K dielectric compositions on the porcelain coated steel substrates have been studied. The test data reported in this paper were obtained on small sample lot sizes. However, most of the formulations have been subjected to preliminary testing and modification to improve the properties obtained from these films. The test results are very encouraging and show potential for a reliable technology employing the porcelain substrates, with further work needed on the inks to make them commercially applicable. Base-metal thick films are a natural complement to the porcelain boards to make the hybrid technology cost effective for consumer applications. The properties of the base-metal thick films obtained on the porcelain-coated steel substrates compare favorably with those obtained from precious metal conductors, ruthenium based resistor systems, and air-firing multilayer dielectric inks on alumina substrates. Considering that the air-firing formulations have been greatly improved since their conceptions 10–20 years ago, we believe that the new base-metal thick film system used on the RCA porcelain-coated steel substrates has great potential for still further improvements.

Acknowledgments

This work was performed within the Electronic Packaging Research Group (L. Onyshkevych, Group Head), in the Consumer Electronics Research Laboratories (D. Holmes, Director). We wish to thank A. Sussman, B. Thaler, D. Dorsey and R. Brown for helpful discussions throughout the course of this work, T. Ward for supplying the porcelain-coated steel samples, W. Anderson for preparing the glass compositions, and A. Miller for the wire bonding evaluations. Many other people, too numerous to mention individually contributed to the success of this undertaking.

References:

[1] D. P. Wisher, Jr., and W. B. Hatfield, "Porcelain Steel Technology: A Bonafide Alternative?", *Proc. 1978 International Microelectronics Symposium.* Minneapolis, Mn.

[2] L. S. Onyshkevych, "New Advances in Porcelainized Steel," ISHM Fall Seminar, Tri-State University, Indiana, Sept. 1980.

[3] K. W. Hang, "High Temperature Porcelain Coated Steel Substrates for Electronic Applications," 83rd Annual Meeting of the American Ceramic Society, Wash., D.C., May 1981.

[4] L. S. Onyshkevych, "Porcelain-Enamel Steel Substrates for Electronic Applications," PEI Technical Forum, University of Illinois, Oct. 1980.

[5] T. T. Hitch, "Adhesion Measurements on Thick-Film Conductors," in *Adhesion Measurement of Thin Films, Thick Films and Bulk Coatings*, K. L. Mittal, Ed., Special Technical Publication 640, American Soc. for Testing and Materials.

Fabrication of Large-Area Thick-Film Hybrid Circuits on RCA Porcelain-Coated Steel Substrates

A. N. Prabhu, E. J. Conlon, A. Z. Miller, J. H. McCusker, and T. T. Hitch

RCA Laboratories, Princeton, NJ 08540

Abstract—This paper describes techniques used for fabricating thick-film hybrid circuits using RCA porcelain-coated steel substrates. The suitability of these porcelain boards as a more versatile thick-film hybrid circuit substrate than the presently used ceramic substrates and commercial porcelain boards is pointed out. The behavior of various thick-film materials developed for use on these substrates is described in terms of the key properties of the thick films, which govern the choice of techniques used for the fabrication of the passive devices and the component attachment methods. The high performance characteristics of thick-film hybrid circuits fabricated on the porcelain boards are attributed to the compatibility between the thick films and the porcelain.

Introduction

Thick-film is an extremely versatile and flexible technology that is being increasingly used in electronic applications. Conductor patterns, as well as resistors and capacitors in a wide variety of combinations, values, and characteristics can be constructed with the basic thick-film materials and substrates. The ability to attach discrete active and passive devices either in packaged or chip form has further enhanced the versatility of thick-film technology. As improvements in the thick-film materials and manufacturing techniques continue to evolve, increased application of thick-film technology into new product areas is certain to occur.

Even though thick-film technology has evolved significantly during the past 20–30 years, its utilization in high volume consumer electronic applications is still limited, primarily due to the high cost of presently

used ceramic substrates and precious-metal thick-film compositions. Attempts made by several companies during the past few years to replace the precious-metal compositions with base-metal compositions have been successful only to a very limited extent. Porcelain-coated steel has attracted a lot of attention as a substrate material for consumer type electronic applications because of its ruggedness, ease of manufacture in large sizes and irregular shapes, as well as its potential for very low cost when compared to ceramic substrates. But so far the commercial acceptance of the porcelain-board technology in the electronic industry has been limited because of the inherent deficiencies of the commercial porcelain-coated steel substrates and the lack of availability of base-metal compositions for use with these substrates.

Both of these drawbacks have been overcome by the development of a high-temperature porcelain-coated steel substrate and compatible base-metal thick-film compositions at RCA Laboratories. A precious-metal conductor, RuO_2 resistor, and dielectric ink system have also been developed for the RCA porcelain-coated steel substrates.

This paper describes techniques for fabricating large-area thick-film hybrids using RCA porcelain-coated steel substrates. The porcelain board can serve as a PC board and/or as a thick-film hybrid substrate. The thick-film conductor ink is screen-printed and fired on these boards to form conductor patterns. This is an additive method and does not involve any etching on the copper, a process that is normally encountered in forming conductor patterns of PC boards. Once the conductors are formed, the porcelain board can be used as a regular PC board and the components can be mounted and soldered. The full potential of the porcelain-board technology is realized when the resistors, capacitors, cross-overs and overcoats are printed and fired on the substrates and component attachment techniques, such as chip bonding and wire bonding, are utilized in addition to soldering to join the active devices. The thick-film materials, their processing on the RCA porcelain coated steel substrates, and component attachment techniques are described here. Throughout this paper, the properties of the thick-film materials and the substrates are emphasized, as they govern the hybrid techniques used to fabricate the circuits.

Thick-Film Materials

The thick-film materials used on the RCA porcelain-coated steel substrates are indicated in Fig. 1. The complete base-metal ink system (copper conductor, base-metal resistor, multilayer dielectric, and overglaze inks) and precious-metal ink system (precious-metal conductor,

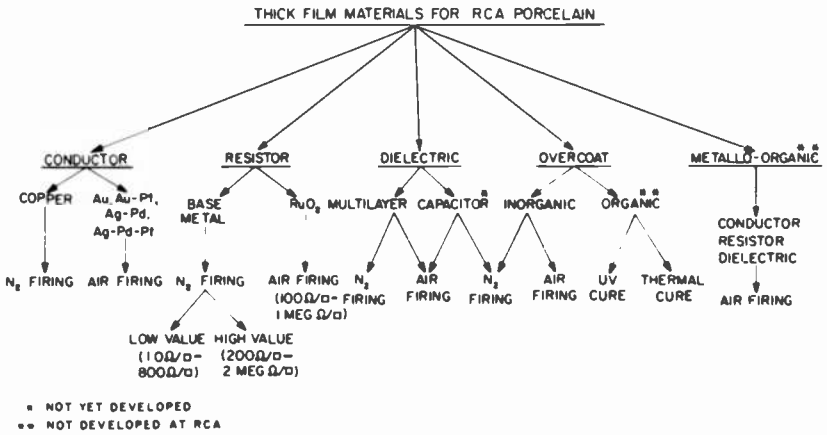

Fig. 1—Thick-film materials for RCA porcelain-coated steel substrates.

RuO_2 resistor, multilayer dielectric, and overglaze inks) have been formulated at RCA Laboratories for use on the porcelain boards.

Conductor Inks

The copper conductor inks are fired in nitrogen and the gold, gold-platinum, silver-palladium and silver-palladium-platinum inks are fired in air. The electrical resistivity is 0.003–0.005 Ω/□ for the copper and the gold films, 0.03–0.06 Ω/□ for the silver-palladium inks, and 0.05–0.1 Ω/□ for silver-palladium-platinum and gold-platinum inks, all for fired film thicknesses of 0.4–0.6 mil. The choice of a particular ink for any application will depend upon the conductor film properties demanded by the circuit and the cost considerations. Other combinations of the precious metals, nickel, or aluminum can also be used to formulate conductor inks for the porcelain-coated steel substrates.

Resistor Inks

Copper-compatible base-metal resistor inks have been developed to give sheet resistivities of 10 Ω/□–2 MegΩ/□. These are based upon two different materials systems. The first system gives sheet resistivities of 200 Ω/□ to 2 MegΩ/□ and the second a range of 10 Ω/□ to 800 Ω/□. For firing in air, RuO_2-based resistor inks have been formulated to give a sheet resistivity range of 100 Ω/□ to 1 MegΩ/□. The gold and the silver-palladium conductors are used to terminate these resistors.

The thick-film resistor materials cover the sheet resistivity range to meet most requirements. Resistors of varying values can be printed at

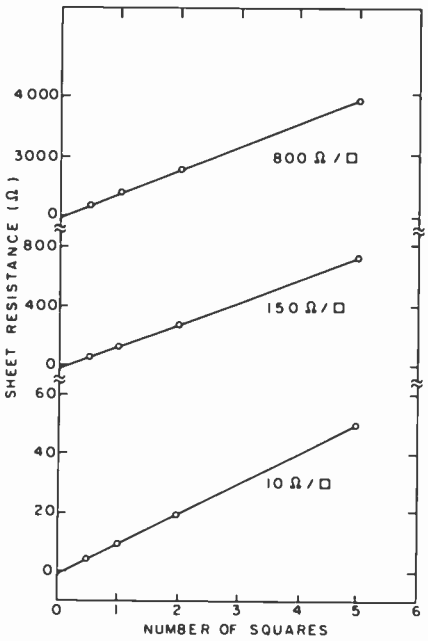

Fig. 2—Sheet resistance versus resistor aspect ratio for base-metal resistors.

the same time by changing the resistor aspect ratio, i.e., the ratio of resistor length to its width. The dependences of the resistor values on the aspect ratio for the low-value base-metal system and for the RuO_2 system are shown in Figs. 2 and 3, respectively. Such a plot for a high-value base-metal system has been previously reported.[1] The plots of sheet resistance versus aspect ratio are linear. The slope of the line gives sheet resistivity for that composition and the intercept on the Y-axis gives the contact resistance between the resistor and its terminations. The aspect ratio for any resistor can be calculated from

$$R = \rho_s (l/W) + C,$$

where R is the sheet resistance, ρ_s the sheet resistivity, l/W the aspect ratio and C is the contact resistance.

Once the aspect ratio is calculated, the actual size of the resistor is determined by considering the power handling characteristics of the resistors and the "real estate" available in the hybrid circuit.

Dielectric Inks

Copper-compatible low-K dielectric inks have been developed for firing

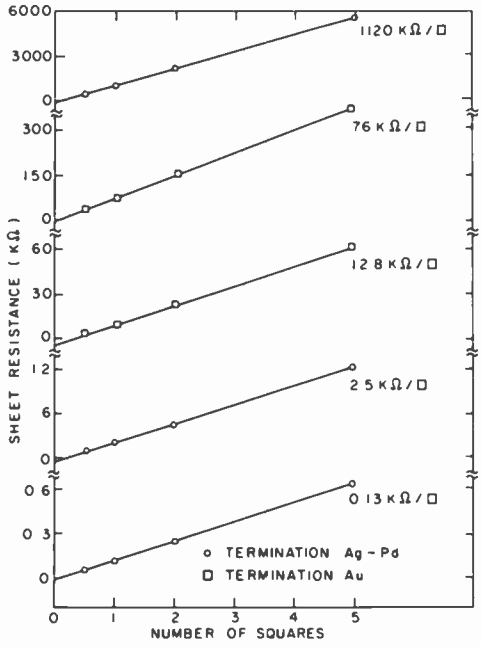

Fig. 3—Sheet resistance versus resistor aspect ratio for RuO_2 resistors.

in nitrogen on the porcelain substrates. Similar compositions are also used with precious-metal electrodes for firing in air. The dielectric constant of the film is 8–9. These inks can be used for fabricating multilayer structures and cross-overs.

Overcoat Inks

Inorganic overglaze inks were formulated for firing in nitrogen and others for firing in air. The ink capable of being fired in nitrogen is used with the base-metal resistor inks and copper conductors, whereas the inks fired in air are used with the RuO_2 resistor inks and the precious-metal conductors. The organic overcoats, such as UV-curing Dynachem–SM18 and thermal-curing ESL–240 SB, can also be used on these substrates.

Metallo-Organic Inks

Metallo-organic deposition is a convenient and economical method of producing thin films (1000–5000 Å) employed in the electronic industry. Thick-film techniques are often used. These materials normally require smooth substrate materials such as pyrex, quartz, and glazed ceramics

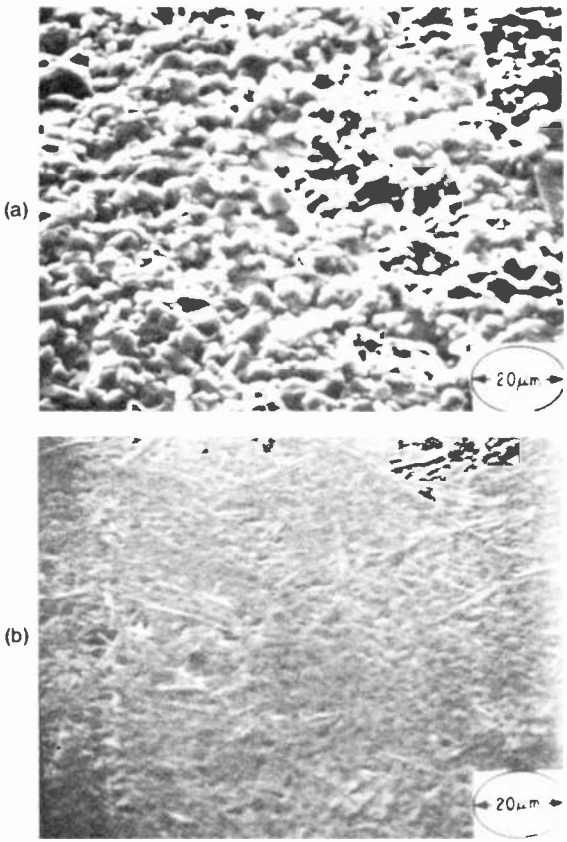

Fig. 4—Scanning electron micrographs of surface (a) of 96% alumina and (b) of porcelain.

and are fired in air at peak temperatures of 500–800°C. The RCA porcelain-coated steel substrates are suitable for use with these materials because of their surface finish and chemical compatibility. The surface finish of the porcelain is compared to that of 96% alumina in the scanning electron micrographs of Fig. 4 and Tallysurf plots of Fig. 5. Metallo-organics also provide means of applying materials by methods other than screen-printing. Such methods are spraying, spinning, brushing, and dipping. Since porcelain-coated steel substrates can be produced in irregular shapes at fairly low prices, some of these techniques can be particularly useful.

In addition to the above, some of the initial materials investigated for computer-driven ink-jet type printing techniques for electronic circuit fabrication were based on metallo-organics. The RCA porcelain is suit-

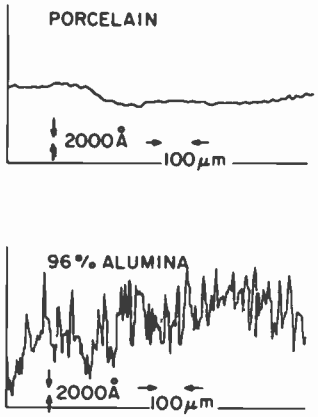

Fig. 5—Tallysurf plots of porcelain and 96% alumina.

able for these new applications. On an area basis, the films made from metallo-organics are considerably cheaper than those made from the conventional precious-metal thick-film inks because the metallo-organic films are orders of magnitude thinner than the conventional thick films. Hence the coverage obtained from the same amount of precious metal is much larger by the metallo-organic processes.

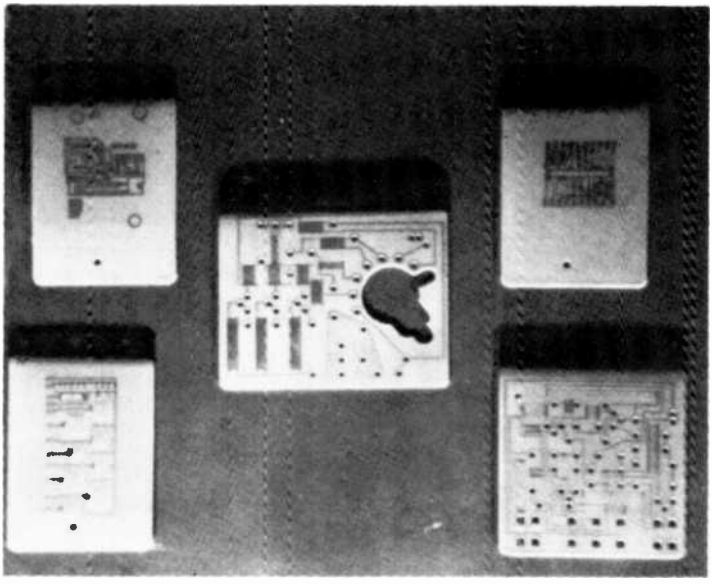

Fig. 6—Porcelain boards with copper conductor, base-metal resistor, and cross-over dielectric films.

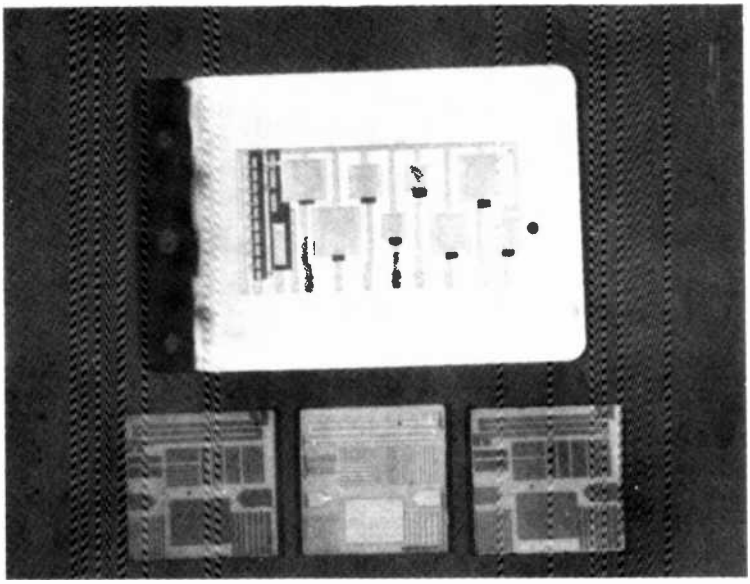

Fig. 7—Porcelain boards with precious-metal conductor (Au, Ag-Pd, Au-Pt) and cross-over dielectric films.

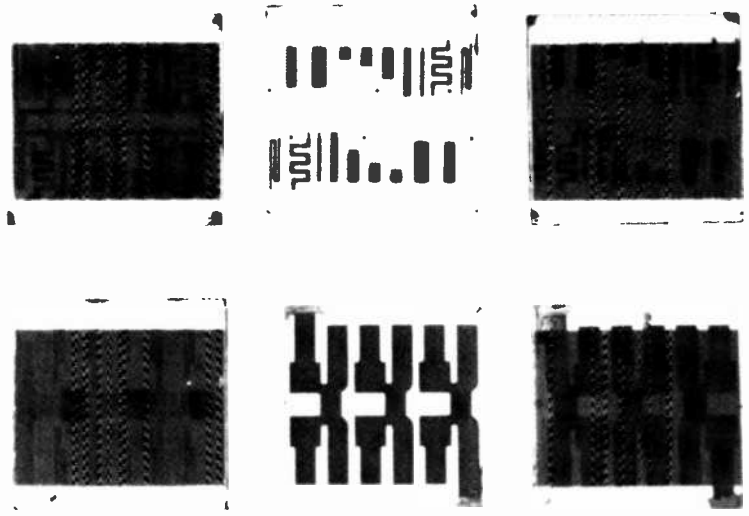

Fig. 8—Porcelain boards with RuO_2 resistor, overglaze, and metallo-organic conductor and resistor films.

Some of the circuits fabricated from the RCA porcelain-coated steel substrates using various thick-film compositions are shown in Figs. 6, 7 and 8. These photographs show conductors, multilayers, resistors, and overglaze films obtained from the base metal and the precious metal ink systems.

Processing the Thick Film Materials

The thick-film materials are generally applied using screen-printing techniques. When the physical nature of the substrate does not permit screen printing, other methods such as spraying, dipping, and brushing can be used. For encapsulation of the thick-film hybrid circuits, either dipping, fluidized bed coating, or hermetic sealing techniques are used.

Firing

This study has been conducted on screen-printed films. Stainless steel screens were used for printing. For through-hole coating, low viscosity conductor inks were printed while suction was applied from beneath the substrate. The films were dried in air at 125 ± 5°C for 5–15 minutes and fired in a belt furnace. The base-metal ink system was fired in nitrogen at a peak temperature of 900 ± 5°C, with a time at peak temperature ranging from 4–6 minutes. The total cycle time was 30–40 minutes. The oxygen content in the firing zone was typically 20–30 ppm. The precious metal system was fired in air at peak temperatures of 700–900°C. Total cycle time was 45–60 minutes, with the time at peak temperature ranging from 5–10 minutes. For the fabrication of multilayer dielectric inks, two layers of dielectric inks were printed and fired separately between each set of electrodes to prevent shorts between them. The overglaze inks were fired at a peak temperature of 500 ± 10°C.

Variables Affecting Film Properties

The physical and chemical properties of the ingredients in the inks, firing parameters, and the substrate characteristics dictate the properties of the films obtained. Fig. 9 shows scanning electron micrographs of copper films obtained from two copper inks on the porcelain substrates. Fig. 9a shows well sintered copper contacts whereas the copper film in Fig. 9b shows a poorly sintered structure. The only difference in the two inks is the particle size distributions of the starting copper powders. A properly developed microstructure is the key to the properties obtained from the thick-film inks. It determines the conductivity, solderability,

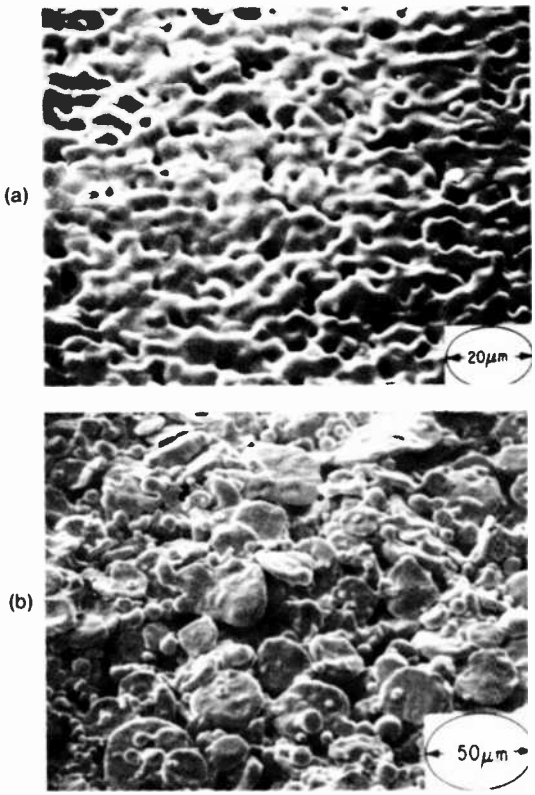

Fig. 9—Scanning electron micrograph of surface (a) of good quality copper film and (b) of poor quality copper film.

solder leach resistance, solder aged adhesion, and wire bondability of the conductor films, as well as the TCR and stability of the resistors and the dielectric properties of the cross-over and the multi-layer films. Fig. 10 shows the power handling characteristics of two resistors measured using a short time overload (STOL) test method. In this test, the resistors are loaded at 6.25 times their rated power for 5 seconds and any permanent changes in the resistances are recorded. The power handling characteristics of the 400 kΩ/□ resistor has been improved significantly over an early 378 kΩ/□ resistor composition by modifications in the glass compositions used for the resistor inks.

The effect of peak firing temperature on the sheet resistivity of the thick-film conductor inks and metallo-organic resistors are shown in Figs. 11 and 12, respectively. With an increase in firing temperature, the sheet resistance decreases due to improved contact sintering. Depending upon the chemical composition of the thick-film inks, peak firing temperatures

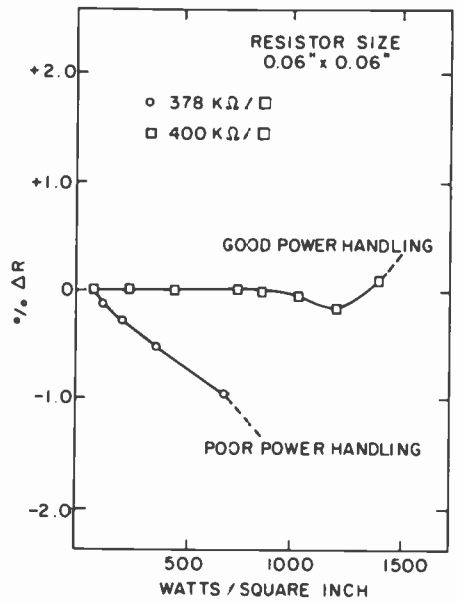

Fig. 10—STOL test data.

of 750–950°C are necessary to obtain fully developed microstructure in the fired films. This is where the importance of the high temperature reheat stability of the RCA porcelain materials is realized in contrast to commercial porcelain materials, which cannot be reheated beyond 650°C. Fig. 12 indicates that the resistance values of the metallo-organic

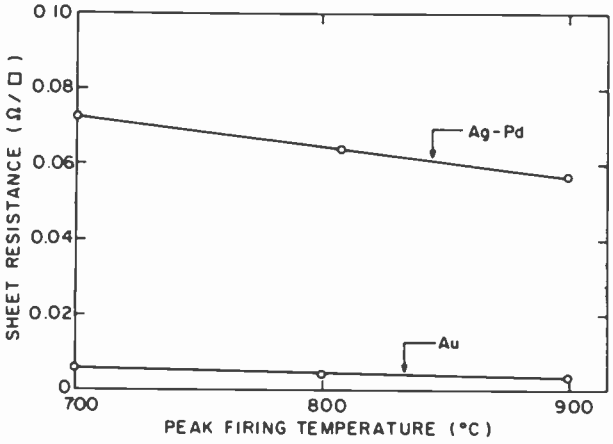

Fig. 11—Effect of peak firing temperature on sheet resistance (precious-metal conductors).

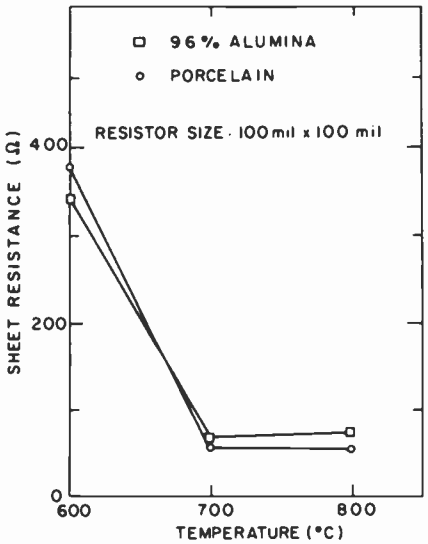

Fig. 12—Effect of peak firing temperature on sheet resistance (metallo-organic resistors).

resistors are similar for alumina and porcelain substrates. But these materials cannot be used on alumina substrates as the surface roughness of the alumina substrates leads to cracks in the conductor and resistor films. Cracks in metallo-organic gold films fired on 96% alumina substrates are shown in the scanning electron micrographs of Fig. 13a. Such cracks are not observed when the same ink is fired on the porcelain substrate as can be seen in Fig. 13b.

Multilayers

For producing multilayer structures, the thermal expansion coefficient of the dielectric should be very close to that of the substrate. This has been achieved in the multilayer paste formulations developed for the porcelain boards by choosing for their base a devitrifying glass composition similar to that in the porcelain boards. These dielectric films have a dielectric constant of 8–10, an insulation resistivity greater than 10^{14} Ω-cm, a dissipation factor less than 0.005, and a break-down voltage greater than 500 volts for 2-mil-thick films terminated with copper electrodes.

Trimming

Since the thick-film process has sufficient inherent variables to result

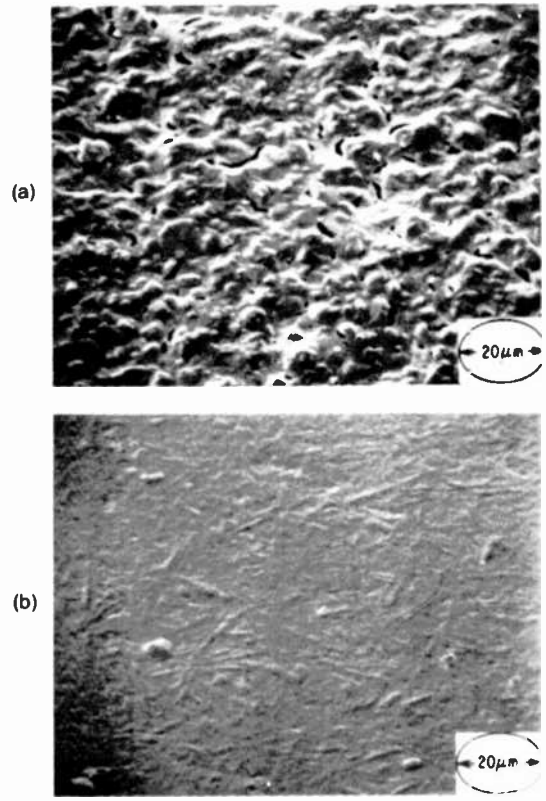

Fig. 13—Scanning electron micrographs of surface of metallo-organic gold film (a) on 96% alumina and (b) on porcelain.

in a distribution of resistor values around the design value, precision resistors must be adjusted by either air-abrasive trimming or laser trimming. These techniques have been successfully employed on the base-metal and the RuO_2 resistor systems fired on the porcelain substrates. Scanning electron micrographs of typical air-abrasive trimmed and laser trimmed resistors are shown in Figs. 14 and 15, respectively.

If the thermal expansion characteristics of the resistors are not matched with those of the substrate, microcracks can form in the laser trimmed resistors. Propagation of the microcracks can lead to increases in the resistance values during the life of the resistors. The glass compositions in the base-metal resistor inks and RuO_2 inks have been chosen to be compatible with the porcelain, and, as a result, microcracks are not visible in the trimmed resistors shown in Fig. 15. Accordingly, the post-trim drift stability of the resistors developed for porcelain boards has been very good.[1]

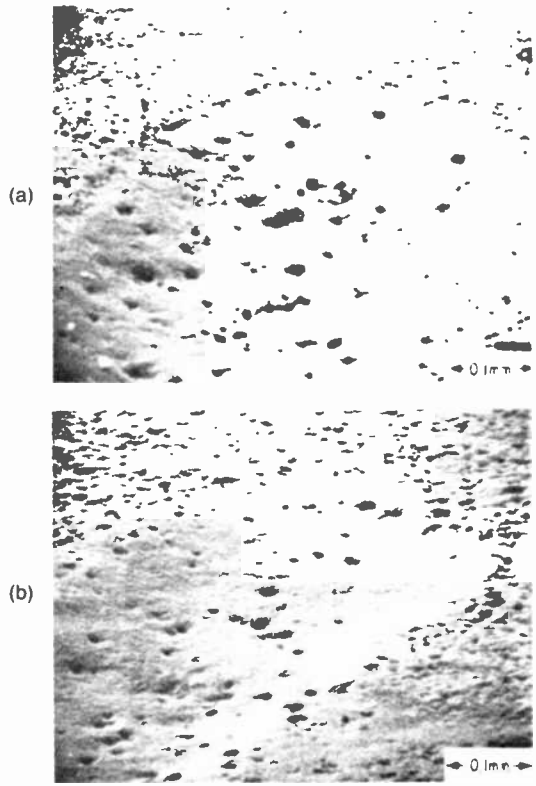

Fig. 14—Scanning electron micrographs of air-abrasive-trimmed base-metal resistors: (a) 2k ohms/□ and (b) 120k ohms/□.

Overcoating

Resistor trimming can be conducted either prior to overcoating or after the overcoating operation, depending upon the resistor tolerances for the circuit being built and the changes occurring in the resistor values during overcoating. The resistance changes of the base-metal resistors during overglazing are about 1–2%.[1] If the organic overcoats are used, these changes will be still smaller. Overcoats can be used as solder masks for conductor areas. The resistance changes after solder dipping are minimal for most of the resistors fired on the porcelain boards. However, overcoating the low value resistors may be necessary to minimize their drifts during wave soldering. Overcoating also helps to minimize the effect of humidity on the resistor drifts. This is illustrated in Fig. 16 for the base-metal resistors.

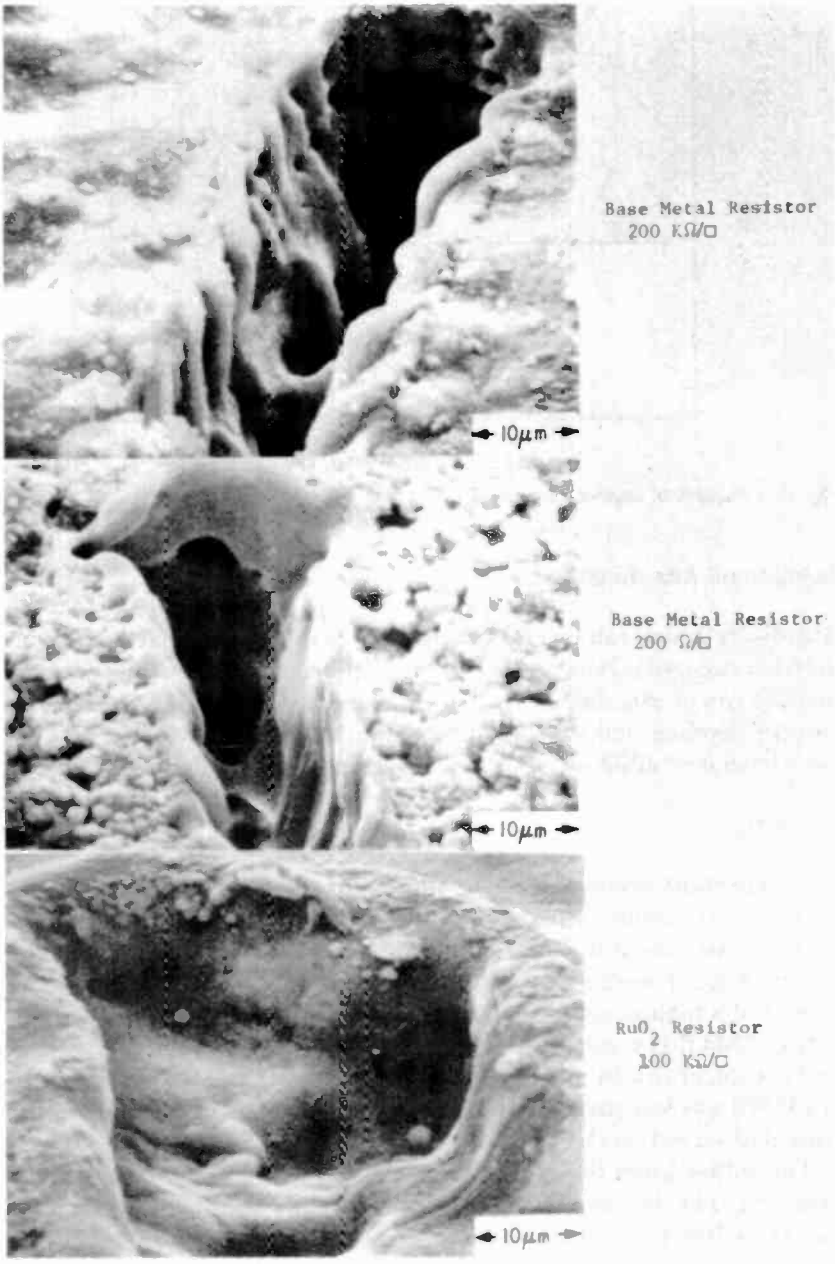

Fig. 15—Scanning electron micrographs of laser-trimmed resistors.

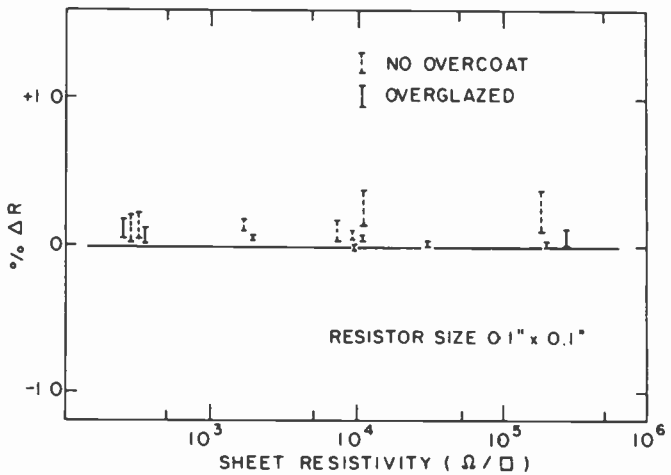

Fig. 16—Stability of laser-trimmed resistors (50°C, 90% R.H., 1000 hours).

Component Attachment

Any discrete electronic part, whether active or passive, that can be soldered or otherwise bonded to a metallic interface can be utilized. Components can be attached by techniques such as soldering, epoxy bonding, eutectic bonding, and wire bonding techniques. Some of these techniques have been evaluated on the porcelain boards and are described below.

Soldering

The important properties of the conductor films to be considered are solderability, solder leach resistance, and solder aged adhesion. The solderability was studied by measuring the contact angle between the solder (after it resolidified) and the film and by observing the solder spread of a molten solder ball on the film. 62Sn/36Pb/2Ag solder and Kester 1544 flux were used. The contact angle between the copper film and the solder (a 0.04 inch diameter solder ball was melted for 5 seconds at 215°C) was less than 15°, and the solder spread was about 75% of the spread observed on OFHC copper foil.

The solder leach resistance of the copper film fired on porcelain is excellent. The decrease in the size of the 0.1 × 0.1 inch copper pads was less than 10% after 21 dips (15 seconds each dip) in 62Sn/36Pb/2Ag solder at 230°C. This means that the leaching of the copper film will be minimal during a standard wave soldering operation. The solder leach resistance of the precious-metal inks fired on the porcelain is shown in Fig. 17. The solder leach resistance of the film improves with increase

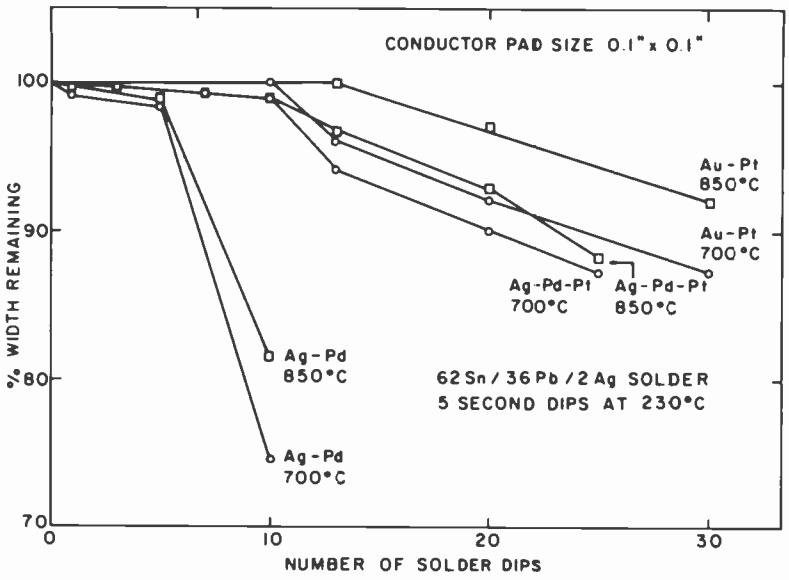

Fig. 17—Solder leach resistance of precious-metal conductors.

in firing temperature. The solder leach resistance of the gold-platinum conductor films is considerably better than the silver-palladium films. Adding platinum to silver-palladium films increases their solder leach resistance.

The solder adhesion of the conductor films was measured on 0.1 × 0.1 inch conductor pads using the soldered wire peel adhesion test method.

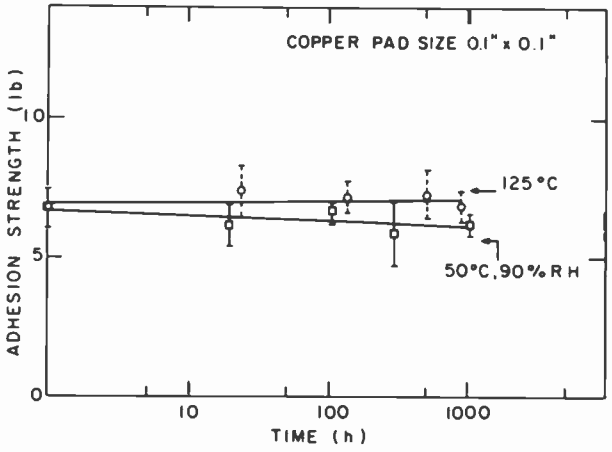

Fig. 18—Effect of heat and humidity on adhesion strength of copper film.

The results for the copper films are indicated in Fig. 18. The peel adhesion of the copper film to the porcelain is good and remains high even after the films are aged at 125°C for 1000 hours. The effect of heat and humidity on the adhesion is minimal. The initial solder peel adhesion values obtained on Au-Pt and Ag-Pd-Pt conductors are also about 6–8 lbs on 0.1 × 0.1 inch conductor pads.

Wave Soldering

It is clear from the above observations that conductor films fired on the porcelain meet the general requirements for component attachment by soldering. The results of wave-soldering experiments specific to the porcelain boards are described here. The thermal behavior of the steel and the porcelain coating during wave soldering is essentially determined by the product of the thermal masses, primarily that of the steel, and the sum of the thermal resistances of one porcelain layer and the porcelain-solder thermal convective resistance. The time constant is about one second. Since the solder contact time for any point on the soldered surface of the board is about 3 seconds for the test conditions used, the board temperature rose approximately to the temperature of the solder.

Propagation of heat in the steel in the travel direction has only a short

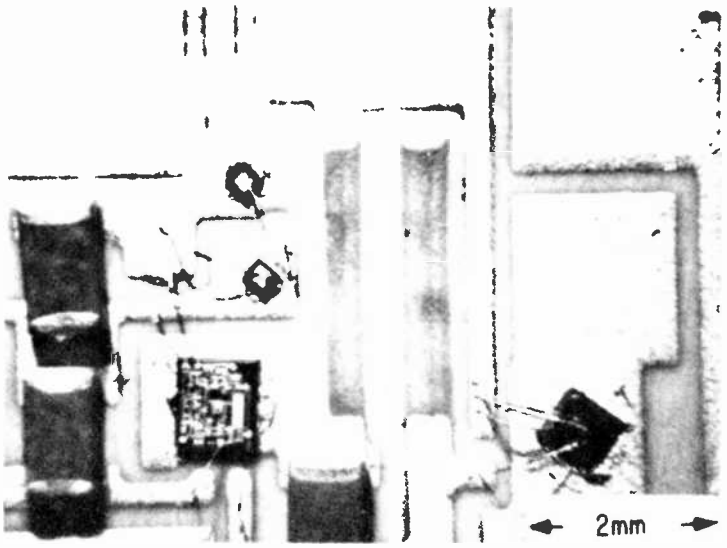

Fig. 19—Optical micrograph of copper film with epoxy bonded chip and ultrasonic aluminum wire bonds.

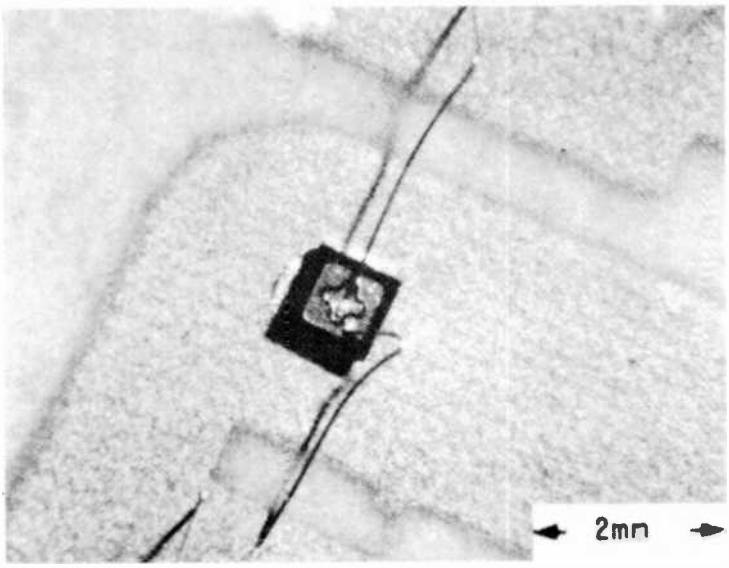

Fig. 20—Optical micrograph of Ag-Fd film with epoxy bonded chip and ultrasonic aluminum wire bonds.

range effect (about 0.1 inch) at the soldering speed used (2.8 feet/minute). The temperature rise starts at the instant of solder contact time.

The thermal behavior of a discrete IC during solder contact is primarily determined by the component itself. The pin temperature rises rapidly (about 1-second time constant) towards a temperature (about 160°C) determined by the temperature divider action of the thermal resistance of the pin section and the other sections, particularly the plastic section, which has a time constant greater than the solder contact time. Cooling of the IC's is affected by the heat stored in the steel. The high emissivity of the porcelain, however, aids in cooling, such that the temperature of a steel board and an epoxy laminated board (160°C top of board during soldering) cool to 100°C in the same time.

Semiconductor Chip Bonding

Chips can be bonded to conductor films on the porcelain boards using epoxy bonding or eutectic bonding. If the epoxy is required to perform a circuit interconnection function in addition to the bonding function, electrically conducting epoxies must be used. These are either silver or gold filled. Epoxy attached chips on copper or Ag-Pd films fired on porcelain are shown in Figs. 19 and 20. A silicon chip device can also be bonded to a gold thick film by means of eutectic bonding between the

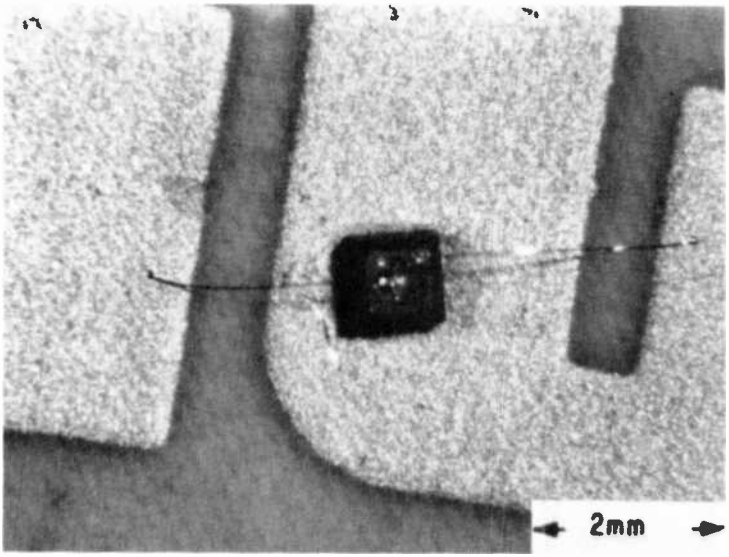

Fig. 21—Optical micrograph of gold film with eutectic bonded chip and thermo-compression gold wire bonds.

silicon and gold. Such die bonds can be made using a gold-backed silicon die, a bare silicon die, or either type of die with a Au-Si preform. A chip eutectically attached to a gold thick film on porcelain is shown in Fig. 21. The chip attachment was done at 410°C using a Kulicke and Soffa model #642 Universal Bench Die Mounter.

Wire Bonding

The interconnections between the thick-film metallizations and IC's can be made by wire bonding methods. Wire bonding is accomplished by thermocompression bonding, ultrasonic bonding, or a combination of the two, commonly called as thermosonic bonding. Figs. 19 and 20 show ultrasonic aluminum wire bonds on copper films and silver–palladium films, respectively. An ultrasonic Al wire bonder (Kulicke and Sofa Model #484) was used to bond 0.0015 inch Al-1%Si wire. The thermocompression bonding of 0.0007-inch gold wire shown in Fig. 21 was accomplished using a Kulicke and Sofa Model #420 nail head bonder. The bonding temperature was 300°C.

The bondability of thick films is determined by the extent of sintering of the conductor particles and the nature of the film surface. The glass compositions in the conductor inks have been selected so that after the

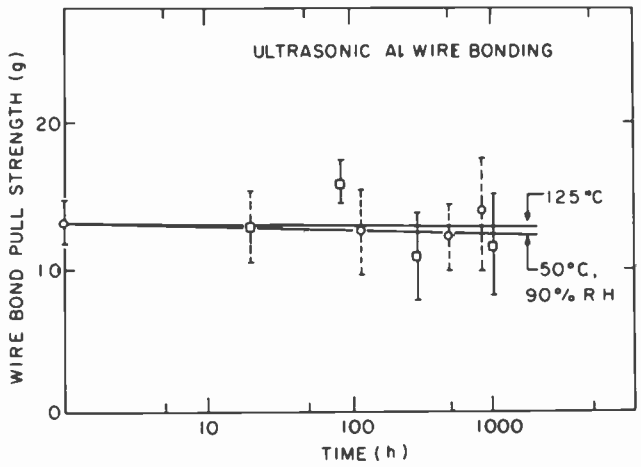

Fig. 22—Effect of heat and humidity on ultrasonic Al wire bonds on copper film.

films are fired, very little glass remains on the surface of the films. Any glass remaining on the surface of the thick films, either in the form of particles or a thin film, can lead to problems in soldering, chip mounting, and wire-bonding. The pull strengths of the aluminum wire bonds formed on copper and silver–palladium films are 10–15 gms; failures are mostly due to wire breaks. The effect of heat and humidity on the wire-bonds was minimal, as shown in Fig. 22 for the copper films.

Conclusions

The properties of RCA thick-film materials fired on RCA porcelain boards meet the requirements for the fabrication of thick-film circuits. Thick-film hybrid circuits for several applications have been successfully fabricated using these materials. The performance of these circuits compares favorably with those fabricated using state of the art ceramic-substrate–thick-film technology. Because of good compatibility between the thick films and porcelain, the long-term testing of soldered conductors, wire bonds, and power loaded resistors have indicated high reliability.

One reason these porcelain-coated steel substrates are more versatile compared to ceramic substrates is because of their ability to be used with metallo-organic inks. In addition, large-area high-reliability thick-film hybrid production has been made possible because porcelain boards can be produced in large sizes considerably cheaper than the ceramic substrates and because a complete base-metal thick-film ink system compatible with these substrates is available.

Acknowledgments

This work was performed within Electronic Packaging Research Group (L. Onyshkevych, Group Head), in the Consumer Electronics Research Laboratories (D. Holmes, Director). We wish to thank D. Dorsey, K. Hang, A. Sussman, and B. Thaler for helpful discussions throughout the course of this work, T. Ward for supplying the porcelain-coated steel samples, A. Kusenko for making the inks, W. Anderson for preparing the glass compositions, and B. Seabury for scanning electron micrographs. Many other people, too numerous to mention, also contributed to the success of this undertaking.

Reference:

[1] A. N. Prabhu, et al., "Characterization of Thick-Film Compositions on RCA Porcelain-Coated Steel Substrates," *RCA Review*, **42**, p. 239, June 1981 (this issue).

Finite Element Analysis of Stresses and Thermal Flow in Porcelain Enamelled Steel PC Boards

J. H. McCusker

RCA Laboratories, Princeton, NJ 08540

Abstract—Finite element analysis was used to determine the effects of the linear thermal expansion coefficients of porcelain on the fired-in thermal stresses in porcelainized steel substrates. Stress concentration effects at coined, partly coined, and uncoined holes in the porcelainized steel boards were investigated for thermal stresses and for 4-point bending stresses. The thermal parameters of the porcelainized steel substrate were used to investigate its thermal behavior for thick-film-resistor heating.

1. Introduction

A high temperature, alkali free, porcelainized steel substrate has been developed at RCA Laboratories. This porcelain material, a partially devitrified glass[1,2] instead of the usual amorphous porcelain, can be refired at temperatures as high as 950°C for fabrication of thick-film patterns and passive components.[3] High-voltage insulating porcelain was obtained by the use of alkali-free materials. The electrical properties are significantly different from commercially available electronic porcelain,[4] but the gross mechanical and thermal properties[5] (not microstructure) of the porcelain are quite similar. The mechanical and thermal properties of the porcelainized steel, however, are significantly different from commercially available nonporcelainized substrates. This paper will use the mechanical and thermal properties of porcelainized steel discussed elsewhere[5] to determine by means of finite element modeling

(1) the stress effects due to firing, applied load, and geometry (especially in a hole region) and (2) the thermal flow due to thick-film-resistor heating on porcelainized steel substrates.

2. Finite Element Modeling of Stresses

The finite element program used was Ansys,[6] which applies finite element methods to stress and thermal flow problems. The element numbers used for 3-dimensional and 2-dimensional stress analyses were 45 and 42, respectively. The 3-dimensional case is the one directly reported on, but the 2-dimensional case is useful for checking the thermal stress induced in a centrally-located hole. The stresses (triaxial) are given in general at the centroids of the elements. The surface stresses (biaxial) are given for an external surface such as the outer porcelain surface. The stresses at the interface between porcelain and steel cannot be obtained with this program.

No interfacial layer between steel and porcelain is used and no slippage at the interface is considered. The corresponding nodes of porcelain and steel at the interface are one common node. These assumptions seem valid for strong porcelain–steel adhesion based on reasonable agreement with experiments reported elsewhere for the four-point bending radii at failure for specimens having good adhesion.[5]

Steel and porcelain are considered as being in the linear stress-strain region. The yield point of steel is considered as the stress at which the linear stress-strain region ends and beyond which the stress-strain curve has a zero slope. The *yield point of steel* is taken as the *failure threshold stress for steel* and, consequently, for the substrate.

The *failure threshold for porcelain* and, consequently, the substrate will be taken as exceeded when *one or both of the biaxial stresses* for the porcelain surface has become *tensile*. This is a conservative failure threshold, but has been observed experimentally.[5] Failure in porcelain is attributed to the propagation of microcracks under tensile stress.

3. Physical Properties and Their Influence on Thermal Stress

Physical properties and parameters normally used in the analysis of stress are listed in Table 1. The physical property exclusive of dimensions that is reasonably changeable is the linear thermal expansion coefficient of the porcelain. This property and the thickness of the porcelain for a fixed steel thickness, f, determine the thermal stresses in the porcelain and steel.

The variations in thermal stresses, bending stresses, and total stresses

Table 1—Physical Properties and Parameters

	Steel α_s	Porcelain α_p
Linear Thermal Expansion[8,1] Coefficient (× 10^{-6}/°C)	14.4	13.0
Poisson's Ratio	0.25	0.25
Young's Modulus,[1,5] psi (×10^6)	30	17.
Yield Point, psi (× 10^3)	30	
Firing Temperature, °C	825	825
Test Temperature, °C	25	25
Thickness, mils	30	7.5 (one side)
Volume Centroids distance from neutral axis, mils (hole region excluded)	11.25	18.75
Surface Centroids, distance from neutral axis, mils (hole region excluded)		22.5

versus f for various $\Delta\alpha$'s, $\Delta\alpha = \alpha_s - \alpha_p$, are shown in Fig. 1. Experimentally the $\Delta\alpha$'s have exceeded the range shown.[1] The four-point bending stresses and radii are based on a moment of 7.9 inch-pounds.

The total stress at the porcelain centroid is in the tensile region for $\Delta\alpha$'s = 0.6 and 1.0 × 10^{-6}/°C. The total stress at the steel centroid is about or above the yield point for $\Delta\alpha$'s = 2.2 and 1.8 × 10^{-6}/°C. A $\Delta\alpha$

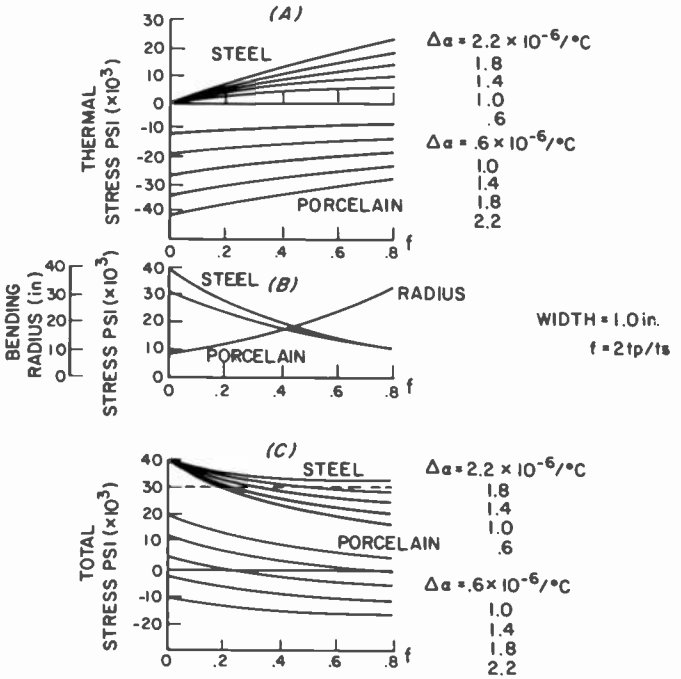

Fig. 1—Thermal and bending stresses for various linear thermal expansion coefficients for porcelain.

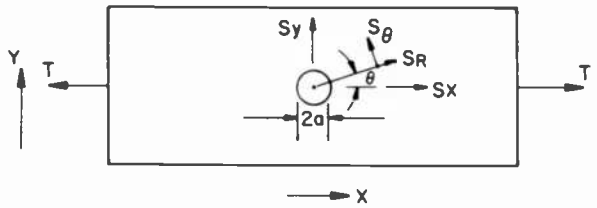

Fig. 2—A centrally located hole in a two-dimensional rectangular plate.

of about 1.4×10^{-6}/°C seems to be most preferable from the failure standpoints used. Different minimum f's or porcelain wall thicknesses are required for all $\Delta\alpha$'s for the given moment. For $\Delta\alpha = 1.4 \times 10^{-6}$/°C, the minimum porcelain wall thickness is about 5 mils. The moment of 7.9 inch-pounds was based on approaching the failure criteria. The bending radius is about 20 inches for $f = 0.5$ which is the radius at which cracking in the porcelain has been observed for the case of good adhesion.[5]

4. Stress Analysis for 3-Dimensional Holes

A circular hole centrally located in a two-dimensional rectangular plate (see Fig. 2) leads to stress concentrations when the plate is subjected to uniaxial tension T.[7] The radial and hoop stresses, S_R and S_θ, for different values of radial distance to hole radius, R/a, are given in Table 2.

At $R/a = 1$, the radial stress is zero due to boundary conditions. The circumferential stresses, however, vary from a compressive stress T at $\theta = 0°$ and 180° to a tensile stress $3T$ at $\theta = 90°$ and 270°. Because of this stress concentration at holes, a quantitative answer was desired for the stress concentration to be expected at porcelainized holes.

Three types of metallic holes have been used experimentally: (1) coined (rounded) cross sections, (2) chamfered or less-rounded cross-sections, and (3) uncoined holes. For simplicity, the porcelain is assumed to conform to the steel; actually, porcelain does not precisely conform due to surface tension. The cost of preparing the holes is directly related

Table 2—Stress Concentration Versus Angular Orientation Under Uniaxial Tension T

R/a	$S_R(\theta = 0°)$	$S_r(\theta = 90°)$	$S_\theta(\theta = 0°)$	$S_\theta(\theta = 90°)$
1	0	0	−T	3T
2	0.47T	0.28T	0.031T	1.22T
4	0.85T	0.089T	0.025T	1.04T
∞	T	0	0	T

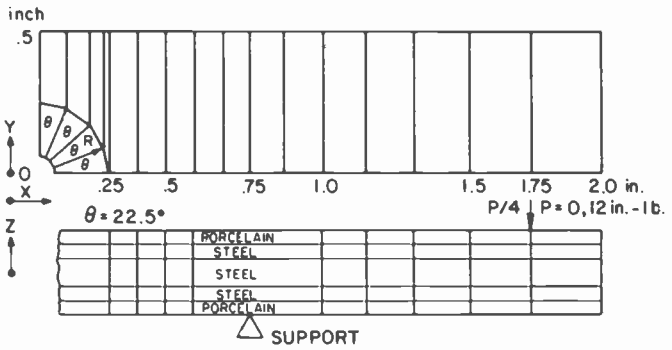

Fig. 3—Element representation of one quadrant of the porcelainized-steel substrate, coined hole.

to the type of hole used. All three types of holes were used in this analysis to determine possible stress differences. A four-point bending test was used rather than a tension test because it was expected that bending or torsion would be the principal stress modes experienced in the field. In the test, a 4 × 1 inch porcelainized steel PC board with a centrally located $\frac{1}{8}$-inch-diameter hole is supported in the thickness direction (Z) at $X = \pm 0.75$ inch and loaded with 0 or 6 lbs ($P/2$) at $x = \pm 1.75$ inches; as shown in Fig. 3 for the quadrant of the board used for finite element analysis for the coined hole. The number of elements in the quadrant is about 260, of which about $\frac{1}{3}$ are located in the radial region of 0.0625 to 0.085 inch.

A cross-section of the elements for the X-Z plane in the neighborhood of the hole is shown in Figs. 4, 5, and 6 for the coined, $\frac{2}{3}$-coined, and rectangular uncoined cases, respectively. Four additional sets of nodes

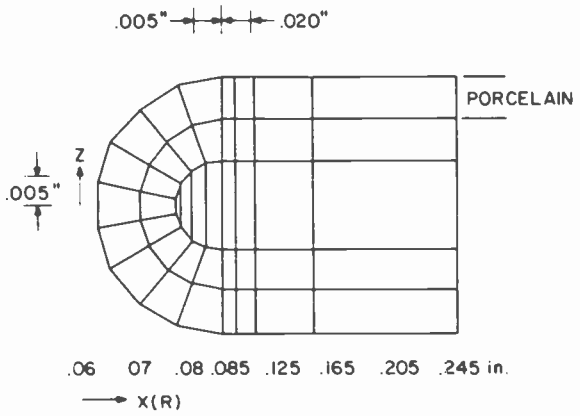

Fig. 4—Elements in XZ plane in vicinity of coined hole.

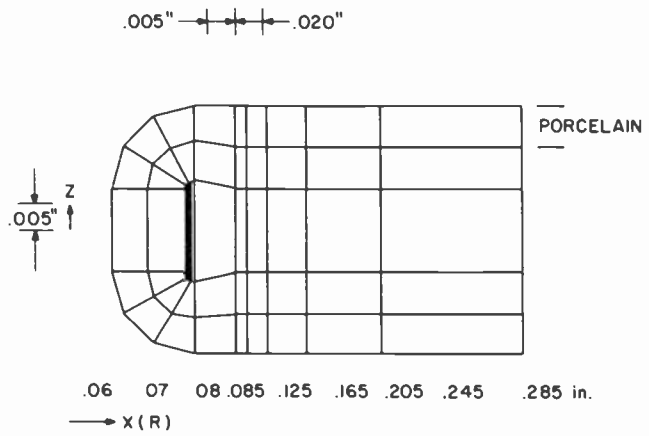

Fig. 5—Elements in XZ plane in vicinity of $^2/_3$-coined hole.

similar to that on the X-Z planes are generated as this plane is rotated in steps of 22.5° about the Z-axis into the Y-Z plane. Circular symmetry is maintained until the stress concentration effect has been reasonably reduced, about $R/a \approx 4$ (see Table 2).

In four-point bending of a board without holes, the stresses at a fixed distance from the neutral plane are independent of X in the region between the supports. The thermal and bending stresses for a board with no holes in the region between the supports are the values of stresses that are approached as the radial distance from the center of the hole is increased to about 0.2 inch, as shown in Figs. 7–15 for the different hole types. The thermal stresses for porcelain (Figs. 7–9) and steel (Figs. 13–15) are -20×10^3 and $+10 \times 10^3$ psi, respectively. The total stresses in the x direction, S_x, due to both thermal and bending stresses are

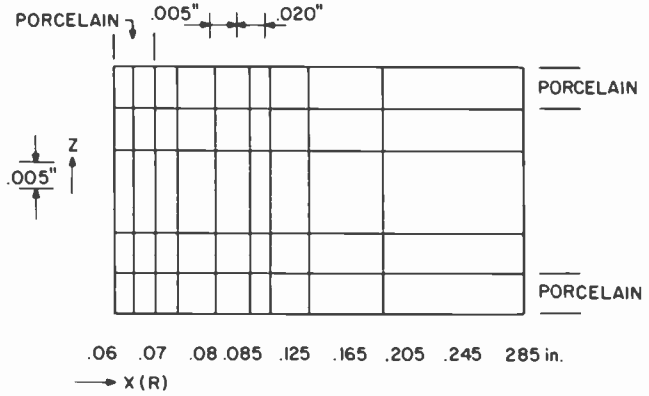

Fig. 6—Elements in XZ plane in vicinity of uncoined hole.

-6×10^3 and 22×10^3 psi for porcelain (Figs. 10–12) and steel (Figs. 13–15), respectively, which are well below the failure thresholds. The total stress in the y direction, S_y, for porcelain is reduced from 20×10^3 psi thermal compression to 17×10^3 psi compressive. This reduction is caused by the Poisson effect due to the tensile bending force in the x direction. This additional compressive strain reduces the compressive stress required to balance the thermal strains.

4.1 Thermal Stresses at Porcelain Surface

The stresses at the porcelain surfaces in the region of the hole are shown in Figs. 7, 8, and 9 for the thermal stress due to recrystallization at 825°C and subsequent cooling to room temperature. Since the thermal stress curves are independent of θ, only one set of curves is required. One component of the biaxial stresses is a hoop or circumferential stress. The other stress component is perpendicular to the hoop stress and is tangential to the surface contour.

The hoop stress for the porcelain surface for the coined hole was essentially constant at -20×10^3 psi, as shown in Fig. 7. The hoop stress for the uncoined hole (Fig. 9) decreases at the top surface of the porcelain at $R = 0.064$ inch. The hoop stress for the ⅔ coined case (Fig. 8) is slightly less than for the coined case.

The tangential stresses in all cases show marked decreases near the hole. In the coined case, however, (Fig. 7) the tangential stress at large distances ($R > 0.085$ inch) is gradually converted from a radial to a thickness stress in the lower walls of the hole ($R = 0.0625$ and 0.063 inch). In the case of the uncoined hole (Fig. 9), the two points on the inner wall ($R = 0.0625$ inch) have thickness stresses but no radial stresses. The point on the top surface ($R = 0.064$ inch) which has almost zero tangential stress has neither a thickness nor a radial stress component. Thus the porcelain at the uncoined rim is not subjected to the usual biaxial

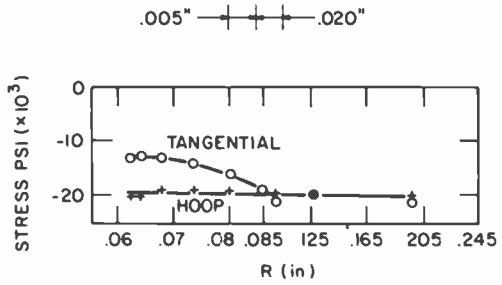

Fig. 7—Thermal stresses at porcelain surface in coined hole vicinity.

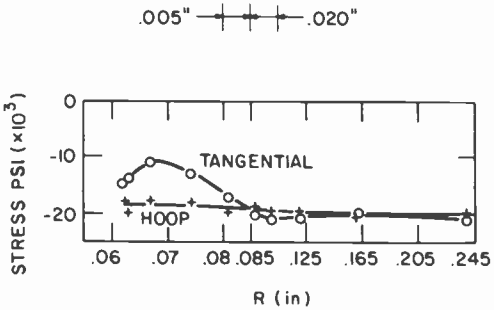

Fig. 8—Thermal stresses at porcelain surface in ⅔-coined hole vicinity.

compressive stresses but essentially only to a uniaxial hoop stress. The hoop stress is −17,000 psi, the thickness stress is −5,000 psi, and the radial stress is zero at the volume centroid of this element. The *failure threshold for the uncoined* hole has been approached at *zero applied stress*. This has been verified on 2-dimensional models that can be readily solved in fine detail for the thermal stress at a centrally located hole. These variations in thermal stresses are confined to the region where $R \leq 0.085$ inch.

4.2 Thermal and Bending Stresses at Porcelain Surface

When external stresses are applied, the resultant hoop stresses are a function of θ for both porcelain and steel. The total stresses in both porcelain and steel are only shown for tensile bending, which is the factor that will contribute to failure. The total stress for the porcelain surface is shown for θ at approximately zero and 90°. The total stress for steel is only shown for θ at approximately 90°. When bending stress is applied, the resultant stresses for the porcelain surface near the hole region are shown in Figs. 10–12 for the coined, ⅔-coined, and uncoined holes, respectively. As can be seen from these figures and from Figs. 7–9 for the

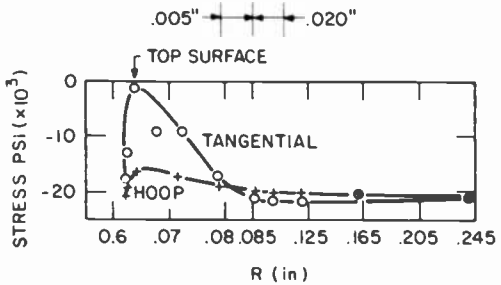

Fig. 9—Thermal stresses at porcelain surface in uncoined hole vicinity.

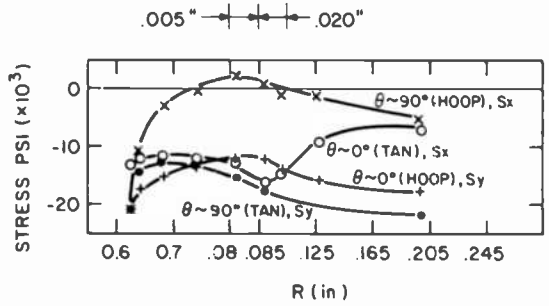

Fig. 10—Combined thermal and tensile bending stresses at $\theta \sim 0°$ and 90° in the coined hole vicinity.

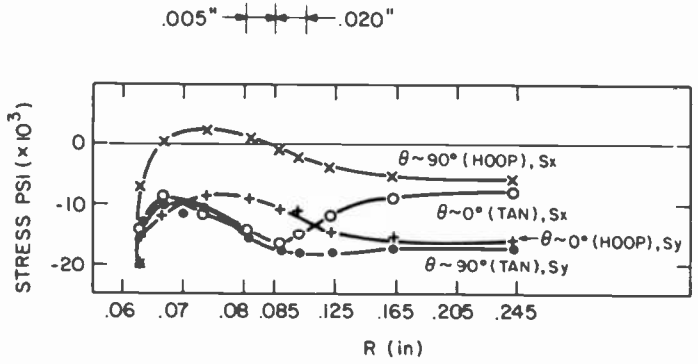

Fig. 11—Combined thermal and tensile bending stresses at $\theta \sim 0°$ and 90° in the $^2/_3$-coined hole vicinity.

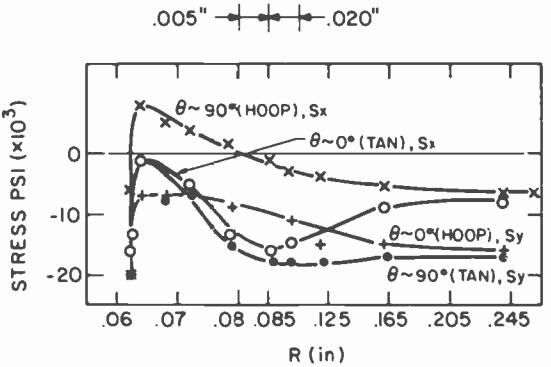

Fig. 12—Combined thermal and tensile bending stresses at $\theta \sim 0°$ and 90° in the uncoined hole vicinity.

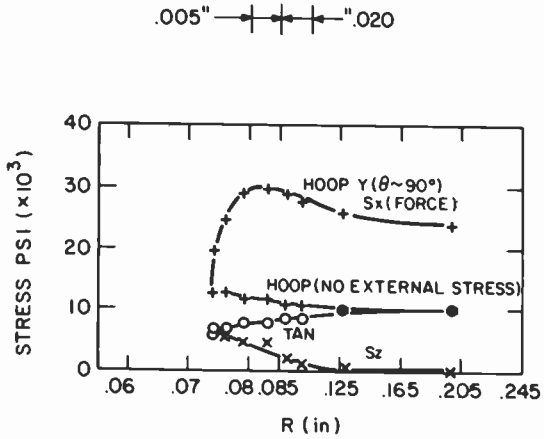

Fig. 13—Thermal stresses and total hoop stresses for steel in coined hole vicinity.

thermal stress, the tangential stresses at the surface of the porcelain irrespective of angle are, surprisingly, the initial thermal stresses up to a radius of 0.085 inch. Beyond 0.085 inch, the tangential stress for $\theta \sim 90°$ approaches S_y whereas the tangential stress for $\theta \sim 0°$ approaches S_x. S_y is $-17{,}000$ psi and S_x is $-6{,}000$ psi.

Hoop stresses are, however, markedly effected by the angle and the bending stresses, as shown in Figs. 10–12. The stress at $\theta \sim 90°$ is the larger. The hoop stresses for the uncoined hole (Fig. 12) at $R = 0.064$ inch (top surface) are considerably greater than for the coined hole (Fig. 10), because (1) the stress due to bending is greatest since the unrounded edge

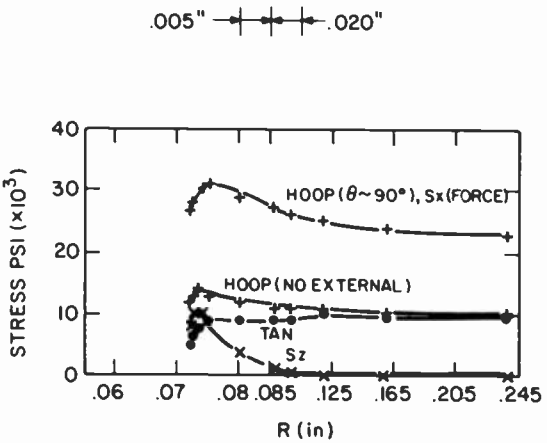

Fig. 14—Thermal stresses and total hoop stresses for steel in $^2/_3$-coined hole vicinity

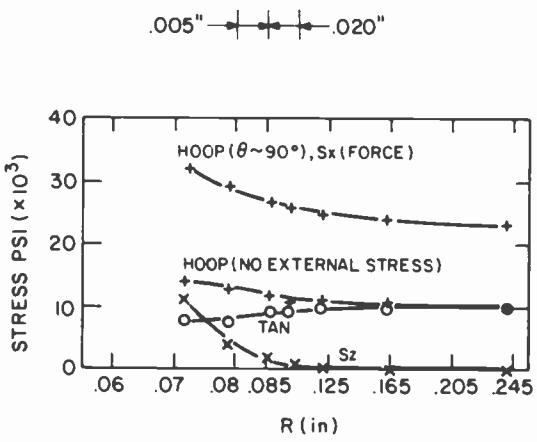

Fig. 15—Thermal stresses and total hoop stresses for steel in uncoined hole vicinity.

has the full thickness associated with the smallest R/a and (2) the thermal compressive hoop stress due to firing is also smaller. For the moment used, the uncoined hole at the edge surface has essentially a tensile hoop stress and a zero tangential stress. Cracks can therefore propagate anywhere in the plane. The coined and ⅔-coined porcelain surfaces are at their failure thresholds, i.e., zero hoop stresses but compressive tangential stresses. For $R > 0.2$ inch, the stress effects due to the hole vanish.

4.3 Thermal Stresses at Steel Centroid

The thermally induced stresses in the steel for the three hole types are shown in the three lower curves of Figs. 13–15. The hoop stresses increase and the tangential stresses decrease for $R < 0.125$ inch. For $R < 0.125$ inch, the thickness or S_z component, normally zero, approaches the hoop stress especially for the uncoined hole.

4.4 Thermal and Bending Stresses at Steel Centroid

For steel, the total hoop stress due to both thermal and bending stresses is a function of θ, but is shown only for $\theta \sim 90°$ in Figs. 13, 14, and 15 for the coined, ⅔-coined, and uncoined holes, respectively. The tangential and thickness stress components for $\theta \sim 90°$ are essentially the same as the thermal stresses, already shown. The total hoop stress is slightly greater for the uncoined case (Fig. 15) as compared to the coined case (Fig. 13). All three cases, however, are at the failure-threshold for steel.

For $R > 0.2$ inch, the stress effects due to the hole vanish for steel also.

4.5 Conclusions

Slightly rounded or rectangular porcelainized holes are undesirable. The porcelain surface near the edges is already near the failure threshold with zero external force, since the tangential thermal stresses are about zero rather than compressive. Maximum roundness is desirable, but the superiority of the coined hole over the ⅔-coined hole is marginal. However, the hoop stresses for $\theta \sim 90°$ for both porcelain and steel are 50% greater in the region of the coined hole than in regions further from the holes. The minimum permissible bending radius is therefore 50 per cent larger ($R = 30$ inches) for a board with a coined hole than for the same board without a hole ($R = 20$ inches). Holes based on this case should be located at least a factor of 3–4 times their radius from the edges of the board. Further study of this separation and the separation from adjacent holes are planned.

5. Thermal Flow Distribution

The element numbers used for 3-dimensional and 2-dimensional thermal analyses[6] are 70 and 57, respectively. The 3-dimensional analysis is used in all cases, but the analysis of the 13.6 × 8.8 inch board also uses the 2-dimensional model. The physical properties and parameters used are listed in Table 3.

Only radiation and convective cooling were used. For vertical convective cooling, the short side was taken as the vertical length. For a high emissivity substrate, the effective radiation coefficient, $E \times h_e$, is at least equal to the convective coefficient, h_c, for short vertical lengths and is the major cooling factor for long vertical lengths or higher ambient temperatures, as shown in Fig. 16.

Table 3—Physical Properties and Parameters Used in Thermal Flow Analysis

	Emissivity (E)			
Porcelain[5]	0.9			
Thin film resistor	0.9			
Alumina[8]	0.75 (0.9 used in model)			
	Thermal Conductivity, W/cm-°C			
	25°C	75°C	125°C	175°C
Steel[8,1]	0.73	0.69	0.66	0.63
Alumina[9] (Coors ADS-96F)	0.26	0.22	0.19	0.17
Porcelain[10]	0.01			
Thin Film Resistor	0.01			

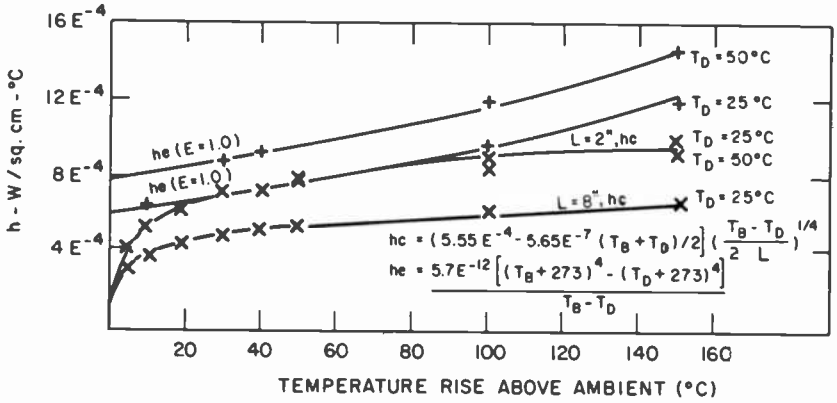

Fig. 16—Radiative and convective coefficients versus temperature rise above ambient.

The effective radiation and convection coefficients were always used as functions of temperature. The thermal conductivity was also used as a function of temperature for the smaller boards.

5.1 Comparison between Experimental and Finite Element Temperature Rises

A 1 × 1 inch thick-film resistor was centrally mounted on a 2 × 2 inch porcelainized steel substrate, with porcelain and steel thicknesses of 9.6 and 37 mils, respectively. The finite element model had the same four thickness layers. The elements with free surfaces had radiation and convection capabilities.

The comparison for temperature rise versus wattage input is shown in Fig. 17 for the hot spot and peripheral locations. The temperature rise for the resistor (T_H) is 20°C above the board temperature (T_E, 90°C) for a thermal input of 10 watts/square inch.

5.2 Thermal Flows for Porcelainized Steel and Alumina Substrates

Figs. 18 and 19 show the calculated temperature distributions of porcelainized steel and alumina with the same overall thicknesses (56.2 mils) versus power input to the centrally located thick-film resistor (1 × 1 inch). Fig. 18 is for a 2 × 2 inch substrate. The rise in temperature at the resistor as compared to the board temperature (about 100°C in each case) is 19°C for the porcelainized steel and 34°C for the alumina substrates at a heat input of 10 W/square inch.

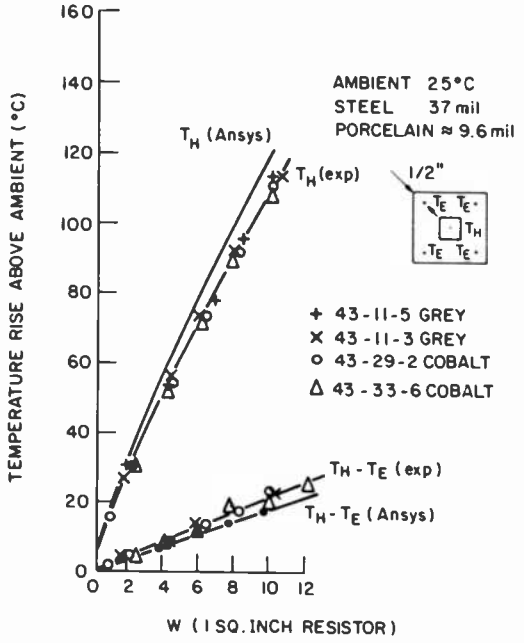

Fig. 17—Temperature rise versus power input, experimental and finite element results.

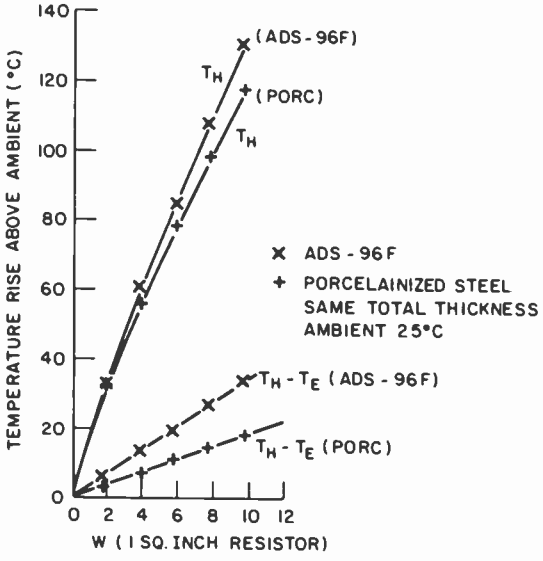

Fig. 18—Thermal distributions of 2 × 2 inch porcelainized-steel and alumina substrates.

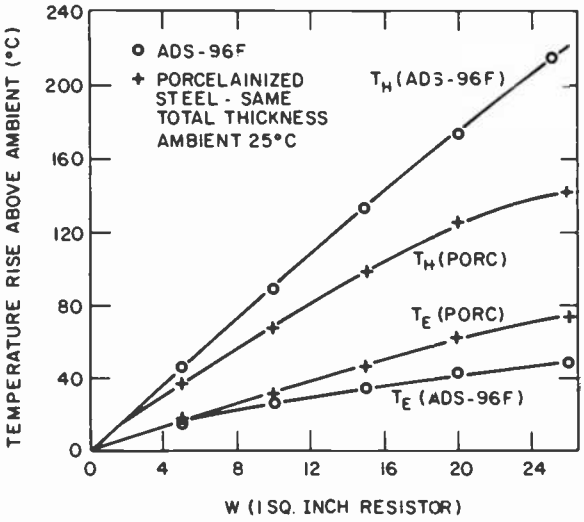

Fig. 19—Thermal distributions of 4 × 4 inch porcelainized-steel and alumina substrates.

Fig. 19 is for a 4 × 4 inch substrate. The resistor on the porcelainized steel substrate is 50°C cooler than that on the alumina substrate for 20 W/square inch thermal heating.

The better thermal behavior of the porcelainized steel is due solely to the steel having a higher thermal conductivity than alumina, since 0.9 emissivity for alumina was used rather than the published value of 0.75.

5.3 Thermal Flow Distribution for 32-Watts Background Heating and 2-Watts Localized Heating

A finite element model was also generated for a porcelainized steel board 13.6 inches long (X) by 8.8 inches wide (Y), with the short side vertical. The porcelain and steel are 7.5 and 32 mils thick, respectively. A 3-dimensional model that is 0.4 × 0.4 inch in the XY plane is used in the localized 2-watt resistor region. The mesh size is 0.05 × 0.05 inch. A 4 × 4 inch transition region with a 0.4 × 0.4 inch square hole is joined to the fine-mesh region. The transition region is then joined to the rest of the board with a coarse mesh (0.8 × 0.8 inch). When the resistor is at or near the edges, the corresponding portion of the transition region that is off the board is eliminated. The transition and the coarse-mesh regions are 2-dimensional elements with the thermal conductivity and thickness of the steel but with the emissivity of porcelain. These elements in the

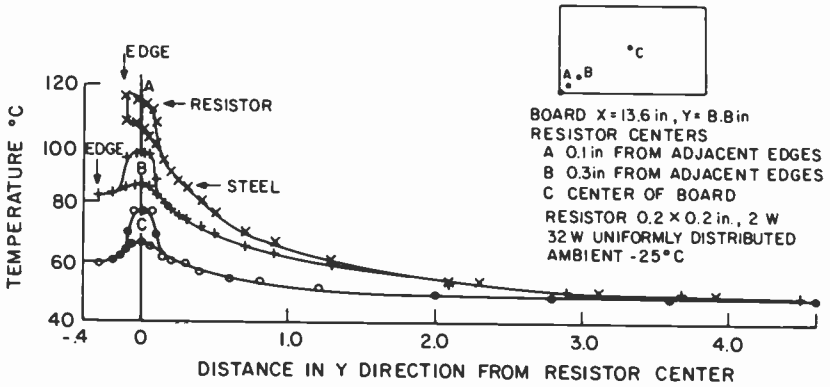

Fig. 20—Thermal distribution for 50 W/square inch localized heating and ¼ W/square inch general heating versus location.

transition and coarse-mesh regions also generate 0.27 watts/square inch (one side only) to give the 32 watts background heating. The 2-watt thick-film resistor located appropriately in the fine-mesh region operates at 50 watts/square inch.

The temperature of the board (due principally to the 32-watt general heating) is 48°C, 23°C above the ambient temperature, as shown in Fig. 20 for $Y \geq 4.0$ inch. Experimental results[5] published elsewhere agree closely. The temperature rise above ambient temperature of a centrally-located 2-watt resistor is 78°C. The temperature rise above the board temperature, however, is only 30°C, of which 10°C is the temperature drop across the porcelain at the high thermal density of 50 watts/square inch. The temperature rise for the 2-watt resistor located exactly at the diagonal edges of the substrate, which is the worst possible location, is 70°C above the board temperature. By moving the resistor only 0.2 inch further away from the edges, the temperature rise above board temperature is reduced to 50°C.

The resistor temperature has decreased to about 2°C of the board temperature at radial distances (Y) of 1.5 inches (central location) and 3.0 inches (edge location). Thus 16 uniformly spaced 2-watt thick-film resistors should not significantly effect the thermal flow characteristics, since the board areas associated with the cooling radii are about $1/16$ of the total area.

5.4 Conclusions

The reasonably high thermal conductivity of steel, the high emissivity of porcelain, and the thinness of the porcelain layers combine to make

a substrate that is thermally suited for thick-film resistors operated at high thermal densities. In many applications, the porcelainized steel substrates are thermally superior to alumina substrates.

Acknowledgments

This work was performed within the Electronic Packaging Research Group (L. Onyshkevych, Group Head), in the Consumer Electronics Research Laboratories (D. Holmes, Director). I wish to thank K. Hang, W. Tsien, and R. Enstrom for helpful discussions throughout this work, T. Ward for supplying the porcelainized steel samples, and J. Honore', III, for his valuable contributions.

References:

[1] K. W. Hang and J. Andrus, "High Temperature Porcelain-Enamel Substrates—Compositions and Interface Studies," *RCA Review*, **42**, p. 159, June 1981 (this issue).

[2] A. Sussman and T. Ward, "Electrophoretic Deposition Coatings from Isopropranol/Glass Slurries," *RCA Review*, **42**, p. 178, June 1981 (this issue).

[3] A. N. Prabhu, K. W. Hang, E. J. Conlon, and S. M. Boardman, "Optimization of RCA Porcelain Composition for Compatibility with Thick Films," *RCA Review*, **42**, p. 221, June 1981 (this issue).

[4] B. J. Thaler, J. H. McCusker, and J. P. Honore, III, "Electrical Properties of RCA Porcelain-Enamelled PC Boards," *RCA Review*, **42**, p. 198, June 1981 (this issue).

[5] W. H. Tsien, J. H. McCusker, and B. J. Thaler, "Mechanical Properties of RCA Porcelain-Enamelled PC Boards," *RCA Review*, **42**, p. 210, June 1981 (this issue).

[6] Ansys is a proprietary engineering analysis computer program developed by Swanson Analysis Systems, Incorporated.

[7] S. P. Timoshenko and J. N. Goodier, *Theory of Elasticity*, McGraw-Hill Book Co., Inc., New York, (1970).

[8] A. Goldsmith, T. Waterman, and H. Hirschhorn, *Handbook of Thermophysical Properties of Solid Materials*, Macmillan Co., New York (1961).

[9] Coors Porcelain Co., Bulletin No. 955, 1976.

[10] E. Sichel, private communication.

[11] F. Keith, *Principles of Heat Transfer*, 3rd Ed., Intext Press, Inc., New York (1973).

The Design, Construction, and Evaluation of a Porcelainized-Steel-Substrate Hybrid-Circuit Module

D. P. Dorsey, R. S. Filson, and W. H. Tsien

RCA Laboratories, Princeton, NJ 08540

Abstract—This paper summarizes the procedures used to build a TV B+ Regulator on a porcelainized-steel substrate. The module employs thick-film-deposited and discrete components. The work was undertaken to gain an appreciation of the implications, strengths, and limitations of a new and novel hybrid technology. As a result of this effort, it has been demonstrated that porcelainized-steel versions of hybrid printed circuits offer an attractive alternative to the conventional phonelic or glass-epoxy printed-circuit boards.

Introduction

An extensive research and development program at the RCA Laboratories has recently led to a family of printed conductors, thick-film resistors, and other dielectric materials that are fully compatible with porcelain-coated steel substrates. It was felt that as the demand for physically large high-volume thick-film printed and/or hybrid circuits increases, porcelain-coated steel may eventually replace the familiar alumina-ceramic substrates or phonelic or glass-epoxy printed-circuit boards on which circuits are typically mounted.

A controlled porcelain layer, 7 to 10 mils thick, is initially deposited and fused to one or both sides of a sheet of soft low-carbon steel that is approximately 32 mils thick. With this strong insulated structure,

high-density printed or hybrid circuitry can be placed on large sized modules instead of being limited to the relatively small and fragile alumina substrates or the typically fragile standard printed-circuit boards.

This new technology allows standard printed-circuit techniques to be used with hybrid elements. For example, through-hole printing and wiring, wave-soldering, and double-sided printing can be used with porcelainized steel circuit boards. Environmentally, porcelainized steel printed-circuit boards offer many advantages. The steel substrate can be molded or bent before porcelainization to form a self-supporting chassis. It can also provide a strong mounting structure for other related electronic hardware (such as transformers) or be folded to produce an effective intracircuit electrostatic shield. In addition, if a portion of the porcelain coating is removed, either in manufacture or later by abrasion, the steel substrate can be connected as a circuit ground-plane or as an effective heat transferring shield. Also, whenever excessive heat and/or vibration may be too severe or hazardous for the typical alumina substrates or the phonelic or glass-epoxy printed-circuit material, porcelain-steel hybrid circuits can offer a reliable, mechanically strong, and cost-effective alternative.

Because of the versatility of porcelainized-steel hybrid-circuits, the electronics industry has been turning to them for solutions to problems that have not been solved by conventional printed-circuit techniques. As this technology continues to grow and new manufacturing techniques evolve, the application of porcelainized substrates into new products is certain to increase.

Initial Considerations

Converting a specific circuit into a thick-film form on a porcelain-coated-steel substrate requires careful consideration of the functional and performance requirements of the final network. Transposing a conventional circuit board or schematic to a thick-film network can be an involved process, but with some experimentation and measurements, to become familiar with the circuit, the conversion can proceed in a very orderly fashion. The capabilities and limitations of the technology must be considered throughout the design process. The size, weight, shape, network performance, and the manufacturing process should be given prime consideration.

During the initial phase of the conversion, it is desirable to be aware of the processing technology and its effect on the electrical characteristics of the substrate. All of the processing techniques in some way affect circuit behavior, and consideration of these effects in the initial design

will minimize the typical development frustrations, provide quick corrective feedback when circuit requirements exceed the process limitation of the thick-film hybrid guidelines, and insure the ultimate desired performance characteristics of the final circuit.

An accurate schematic diagram must be obtained or prepared for the circuit that is to be converted to a porcelain-steel thick-film hybrid network. If at all possible, the circuit should be "breadboarded" and analyzed until the circuit's behavior is clearly understood. As an alternative, computer-aided-design programs can be effectively used to analyze circuits for conversion. During this initial step, consideration must also be given to logical circuit partitioning, thermal distributions, potential signal cross-coupling effects, and maximum allowable component tolerances. A worst-case analysis should be performed on the circuit to fully understand the effects component variations may have on the circuit. In addition, cursory consideration should be given to the circuit layout so that it will approximate the final hybrid configuration. All of these "action" items will increase the probability that the converted circuit will provide excellent and reliable performance.

It is important to remember that thick-film resistors can be screened and adjusted to any desired value; it is not necessary to use standard EIA values. With this in mind, some resistors may even be eliminated. The cost of a thick-film resistor will increase as the resistive tolerance decreases. Therefore, it is best to avoid close tolerance resistance values. In many instances, using two thick-film resistors and establishing a controlled impedance ratio will avoid the relatively expensive process of dynamic trimming. Since a thick- film resistor can be screened to any initial value, resistors sometimes can be specified so as to increase, or broaden, tolerance requirements. For example, a 3.0 kΩ $\pm$ 5% resistor may be designated as 2.87 kΩ $\pm$ 10%. Although 3.0 kΩ is a standard value, its tolerance (5%) is generally specified for an expected circuit performance. However, if the same resistor can be specified as the lower tolerance level, and at a more exact value (2870 Ω), its tolerance may be increased to $\pm$10%.

Before selecting the discrete components for conversion to thick-film resistive and capacitive devices, the components used in the network should be tallied and a component-profile plotted for all resistors and all by-pass capacitors. This will result in a bell-shaped curve with the components plotted as the independent variable and the total number of components plotted as the dependent variable. These graphical representations will accurately show the resistive and capacitive distributions for the entire network. Our development program allows two different inks to be selected and processed per circuit board. Therefore, based on the resistive profile-curve, the inks should be selected with

corresponding length-to-width and width-to-length aspect ratios to cover the greatest number of potential resistors for the screening process. The inks should be selected to fall somewhere from the 50% to 70% level on the slope of the "bell-shaped" distribution curve. The aspect ratios should be adjusted to allow for a 2:1 or 4:1 overlap of selectivity, i.e., the greatest number of possible thick-film resistors to be screened can be screened by using either resistive ink.

By using this approach, a designer can gain valuable design flexibility around the largest portion of potential thick-film resistive components. This is important when considering the effects of distributed capacitance on a particular network. With an overlapping aspect ratio, any critical resistor can easily be altered in size and shape to control distributed capacitance. For example, the capacitance measured from a given resistor to the substrate is directly proportional to the thick-film-resistor area. If a large distributed capacitance is desired, then the lower value of selected ink should be used to fabricate high value resistor. Or, to minimize the effects of stray-capacitance, the higher value of selected ink should be used. Resistors can also be shaped or tapered to linearly increase or decrease the distributed capacitance along the length of the resistor. This may be very effective with certain frequency peaking circuits.

Usually, some resistors will fall outside the boundaries of the aspect ratios of the selected inks. These are primarily resistors that are either very small in value (10 Ω or less) or very large in value (1 MΩ or greater). Fortunately, for any given network, there are not many of these types. These resistors will become discrete EIA standard resistive components. For layout purposes, use of some discrete resistors can be an advantage. When resistors are screened as thick-film components, layouts can become rather difficult because screened resistors must be insulated from conductor leads and all cross-overs. Discrete resistors, however, can effectively be used as "bridges" to jump over conductor pads, screened thick-film components, or conductor lines. Therefore, with complex circuitry, extending aspect ratios to include all resistive components may be a mistake, and saving a few discrete resistors may significantly ease potentially difficult layout problems. In addition, fabrication of extremely high or low resistive values usually require a great deal of surface area. Sometimes these resistors can be included in the hybrid circuit using either "serpentine" or "interdigitated" screening techniques. Only the physical size limitations will dictate the availability of surface area to accommodate very small or very large resistors. This is left to the discretion of the designer.

Although screened thick-film resistors on porcelainized-steel substrates will stabilize to operating temperatures much lower than their discrete counterparts, thermal problems should be carefully considered

when selecting power resistors for screening. For high-power dissipations (in excess of 10 watts), it may not be practicable to use screened resistors because of the surface area required. Even at a conservative estimate of 50 W/inch^2 per ink, circuit board surface area can be depleted very quickly if all power resistors are converted to thick-film components. Furthermore, special consideration must be given to the size of these resistors after "trimming" to insure that enough surface area remains to handle the required power dissipation.

As an example, let us assume it has been determined that a 2 W resistor will require 4×10^5 mils^2 as a minimum resistive surface area after "trimming" to final value. Therefore, the pretrimmed area (a) for a thick-film resistor de-rated by 30% is

$$0.7\,a = 4 \times 10^5,$$

or, solving for a,

$$a = 1.43\,(4 \times 10^5).$$

In other words, the initial or pretrim resistive area should be 43% larger so that the resistive surface area remaining after trimming is sufficient to handle the required power. Increasing a power resistor's initial area, only to have it "trimmed" away later, complicates high-density hybrid-circuit layouts. High-power dissipating resistors can be an integral part of the thick-film hybrid circuit if (1) there is ample surface area available or (2) double-sided printed-circuit techniques can be used.

The component-profile for by-pass circuit capacitors will show the distribution of the capacitors for the network. "Inks" are not used for the capacitors. They are created by (1) depositing an area of conductor material to be used on one plate of the capacitor, (2) controlling the thickness of the dielectric enamel, and (3) grounding the substrate and effectively using the substrate for the other capacitive plate. The capacitance can readily be determined from the equation:

$$C = \frac{0.255\,kA}{t} \qquad [1]$$

where C is the capacitance in pF, k the dielectric constant of the material, A the conductor area in inches squared, and t is the thickness of the dielectric in inches.

The dielectric constant of the porcelainized steel substrate measures nearly 6.00. Therefore, it will require approximately one square inch of conductor material to produce 200 pF of capacitance. From the component-profile, a family of capacitors can be selected for screening. Usually, only the smaller value capacitors (200 pF or less) can be generated using the conductor material because of the relatively large sur-

face areas required. Coupling-type capacitors can be fabricated on porcelainized circuit boards by using two overlapping conductors separated by an insulator. However, the stray-capacitance measured to the substrate may drastically alter the effects of a coupling capacitor. For any given capacitance, consideration must be given not only to the area calculated for a selected capacitor, but also to the effective area of the conductor leads connecting the capacitor to the other elements of the circuit. The same mathematical formulas can be applied to the two interconnecting leads and must be considered in the total capacitive description. Larger values of capacitance have the same limitations as high-power resistors. That is, capacitors greater than 200 pF can be added to any thick-film hybrid circuit if (1) there is adequate surface area available or (2) double-sided printed-circuit techniques can be used.

As previously mentioned, an analysis should be made on any circuit that is to be converted to a thick-film hybrid equivalent mounted on a porcelain-coated steel substrate. In particular, a worst-case analysis should be performed since it will show the behavior of the circuit while the component values are varied over their known tolerance limits, temperature limits, power dissipation limits, and other parameter variations. Depending on the methods used for this analysis, a wide variety of critical information can be obtained, such as (1) allowable tolerance levels, (2) output parameters, (3) reliability, and (4) maximum or minimum temperature range. A thorough analysis is necessary to establish proper component values and tolerances to assure the circuit specifications will be maintained when all specified components are converted to thick-film devices. A worst-case type of analysis can be accomplished empirically but computer-aided design programs are extremely useful in obtaining this type of data. Many programs are available that can perform dc, ac, and transient analyses as well as worst-case analyses. Because these programs are relatively easy to use, they will readily find wide application, especially in the conversion and development of thick-film hybrid-type circuitry.

Description of B+ Regulator Circuit

One of the circuits selected for conversion to a thick-film hybrid module using the porcelanized steel substance is the B+ Regulator module shown schematically in Fig. 1. This circuit has been used in recent RCA color receivers. Briefly, the operation of the circuit can be described as follows.

The unregulated +150-V dc source provides power to the regulator and SCR anode circuit. The regulator drives an SCR switching network

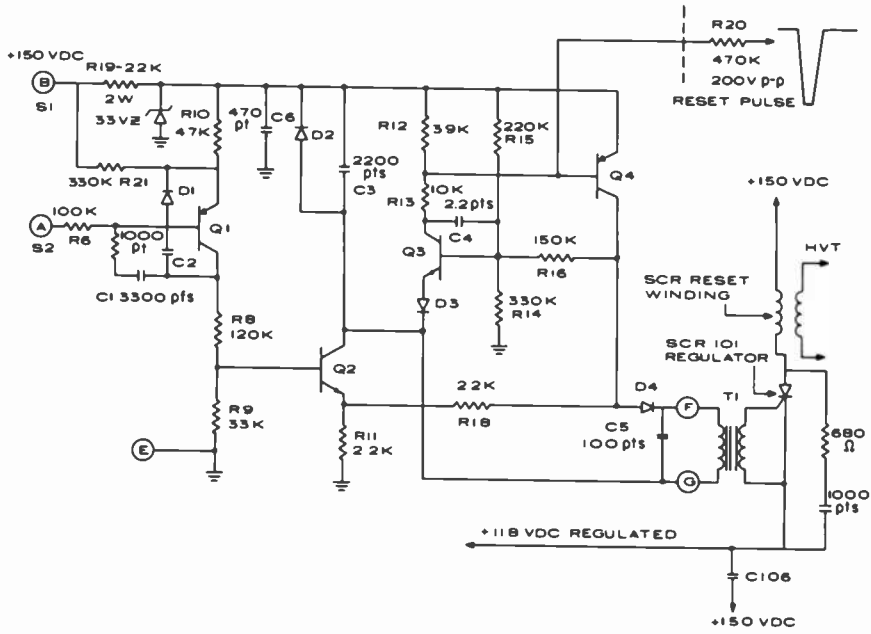

Fig. 1—B+ regulator circuit.

that turns the unregulated source on and off repeatedly, charging the filter capacitor C106. The capacitor, in turn, acts as a filter allowing the stored energy to be discharged into the horizontal output network at a constant rate. The regulated source at the cathode of the SCR, is sampled by the regulator's input stages at the horizontal frequency rate. Since the system is a closed-loop system, the SCR turn-on signal applied to the SCR's gate network maintains the regulated source voltage at exactly +118 V dc.

The gate of the SCR is turned-on by a pulse near the end of the horizontal scan. This charges the filter capacitor C106. The SCR is turned-off by forcing the anode current to zero by applying a 270 V negative pulse to the anode through L103. Therefore, between the regulator generated turn-on and the anode turn-off pulse, the SCR operates as a switching mode power regulator. Using a switching-type regulator to provide the regulated dc requirements of the circuit will significantly reduce the receiver's power consumption.

The longer the SCR is conducting, the higher the regulated voltage will be at the SCR cathode. Conversely, the shorter the SCR conducting period, the less the regulated output voltage will be. Therefore, the length of time the SCR is on determines the relative magnitude of the regulated output voltage.

The regulator's control and oscillator circuits, the SCR, and the transformer are part of the closed-loop regulated system. The oscillator transistors (Q1 and Q2) generate the turn-on gating pulse to the SCR as the developed +118 V dc regulated source is resistively sampled and applied to the base-network of the Q1 error amplifier. The unregulated +150 V dc source is tightly zenered and coupled to the emitter-network of the error amplifier. The difference voltage, i.e., the relative difference between the regulated and unregulated voltage, appears at the collector of the error amplifier Q1. This difference voltage is resistively divided and applied to the base-network of a constant-current generator or oscillator frequency controller Q2. The frequency controller discharges capacitor C3 from the reference zener voltage (+33 V) negatively in a linear fashion. When the collector voltage of Q2 drops approximately 20 volts below +33 V dc, Q3 conducts. Through regenerative action, Q3 will provide base-current drive for transistor Q4 driving it into saturation. The current that flows through Q4 will now flow through transformer T1 generating the turn-on pulse for the SCR.

If the sampled regulated voltage is high (> +118 V dc), the difference voltage measured at the error amplifier collector is low and the discharging current for C3 is low. Therefore, the pulse to turn-on the SCR takes longer to produce and the period between SCR turn-on and turn-off is short. With the closed-loop system, this is in a direction to lower the regulated voltage. If the sampled voltage is low (< +118 V dc), however, the difference voltage is high and the discharging current for C3 is correspondingly high. In this instance, the generated SCR turn-on pulse is produced more quickly and a longer turn-on period is developed for the SCR. Again, with the closed-loop system, this is in a direction to increase the regulated voltage. Thus, the gating of the SCR is "advanced or retarded" as necessary to regulate the B+ (+118 V dc) with respect to the horizontal output requirements.

The error amplifier Q1, constant-current generator Q2, and the regenerative switch Q3 and Q4 provide the turn-on pulse for the SCR gate. The switch and the SCR are turned off synchronously at the horizontal frequency rate. A pulse (S4) is applied to the regenerative switch resetting the regulator and another pulse is coupled through the high-voltage transformer (HVT) momentarily driving the SCR anode to its cathode potential, resetting the SCR. The regulator turn-on occurs near the beginning of the horizontal blanking period and the turn-off occurs at the end of the horizontal blanking period when the system is in the closed-loop mode of operation. With the system functioning in an open-loop mode, the ramp generating period of the constant-current source is nearly 30 μseconds. When the feedback-loop is closed, the system error function indicates an initial high regulating potential. The

network will automatically increase the ramp's linear decay period toward the back edge of the horizontal scan interval (1) narrowing the SCR turn-on pulse and (2) stabilizing the regulated source voltage to +118 V dc. With the SCR turn-on and turn-off occurring within or very close to the horizontal blanking interval, there will not be any objectionable SCR switching transients appearing in the video portion of the picture.

Analysis of Passive Resistive Elements

A computer-aided-design program was written for the error amplifier and constant current source to analyze the open-loop frequency response of the system and to determine the power dissipation in the passive resistive elements. Fig. 2 is a plot of the output response curves of the two input stages. Node voltage-9, the collector of Q2, decays to nearly 0 V dc in approximately 34 μseconds when the regulated sampled input is set to 31 V dc. The regenerative switch, however, will "turn-on" when the ramp voltage decays to about +118 V dc. When the feedback loop is closed, the slope of voltage at node-9 will decrease stretching the linear

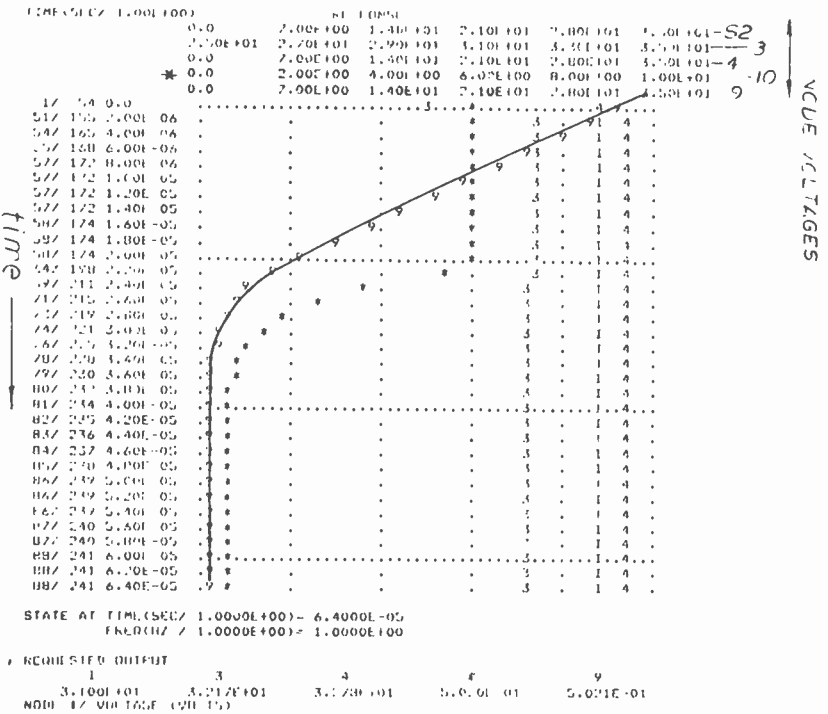

Fig. 2.—Printout from computer-aided design program.

ramp voltage toward 63.5 μsec, the horizontal scanning time. Fig. 3 shows the closed-loop ramp voltage and the synchronizing or resetting pulse applied to the regulator circuitry. Note that the ramp reaches its maximum negative excursion just before the synchronizing pulse is applied. The signal that turns-on the SCR switching regulator begins at the end of the ramping voltage and ends with the positive transition of the synchronizing signal. It is shown in the Q2-collector signal in Fig. 3.

As can be seen in the figure, there is a secondary ramp just before the regulator is fully reset by the synchronizing signal. This is of no consequence since the SCR has already been "turned-on" by the first positive excursion of Q2's collector. Although this lower level ramp has started to recharge capacitor C3, it is completely reset by the trailing or positive edge of the applied synchronizing signal. Once reset, the rgulator repeats the cycle sequence.

The power dissipated in the regulator's discrete resistors averages less than ¼ W per resistor except for the zener reference load resistor. It will dissipate nearly 600 mW under normal operation. Using the waveform analysis of Fig. 2, the power dissipations in the remaining resistors can easily be calculated. For example, at worst-case, the current through R8, R9, and R10 when Q1 is fully saturated is just 0.21 mA. Therefore, the power dissipated in R8 (the largest resistor) is less than 10 mW. Under normal operation, the regenerative switch Q3 and Q4 has a very low conduction duty cycle. Typically, the "on" duty cycle for this electronic switch is less than 15 μs. For this particular circuit, power dissipation is not a serious problem. However, for circuit conversion to resistive thick-film components, the circuit must be thoroughly understood to

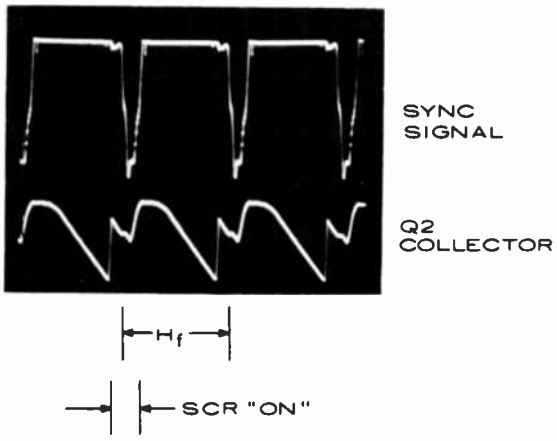

Fig. 3—Original B+ regulator network synchronizing signal and ramping signal.

insure the final thick-film resistor areas are capable of handling the required network power.

Thick-Film Resistor Design

The circuit selected for conversion to a porecelainized steel thick-film hybrid network is not a complex network. It was selected primarily to show the concepts and techniques used for a successful conversion to an operational thick-film regulating circuit. There are fourteen possible resistors that can be converted to thick-film resistive components (see Figure 1). These resistors are tabulated in Fig. 4. The resistor schematic numbers are in column R and their magnitudes are in column V. The resistor wattage rating is shown in column WT. For this example, a single ink was selected to cover the range of resistors, although several inks could have been used. The regulator resistors vary from a low value of 2.2 kΩ to a high value of 330 kΩ. An ink with a resistivity of 10 kΩ per square was chosen for this development and it is designated as column P.

The final thick-film resistors will be trimmed to a final size. Therefore, the resistors are devalued to a new calculated range 33% below the final magnitude. The recalculated value is designated as column RV. Column S is the number of squares required for the initial resistor; it is simply the ratio of RV to P. The number of squares (S) is also related to the ratio of the actual length (LA) to the actual width (WA). It is evident at this juncture, that many combinations of LA and WA will satisfy the number of squares (S) to generate a given value of resistor (RV). However, power

B + REGULATOR						· MILS · in²				MILS			← MILS →	
R	V	WT	P	RV	S	WA	LA	A	Cs	PAD SIZE	Cp	Ct	Wr	Lr
19	22K	2	10K	14.7K	1.47	205	300	.062	12.4	205/30	2.46	14.86	205	360
9	33K	¼	10K	22K	2.20	100	220	.022	4.4	100/30	1.20	5.60	100	280
11	2.2K	¼	10K	1.47K	.147	680	100	.068	13.6	680/30	8.16	21.70	680	160
18	22K	¼	10K	14.7K	1.47	100	147	.015	3.0	100/30	1.20	4.20	100	207
6	100K	¼	10K	66.7K	6.67	100	667	.067	13.3	100/30	1.20	14.5	100	727
8	120K	¼	10K	80K	8.0	100	800	.080	16.0	100/30	1.20	17.2	100	860
10	4.7K	¼	10K	3.13K	.313	200	63	.013	2.6	200/30	2.40	5.00	200	123
12	3.9K	¼	10K	2.6K	.260	200	52	.010	2.0	200/30	2.40	4.40	200	112
13	10K	¼	10K	6.7K	.670	200	133	.027	5.4	200/30	2.40	7.80	200	193
15	220K	¼	10K	147K	14.7	100	1470	.147	29.4	100/30	1.20	30.6	100	1530
16	150K	¼	10K	100K	10	X								
14	330K	¼	10K	220K	22	X								
7	47K	¼	10K	31.3K	3.13	100	313	.031	6.2	100/30	1.20	7.40	100	373
21	330K	¼	10K	220K	22	X								

Fig. 4—Thick-film resistor calculations.

considerations dictate the minimum resistive surface area permitted by the network, and the restrictions on the modules final physical size usually determines the maximum resistive surface area. For each resistor, a compromise in actual width and actual length was empirically selected and they are indicated as columns WA and LA. The thick-film resistive area (A) was then calculated and, based on the dielectric constant of the insulating material, the capacitance associated with each screened resistor was determined with respect to the substrate. This capacitance is column Cs in Fig. 4.

Each resistor must be terminated in bonding pads connected to the conductor leads of the copper conductor lines of the circuit. These pads have been standardized to a width of 30 mils and are a width equal to WA. These pads add additional distributed capacitance (Cp) to the network and must be included in the final analysis of the circuit. The total capacitance (Ct), associated with the thick-film resistance, is simply the sum of Cs and Cp. Wr and Lr are the real width and real length of the resistors to be screened as thick-film resistive devices. Notice that WA equals Wr but Lr is 60 mils longer than LA to accommodate the bonding pads, i.e., two 30 mil pads, one at each end terminating the resistor. The basic calculations for the resistors is now complete and all other critical information can be obtained from the data given in Fig. 4. Three resistors, namely 14, 16, and 21 are not included in the total resistive components to be screened. They were omitted due to reasons alluded to in the early parts of this paper.

Capacitor Design

For this sample, screen-printed thick-film capacitors, either by-pass or coupling types have not been considered. Coupling type screen-printed capacitors are formed by screening a dielectric insulator over a base electrode and co-firing a second electrode pattern on top of the first dielectric. By-pass type capacitors take advantage of the steel substrate as one electrode, utilize the porcelain as an insulator, and simply require a screened second conductive electrode over any available module area.

Although the screen printing process is an economical and a very practical method of obtaining capacitors in thick-film hybrid circuits, there are certain limitations and problems. First, it is very difficult to fabricate coupling capacitors to close tolerances and there will always exist a second-order effective capacitance with respect to the substrate. For either type of capacitor the final value is a function of the dielectric thickness and dielectric constant. Both of these crucial factors are very difficult to control. Unless extreme care is taken during the screening

process and the fabrication, the thickness of the dielectric may vary appreciably. This is particularly true during a double screening. Also, the dielectric constant of available insulating materials and the porcelain itself can and will vary with formulation during the firing profile, time, and temperature. As a result, capacitors with tolerances better than ±20% are difficult to achieve with high yields. Despite these problems, screen-printed capacitors have a definite practical advantage wherever low-value wide-tolerance capacitors are readily acceptable.

The second major limitation of screened hybrid-type capacitors is one of physical size. For this module, the dielectric constant of the porcelain insulator is about 6.00. Therefore, it will require nearly 1 square inch of board area to fabricate a 200 pF capacitor.

Because of the uncertainty in screening acceptable capacitance values and a limitation on physical size, discrete capacitive components were selected.

Designing the Taping or Rubylithe Master

With the schematic (Fig. 1) a preliminary board layout should be drawn free-hand, sketching all of the interconnections, discrete components, and potential screened parts. Consideration should be given to the physical size of all components, i.e., the active and passive discrete parts as well as those to be screened as thick-film components. After the preliminary layout is checked for accuracy, the circuit can then be taped or rubylithed from 2 to 4 times actual size, depending on the complexity of the circuit. Working with oversized taping or rubylithed masters will insure the proper spacing between conductors, the correct dimensioning of bonding pads and holes, and location of discrete parts. One master taping will be required for the conductor pattern, including the single plate of any by-pass type capacitor, and separate independent tapings will be required for every set of screened thick-film resistors utilizing a common ink. All of these master tapes must be continually coordinated and repeatedly cross-checked by superimposing the tape masters over one another to guarantee proper circuit continuity and layout accuracy among the conductors, screened parts, and discrete parts.

Bonding Pads, Holes, and Connectors

When generating the conductor master tape, connecting or bonding pads are generally used to connect the board's conductive circuitry to leaded components. In some cases, connections must be made to other outside circuitry or crucial test points. The design of the proper bonding pad should be optimized for the particular purpose. The pads used to su-

round round leaded components, wires, connectors, etc., should be designed as shown in Fig. 5. The minimum reliable and consistent hole size that can be punched and coined into the steel substrate is 0.052 inch. After porcelainization, the hole diameter will be reduced to 0.030 inch. In addition, edges of holes should not be closer than 0.040 inch. The diameters of holes processed in porcelainized steel substrate circuit modules can be related by the equation

$$D_P = D_S - \left[\frac{(2T_P)D_s}{D_S - 2T_P}\right] \qquad [2]$$

where D_P is the final porcelainized hole diameter, D_s the original hole diameter in the steel substrate, and T_P is the average thickness of the porcelain insulator.

Slots are somewhat more complex but the same equation can be used as an approximation to the final hole size. This change in the final hole and slot dimensions is primarily governed by the preparation and application of the porcelain insulator. Of secondary importance is the actual location of the hole. However, if the porcelainization can be carefully controlled over the entire surface area, the final hole and slot sizes will generally follow Eq. [2]. Therefore, the master conductive taping or rubylithe must be adjusted accordingly. Fig. 6 is a partial chart showing the predicted reduction in size of feedthrough holes and slots due to the processing of the porcelain insulator during electrophoresis.

This new technology has lead to a porcelain processing technique that has practically eliminated the common convex meniscus associated with liquid or fluid flows around punched and coined holes and/or slots. As a result, the conductive pattern typically used to interconnect holes and slots can be successfully printed right up to the very edge of the opening and, in some instances, through hole printing can be accomplished. When interconnecting holes and slots, the minimum conductive line width should be 0.025 inch. (This minimum can be reduced to 0.010 inch if certain integrated circuits are required in the network.)

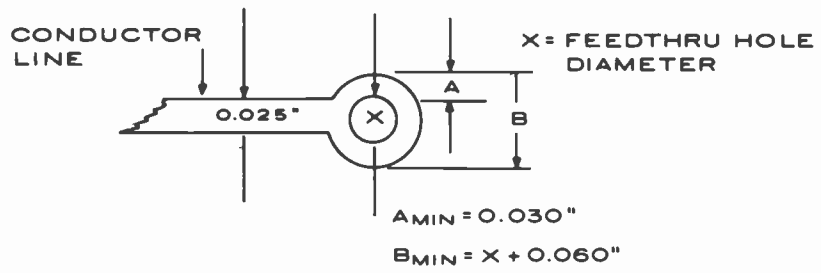

Fig. 5—Bonding-pad dimensions.

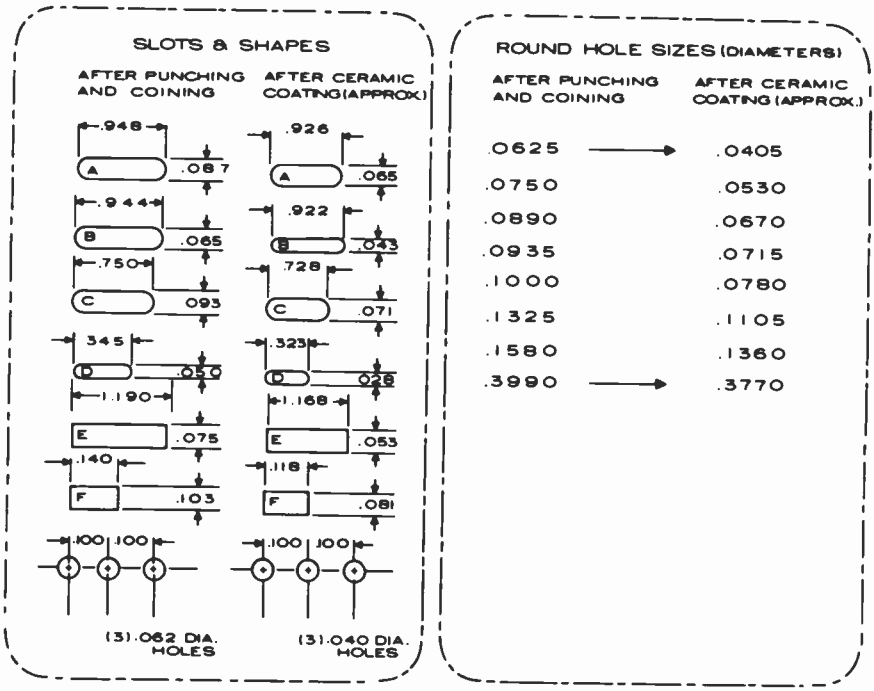

Fig. 6—Reductions in feed-through hole after porcelaining.

Referring to Fig. 5, the hole diameter (X) is the final hole size after porcelainization. The taping masters must be adjusted accordingly. Notice the minimum bonding pad around the hole is 0.030 inch which guarantees a secure bond to leaded components or wires. The conductor is shown as a 0.025 inch line. The minimum spacing between parallel 0.025-inch conductors should also be 0.025 inch but care must be taken to observe the voltage limitations imposed on conductors spaced that close together. For obvious reasons, high-voltage lines should be separated at distances greater than 0.025 inch, and heavy currents should not be routed along conductive lines of this size. Finally, conductors should not be placed closer than 0.100 inch from the outside edge of the board in its final version. In general, good circuit-board layout techniques should be adhered to throughout the process of converting a circuit to a porcelainized steel hybrid network.

The conductor lengths should be as short as possible to minimize the stray-capacitance associated with the metal substrate. This will usually involve several iterations before the master tapings are finalized and prepared for the photo reductions. Conductive lengths should be run in straight horizontal or vertical lines. Angled and curved conductors are permissible but they will be printed as sawtoothed, or serrated, edges

because of the nonalignment of the photographic artwork with screen meshes. This is particularly true of narrow conductive lines. Any insulated cross-over will require an extra printing and firing and should be avoided if possible. If there are many crossovers per unit area, insulated crossovers should be used to (1) improve the aesthetic value of the module and (2) to eliminate excessive component-side conductive jumper wires. However, if there are only a few crossovers, it is best to use a jumper wire on the component side of the board.

Resistor Considerations

Always orientate the thick-film resistive components horizontally or vertically, never at an angle. This is particularly true with the segments of either serpentine or interdigitated resistive structures. Curved or angled thick-film resistors will experience the same problems associated with similar conductive lines during the screening process. Also, locate the thick-film resistors so that all trimming can be accomplished in just two directions. This will minimize the trimming setup and reduce the time required to trim the resistors to their proper value. Finally, it is important to be aware of the instrument used to trim the thick-film resistors to size. For example, if the thick-film resistors are physically spaced too close together, the overspray from an abrasive trimmer may cut into adjacent resistors.

Closed loops should also be avoided. For any given network, the design may necessitate a resistor-conductor loop or the parallel combinations of resistors. To trim resistors to the appropriate value within a loop, the loop must be open until all adjustments are complete. Usually, with the hand or automatically inserted parts removed, most or all potential loops are open. In some cases, closed loops cannot be avoided and the loop must be opened deliberately on the original tape or photomaster. The actual opening can be very narrow and is typically 0.010 inch or less. After the thick-film resistive components are trimmed to the proper value, the loop must be closed either during a reflow solder application or with a jumper wire. (This stresses the advantage of occasionally using a discrete resistive component to open a loop rather than screening every resistor as thick-film components.) When two resistors have the same sheet resistivity (ρ), they may be printed as a single pattern completely overlapping a common conductor.

Soldering Considerations

Most components generally associated with thick-film hybrid circuits are of chip-form. However, it is sometimes necessary to use lead-attached

components such as in this B+ Regulator. The preferred way to secure lead-attached components is by soldering, although a conductive epoxy can be used. To properly secure the leaded components to the hybrid circuit it is necessary to (1) adjust the original artwork for the proper through-hole size (see Figs. 5 and 6) and (2) have the surrounding solder bonding pad at least three times the lead diameter in width. Terminals and/or fasteners should be designed with some resilience to insertion, especially during automatic insertion. Sharp impact by insertion tools or components should be avoided during construction. The steel substrate is virtually indestructable, but the porcelain insulator is somewhat brittle at 0.007 inch and therefore not immune to sharp impacting stresses and loads.

For best results, the porcelainized-steel printed-circuit boards should be preheated slightly before soldering. The preheat temperature depends on the module's total surface area and porcelain thickness and is usually determined empirically. The solder composition should be 62/36/2-Sn/Pb/Ag with a particle size of 300 mesh (0-53 microns). A solder of this nature is virtually oxide-free so that the solder will melt and flow quickly and cleanly on the surface of the module. The soldering iron or station is also important. A pulse-heat type probe for preheat and a reflow tip generally gives the best results.

Film Masters

After completing the tape or rubylithe masters, they should be rechecked for accuracy against the original schematic diagram. The final photoreductions of the master layouts can then be made and reduced to actual size film masters that are (1) emulsion side-up, (2) right reading, with (3) conductive and screened patterns black on a clear field. An extra film-master will make an excellent template for the mechanical punching and coining operation. Also, a final film-master can be used to shear the module to the exact required size. From these film-masters, "silk" screens or fine "wire-mesh" screens can be generated for the conductor, thick-film, and/or insulator patterns.

Final Preparation of Steel Substrate

As the steel is prepared for the punching and coining operation, an electrophoretic contact and firing support hole should be added as a tab at the center line of one side of the module. A typical tab is shown in Fig. 7. This tab will not be porcelainized but used as a guide during the porcelainization. All critical vertical positions should be specified in inches from the bottom of the board; all critical horizontal positions should be

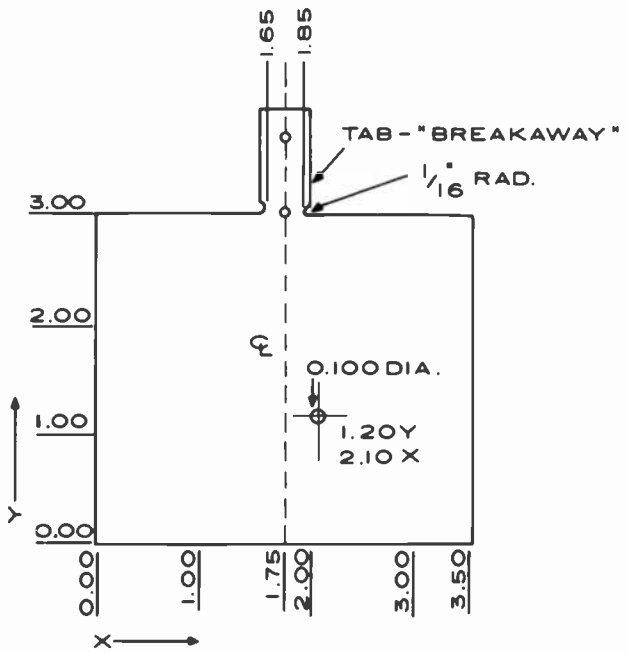

Fig. 7—Tab electrophoretic contact and firing support hole.

specified in inches from the left-hand edge of the board. All holes and "starting" edges of slots for either hand inserted or automatic insertion should be kept on 0.010″ centers. Features that are to be sheared into or from the module should be dimensional from the 0,0 position to the nearest 0.001 inch. In general, all dimensions and positions on the accompanying mechanical drawing should be referred to the steel substrate and designated "before porcelainization." After the porcelainizing process the exact position of all holes, slots, and sheared areas will be slightly altered as discussed previously (see Fig. 6).

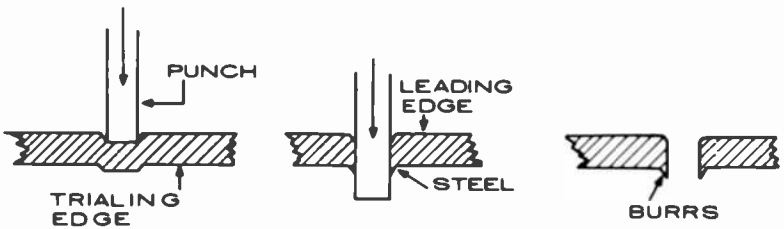

Fig. 8—Effects of hole punching.

Punching and Coining

When a hole or slot is punched into the low-carbon steel board, the punch has a tendency to pull the surrounding steel into the hole before the actual shearing process begins. This will round the leading, or top, surface of the hole, but steel is forced out the trailing or bottom surface of the hole, usually leaving sharp and abrasive burrs around the bottom edge. During the electrophoretic process, the porcelain will uniformly coat the rounded top surface and also penetrate the inside edges uniformly. The porcelain will not, however, cover the burrs, even if the burrs are ground flat, because the bottom edge will remain sharp and abrasive at 90°. Fig. 8 is a series of diagrams showing the effects of punching a hole in low-carbon steel.

To insure uniform porcelainization over the entire steel surface area, the top *and* bottom surface edges of all punched holes and slots must be rounded or coined. Attempts have been made to round the edges of holes by the use of dies and special punches. These attempts have not been consistently successful because they distort the material around the holes causing bulges and other uneven surface distortions. Some research has been directed to beveling the trailing edges with counter bores and drills, but this has proven to be a slow and costly process. The problems associated with previous attempts to coin holes and slots is readily solved by using two dies or coining punches simultaneously that are the exact mirror images of each other. Fig. 9 is a diagram of this mechanical arrangement. As pressure is gradually applied, each coining punch rounds the hole from the top and bottom into a final smooth curve of radius r. The angle (α) is critical for proper rounding of the holes. Through experimentation, an angle α of 2° to 3° was found to be the most satisfactory in coining holes in low-carbon-steel substrate material.

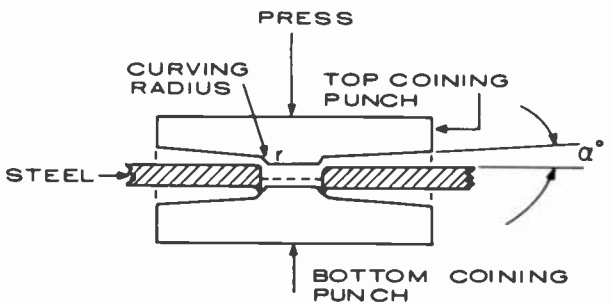

Fig. 9—Mechanical arrangement to punch and coin hole from both sides of steel simultaneously.

B+ Regulator Circuit Module

Figure 10 is the conductor side detail of the converted B+ Regulator circuit. The tape-master has been photographically reduced to actual size and clearly shows the network's interconnections, the mounting hole locations, and the conductive bonding pads for the thick-film resistors. Figure 11 is the photoreduced thick-film resistive pattern before trimming and Fig. 12 is the superposition of Figs. 10 and 11. Fig. 13 is a photo of the conductor side of the module and shows the trimming

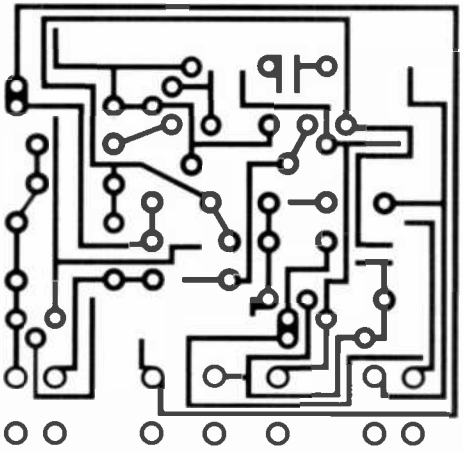

Fig. 10—Conductor side of B+ regulator circuit.

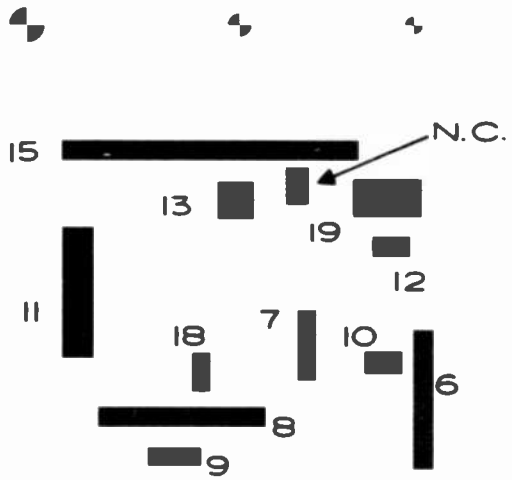

Fig. 11—Thick-film resistor pattern of B+ regulator circuit.

necessary to bring the thick-film resistors into their proper range. Fig. 14 is a side-by-side comparison of the original module (on the right) and the new and fully compatible porcelainized steel module (on the left). The component side of the porcelain model is not as dense with components since most resistors are screened parts on the reverse or conductor side. The porcelain model shown is physically larger than the original unit, but the actual circuit falls within the printing or layout bounds of the original. The top portion of the porcelain module shows the electrophoretic contact and several supporting guide holes. The center-line tab along with its firing support holes has been removed for insertion into the receiver.

Experimental Results

After the porcelainized steel substrate hybrid unit was installed and operated for nearly 100 hours, a series of measurements and oscilloscope pictures were taken and evaluated. They compared very favorably with an identical series taken on the original module. The oscilloscope picture in Fig. 15, which shows the porcelain board's synchronizing signal and collector Q2 waveform, should be compared with Fig. 3 for the original module. The two are nearly identical in nature. The synchronizing signal, as expected, is unaffected by the input characteristics of the porcelain-steel hybrid network. The Q2 collector ramping slopes are almost iden-

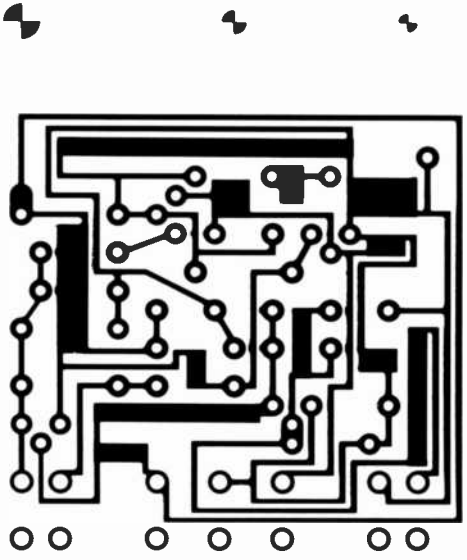

Fig. 12—Composite of conductors and thick-film resistors.

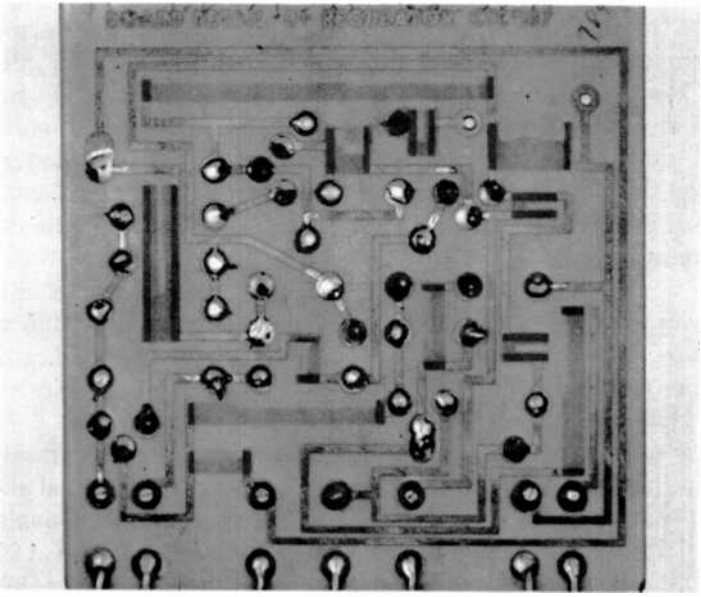

Fig. 13—Conductor and thick-film resistor side of porcelainized-steel module.

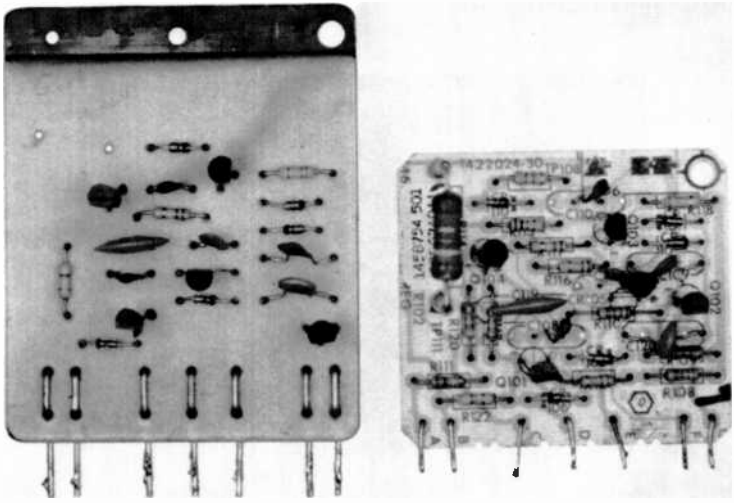

Fig. 14—Comparison of "parts side" of porcelainized-steel (left) and original (right) modules.

tical. In the porcelain-board version (Fig. 15) the downward slope lasts approximately 5 μsec longer, resulting in a shorter "turn-on" time for the SCR switching regulator. Therefore, the regulated voltage has stabilized at +116.8 V dc as opposed to the nominal regulated voltage of +118 V dc. This slight reduction in regulated voltage had no detrimental effect on the TV receiver. In fact, the regulated voltage could have been adjusted to exactly +118 V dc by externally altering the feedback sampling resistors.

The thick-film resistors drifted from their original values less than ±2% after prolonged use and generally remained well within circuit tolerance. At horizontal frequencies, the stray-capacitance, i.e., the capacitance measured with respect to the substrate, did not affect the basic performance of the network.

As far as power considerations are concerned, both units dissipated the same power. However, the 22 kΩ 2-W resistor on the original phonelic printed-circuit board stabilized at 133.7°F, whereas, the equivalent 22 kΩ 2-W thick-film resistor on the porcelain module stabilized at 97.3°F. If the phonelic module was overstressed, e.g., through excessive loading, the discrete resistors changed values and did not recover to their original values. The thick-film version would completely recover from an overload condition and the resistors would return to the original trimmed values. This was attributed to the fact that the porcelainized steel substrate quickly and effectively dissipated any of the destructive resistive heating phenomenon.

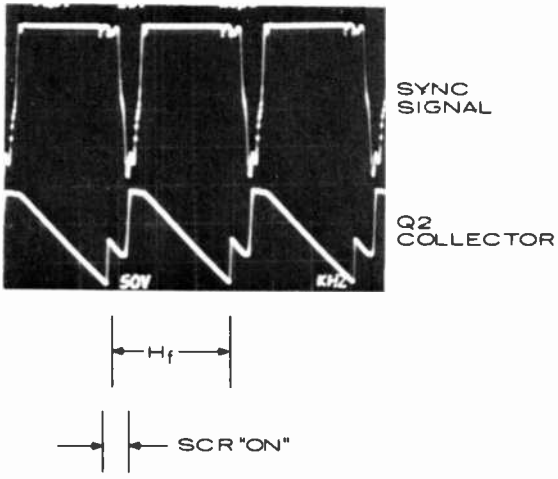

Fig. 15—Porcelainized-steel B+ regulator network synchronizing signal and ramping signal.

Conclusion

Although this module represented a very small portion of an entire television receiver's circuitry, the porcelainized steel circuit board offered a reliable and durable alternative to the conventional printed-circuit technology. The module exhibited high mechanical strength, good-to-excellent thermal conductivity, and was certainly very compatible within the television receiver environment. It could have provided electromagnetic shielding for other portions of the circuitry. The design was very flexible and could have been utilized as an integrated structural support for other networks. Over its present life, it has been a highly reliable B+ regulating circuit compatible with automatic insertion equipment and wave-soldering baths; it is resistant to chemicals and high ambient temperatures. It is also potentially less expensive.

There are some disadvantages to the new technology. It is indeed a new technology. It does not lend itself well to a redesign cycle, i.e., it is difficult to change a screened component. Also it has inherent parasitic capacitance with respect to the substrate, and it adds some additional weight.

Acknowledgments

This effort was undertaken within the Electronic Packaging Research Group headed by L. Onyshkevych. We wish to thank all members of this group for their cooperation and considerable efforts in making this project a success. In addition, we wish to thank Mr. Paul Smith who developed the mechanical punching and coining dyes and Mr. John Furda who provided the prepared metal substrates.

Bibliography:

[1] C. A. Harper, *Handbook of Thick-Film Hybrid Microelectronics*, McGraw-Hill Book Co., N.Y. (1974).

[2] M. Kaufman and A. Seidman, *Handbook of Electronics Calculations*, McGraw-Hill Book Co., N.Y. (1979).

[3] Television Workshop 20, "Servicing the CTC 99 and 101 Color Chassis," 1979 RCA Consumer Electronics.

AUTHORS

Wayne M. Anderson received the B.S. degree in Chemistry from the University of Delaware in 1949. Following graduation he was with Heyden Chemical Corp. in the control laboratory at Princeton, N.J. Mr. Anderson joined RCA Laboratories in 1953 as a Research Technician. He was named Research Associate in 1967 and Senior Technical Associate in 1978. He is presently in the Display Materials and Process Research Group in the Display and Energy System Research Laboratory, engaged in research on glass and ceramic materials for the porcelain enamel printed-circuit-board substrate and the gentle arc program.

Mr. Anderson, with Dr. Kenneth Hang, received an RCA Laboratories Outstanding Achievement Award in 1978 for contribution to a team effort leading to innovations in the development and processing of glass and ceramic materials.

James Andrus joined RCA in 1973. He has been engaged in research into various aspects of surface and thin-film Chemistry. He holds a BS degree in Chemistry from Delaware Valley College, and is now pursuing a degree in Electrical Engineering.

Simon M. Boardman received an Associate degree in Electronics Technology from Temple University in 1961 and a BS in Business Administration from Rider College in 1978. Mr. Boardman worked in the microcircuit thin-film applications laboratory and thick-film service group at IRC, from 1961 to 1965. From 1965 to 1968 he worked for Fairchild Hiller Corporation in the physical chemistry group, having responsibility for the thin-film services and assisted with the PC facility, doing NASA and defense contracts. Mr. Boardman joined RCA Laboratories in 1968. He has worked on various device development projects and is currently engaged in the development of polymer thick-film materials.

Mr. Boardman is a member of ISHM.

Edward J. Conlon has worked in microelectronics since 1960, and has broad experience with thick- and thin-film processes. Prior to his present work at RCA, he worked for eight years at Electra-Midland Corporation, a division of North American Phillips Co., Inc., where he developed thick-film resistor pastes with very low TCR's. At Electra-Midland he also developed thick-film dielectric and resistor processes. Mr. Conlon worked on silicon processing at General Instrument Corporation. Earlier he worked on a variety of electronic materials processing projects at Burroughs Corporation. In 1973 he joined the hybrid study effort at RCA's David Sarnoff Research Center as a Research Technician. He has fulfilled a key role in the performance of the 1974 and 1975 Naval Air Systems Command contract studies of thick-film conductor adhesion. Mr. Conlon has two and a half years of engineering school credits from Columbia University and Newark College of Engineering. Presently he is an associate member of the Technical Staff.

Denis P. Dorsey received his B.S.E.E. degree in 1958 from the University of Delaware in 1958 and an M.S.E.E. from Drexel Institute of Technology in 1962. In 1959 he joined RCA Astro-Electronics as an electronic circuit designer. He was involved in the first TIROS weather satellite, the NIMBOS HRIR system, the TOS check out system, and the RANGER moon launch camera. In 1966 he joined RCA Laboratories and participated in the design and development of the Homefax Message System, the SRI single vidicon color encoding television system, silicon-dioxide storage vidicons, VIDEOVOICE, and the OMS Dewline PPI radar image transmission system. In 1971 Mr. Dorsey was sent to mainland China to participate in coordinating and establishing television coverage of the Presidential visit and in 1975 he completed several tours to the Artic, installing and evaluating new surveillance equipment for the AIR FORCE and NORAD. Since 1975, Mr. Dorsey has been a member of RCA's Consumer Electronic Research Laboratory, where he is actively engaged in the design and development of television baseband circuitry. He has the responsibility for converting receiver circuits to hybrid-microelectronic thick-film technology and modeling television networks using analog and digital computers.

Mr. Dorsey received an Outstanding Research Award and the David Sarnoff Award for his contributions to the RCA Videovoice System. He is a member of the IEEE and a member of Eta Kappa, N.J.

Ralph S. Filson served four years in the United States Navy and received electronics training in Class A and Class C schools. While attached to the Navy, he also attended Rider College. In 1957 Mr. Filson joined the RCA Laboratories and continued his education at the RCA Institutes. His research activities have included photomechanical processing, the RCA Hometax System, the video-voice project, and the OMS Radar Surveillance Dewline Project for the United States Air Force. Since 1978, Mr. Filson has been a member of the Electronic Packaging Research Group and has been participating in the conversion and evaluation of electronic circuits on porcelain-coated-steel substrates and the generation of low-temperature thick-film hybrid networks.

Kenneth W. Hang received the B.S. degree in Ceramic Engineering from the University of Illinois in 1966. He received the M.S. degree in 1967 and completed the Ph.D. in Ceramic Engineering in 1970. Dr. Hang joined RCA Laboratories in 1970 as a Member of Technical Staff with the Display Materials and Process Research Group, specializing in the area of glass research, synthesis, and materials measurements in the Display and Energy Systems Research Laboratory. He has been responsible for the synthesis and characterization of glasses for passivating the surface of silicon power devices. He has invented and developed a glass ceramic coating on steel that has application as a thick-film hybrid circuit substrate. Dr. Hang has also developed a process for power transistor glass passivation and has developed a coating for TV picture tube funnels to control arc currents.

Dr. Hang has been the recipient of RCA Laboratories Achievement Awards in 1973 and in 1978. He holds six U.S. patents. He is a member of the American Ceramic Society and Sigma Xi.

Thomas Tipton Hitch received his B.S. degree in Metallurgical Engineering from the University of Tennessee in 1961 and the Ph.D. in Materials Engineering from Rensselaer Polytechic Institute in 1973. He joined the Martin Co. in Baltimore, Maryland, in 1961, where he worked on a nuclear fuel project and on several environmental effects projects. In 1969, Dr. Hitch joined the Process Research Group of RCA Laboratories, where he initially worked on the analysis of failures of silicon electronic devices and interconnections. Since 1970 he has been concerned with thick-film hybrid materials and their processing. From 1974 to 1978 Dr. Hitch was a principal scientist on a series of contracts for Naval Air Systems Command and Naval Avionics Center, Indianapolis. These studies have contributed significantly to the understanding of the fundamental mechanisms of adhesion and bondability in thick-film conductors. Through this research, advances were also made in adhesion testing, the chemical analyses of conductor inks, and other areas. More recently, Dr. Hitch helped to form the Electronics Packaging Research Group in the Television Research Laboratory at RCA Laboratories. His work there has involved thick-film, porcelainized steel for printed circuit boards/hybrid substrates, and leadless passive components.

Dr. Hitch is inventor or co-inventor on three U.S. patents, and is a member of ASM, ISHM and the American Ceramics Society. He was president of the Metal Science Club of New York for 1980–1981.

Jack P. Honoré III is currently a student at Drexel University where he is completing work towards a Bachelor degree in Electrical Engineering. From 1972 to 1974 he worked as a Engineering Technician for Dow Jones Inc. on the conversion from hot lead type to computer controlled offset printing. He then joined Princeton Applied Research Corp. where he was employed as an Electronics Analyst. His primary duty was to evaluate the performance of Photon Counters, Signal Averagers and Polargraphic Analyzers. Since 1978, he has been employed with RCA Laboratories in the Electronic Packaging Research Group, where he is currently working on porcelanized steel boards and an integrated high voltage transformer.

Adrian Kusenko worked with Thiokol Chemical Corporation from 1962 until 1979 as a senior research technician in the Process Development Department, specializing in urethane, elastomers, liquid polymers, sealers, urethane, gas-liquid chromatography, physical testing, analytical procedures, technical service, customer assignments and special chemicals and monomer development. He joined RCA in 1979 as a research technician in the Consumer Electronic Research Department and is engaged in thick film and printed circuits development research.

Joseph H. McCusker received a B.S. in Electrical Engineering from Northeastern University, Boston, Mass., in 1947, and his M.S. in Electrical Engineering from Massachusetts Institute of Technology, Cambridge, Mass., in 1949. At M.I.T., he worked as a research assistant in the Digital Computer Laboratory on the development of an electrostatic storage tube for use as a high-speed random-access memory. From 1949 to 1951, he was an instructor in the Electrical Engineering Department at Pennsylvania State University, State College, Pennsylvania. From 1952–1956, he worked at Lincoln Laboratories, Bedford, Mass., where he was the leader of the Magnetic Section which, in cooperation with other sections, developed the first working random-access high-speed ferrite memory. In 1956, he joined RCA, where he helped set up the RCA Needham Materials Laboratory. He was the Manager of Advanced Development which synthesized ferrites with better temperature characteristics in both memory and high-frequency ferrite cores. Since then he has been a member of the technical staff at RCA Laboratories, where he has worked on fabrication of diode matrices by electron-beam bombardment, packaging of MOS transistors, the development of thin-film transistors, solid-state adaptive devices, and microsonic surface wave filters for signal processing. Recently he has been working on porcelainized-steel substrates for consumer applications.

Anthony Z. Miller received his B.A. degree in Chemistry from Rutgers University in 1964. As employee of RCA-Solid State Division in Somerville from 1962 until the end of 1975, he was responsible for the development of a chromium thin-film mask for photolithograhic processing of semiconductor devices. He also contributed to the development of a beam-lead bonding process used in the Safeguard project and developed and improved ultrasonic wire bonding processes for semiconductor devices and packages. Additional contributions included improved solder reflow joining methods for diverse semiconductor device packages. He has experience in metallography and diffusion of silicon devices. In April 1976, Mr. Miller joined RCA Laboratories and works in thick-film technology, including ink material synthesis, process development, ultrasonic wire bonding and solder reflow studies. Currently, his main efforts are in development of adhesives for chip attachment to printed circuit boards.

Mr. Miller holds two patents and is a member of the American Chemical Society, and American Society for Metals.

Lubomyr S. Onyshkevych obtained his B.E.E. degree at the City College of New York in 1955, and his M.S. degree in electrical engineering at M.I.T. in 1957 and an advanced E.E. degree at M.I.T. in 1962. From 1955 through 1957 he worked at the Research Laboratory of Electronics, M.I.T. In 1957 he joined RCA Laboratories in Princeton, N.J., where he worked in the field of computer magnetics; for this work he received an Outstanding Achievement Award. Presently he is involved in the areas of magnetics, thin films, thick films, ultrasonics, surface-waves, microsonics, and television. For this work he has received a second Outstanding Achievement Award, the IR1000 Award, and three other awards. At the present time he heads the Electronic Packaging Research Group at the RCA Laboratories. Mr. Onyshkevych holds 12 U.S. patents and is a member of IEEE, ISHM, Sigma Xi, Tau Beta Pi, and Eta Kappa Nu.

Ashok N. Prabhu received the B.Tech. degree in Metallurgical Engineering from Indian Institute of Technology, Bombay, in 1970 and the M.S. and Ph.D. degrees in Metallurgical Engineering from Purdue University in 1972 and 1975, respectively. He worked as an IMB research-fellow at Northwestern University during 1975–1976 and as a senior application metallurgist at Engelhard Industries during 1976–1979. He joined RCA Laboratories in 1979 as a member of the technical staff. Dr. Prabhu has done extensive research and development work in hybrid microelectronic materials and processes, especially thick-film resistors, conductors and dielectrics. He is currently engaged in the development and use of base metal thick-film technology on porcelain-coated steel boards and polymer thick-film technology on PC boards.

Dr. Prabhu is a member of the American Ceramic Society, the International Society for Hybrid Microelectronics and Sigma Xi.

Alan Sussman received a bachelor's degree in chemistry from Rensselaer Polytechnic Institute and a Ph.D. in physical chemistry from Yale University, investigating self-diffusion in polymers. At RCA Laboratories, he has worked on solid state optical amplifiers, thin film organic semiconductors, and liquid crystals. He continued the studies of liquid crystal displays at Hewlett-Packard, Optel Solid State (Somerville), and Timex. He returned to RCA Laboratories to investigate the electrochemistry of glass deposition for the porcelain enamel project, and is now working on the chemistry associated with integrated high voltage transformers. He is the holder of 4 patents and has been awarded 2 outstanding achievement awards.

Barry J. Thaler graduated in 1972 from SUNY at Stony Brook cum laude with honors in physics. He received his M.S. and Ph.D. degrees in physics from Michigan State University in 1974 and 1977, respectively. His doctoral thesis was an investigation of the high field magneto transport properties of metals at liquid helium temperatures. After graduation, he became a Research Associate in the Department of Physics at Northwestern University. There, and as a Visiting Scientist in the Solid State Sciences Division of Argonne National Labs (1978), he was engaged in research in the preparation of and magnetic properties of metallic thin films having microscopic composition modulations. In 1979 he joined RCA Laboratories, Princeton, N.J., as a member of the technical staff where he has participated in studies of insulating materials. He is presently studying the effects of processing variables on the physical properties of polymeric materials.

Dr. Thaler is a member of the American Physical Society, Sigma Xi, and the Metals Science Club of New York.

Wei H. Tsien received a B.S.M.E. from Chiao-Tung University, Shanghai, China and an MSME from M.I.T. He worked from 1953 to 1977 in RCA Commercial Electronic System Division, designing broadcasting cameras, recorders, and related equipment. He is now a consultant to RCA in the Electronic Packaging Research Group in Princeton, N.J. In 1937, he was a winner of the National Scholarship Contest for advanced studies sponsorec by Tsing-Hua University, Peking, China. He was the first prize winner of RCA Tape Recorder Design Contest in 1953, and the first prize winner of RCA Victor Television's TV "Imagineering" Contest for television receiver remote control concept design in 1958.

Thoms J. Ward joined RCA in 1959, after 3 years with Remington Rand Univac, where he was involved with components of Ferrite Memories. Since joining RCA, he has worked with magnetic materials for sonic-film memory and magnetic bubble memory. Work on sonic-film memory won an IR-100 award. He has also worked on epoxy-metal PC boards for television receivers, porcelain-enamelled PC boards for television receivers, and is recently involved with integrated high voltage transformer encapsulation. He was an associate member of technical staff in 1978.

Patents Issued to RCA Inventors—First Quarter 1981

January

A. R. Balaban and S. A. Steckler Voltage Controlled Oscillator Presenting High Impedance to Parallel Resonant Tank Circuit (4,243,953)
D. P. Bortfeld and L. J. Vieland Simplified Resistive Lens Electron Gun With Compound Linear Voltage Profile (4,243,912)
R. J. Bosselaers Apparatus for Computing the Change in Bearing of an Object (4,247,898)
F. Caprari Flash Lamp Drive Circuit (4,243,917)
A. R. Dholakia Method for Precision Grinding of Hard, Pointed Materials (4,243,395)
J. S. Fuhrer Non-Linear Processing of Video Image Vertical Detail Information (4,245,238)
S. T. Hsu and R. J. Hollingsworth High Performance Electrically Alterable Read-Only Memory (EAROM) (4,247,861)
H. Huang and F. N. Sechi Design Method for Linear Amplifier (4,246,535)
L. M. Hughes Record Side Identification Apparatus for VideoDisc Player (4,247,119)
A. C. Ipri Fabrication of an Integrated Injection Logic Device with Narrow Base Width (4,244,001)
R. W. Kipp and H. C. Johnson FM-CW Radar Ranging System with Automatic Calibration (4,245,221)
W. F. Kosonocky and R. L. Rodgers, 3rd CCD Imagers (4,246,591)
W. A. Lagoni Controllable Non-Linear Processing of Video Signals (4,245,237)
N. R. Landry, R. L. Schelhorn, and S. L. Williams Thick Film Resistor Element and Method of Fabrication (4,245,210)
D. D. Mawhinney Smart Noise Generator (4,247,946)
J. F. McSparran Circuit Board Guide and Ground Connector (4,243,283)
W. H. Meise Signal Integrator With Time Constant Controlled by Differentiating Feedback (4,243,918)
R. S. Mezrich and W. C. Stewart Acoustic Variable Focal Length Lens Assembly (4,242,913)
L. W. Nero Color Picture Tube Magnetic Shielding and Degaussing Structure (4,243,913)
M. Nowogrodzki Frequency Translation Means (4,247,822)
D. R. Patterson Temperature Compensated Bias Circuit for Semiconductor Lasers (4,243,952)
T. W. Pote and W. E. Ham Method for Cracking and Separating Pellets Formed on a Wafer (4,247,031)
C. E. Profera and J. J. Campbell Multimode Feed for a Monopulse Radar (4,246,583)
O. H. Schade, Jr. Substantially Temperature-Independent Trimming of Current Flows (4,243,948)
S. Shai Digital Open Loop Programmable Frequency Multiplier (4,244,027)
S. A. Steckler and A. R. Balaban AFPC Phase Detector With No Output From Alternate Sync Pulses (4,245,251)
H. Stietenroth Electronic Tone Generator (4,245,336)
J. Tults AFT Arrangement for a Phase Locked Loop Tuning System (4,245,351)
M. H. Wardell, Jr. Convergence Adjustment Arrangement Using Magnetic Tabs With Differential Motion and Rotary Drive (4,245,205)
C. F. Wheatley, Jr. Multivibrator Circuit (4,246,551)
J. A. Wilbur and T. J. Christopher Nested Loop VideoDisc Servo System (4,247,866)
N. D. Winarsky, D. P. Bortfeld, R. W. Cohen, and L. J. Vieland Resistive Lens Electron Gun With Compound Linear Voltage (4,243,911)
H. J. Wolkstein, B. R. Dornan, and J. Goel High Repetition Rate Driver Circuit for Modulation of Injection Lasers (4,243,951)

February

A. A. Ahmed Circuit With Electrically Controlled Gain (4,251,778)
L. R. Avery Plural Sequential Operating Mode Automatic Kinescope Beam Current Limiter (4,253,121)
H. R. Beelitz Current Source, as for Switching PIN Diodes (4,251,742)
S. Berkman, R. Metzl, R. E. Novak, and D. L. Patterson Apparatus for and Method of Supporting a Crucible for EFG Growth of Sapphire (4,251,206)
W. M. Boyd Exciter Having Incidental Phase Correction Compensation in Consonance With Output Power Level (4,249,214)
Z. F. Chang and R. Minton Push-Push Resonant Power Inverter (4,250,541)
P. Datta and G. Kaganowicz Perfluorinated Polymer Thin Films (4,252,848)

E. J. Denlinger Flip Chip Mounted Diode (4,250,520)
J. J. Fabula Low Leakage N-Channel SOS Transistors and Method of Making Them (4,252,574)
R. E. Fernsler and D. H. Willis Television Horizontal AFPC With Phase Detector Driven at Twice the Horizontal Frequency (4,251,833)
N. Goldsmith and S. T. Hsu Gate Injected Floating Gate Memory Device (4,253,106)
D. F. Griepentrog Continuous Tuning Arrangement for a Multiband Television Receiver (4,249,132)
L. A. Harwood and E. J. Wittmann Phase Compensated Controller Oscillator (4,249,199)
L. A. Harwood, R. L. Shanley, 2nd, and E. J. Wittmann Automatic Kinescope Beam Current Limiter With Sequential Control Modes (4,253,110)
R. J. Himics, N. V. Desai, and M. Kaplan Novel Resists and Recording Media (4,252,886)
R. J. Hollingsworth Blocked Source Node Field-Effect Circuitry (4,253,162)
S. T. Hsu Comparator, Sense Amplifier (4,249,095)
R. W. Jebens Solar Cell Construction (4,249,959)
K. Knop and J. Kane Tunable Diffractive Subtractive Filter (4,251,137)
P. A. Levine Defect Detection Means for Charge Transfer Imagers (4,253,120)
A. L. Limberg Current Mirror Amplifier (4,250,461)
G. A. Lucchi and R. H. Aires Aircraft Weather Radar System (4,249,174)
M. E. Malchow Amplifier System With AGC, as for an AM Radio (4,249,137)
M. E. Malchow Frequency Converter, as for First Detector of Heterodyne Radio Receiver (4,253,196)
T. E. Molinari Continuous Tuning Arrangement for a Multiband Television Receiver (4,249,255)
T. E. Molinari and D. F. Griepentrog Continuous Tuning Arrangement for a Multiband Television Receiver (4,249,256)
J. A. Olmstead and S. W. Kessler, Jr. Semiconductor Power Device Incorporating a Schottky Barrier Biode Between Base and Emitter of a PnP Device (4,253,105)
A. D. Robbi Digital Drive Circuit for Electric Motor or the Like (4,249,119)
R. L. Rodgers, 3rd Television Synchronizing System Operable From Nonstandard Signals (4,253,116)
O. H. Schade, Jr. Multi-Mode Relaxation Oscillator (4,250,464)
O. H. Schade, Jr. Smoke Detector (4,250,500)
G. L. Schnable and C. P. Wu Laser Rounding a Sharp Semiconductor Projection (4,249,960)
A. Schwarzmann Adjustable Passbank Filter (4,250,475)
S. A. Steckler and A. R. Balaban Television Horizontal AFPC With Phase Detector Driven at Twice the Horizontal Frequency (4,250,525)
M. H. Wardell, Jr. Yoke Tabbing Device (4,253,077)
G. J. Whitley Method of Forming Aperture With Rounded Edges in Sheet Material (4,248,075)
D. H. Willis Regulated Deflection Circuit (4,251,756)
H. A. Wittlinger Battery Test System, as for Smoke Detector Alarm (4,251,811)
J. J. Wolford and J. B. George Short-Term Power Dropout Arrangement Useful in a Televison Receiver (4,249,089)
D. I. Wright Video Signal Dropout Compensator (4,250,521)

March

J. A. Allen and M. E. Miller VideoDisc Stylus Retractor (4,256,311)
F. Aschwanden Self-Adjusting Bell Filter Circuit for Use in SECAM Coders (4,255,758)
V. Christiano and C. B. Carroll Faceplate Assembly for a Flat Panel Color Display Device (4,259,612)
R. J. D'Amato Projection Kinescope and Method of Operation (4,259,692)
R. G. Ferrie Systems for Comparing and Ranking a Plurality of Signal Inputs (4,255,740)
A. Goldman Improving Etch-Resistance of Casein-Based Photoresist Pattern (4,259,421)
P. D. Griffis Integrated Circuit Heat Dissipator (4,254,447)
D. F. Hakala Method for Producing CRT Screen Structure (4,255,504)
K. W. Hang and W. M. Anderson Partially Devitrified Porcelain Composition and Articles Prepared With Same (4,256,796)
J. R. Harford Noise Cancellation Circuit (4,254,436)
J. G. N. Henderson and R. J. Maturo Channel Identification Apparatus Useful in a Multiband Sweep Type Tuning System (4,254,506)
R. V. Johnson and D. P. Biondi Temperature Gradient Means in Reactor Tube of Vapor Deposition Appratus (4,256,052)
L. B. Johnston System for Periodically Reversing the Order of Video Data in a Flat Panel Display Device (4,257,068)
S. T. Jolly Method of Depositing Layers of Semi-Insulating Gallium Arsenide (4,253,887)

J. Kane Method for Fabricating a Diffractive Subtractive Filter Embossing Master (4,255,514)
S. W. Kessler, Jr. Minimum Pressure Drop Liquid Cooled Structure for a Semiconductor Device (4,258,383)
P. R. Knight Side Pincushion Correction Modulator Circuit (4,254,365)
K. Knop Diffractive Color Filter (4,255,019)
H. L. Levin Antenna Deicing Apparatus (4,259,671)
A. Month and D. B. Kaiser Electron Tube Having Electrode Centering Means (4,258,284)
A. Month and T. E. Benner Pick-Up Tube Having Light Controllable Furcated Light Pipes (4,259,609)
J. I. Pankove Method and Structure for Passivating Semiconductor Material (4,254,426)
F. C. Raih Method for Slurry Coating a Faceplate Panel Having a Peripheral Sidewall (4,254,160)
A. Rosen GaAs Dual-Gate FET Frequency Discriminator (4,255,714)
E. D. Simshauser Track Skipper Apparatus for VideoDisc Player (4,258,233)
T. Takahashi and O. Yamada X-Ray Luminescent Glasses (4,259,587)
W. Truskalo Regulated Deflection Circuit (4,254,366)
J. A. VanRaalte Segmented Shadow Mask (4,259,611)
C. F. Wheatley, Jr. Balanced-to-Single-Ended Signal Converters (4,254,381)
M. L. Whitehurst Shield for Plating Substrate (4,259,166)
R. Williams Non-Air Polluting, Non-Pyrolytic Upgrading of Coal for Cleaner anbd More Effective Electrical Power Generation (4,259,414)
W. Wilson and F. J. Egenski Free Hold Down of Wafers for Material Removal (4,258,508)
W. R. Witte Method of Making Transformer (4,258,467)
B. J. Yorkanis Inhibit Circuit for a Differential Amplifier (4,257,009)